Propagation of suspended sediment flux in the Amazon river from Tamshiyacu gauging station in Peru to Obidos gauging in Brazil : spatio-temporal variability

Elisa Natalia Armijos Cardenas

Université de Toulouse

THÈSE

En vue de l'obtention du

DOCTORAT DE L'UNIVERSITÉ DE TOULOUSE

Délivré par :
Université Toulouse 3 Paul Sabatier (UT3 Paul Sabatier)

Cotutelle internationale avec :
Instituto Nacional de Pesquisas da Amazônia - INPA

Présentée et soutenue par :
Elisa Natalia ARMIJOS CARDENAS

Le mercredi 10 novembre 2015

Titre :
Propagation des flux de sédiments en suspension sur l'Amazone de Tamshiyacu (Pérou) à Óbidos(Brésil)-Variabilité spatio-temporelle

---

École doctorale et discipline ou spécialité
ED SDU2E : Hydrologie, Hydrochimie, Sol, Environnement

Unité de recherche :
UMR Géosciences Environnement Toulouse (GET)

Directeur(s) de Thèse :
Dr. Jean Loup GUYOT
Dr. Naziano Pantoja FILIZOLA Jr.

Rapporteurs :
Dr. Gustavo Henrique MERTEN
Dr. José Cândido STEVAUX

Autre(s) membre(s) du jury :
Dr. Luiz Antonio CÁNDIDO
Dr. Jean Michel MARTÍNEZ

INSTITUTO NACIONAL DE PESQUISAS DA AMAZÔNIA - INPA -
MANAUS-BRASIL

PROGRAMA DE PÓS-GRADUAÇÃO EM CLIMA E AMBIENTE - CLIAMB

TESE EM COTUTELA COM A
UNIVERSITÉ PAUL SABATIER- UPS- TOULOUSE-FRANÇA

Propagação dos Fluxos de Sedimentos em suspensão do Rio Amazonas- Trecho Tamshiyacu (Peru) até Óbidos(Brasil)-Variabilidade Espacial e Temporal

Elisa Natalia Armijos Cárdenas

Manaus, Amazonas
Novembro, 2015

Elisa Natalia Armijos Cárdenas

Propagação dos Fluxos de Sedimentos em suspensão do Rio Amazonas- Trecho Tamshiyacu (Peru) até Óbidos(Brasil)-Variabilidade Espacial e Temporal

Orientadores:
Naziano Pantoja Filizola Jr.
e Jean Loup Guyot.

Fonte Financiadora: Capes

Tese apresentada ao Instituto Nacional de Pesquisas da Amazônia - INPA em cotutela com a Universidade de Toulouse Paul Sabatier como requisito para a obtenção do Título de Doutora em Clima e Ambiente e em Ciências da Terra.

Manaus, Amazonas
Novembro, 2015

A729p Armijos Cárdenas,Elisa Natalia.

Propagação dos fluxos de sedimentos em suspensão do Rio Amazonas. Trecho Tamshiyacu (Peru) ate Óbidos (Brasil)-Variabilidade Espacial e Temporal./Elisa Natalia Armijos Cárdenas.
– – – Manaus: [s.n.], 2016.
177 f. : il., color.

Tese de Doutorado em cotutela INPA e UPS, Manaus, 2015
Orientadores: Naziano Pantoja Filizola Jr e
Jean Loup Guyot

Área de concentração : Clima e Ambiente.

1.Sedimentação, 2.Iteração biosfera-atmosfera, 3. Hidrologia, 4. Bacia Amazônica. I. Titulo

CDD 551.354

Sipnose:
Estudou-se a distribuição espacial e temporal dos sedimentos em suspensão no Rio Amazonas, se quantificou o fluxo sedimentar na bacia Amazônica Peruana e no Brasil na estação de Óbidos. Implantou-se uma nova metodologia para predizer modelos de concentração em base na turbidez.
Palavras chave: sedimentos em suspensão,Bacia Amazônica,turbidez, granulometria, sub-bacias Andinas, Amazônia.

Comissão Julgadora:

Revisores/ Rapporteurs:

Dr. Gustavo Henrique MERTEN	University Minnesota Duluth- Department of Civil Engenniering.
Dr.José Cândido STEVAUX	Instituto de Geociências e Ciências Exatas-Universidade Estadual Paulista Rio Claro

Miembros da banca/ Examinateurs:

Dr.Jean Michel MARTÍNEZ	Laboratoire Géosciences Environnement Toulouse Université de Toulouse Paul Sabatier.
Dr. Luiz CÂNDIDO	CLIAMB- Instituto de Pesquisas da Amazônia(INPA)-Universidade do Estado de Amazonas (UEA).

Orientadores/Directeurs:

Dr. Naziano FILIZOLA	CLIAMB- Universidade Federal do Amazonas.
Dr. Jean Loup GUYOT	Laboratoire Géosciences Environnement Toulouse Université de Toulouse Paul Sabatier.

Agradecimentos

Este estudo faz parte do projeto de pesquisa do Observatório SO-HYBAM que envolve os Países da bacia Amazônica e que com ajuda de Instituições interessadas no desenvolvimento da pesquisa tem apoiado na realização deste estudo como são, ao Serviço Nacional de Meteorologia e Hidrologia do Peru (SENAMHI), a Agencia Nacional de Águas do Brasil (ANA), o Serviço Geológico do Brasil (CPRM) e a Laborátorio de Potamologia da Amazônia (LAPA) e ao Institut de Recherche pour le Devéloppement da França (IRD).

Tenho que dar meu infinito agradecimento ao Brasil por estender as fronteiras do conhecimento e apoiar a estrangeiros como eu a realizar estudos de post-graduação. As Instituições de ensino Universidade Agraria La Molina do Peru, a Universidade Estatal do Amazonas UEA, a Universidade Paul Sabatier de Toulouse-França e ao Instituto Nacional de Pesquisas da Amazônia (INPA) onde literalmente fez com agrado minha segunda moradia. Aos professores do programa Clima e Ambiente (CLIAMB) em especial a Dra. Rita Andreoli, Dr. Antônio Manzi, Dr. Luiz Cândido e Dr. Alberto Quezada. Igualmente agradeço as secretárias Priscylla, Rita e Mme. Cathala que sempre tentam ajudar aos alunos com um sorriso.

Agradeço a meus Orientadores Dr. Naziano Filizola e a Dr.Jean Loup Guyot que me deram sua confiança para realizar este trabalho e caminharam comigo esses quatros anos. Tenho que agradecer ao Dr. Alain Crave, quem me ensino o prazer de fazer pesquisa, as largas horas de skype e de campo deram como fruto este trabalho, ao Coordenador do Observatório SO-HYBAM, Dr. Jean Michel Martínez pela ajuda e colaboração durante estes anos.

Agradeço aos co-autores dos artigos, por suas valiosas contribuições na elaboração dos artigos. Tenho que dar meus agradecimentos a Pascal Fraizy e Phillipe Vauchel por seus aportes nestes trabalho, grandes professores no campo.

Fico grata com os revisores/rapporteurs que deram importantes aportes no texto final Dr. Gustavo Merten, Dr. José Stevaux.

Um muito obrigado a meus amigos e grandes pesquisadores Jean Sebastién Moquet, Jhan Carlo Espinoza, Raúl Espinoza e Jamesito, Isa, eles traçaram meu caminho e sempre es um prazer trabalhar juntos. Aos amigos da Casita Verde que cada vez que volto para Peru fazem que seja como voltar a casa Hector, el Gato, Elmo, Margot.

Tenho que dar meu agradecimento ao equipe do IRSTEA, Jérôme Le Coz, Benoît Camene e Guillaume Damaris, que me ajudaram durante minha estadia em Lyon.

Tenho que agradecer a Manaus, uma cidade que depois que a conheces impossível de deixar lhe, aqui meus colegas de trabalho se transformaram em grandes amigos, Nilda, Eurides, Marco, Luna, Daniel, Paulo, Alice, Bosco, Menino Lindo, os meninos do LAPA, ao Capitão Zé e Baixinho.

Graças Taty e o Zé, por ser um exemplo de vida e por sua acolhida, obrigada pelas risadas e os dias de música junto Newton e Marluce com os integrantes de Eletricidade Mambembe.

Ao amigos do CLIAMB que me deram força no caminho, Cléo, Raoni, Paulo, outro Paulo, Aline, Claudia, Lore, Bruna, Stephan e a Rosy. A Sylvain, minha voz em Toulouse. Também as funcionários do LBA sempre ajudando a gente.

A Marcela, Polly, Paula minhas amigas que ficam pendentes de mim e são minhas profes de português, francês e inglês.

A o maître que desde o primeiro dia virou um grande amigo.

Agradeço a minha família, meus padres Dina e Alberto minha irmã Nadia e minha tia Luz que me apoiaram a pesar da ausência. A mi outra família que me quere tanto e que também suporto minhas ausências Merci Marie, Fernand, Michel, Pascal, Françoise, Helene, Marie e Martin. Graças pelo apoio Pierric, Doriam e Pat. A meus amigos da vida um grand merci Brigitte, Jacky, Dennis, Lyka, Françoise e Tony.

E finalmente a meu esposo, o homem que levo a parte difícil nestes anos, obrigada pela compreensão e amor Pascal Fraizy, je t'aime.

Resumo

Na bacia Amazônica, os fluxos de sedimentos em suspensão têm um papel importante na biodiversidade aquática e na riqueza das zonas inundadas, pois, os nutrientes e matéria orgânica que estão aderidos aos sedimentos são depositados nestas zonas. Os sedimentos influenciam na geomorfologia do curso do rio Amazonas ao serem depositados em zonas de menor velocidade, criando novas ilhas. O fluxo sedimentar tem a capacidade de influir na movimentação dos meandros e em certos casos até no desligamento destes, formando assim novos lagos. Estas mudanças e riquezas, têm influência direita nas populações que moram na Amazônia.

A bacia Amazônica é considerada como uma das principais fontes de sedimentos para o Oceano Atlântico em termos mundiais, porém, os Andes e as zonas sub-Andinas produzem aproximadamente o 90% desses sedimentos para a bacia Amazônica.

Entender o a distribuição espacial e temporal dos fluxos sedimentários é o objetivo deste estudo, no qual foram escolhidas quatro estações de monitoramento de água e sedimento ao longo do rio Amazonas, desde o Peru até o Brasil. Para cumprir com este objetivo, foram feitas coletas superficiais a cada 10 dias em cada estação e amostragens distribuídos na seção em diferentes épocas do ano. Perfis de turbidez e amostragem para granulometria ao longo da seção também formaram parte do monitoramento.

Na zona Andina, os fluxos de sedimentos em suspensão têm uma relação direita com os fluxos de água, no entanto, está relação se transforma em uma histereses ao se aproximar da planície, tornando-se bem marcada em Óbidos, localizada a 870 km antes da desembocadura. Atribui-se este resultado à contribuição de fluxos de água de tributários pobres em sedimentos provenientes principalmente dos Escudos Brasileiro e Guianês.

Tanto na planície peruana quanto na planície brasileira, em aproximadamente uma longitude de 3000 km, observa-se que a concentração de sedimentos em suspensão está composta de dois tipos de granulometrias bem definidos: sedimentos finos (10-20 µm) e sedimentos grosseiros de tipo areias (100-250 µm). A porcentagem de cada tipo de sedimentos presente no curso principal está em função do regime hidrológico. Picos de concentração de sedimentos finos são presenciados nas épocas de máximas chuvas (Dezembro a Março) e picos de areias em época de cheia (Maio a Julho).

Nas estações Andinas e sub-Andinas, a turbulência junto com as baixas profundidades permitem a ascensão de sedimentos grosseiros à superfície. Consequentemente,

observa-se uma relação direita entre concentração de sedimentos em suspensão na superfície com a concentração de sedimentos média da seção, o que permite o cálculo de fluxos sedimentários, sendo que, a bacia peruana contribui com 540 Mt ano^{-1}. Na planície brasileira o contexto muda, onde as profundidades atingem de 40 á 100 m, tornando quase nula a presencia de areias na superfície. Está é, por tanto, a maior incerteza ao utilizar a relação da concentração de superfície com a média da secção. Analisando a estação de Óbidos constatou-se que existe uma relação direita entre a concentração de sedimentos da superfície e a concentração média de sedimentos finos da seção. Observou-se também que, a concentração média de sedimentos grosseiros da seção têm relação direita com a vazão. Esta diferenciação dos tipos de sedimentos permite o cálculo de fluxos do rio Amazonas, concluindo que 1100 Mt ano^{-1} de sedimentos são transportados para el Oceano Atlântico na estação de Óbidos, sendo que 60% corresponde ao fluxo de sedimentos finos e 40% ao fluxo de areias. Observou-se que os sedimentos são sensíveis à variabilidade climática, em geral eventos El Niño estão relacionados com maiores quantidades de sedimentos finos e eventos La Niña incrementam a porcentagem de sedimentos grosseiros no rio Amazonas.

Utilizou-se a turbidez para obter dados de concentração por ser uma medida de alta frequência, na qual, foram feitas curvas de calibração em função do diâmetro da partícula. Observou-se que o sinal de turbidez é uma adição do sinal emitido pelas partículas presentes em uma amostra, com esta premissa utilizou-se o modelo de Rouse para separar o sinal de concentração obtido pela turbidez dos tipos de sedimentos presentes no rio Amazonas, partículas finas e areias. Deste modo conseguiu-se perfis de concentração para sedimentos finos e perfis de concentração para as areias. Observa-se que na época de enchente os perfis de concentração tem um gradiente bem marcado para os sedimentos finos, no entanto, em épocas de cheia o gradiente é governado pelas areias e os perfis de finos são verticais e constantes em toda a seção. Estes resultados indicam que, pode-se predizer perfis de concentração com base na turbidez em rios da Amazônia.

Palavras-chave: sedimentos em suspensão, Bacia Amazônica, turbidez, granulometria, sub-bacias Andinas.

Résumé

Dans le bassin amazonien, les flux de sédiments en suspension jouent un rôle important pour la biodiversité aquatique et pour la richesse des zones inondées car les nutriments et la matière organique adhérants aux sédiments sont déposés dans ces zones. Les sédiments influencent également la géomorphologie du cours de l'Amazone en se déposant aux endroits de plus faible vitesse et en créant des îles. Le flux sédimentaire influe sur le déplacement progressif des méandres et dans certains cas peut aller jusqu'à couper le méandre du fleuve créant ainsi de nouvelles lagunes. Cette dynamique sédimentaire a donc un impact direct sur la vie des populations vivant en Amazonie.

Le bassin amazonien est considéré au niveau mondial comme l'un des principaux apports de sédiments à l'Océan Atlantique, cependant approximativement 90% des sédiments du bassin proviennent des Andes et des zones sub-andines.

Comprendre la distribution spatiale et temporelle des flux sédimentaires est l'objectif de cette étude pour laquelle on a choisi quatre stations hydrométriques de suivi réparties tout au long de l'Amazone depuis sa formation au Pérou jusqu´à environ 800 km de son embouchure au Brésil. Pour atteindre cet objectif, on a mis en place pour chaque station un échantillonnage décadaire en surface et une exploration totale de leur section à différentes périodes de l'année. Des profils de turbidité et des échantillons pour la granulométrie sur toute la section faisaient également partie de ce suivi.

Dans la zone andine, les flux de sédiments en suspension sont en relation directe avec les débits liquides mais cette relation laisse peu à peu apparaître un hystérésis au fur et à mesure que l'on pénètre dans la plaine et celui-ci est alors nettement marqué à Óbidos, 870 km avant l´embouchure. On attribue cet effet d'hystérésis aux apports en eaux peu chargées de sédiments de tributaires en provenance, pour la plupart, des boucliers Brésiliens et Guyanais.

Sur une distance d'environ 3000 km , tant sur la plaine péruvienne que brésilienne, on a pu observer que le matériel en suspension se compose en fait de deux types de sédiments bien définis : des sédiments fins (10-20 µm) et des sédiments grossiers, des sables(100-250 µm). La quantité de chaque type de sédiment présent dans le cours principal du fleuve est fonction de son régime hydrologique annuel. On relève des pics de concentration en sédiments fins aux époques de plus grandes précipitations (décembre à mars) alors que ceux des sables apparraissent pendant la période de crue (mai à juillet).

Sur les stations andines et sub-andines, la turbulence de l'écoulement jointe aux faibles profondeurs permet l'ascension de sédiments grossiers vers la surface. Par conséquent, on observe une relation directe entre la concentration de sédiments en suspension de surface et la concentration moyenne dans la section, ce qui permet un calcul simple des flux sédimentaires et d'arriver à une valeur de 540 Mt an^{-1} pour qui concerne l'apport du bassin péruvien de l'Amazone. Dans la plaine brésilienne, le contexte change, les profondeurs moyennes se situent entre 40 et 100 m de telle sorte que la présence de sable en surface est quasi nulle. D'où une incertitude plus grande à vouloir utiliser une relation entre concentration de surface et concentration moyenne dans la section. Cependant, l'analyse des résultats à la station d'Óbidos montre qu'il existe encore une relation directe entre la concentration de sédiments de surface et la concentration moyenne de sédiments fins dans la section alors que la concentration moyenne de sédiments grossiers dans la section est, elle, en relation directe avec le débit liquide. En différenciant ainsi le calcul suivant ces deux types de sédiments, on arrive pour l'Amazone à une valeur de flux de 1100 Mt an^{-1} transitant par Óbidos, dont 60% correspond au flux des sédiments fins et 40% respectivement aux grossiers.

On a utilisé la turbidité car c'est une mesure à haute fréquence et pour parvenir aux valeurs de concentration à partir de celles-ci, on a dû établir différentes courbes de calibration en fonction du diamétre des particules. On a pu observer que le signal de turbidité est le résultat de l'addition des signaux émis par les particules de différents diamètres présentes dans l'échantillon et avec cette prémisse, on a utilisé le modèle de Rouse pour différencier le signal de concentration obtenu avec la turbidité. On a constaté que les granulométries en présence sont les mêmes tout au long du régime hydrologique mais que ce sont les proportions de chacune d'entre elles qui varient. Aussi a-t-on abouti à des profils de concentration pour sédiments fins et des profils pour sédiments grossiers. En montée de crue, les profils de concentration présentent un gradient bien marqué pour les sédiments fins, alors qu'en période de crue ce gradient est contrôlé par les sables et les profils de fines sont alors verticaux et constants sur toute la section. Ces résultats montrent qu'il est possible de prédire, en Amazonie, les profils de concentration à partir de la turbidité.

Mots clés: sédiments en suspension, Basin Amazonian, turbidité, granulométrie, subbasin Andean.

Abstract

The sediments flux in Amazon Basin have an important role on the aquatic biodiversity and richness in the floodplains because the nutrients and organic matter attached on suspended sediments are deposited in these zones. The suspended sediments have influence in the geomorphology of Amazon River too, because where they are deposited in zone of low turbulence new isle are create. The sediments flux have influence in the meandering movement and sometimes this movement can cause meanders to cutoff and create new lakes. These changes and richeness have influence in the Amazonian population.

The Amazon Basin is considered in global terms as one of main source of suspended sediments of Atlantic Ocean, but the Andean region and foreland provide 90% of sediments at the Amazon Basin.

The aim of this study is to understand the spatial and temporal distribution of sediments flux in the Amazon River, therefore were select four gauging station located along of Amazon Riven from Peru to Brazil. In each gauging station was make superficial samples each ten days and samples in the section in different times of hydrological period. Turbidity profiles and granulometry measuring were made too in each gauging station.

In the Andean region, it is observed a relationship between the suspended sediments concentration and discharge, however, this relationship become a hysteresis in the plain especially in the Óbidos gauging station located at 870 km before of mouth. This result can be by the contribution of influx poor in suspended sediments from Guyanese and Brazilian shields.

In 3000 km of long from Peru to Brazil plain, the suspended sediments is composed by two well defined types of suspended sediments: fine sediments (10-20 µm) and coarse sediments (100-250 µm). The percentage of each type of sediments in the main river is different during the hydrologic regime. Peak of fine sediments is observed in the same period of peak of rainfall (December to March) and peak of coarse sediments is observed in flood period (May to July).

The Andean and sub-Andean basin gauging station show the coarse sediments in surface due to great turbulence and low depths. Therefore, this gauging station show a relationship between the suspended sediments concentration in surface and average

suspended sediments concentration in section, with this relation is possible to calculate the suspended sediments flux. Hence the Peruvian basin provide 540 Mt year^{-1}. However in the Brazilian plain the context is different, the depth is from 40 to 100 m, becoming almost null the presence of coarse sediments in the surface. Therefore, cannot use the relationship between suspended sediments concentration in surface and average suspended sediments concentration in section. When the Óbidos gauging station is analysed, it found there is a relationship between suspended sediments concentration in surface and average of fine suspended sediments concentration. It is observed too, that there is the relationship between coarse suspended sediments concentration and discharge. Therefore, it is possible to calculate of suspended sediments flux using this two relationships. The Amazon River export 1100 Mt year^{-}1 of suspended sediments at Óbidos gauging station, of which 60% correspond at fine sediments flux and 40% to coarse sediments flux. It is observed that the suspended sediments are sensitivity of climate variability, generally El Niño events is associate with increase of fine suspended sediments and La Niña events increase a percentage of coarse sediments in Amazon River.

It is using the turbidity for determinate of suspended sediments concentration, we use this technique due the high frequency in acquisition of data. However for use the turbidity is necessary the previous calibration. It was observed that the turbidity signal is an addition to the signal emitted by the particles in one sample and with this assumption the Rose model was used to separate the concentration signal obtained by the turbidity of these two types of sediments present in the Amazon River, fine particles and sand. Therefore, it was obtained the concentration profiles to fine sediments and the concentration profiles to the sand. It is observed during the rising period that the fine sediments profiles show a strong gradient, however in the flood periods this gradient reduce come a constant in all section. These results show that turbidity and Rouse model can be used for prediction of suspended concentration in Amazon River.

Keywords: suspended sediments, Amazon Basin, turbidity, granulometry, sub-basin Andean.

Lista de Figuras

Lista de Tabelas

Sumário

Introdução Geral

Considera-se a teoria de *feedback* da erosão junto com os efeitos do clima, como a explicação para formação de montanhas (Pinter e Brandon, 2002). Quando as montanhas e a crosta se erodem, os sedimentos são depositados no sopé causando a subsidência desta zona. Para compensar o material perdido e manter o equilíbrio produz-se o soerguimento da cadeia montanhosa. Esta hipótese é complementada com a teoria das placas, que estabelece à Terra como um sistema dinâmico, com movimentos e interações entre placas, provocando alterações e deformações na crosta e litosfera e dando lugar as grandes cadeias montanhosas. Assim, os Andes são consequência da subducção ocasionada pela colisão de duas placas: a placa Oceânica do Pacífico com a placa Continental da América do Sul (Paleogéno 65-34 Ma). A placa Oceânica, que é mais densa, afundou sobre a continental, criando o levantamento da Cordilheira Andina. O norte Andino é produto da colisão da placa Sul-Americana e a placa do Caribe (Mioceno 23 Ma). Mora et al. (2010) indicaram que a formação do rio Amazonas com o fluxo no sentido para o Atlântico, aconteceu no final do Mioceno-Pleistoceno (11 Ma), resultado do desnudamento dos Andes e da precipitação orográfica.

A água cumpre um papel fundamental no ciclo dos sedimentos por ser um dos principais fatores que causam a denudação do solo. Também é um dos agentes mais importantes no transporte e deposição de sedimentos através dos sistemas fluviais. A nível mundial, nestas últimas décadas, observaram-se mudanças nas descargas líquidas que correspondem às modificações nas precipitações (Fig.1). Os rios da Ásia, África e Austrália têm sofrido um decréscimo de 50% nas descargas médias. Em contrapartida, rios da América do Norte (exceto o Canadá) apresentam aumento médio de 30%. Os rios da América do Sul (Amazonas, Orinoco, Magdalena) em termos de média mantêm-se em situação de estabilidade (Milliman et al., 2008). No entanto, no caso do rio Amazonas, Espinoza et al. (2009a) mostraram um aumento significativo nos valores máximos de precipitação e uma diminuição nos valores mínimos. Estas alterações influem nos fluxos de sedimentos e materiais dissolvidos, como exemplo o aumento significativo da concentração de sedimentos em suspensão depois de uma mudança abrupta de uma seca extrema (2010) para uma cheia (2011) no rio Amazonas no Peru observado por Espinoza et al. (2011).

A importância de estimar a carga de sedimentos nos rios reside em: desde o ponto de vista ambiental, na quantidade de nutrientes e contaminantes transportados pelos sistemas fluviais, até o impacto que causaria as mudanças dessas concentrações ao longo

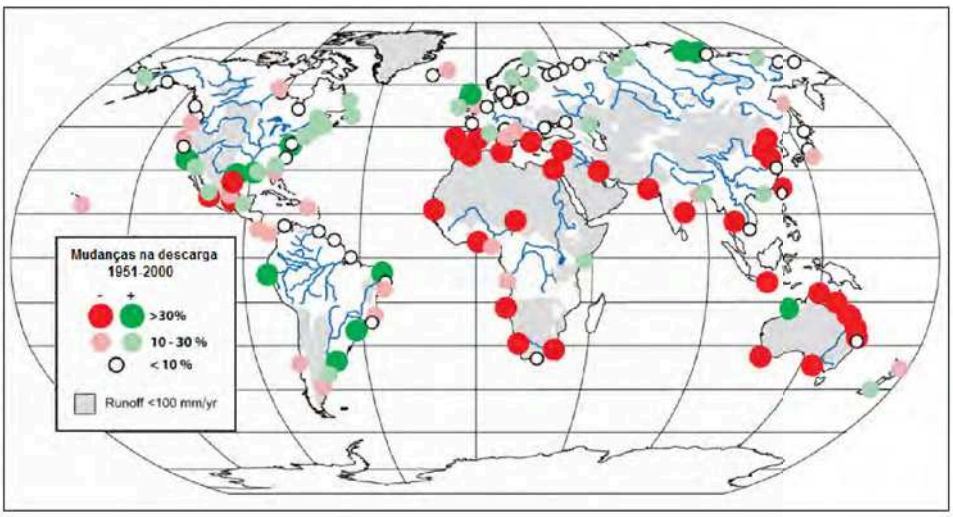

Figura 1: *Mudanças na descarga líquida por consequência das mudanças nas precipitações em escala mundial. Adaptado de Milliman et al. (2008)*

do tempo (Walling, 2005; Restrepo et al., 2006). Na planície Amazônica, os nutrientes e matéria orgânica associados aos sedimentos resultante das trocas entre o canal principal e as várzeas ou zonas de inundação tem um papel importante na biodiversidade aquática (Dunne et al., 1998; Melack e Forsberg, 2001). Do ponto de vista geomorfológico os fluxos de sedimentos modelam a paisagem, tendo em vista que sedimentos acumulados em zonas de menor velocidade geram novas ilhas. Constantine et al. (2014) indica que a movimentação e o isolamento dos meandros tem uma relação direita com os fluxos de sedimentos. Do ponto de vista energético, os projetos de implantação de novas usinas para a geração de energia hidroelétrica tem-se expandido nos últimos anos na Amazônia, pelo qual se faz necessário conhecer a taxa de sedimentação no momento do planejamento das represas. Na bacia Amazônica estão previstas a construção de 151 hidroelétricas, e a maioria encontram-se localizadas na parte andina do Peru, Colômbia, Equador e Bolívia. No Brasil os principais projetos estão focalizados nos rios Madeira, Branco, Tapajós e Xingú (Finer e Jenkins, 2012). Cabe notar que os Andes são a fonte de sedimentos da bacia Amazônica, sendo o Madeira um dos principais caminhos de transporte deste material, ademais, estas mudanças nos cursos d'água modificam também a vida aquática (Pouilly et al., 2004; McClain e Naiman, 2008).
Igualmente, a bacia Amazônica tem sido exposta a mudanças no uso da terra, especialmente com a introdução da pecuária e cultivo da soja. O desmatamento e a construção de estruturas hidráulicas geram alterações nas quantidades de fluxos líquidos e sólidos (Davidson et al., 2012).

Segundo Milliman e Farnsworth (2011), o aporte de sedimentos dos rios para os oceanos é de 19.100 Mt ano^{-1}. Aproximadamente 70% destes fluxos correspondem a contribuição das bacias do sul da Ásia e das ilhas maiores dos oceanos Pacífico e Índico (Fig.2). O fluxo de sedimentos da bacia Amazônica é considerado o maior da América e o terceiro do mundo, depois dos rios Huang He (Rio Amarelo) na China e Ganges-

Bamaputra na Índia e Bangladesh (Walling e Webb, 1988; Chakrapani, 2005). Estima-se que a carga de sedimentos que ingressa no Brasil pelo rio Madeira seja de 319 Mt ano^{-1}, valor que representa 46% do total de sedimentos em suspensão do que é produzido pelos rios Beni e Mamoré (Guyot, 1993; Leite et al., 2011). Entretanto, as bacias de piemonte do Equador e Peru aportam 47 e 413 Mt ano^{-1}, respetivamente (Armijos et al., 2013b; Guyot et al., 2007a; Armijos et al., 2013a). Na planície Amazônica Dunne et al. (1998) mostra que existe uma dinâmica de intercâmbios de sedimentos entre o rio principal e as várzeas. Aalto et al. (2003) e Santini et al. (2014) mostram que as zonas de *Antepais* de Bolivia e Perú saõ regiões de acumulo de sedimentos.

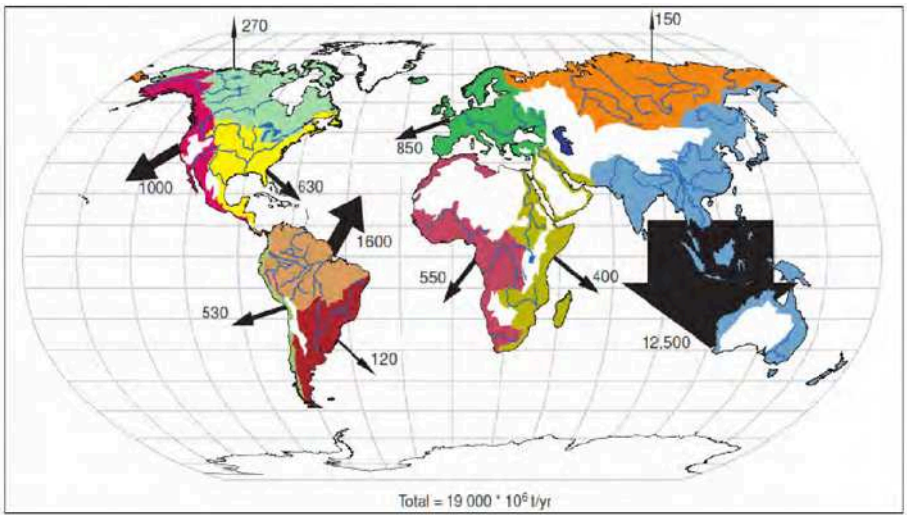

Figura 2: *Fluxos de sedimentos em suspensão para os oceanos. Adaptado de: Milliman e Farnsworth (2011)*

A estimativa do fluxo de sedimentos do rio Amazonas em Óbidos (última estação de monitoramento a 870 km antes da foz) ainda está em discussão e os valores indicados oscilam entre 500 e 1.300 Mt ano^{-1} (Gibbs, 1967a; Meade et al., 1985; Filizola, 2003; Guyot et al., 2005). As diferenças entre as estimativas devem-se principalmente aos diferentes métodos de calculo dos fluxos, os períodos de monitoramento devido às dificuldades para medir regularmente o maior rio do mundo, com 6.850 km de extensão, com profundidades que ultrapassam os 60 m e larguras do canal de 2-6 km. Por estes motivos os métodos indiretos (a través de sensores óticos,imagens de satélite) vêm ganhando força pois são técnicas que permitem obter melhor resolução espacial e temporal.

Walling et al. (2003),2005 indicam que é importante quantificar com melhor precisão a carga de sedimentos e buscar o melhoramento das técnicas de amostragem, com equipamentos e tecnologias que permitam levar em conta as propriedades do material sem mudar suas características no momento da coleta. Atualmente, por meio de sensoriamento remoto, com o uso de imagens do sensor MODIS, pode-se obter resultados de fluxos de sedimentos em suspensão na superfície da água e sua evolução no tempo (Martinez et al., 2009; Espinoza Villar et al., 2012). Igualmente, a turbidez mostra-se como uma alternativa para medir a concentração de sedimentos em suspensão, permitindo

um maior número de medidas com um equipamento mais versátil (Tessier, 2006; Restrepo e Pierini, 2012). A utilização de modelos verticais também tem sido testados para predizer o fluxo de sedimentos nos rios Solimões e Amazonas (Bouchez et al., 2011b), no entanto, tem-se encontrado dificuldade para gerar um modelo geral no espaço e no tempo. Guyot et al. (2005) mostraram que não existe uma relação direita entre vazão e concentração de sedimentos em suspensão, pelo que recomendam realizar um monitoramento contínuo para determinar o fluxo de sedimentos em suspensão.

O objetivo deste trabalho é estudar a distribuição espacial e temporal dos sedimentos em suspensão ao longo do rio Amazonas no trecho Tamshiyacu (Peru) até Óbidos (Brasil). Este trabalho propõe uma estimativa do fluxo de sedimentos na zona Andina e sub-Andina do Peru. Estuda a distribuição espacial e temporal dos sedimentos em suspensão e seu comportamento, durante o regime hidrológico nas estações andinas e da planície peruana logo depois da saída dos Andes (Capitulo 3). Apresenta uma nova estimativa de fluxos na estação de Óbidos baseado em 19 anos de monitoramento e a influência da variabilidade climática nos fluxos sedimentares na bacia Amazônica (Capítulo 4), e finalmente este estudo propõe uma metodologia para caracterizar o gradiente vertical e horizontal dos sedimentos em suspensão baseada na turbidez e no modelo de Rouse (Capítulo 5).

O estudo se apoia nos dados de estações do observatório ORE-HYBAM (www.ore-hybam.org) estabelecido no contexto de convênios bilaterais entre o IRD (*Institut de Recherche pour le Dévelopement*) da França e instituições interessadas na hidrologia e geodinâmica da Bacia Amazônica. No Brasil, as Instituições parceiras são a Universidade Federal do Amazonas (UFAM), a Agência Nacional de Águas (ANA) e a Companhia de Pesquisa de Recursos Mineiros (CPRM). Além disso, esta tese está inserida escopo do Projeto IHESA (Iniciativa de Hidrologia Espacial na Amazônia) da Rede de Hidrologia Amazônica (Projeto FINEP) do qual participam a UFAM, CPRM, ANA, IRD, INPA (Instituto de Pesquisa da Amazônia), UEA (Universidade do Estado de Amazonas), UFPA (Universidade Federal do Pará), UFRGS (Universidade Federal do Rio Grande do Sul), SIPAM (Sistema de Proteção da Amazônia), UNIR (Universidade Federal de Rondonia) e *The University of Texas at Austin*.

A tese está escrita no formato de artigos, composta por 6 Capítulos:

Capítulo 1 : Revisão Bibliográfica;

Capítulo 2 : Metodologia- Área de Estudo

Capítulo 3 : Suspended sediment dynamics in the Amazon River of Peru. Publicado no Journal South American Earth Sciences.

Capítulo 4 : New estimation of suspended sediments yields of the Amazon River and its sensitivity to climate variability. Artigo submetido para o Science.

Capítulo 5 : Measuring and modelling vertical gradients of suspended sediments in the Amazon River. Artigo submetido ao Hydrological Processes.

Capitulo 6 : Conclusões

Apendice :

- Características das sondas de turbidez.
- Determinação granulométrica em amostras dos Rios da bacia Amazônica.
- Yields of suspended sediment and dissolved solids from the Andean basins of Ecuador. Artigo publicado no Hydrological Sciences Journal durante o período de doutorado como primeira autora.
- The optical properties of river and floodplain waters in the Amazon River Basin: Implications for satellite-based measurements of suspended particulate matter. Artigo publicado Journal of Geophysical Research: Earth Surface, como colaboradora

Capítulo 1

Revisão Bibliográfica

1.1 A bacia Amazônica

A bacia Amazônica localiza-se na América do Sul entre as latitudes 5^oN (rio Cotingo no Brasil) e 20^oS (rio Parapeti na Bolívia) e as longitudes 50^oE (rio Pará no Brasil) e 80^oW (rio Chamaya no Peru). Drena uma superfície de 5.961.000 km^2 (Callède et al., 2010) que abrange os países do Brasil (62,61%), Peru (16,61%), Bolívia (11,67%), Colômbia(6,02%), Equador (2,35%), Venezuela (0,60%) e Guiana (0,1%) (Wolf et al., 1999). Estruturalmente a bacia Amazônica é formada por quatro zonas geomorfológicas (De Almeida et al., 1976; Roddaz et al., 2005): 1) ***Os Andes que incluem a zona sub-andina***, caracterizada por forte declividade e submetida a uma forte erosão; 2) ***A zona de Ante-país ou região Pré-Andina***, é a zona de transição entre os Andes e a planície, formada pela erosão recente dos Andes de idade Quaternária ou Terciária. Atualmente esta região tem áreas receptoras de sedimentos que proveem da erosão dos Andes e outras áreas que fornecem sedimentos. Inclui-se nesta zona o Arco de Fitzcarraldo, este arco constitui a linha divisória das águas entre o alto Solimões e o alto Madeira (Espurt et al., 2008), e o Arco de Iquitos, divisor das águas do Marañón e alto Solimões (Bernal e Tavera, 2002); 3) ***A planície Amazônica***, que atua como uma depressão, acumula o material sedimentar resultante da erosão dos Andes desde que foi formada no Mioceno médio e 4) ***Os escudos Guianês e Brasileiro***, localizados respectivamente ao norte e sul da bacia Amazônica, correspondem a porções do continente Sul-Americano da idade do Pré-cambriano já bastante erodidos (Fig.1.1).

1.1.1 Solos

Os solos que estão presentes na Amazônia, segundo Gardi et al. (2014) são o resultado dos processos de formação da Bacia (Fig.1.2). Na parte Andina e piemonte encontram-se *Regosols* e *Leptosols*, solos pouco alterados que recebem e exportam continuamente a matéria da cadeia Andina, caracterizados por serem rasos e armazenarem pouca água, tendem a ser utilizados para pastagens e floresta. Estes tipos de solos encontram-se também de forma pontual nos escudos Brasileiro e Guianês.

A zona sub-Andina é formada por *Cambisols*, solos com moderado grau de altera-

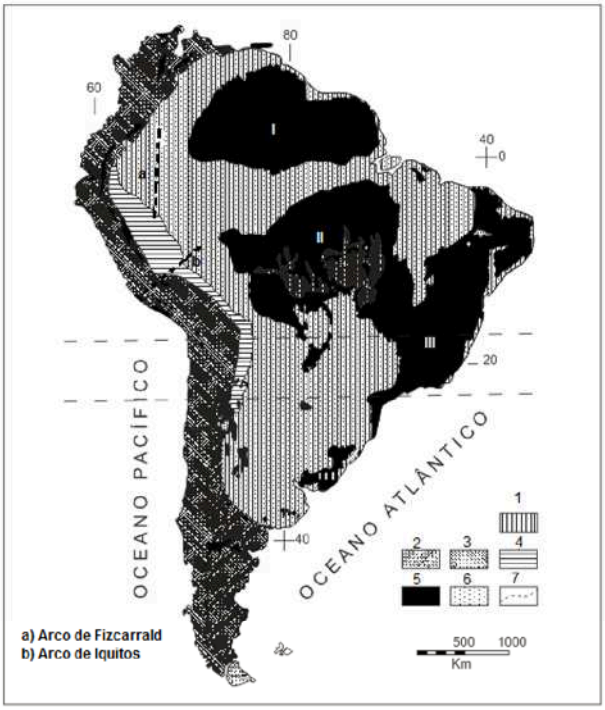

Figura 1.1: *Unidades tectônicas da América do Sul. 1-Plataforma Sul Americana. 2-Platafoma Patagônica. 3-Cadeia Andina. 4-Região Pré-Andina. 5-Ecudo Guianês(I), Escudo Brasileiro (II), Escudo Atlântico (III). 6-Coberturas sedimentares fanerozóicas e vulcano-sedimentares. 7-Limite meridional da Plataforma Sul-Americana. Adaptado de: De Almeida et al. (1976)*

ção, formados pela deposição sedimentar de material orgânico dos Andes. Muitos destes solos podem ser férteis dependendo do conteúdo de matéria orgânica e do valor de pH. A planície Amazônica e as zonas de Ante-país são formadas por *Acrisols*, caracterizados pela alteração avançada e presença de caulinita. São solos susceptíveis à estresse hídrico, encrostamento, compactação e erosão. Entre o Arco de Iquitos e o ingresso do Amazonas no gargalo inter-cratônico, encontram-se *Plinthosols* que são ricos em óxido de ferro e pobres em matéria orgânica. São diferentes de outros solos tropicais por possuírem elevadas porcentagens de caulinita. A presença de elevadas quantidades de petroplintita (petroplinita=resultado do umedecimento e secagem da plintita) pode restringir o uso destas áreas para pastagem e reflorestamento, pois requerem ações de proteção para evitar erosão e endurecimento.

A planície do Amazonas ao longo de seus grandes rios é dominada por *Fluviosols*, solos jovens, continuamente reciclados pelo aporte de novos sedimentos provenientes dos cursos d'água de seu entorno. As zonas inundadas do canal do Amazonas na parte central e oriental e as zonas de Ante-país dos rios Marañón, Ucayali, Beni e Mamoré são formadas por *Gleysols*, solos mal drenados ricos em matéria orgânica. O escudo Brasileiro, uma parte do escudo Guianês e o sul da zona de Ante-país do rio Mamoré são constituídos por *Ferrosols*, solos profundos intensamente intemperizados e formados sobre condições de clima tropical úmido, de cores vermelho e amarelo e estrutura bastante porosa. Estes solos menos suscetíveis à erosão. Devido à sua baixa capacidade de

retenção de nutrientes, estes solos têm baixa fertilidade, seu uso para o cultivo requer a adição de calcário e fertilizantes.

O Escudo Guianês, essencialmente nas regiões do alto rio Negro e alto rio Branco, é coberto por *Podzsols* e *Arenosols*, solos extremamente pobres. Os *Podzsols* têm grande quantidade de quartzo e são desprovidos em de argila (Gardi et al., 2014; Quesada et al., 2011).

Figura 1.2: *Mapa de solos Fonte: Atlas de Solos 2014 (Gardi et al., 2014)*

.

1.1.2 Natureza dos sedimentos em suspensão

A natureza dos sedimentos em suspensão que formam os rios da bacia Amazônica está ligada a fatores como o relevo, umidade, temperatura e sobretudo aos processos geológicos que têm acontecido nesta zona. Do ponto de vista da granulometria, o tamanho das partículas aumentam conforme aumenta o relevo e a sazonalidade da precipitação (Mertes e Meade, 1985). No entanto, os rios de montanha podem ter 100 vezes mais argila que os rios da Planície devido à erosão física e alteração química que ocorre nesta zona. Martinelli et al. (1993) indicaram que a quantidade de caulinita aumenta a medida que se aproxima do Oceano Atlântico, e inversamente a quantidade de esmectita diminui. Esta observação indica que a maturidade dos sedimentos aumenta na direção do Oceano que recebe mais umidade tropical.

Guyot et al. (2007b), concluíram que nos Andes (nas bacias do alto Marañón, alto Napo e alto Madeira) os sedimentos em suspensão estão compostos por ilita+ clorita em porcentagens de 46 a 63%, sendo que também encontraram valores de 20 a 30% de caulinita e esmectita devido à processo de alteração nos sedimentos do Terciário. Nos

Escudos, onde se constata uma constante alteração química e elevada umidade tropical, observa-se uma predominância de caulinita, em percentuais maiores que 90%. Na planície dos rios Napo, Pastaza, Javari, Juruá e o baixo Beni, predominaram a caulinita e a esmectita, por serem zonas de forte alteração recebendo sedimentos oriundos dos processos de constante erosão dos Andes. Na planície brasileira, observa-se uma mistura da composição dos elementos erodidos das montanhas e dos Escudos como também dos sedimentos do Terciário que são remobilizados das margens, notadamente nas áreas de várzea.

1.1.3 Climatologia

A bacia Amazônica é uma das maiores zonas de chuva e fonte de vapor d'água no mundo (Salati et al., 1978; Espinoza et al., 2009b). Apresenta contrastes climatológicos acrecidos a uma forte variabilidade espacial e temporal, produzidas pelas influências da Zona de Convergência Inter-Tropical (ZCIT), da Zona de Confluência do Atlântico Sul (ZCAS) e pela presença da barreira Andina. As regiões mais chuvosas acima dos 3.000 mm.ano^{-1} encontram-se no delta do Amazonas e no noroeste da Bacia (Colômbia, norte do Equador, nordeste do Peru e noroeste do Brasil) devido à sua exposição à ZCIT. As precipitações também são abundantes perto da posição média da ZCAS durante o verão austral desde o noroeste da bacia Amazônica até o sudeste da costa do Atlântico Sul (Carvalho et al., 2004). No sudeste da Bacia, as precipitações diminuem à 2.000 mm.ano^{-1} e na planície peruana-boliviana até o Estado de Rondônia no Brasil, as precipitações decrescem a menos de 1.500 mm.ano^{-1}. Nos Andes a 3.000 metros sobre o nível do mar, os valores de precipitação são aproximadamente 1.000 mm ano^{-1}. Em cotas menores aos 3.000 m nota-se uma variabilidade espacial com precipitações entre 500 e 3.000 mm ano^{-1}. A variabilidade espacial está relacionada com a predominância dos ventos Alísios e às exposições de barlavento e sotavento (Fig.1.3). O ciclo sazonal das precipitações na Amazônia evidencia uma oposição entre as regiões tropicais norte e sul durante o verão e inverno austral. Ao longo do inverno austral (Junho-Julho-Agosto) 50% das precipitações acontecem no norte da região e abaixo dos 20% na região sul (Peru, Bolívia e Sul do Brasil). O comportamento inverso (Espinoza et al., 2009b) é observado no verão austral (Dezembro,Janeiro e Fevereiro).

A temperatura na bacia Amazônica também é contrastante, encontrando-se valores médios de 24 a 28 °C na parte da planície. No entanto, estes valores podem diminuir a 20 °C devido às friagens que ocorrem pela penetração de massas de ar polares que vêm do sul, resfriando a zona central da Bacia. Na parte Andina a temperatura pode atingir valores de até -20 °C (Salati et al., 1978; Fisch et al., 1998).

1.1.4 Hidrologia

O rio Amazonas ou Santa Maria de la Mar Dulce, como foi denominado pelo espanhol Vicente Yáñez Pinzón no ano 1500, verte 210.000 m^{3}s^{-1} d'água para o Oceano Atlântico, o que representa cerca de 20 % do volume de água doce do mundo (Callède et al., 2010). O rio Amazonas se forma a partir da confluência dos rios Ucayali e Ma-

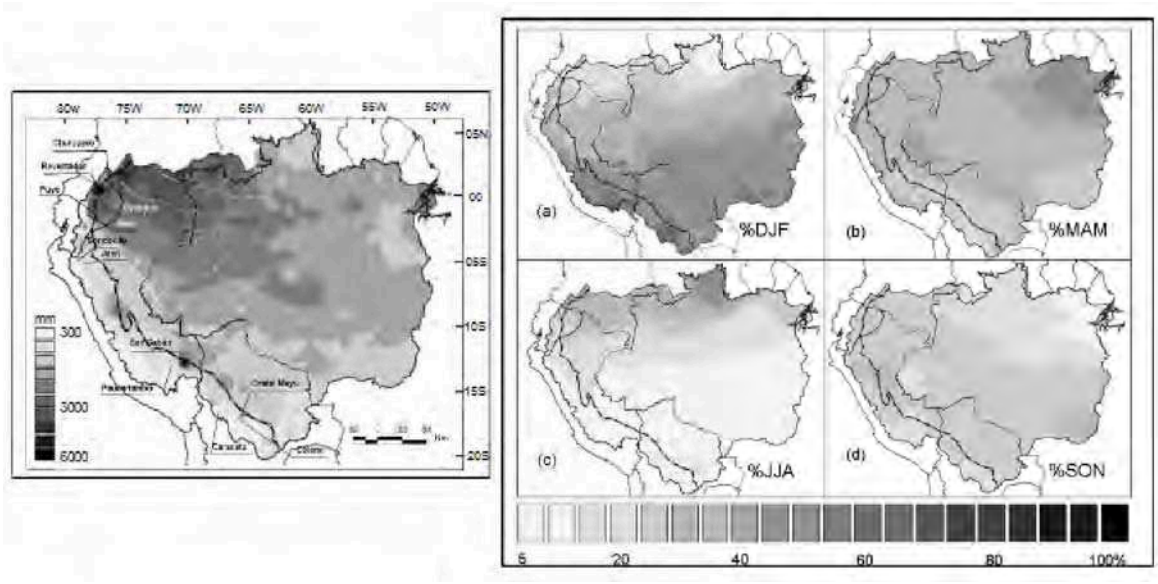

Figura 1.3: *A) Precipitação média ($mm.ano^{-1}$). B) Porcentagens de precipitação trimestral a) Dezembro-Janeiro-Fevereiro (DJF), b) Março-Abril-Maio (MAM), c) Junho-Julho-Agosto (JJA) e d) Setembro-Outubro-Novembro (SON). A região Andina acima dos 500 m é limitada com uma linha preta e branca Adaptado de: Espinoza et al. (2009b)*

.

rañón no Perú. Estes rios têm por sua vez seu nascimento nos Andes peruanos. O rio Amazonas recebe o nome de Solimões ao entrar no Brasil e só depois da confluência com o rio Negro retorna a receber o nome de Amazonas conservando-o assim até a desembocadura. O grande Amazonas percorre um trajeto de aproximadamente 6.850 km desde sua origem nos Andes peruanos até a sua desembocadura no Oceano Atlântico. Os principais afluentes do Norte são os rios Napo, Putumayo-Iça, Caqueta-Japurá e Negro. Entre os principais afluentes do sul encontram-se os rios Javari, Jutaí, Juruá, Purus, Madeira, Tapajós e Xingu (Fig.1.4).

A hidrologia da bacia Amazônica reflete a distribuição sazonal e anual da precipitação. Espinoza et al. (2009a) descreve os regimes hidrológicos da bacia Amazônica. A região que está localizada ao sul da Bacia apresenta os níveis máximos de vazão nos meses de março até maio e as mínimas de agosto até outubro [Portovelho (PVE), Fazenda Vista Alegre (FVA), Gavião (G), Lábrea (L), Altamira (ALT) e Itaituba (ITA)]. Em contraposição, na porção norte, as vazões máximas ocorrem entre junho e agosto e as mínimas de dezembro a março [Caracaraí (CAR), Serrina (SER) e Acanaui (ACA)].

A oeste, Sõ Antônio de Iça (SAI) e em Tamshiyacu (TAM) no Peru a vazão máxima é observada entre abril e maio e as mínimas nos meses de setembro a outubro. Na região central [Manacapuru (MAN), Óbidos (OBI)] as vazões máximas aparecem nos meses de maio a junho e as mínimas nos meses de outubro a novembro.

Na zona Andina do Peru observa-se uma alta frequência na variação sazonal. O período de águas altas na bacia do Marañón acontece de janeiro a março para a estação de Chazuta (CHA) e fevereiro-abril na estação de Borja (BOR), o período de estiagem

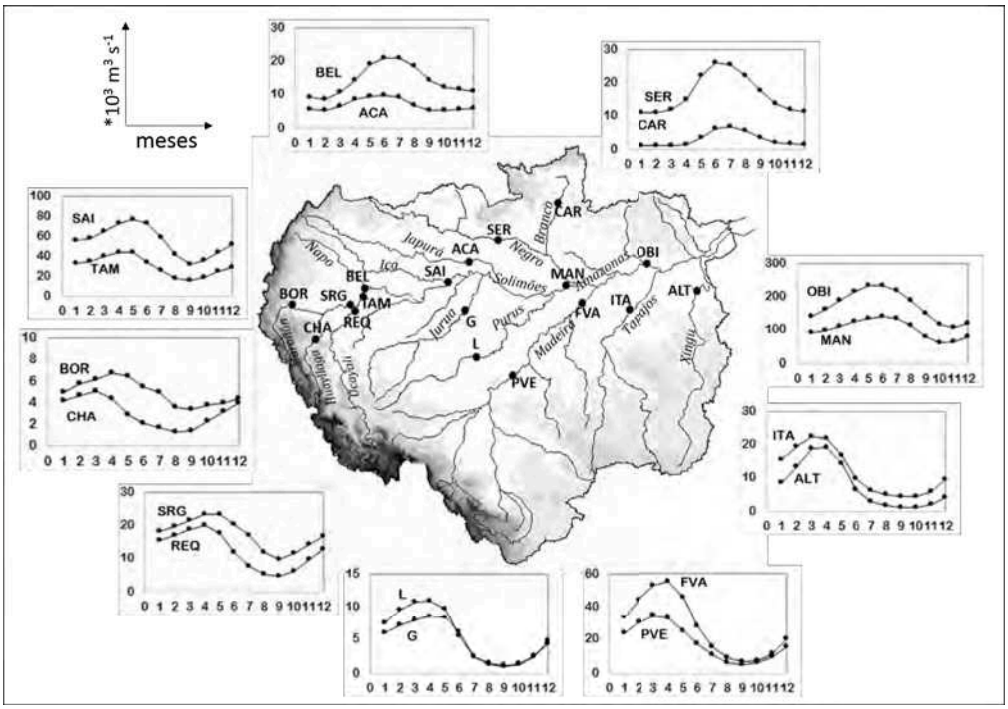

Figura 1.4: *Vazão média mensal no período 1974-2014 em ($*10^3 m^3.s^{-1}$) para as sub-bacias de:*
SAI,ACA,SER,CAR,G,L,OBI,MAN,ITA,ALT,FVA,PVE, e no período de 2000-2014 para as sub-bacias de BOR,CHA,SRG,REQ,TAM,BEL. O eixo X corresponde aos meses a partir de janeiro (1) a dezembro (12). Adaptado de: Espinoza et al. (2009a) e atualizado do (http://www.ore-hybam.org/)

ocorre entre julho-setembro para as duas estações. No baixo Marañón (SGR) e Ucayali (REQ) observam-se as máximas vazões entre abril-maio e as vazões mínimas entre agosto-setembro.

O rio Napo, proveniente do Equador mostra uma alta variabilidade hidrológica podendo-se distinguir os picos de cheia de abril a junho e estiagem de dezembro a fevereiro na estação de Bellavista (BEL).

A Tabela 1.1, apresenta os dados de vazão média (Qmédia), máxima (Qmáx) e mínima (Qmín) e vazão específica (Qespecífica) das principais estações hidrológicas da bacia Amazônica em termos de área drenada. A vazão específica indica a quantidade de água produzida pela bacia por área drenada. As estações localizadas no norte da Bacia apresentam maior vazão específica (ACA e SER) seguidas pelas estações da região andina (BOR,CHA,REQ,SRG,TAM,SAI). As estações de SAI e MAN são resultado da influência Andina, que também apresentam um elevado valor de vazão específica. As estações com vazões específicas menores encontram-se nos rios que vem do sul (ALT, PVE, FVA, ITA). Nos rios Madeira e Negro, os principais afluentes do Amazonas, observa-se um aporte da vazão de 15% e 14% respectivamente (Filizola e Guyot, 2011). As estações têm um contínuo monitoramento por parte das Instituições Nacionais de cada país: No Equador a entidade responsável é o Instituo Nacional de Meteorologia e

Hidrologia (INAMHI), no Peru o monitoramento é realizado pelo o Serviço Nacional de Meteorologia e Hidrologia (SENAMHI) e no Brasil, a Agência Nacional de Águas (ANA) junto com o Serviço Geológico do Brasil (CPRM). Estes dados encontram-se disponíveis no site web das Instituções correspondentes e no site do Observatório ORE-HYBAM (http://www.ore-hybam.org/).

Segundo, Callède et al. (2004) e Espinoza et al. (2013) a partir dos anos 1970 foram registrados em torno de 17 eventos de cheia máxima (>250.000 m^3s^{-1}) e depois de 1990 foram observados, eventos de estiagem mais severos (Fig.1.5). A corrença de eventos extremos na bacia Amazônica tem aumentado na ultima década, como por exemplo os casos das seca de 2005 e 2010 e as cheias excepcionais de 2009 e 2012. Os eventos de seca foram associados a corrença de eventos do El Niño e episódios quentes do Atlântico Norte. E os episódios frios do Atlântico Norte com eventos de La Niña geram as cheias extremas (Marengo et al., 2008, 2011, 2012; Espinoza Villar et al., 2012).

Tabela 1.1: Principais sub-bacias da bacia Amazônica. Vazão média (Q_{mdia}), vazão máxima (Q_{mx}) e vazão mínima (Q_{mm}). Período de monitoramento para as estações brasileiras 1974-2014 (http://www.ore-hybam.org/). Para as estações do Peru o período de monitoramento foi 2000-2014 (http://www.ore-hybam.org/)

Codigo	*Estação*	*Rio*	*Lat.*	*Log.*	*Area* km^2	*Qmédia* $m^3\ s^{-1}$	*Qmáx* $m^3 s^{-1}$	*Qmín* $m^3 s^{-1}$	*Qespecífico* $l\ s^{-1}\ km^{-2}$
BOR	*Borja*	*Marañón*	*-4.4702*	*-77.5483*	*114*	*5000*	*1550*	*60*	*44*
CHA	*Chazuta*	*Huallaga*	*-6.5704*	*-76.1193*	*69*	*2980*	*13200*	*220*	*43*
SRG	*San Regis*	*Marañón*	*-4.5134*	*-73.9068*	*362*	*16200*	*26870*	*5400*	*45*
TAM	*Tamshiyacu*	*Amazonas*	*-4.0034*	*-73.1161*	*726.4*	*31700*	*46700*	*16400*	*44*
ALT	*Altamira*	*Xingu*	*-3.2122*	*-54.0008*	*446203*	*7900*	*22670*	*960*	*18*
ITA	*Itaituba*	*Tapajós*	*-4.2833*	*-57.5833*	*451600*	*11700*	*24900*	*3000*	*26*
PVE	*Porto Velho*	*Madeira*	*-8.7367*	*-63.9203*	*954285*	*18800*	*38800*	*4000*	*20*
G	*Gavião*	*Juruá*	*-4.8392*	*-66.8500*	*162000*	*4700*	*9100*	*850*	*29*
L	*Lábrea*	*Purus*	*-7.2522*	*-66.1833*	*220351*	*5500*	*11200*	*900*	*25*
SAI	*Santo Antônio do Iça*	*Solimões*	*-3.0850*	*-67.9320*	*1134540*	*55700*	*78500*	*25800*	*49*
ACA	*Acanaui*	*Japurá*	*-1.8167*	*-66.6000*	*242259*	*13400*	*20700*	*5600*	*56*
SER	*Serrinha*	*Negro*	*-0.4819*	*-64.8289*	*279945*	*16700*	*28500*	*6470*	*60*
CAR	*Caracaraí*	*Branco*	*1.8214*	*-61.1236*	*124980*	*3000*	*9800*	*600*	*24*
FVA	*Fazenda Vista Alegre*	*Madeira*	*-4.8972*	*-60.0253*	*1324727*	*27800*	*55700*	*4900*	*21*
MAN	*Manacapuru*	*Solimões*	*-3.3083*	*-60.6094*	*2147736*	*104000*	*145200*	*56300*	*48*
OBI	*Óbidos*	*Amazonas*	*-1.9197*	*-55.5134*	*4680000*	*181700*	*248600*	*97500*	*39*

1.2 Sedimentos

A superfície da Terra está continuamente sendo modelada como consequência da erosão. A erosão pode ser analisada em diversas escalas de tempo em função das forças exteriores e de suas próprias características, como por exemplo: processos de erosão local de poucos segundos até processos de formação de montanhas de milhões de anos (Laguionie, 2006). A erosão fluvial é o agente mais importante na denudação e depósito dos sedimentos. Os sedimentos são definidos como fragmentos de rochas e solos desagregados pela erosão e intemperismo (Bordas et al., 2004).

O transporte de sedimentos é definido pela hidráulica fluvial e pelo gradiente da granulometria das partículas carregadas. Consequentemente, podem-se distinguir quatro formas de deslocamento das partículas (Fig.1.6): 1) *Carga do fundo*, é necessário um

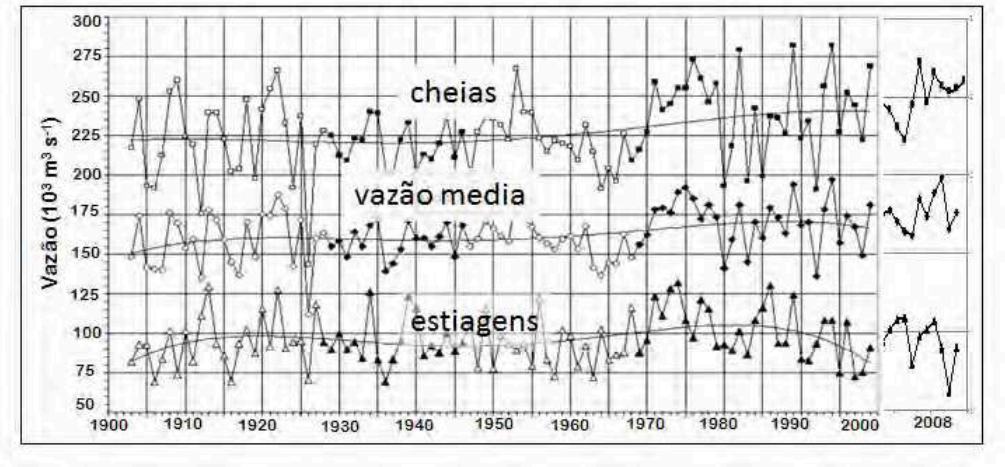

Figura 1.5: *Eventos extremos na estação de Óbidos. Adaptado de: (Callède et al., 2004) e https://sites.google.com/site/jhancarloespinoza/ .*

mínimo da energia hidráulica para movimentar as partículas do tipo cascalho e areias por rolamento ou arrastamento. O fator predominante no movimento é a força de tração, assim a maior vazão, maior força de fricção e maior capacidade de deslocamento das partículas grossas; 2) *Transporte por saltação*, parte da carga do fundo desloca-se e se mantém em suspensão por curtos períodos; 3) *Transporte em suspensão*, corresponde aos sedimentos do tipo argila, silte e areias finas que são transportados com a mesma velocidade que do fluido. A presença destes sedimentos na coluna d'água resulta do equilibro entre as forças gravitacionais e as forças turbulentas; 4) *Estado de solução* são os sais dissolvidos em forma iônica (Coynel, 2005; Laguionie, 2006).

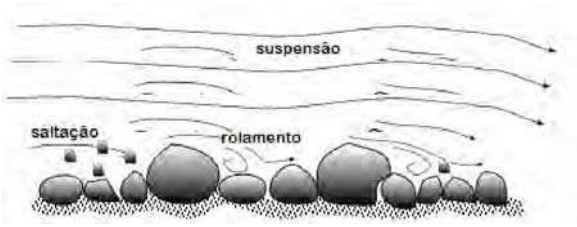

Figura 1.6: *Tipos de transporte das partículas dentro do fluxo de água Adaptado: (Niño, 2004)*

A capacidade de transporte do rio é determinada pela quantidade de material que ele pode transportar. A carga de sedimentos ou fluxo de sedimentos, consiste na quantidade de detritos transportados pelo fluxo líquido, expresso em kg.s^{-1}, t.dia^{-1}. Concentração de sedimentos, é a quantidade de massa de sedimentos que se encontra em um volume unitário de água, usualmente expressada em g.L^{-1}. Produção de sedimentos (*sediment yield*) é a quantidade de sedimentos que passa por uma seção transversal de um rio em uma unidade de tempo dividida pela área da bacia de contribuição, expressa em t.ano^{-1}km^2. Quando a corrente não possui energia suficiente para transportar toda a carga de material, o sedimento se deposita no fundo, e este processo é conhecido como sedimentação. O decréscimo na capacidade de transporte depende da redução no

potencial hidráulico da corrente devido a diminuição da declividade ou da quantidade de água (Niño, 2004).

A distribuição vertical dos sedimentos em suspensão pode ser homogênea ou pode apresentar um gradiente. De Oliveira Carvalho (1994), mostra a distribuição vertical que geralmente é encontrada nos curso d'água em função da granulometria. O maior gradiente de concentração é observado na distribuição vertical de areias, enquanto que para a distribuição de sedimentos finos, este gradiente de concentração decresce. (Fig.1.7).

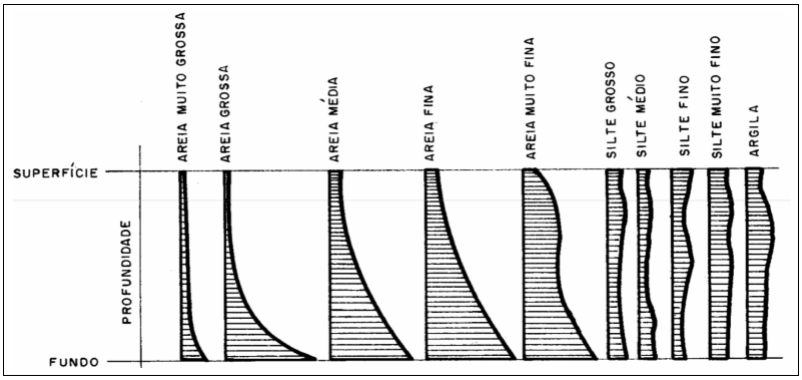

Figura 1.7: *Distribuição da concentração de material em suspensão para diferentes granulometrias Adaptado: (De Oliveira Carvalho, 1994)*

1.2.1 Amostragem de sedimentos em suspensão

Devido às condições hidráulicas e altas concentrações de sedimentos que apresentam as águas dos rios amazônicos, são necessários métodos e equipamentos robustos para realizar a coleta desse material em suspensão. A bibliografia mostra que os procedimentos mais adaptados para grandes rios são: *a*) *por integração* e *b*) *pontual* (Fig.1.8). Estes métodos têm por base, considerar que a seção transversal está bem representada com medições realizadas em diversos perfis (Nordin et al., 1983; Diplas et al., 2008). O número de perfis é definido em função de dois critérios: seja dividir a seção em segmentos de igual largura ou, seja dividir em áreas de igual descarga líquida (De Oliveira Carvalho et al., 2000). No entanto, o protocolo do observatório ORE-HYBAM recomenda considerar também a presença de fundo móvel e a existência de nuvens de sedimentos se deslocando com a corrente http://www.ore-hybam.org/index.php/eng/Tecnicas/L-echantillonnage-complet-de-la-section-avec-suivi-ADCP.

1.2.1.1 Método por integração vertical - saca compressível (AMS-8)

Este método consiste em coletar uma amostra homogênea composta de uma mistura de água e sedimento acumulada continuamente em um recipiente. O amostrador usado *in situ* se move verticalmente suspenso por um cabo fixo à embarcação, à uma velocidade de trânsito constante entre a superfície até as proximidades do leito sem tocar o fundo para evitar a suspensão do material de arrastre. No Brasil, as Instituições Nacionais utilizam o amostrador de saca compressível AMS-8, composto de um recipiente de

alumínio com leme para direcionar seu posicionamento em relação à corrente, dentro do recipiente coloca-se a saca plástica comprimida de 3.8 a 7.6 litros com um bico de admissão d'água. O princípio deste método é que a pressão hidrostática agindo numa superfície macia, perfeitamente flexível, isenta de ar internamente, cria uma pressão na entrada do bico de admissão d'água igual à pressão interna do amostrador. O ingresso da água é controlado pela abertura do bico, cujo tamanho depende da velocidade da corrente do rio (De Oliveira Carvalho et al., 2000).

1.2.1.2 Método pontual - amostrador horizontal

Este método se caracteriza por obter medições pontuais em determinadas profundidades do perfil em uma seção. No Brasil, se utiliza um amostrador horizontal de 7 litros de capacidade, fabricado pelo Programa ORE-HYBAM chamado *"Callede II"* em homenagem a seu projetista. Este amostrador está composto por um tubo de PVC, disposto na horizontal e válvulas de borracha que vedam as extremidades. O fechamento do tubo se dá pela ação de um peso metálico (mensageiro) junto a um mecanismo de fechamento que quando enviado comanda o fechamento do dispositivo na profundidade desejada. A orientação vertical e isocinética do amostrador é mantida por um leme apoiado com um peso de 50 kg de peso colocado em a parte inferior do amostrador. A isocinética do amostrador é importante para evitar distúrbios na velocidade da corrente no momento de pegar a amostra. Para cumprir com este objetivo posiciona-se o barco contra a corrente entre 50 e 100 m e depois em deriva na direção do ponto de amostragem, o amostrador se coloca em posição vertical e segue o fluxo, no momento que se encontra na posição do amostragem são fechadas as válvulas de borracha.

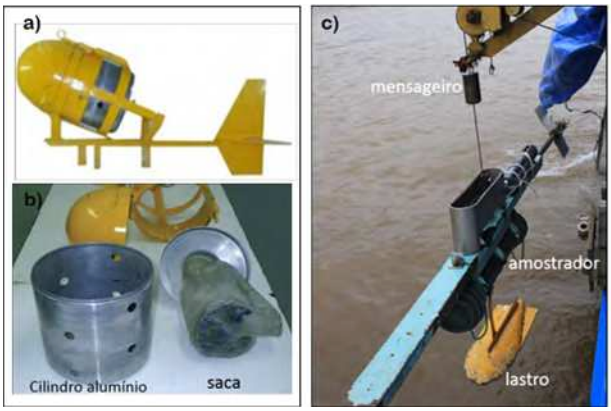

Figura 1.8: *a) amostrador AMS-8 de saca compressível, b) Componentes do amostrador AMS-8, c) amostrador pontual horizontal "CalledeII" - Programa ORE-HYBAM Fonte: (De Oliveira Carvalho, 1994)*

1.3 Técnicas Óticas

Os métodos óticos analisam a faixa de luz depois de passar por um meio de interesse. Este estudo coloca enfases nas partículas em suspensão dentro da água, estas podem ser

detectadas por difusão ou absorção da faixa de luz incidente, dependendo do sistema de medida de cada aparelho. Dentro destes métodos, temos a Granulometria e a Turbidez (Maréchal, 2000).

1.3.1 Granulometria

O tamanho da partícula pode ser considerado como a característica física mais importante no controle do transporte e da dinâmica geoquímica dos sedimentos, e como tal é incluído direta o indiretamente na maioria dos modelos em termos da velocidade de sedimentação (Phillips e Walling, 1995). A medição *in situ* é a mais adequada para determinar as características dos sedimentos sem ter que modificar o tamanho natural da partícula e seu equilíbrio com o regime turbulento da coluna d'água. Mas esse tipo de equipamento tem custo elevado e precisa de dispositivos adaptados para rios de grande porte (Gibbs, 1981). No entanto, os equipamentos de laboratório têm evoluído, permitindo a obtenção de bons resultados se comparados à distribuição dos tamanhos das partículas presentes no ambiente natural.

Neste contexto, depois dos anos 70, a granulometria à laser se apresenta como uma ótima ferramenta para medir o tamanho das partículas. A granulometria à laser utiliza o princípio da difração de luz (Wedd, 2003). A difração à laser se baseia na relação que existe entre o tamanho de uma partícula e a intensidade e o ângulo da luz espalhada. Quando a luz monocromática passa através das partículas em suspensão se cria um padrão de difração que depende do tamanho dos difusores (Fig.1.9). Para partículas grandes, a luz será espalhada com maior intensidade e com ângulo menor do que para partículas pequenas (Moore, 2012). Desse modo o granulômetro à laser mede a intensidade e tamanho do angulo de difusão de cada amostra e transforma estes dados em valores de distribuição de granulometria. A grande maioria dos equipamentos consideram que partículas maiores a 20 µm difundem a luz por difração, no entanto, quando as partículas são menores que este tamanho a luz é espalhada mais por refração, consequentemente faz-se necessário conhecer as propriedades óticas do meio de difusão. Atualmente os equipamentos dispõem de alternativas para a escolha dos índices de refração do meio *(http://www.horiba.com)*.

1.3.2 Turbidez

A turbidez é a medida da redução da transparência de uma amostra de água devido à presença de partículas coloidais e/ou material em suspensão. A turbidez pode ser medida através de Nefelômetros ou Absorvímetros. Os Nefelômetros são aparelhos que detectam a porção do feixe de luz que se dispersa pelas partículas suspensas em um ângulo específico em relação à luz incidente, este pode variar de 90°a 160°dependendo dos aparelhos. Pelo contrário, os absorvímetros medem o grau de atenuação e absorção que experimenta a luz pela presença de partículas (Lawler, 2005; Maréchal, 2000). Quando um feixe de luz passa através de uma amostra, as partículas interagem com a luz incidente absorvendo e espalhando a luz em todas as direções. A distribuição espacial da luz dispersa depende do tamanho das partículas em relação ao comprimento de

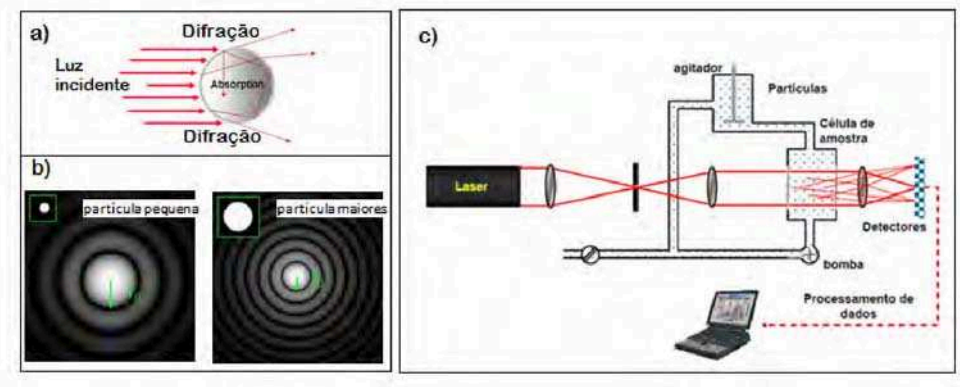

Figura 1.9: *a) Efeitos da incidência da luz em uma partícula; b) padrões de difração para partículas < 20 μm e partículas > 20 μm; c) esquema do funcionamento do granulômetro à laser. Fonte:https:// www.sympatec.com*

onda da luz incidente. Partículas muito menores do que o comprimento de onda da luz incidente, exibem uma distribuição de dispersão bastante simétrica com quantidades iguais de luz difundida, tanto para a frente quanto para trás. Quando o tamanho das partículas aumenta em relação ao comprimento de onda, a luz dispersa se espalha na frente com uma intensidade maior do que em outras direções (Fig.1.10). Além disso, as partículas menores espalham mais intensamente em curtos comprimentos de onda (azul) e têm pouco efeito sobre comprimentos de onda mais longos (vermelho). Por outro lado, as partículas maiores dispersam mais facilmente em longos comprimentos de onda do que em curtos comprimentos de onda. A forma das partículas e o índice de refração também afetam na distribuição de dispersão e intensidade da luz. A dispersão de luz intensifica-se quando a concentração de partículas aumenta. Se a concentração for superior a um certo ponto, maior aos níveis detectáveis, a luz difundida e transmitida diminuem rapidamente, marcando o limite superior de turbidez mensurável. Para diminuir este efeito deve-se reduzir o comprimento do percurso da luz através da amostra, o que reduz o número de partículas entre a fonte de luz e o detector de luz, estendendo-se assim, o limite superior da medição de turbidez (http://www.omega.com).

Anderson (2005) indica como mostrado na Tabela 1.2 as características necessárias que teria que ter um turbidímetro em função das condições naturais dos cursos d'água. A medição da turbidez fornece uma leitura da quantidade de luz dispersa e não pode ser diretamente relacionada com um equivalente gravimétrico, a menos que uma curva de calibração seja criada (Minella et al., 2008).

O uso da turbidez no contexto aqui referenciado por ser uma ferramenta que permite determinar a concentração de sedimentos em suspensão em eventos pontuais que ocorrem em curto espaço de tempo sem interferir com a dinâmica hidro-sedimentar (Restrepo e Pierini, 2012). Esta ferramenta soluciona problemas associados com a extrapolação de dados, principalmente quando se tem uma curta série de dados da relação entre a concentração de sedimentos em função da descarga líquida, ou em estações que apresentam histereses (Walling e Collins, 2000). A turbidez também pode ajudar a resolver os problemas relacionados ao custo econômico elevado à longo prazo, de coletas

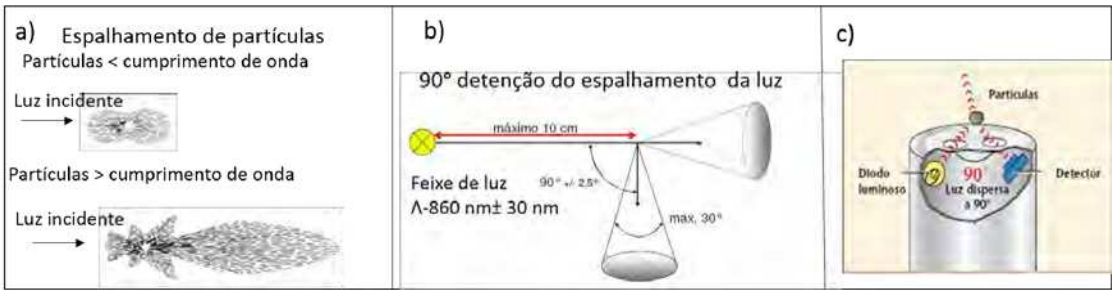

Figura 1.10: *a) Partículas de tamanho* 1/10 *do comprimento de onda com espalhamento simétrico. Partículas maiores do comprimento de onda com espalhamento para a frente; b) esquema do funcionamento do tubidímetro com um angulo de 90 graus; c) esquema do sensor de turbidez Fonte: http://www.vliz.be/wiki/Turbidity/sensors*

.

Tabela 1.2: Propriedades das águas naturais, os efeitos sobre a medição da turbidez e as características dos instrumentos para contornar o problema. IR= infravermelho. Adaptado de Anderson (2005)

Propriedades da água natural	**Efeito sobre a medida**	**Características do equipamento**
Cor partículas	Absorção do feixe de luz	Fonte de luz IR-cercano 980-900 nm,detetores múltiplos
Cor material dissolvido	Absorção no feixe de luz, se os comprimentos de onda de luz incidente sobrepor os espectros de absorção no interior da amostra	-Fonte de luz IR-cercano 980-900 nm, -detectores múltiples
Tamanho da partícula	*comprimento de onda depende:*	
Partículas grandes	espalha longos cumprimentos da onda de luz mais facilmente que as partículas pequenas	-fonte de luz: luz branca de amplo especto
Partículas pequenas	espalha comprimentos de onda curtos de luz mais eficientemente do que em comprimentos de onda longa	-fonte de luz: IR-cercano 980-900 nm
Densidade das partículas	Aumenta o espalhamento da luz na frente e atras em altas densidades	-detetores múltiplos -retroespalhamento

de amostras realizadas de forma muito frequente, permitindo assim, maior resolução na aquisição de dados. No entanto, esta técnica tem limitações ligadas à calibração e comparação de resultados entre um aparelho e outro, pois é necessária uma calibração para cada aparelho. Não existe um método definido para calibrar a concentração de sedimentos em função da turbidez. Os protocolos propostos variam de acordo com o tipo de estudo, das características dos sedimentos, da geografia do lugar (Lawler, 2005; Minella et al., 2008; Williamson e Crawford, 2011).

1.4 Hidrometria

1.4.1 Nível d'água

A determinação do regime hidrológico de um rio refere-se às variações estacionais e cíclicas do nível e volume d'água de uma determinada estação. Para realizar o monitoramento do nível do rio utiliza-se um jogo de réguas referenciadas localmente e deve-se realizar um mínimo de duas leituras diárias a cada 12 horas (padrão da OMM-Organização Mundial de Meteorologia (OMM, 1994)). As leituras das cotas dos rios são transformadas em vazão através do uso da relação cota (vs) vazão, conhecida como curva chave. A curva chave obtém-se das medições conjuntas do nível d'água e vazão em diferentes períodos, onde se busca cobrir todo o período/ciclo hidrológico.

Em um canal estável a relação entre nível do rio e vazão é unívoca e são necessárias poucas medidas para estabelecer a curva chave. No entanto, existem diversas condições de canal que não permitem estabelecer uma curva unívoca, como para os casos de: canais com leitos de areia, mudanças no leito do rio com vegetação aquática, rios com baixa declividade, rios com barragens naturais à jusante ou importantes zonas de inundação (como é o caso dos rios tropicais), rios onde formam-se capas de gelo, e rios onde ocorrem mudanças nos fluxos (Fig.1.11.)

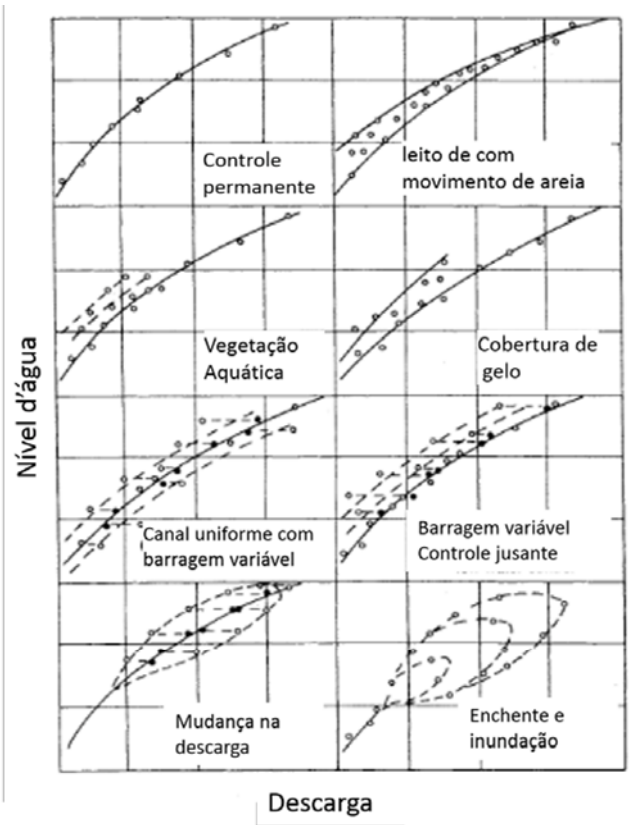

Figura 1.11: *curvas chaves em função das diferentes condições hidráulicas Fonte: (Herschy, 1995)*

.

A avaliação das curvas chaves na Amazônia é um trabalho que vem sendo realizado

desde os anos de 1980 (Guimaraes e Jaccon, 1983; Jaccon e Guimaraes, 1985; Jaccon e Cudo, 1987) e continua sendo realizado pelo observatório ORE-HYBAM em conjunto com as Instituições Nacionais do Peru e Brasil. Observa-se que para as estações no Peru e no alto Solimões a relação é unívoca, ou seja, para um valor de nível d'água corresponderá um único valor de vazão independente da época do ano. No entanto, as estações localizadas nos rios Madeira, Solimões e no próprio Amazonas apresentam uma relação não univoca entre a vazão e o nível d'água. Este efeito deve-se principalmente a influência do barramento natural[1] à jusante da seção, em períodos de enchente (Jaccon e Cudo, 1989). Já no rio Amazonas, este efeito é devido à influência da maré, às baixas declividades e às grandes zonas de inundação (Dubreuil et al., 1970; Callède et al., 2001). Em consequência não se pode aplicar uma curva chave, e a melhor solução é utilizar a fórmula de Manning-Stricler (Equação 1.1)

$$Q = \frac{AR^{2/3}S^{1/2}}{n} \tag{1.1}$$

Onde: Q= descarga (m^3 s^{-1}); A= área da seção transversal (m^2); R= raio hidráulico (m); S= gradiente da linha d'água (m/m); n= coeficiente de rugosidade. O gradiente diário da linha d'água é calculado entre uma estação à amontante e outra à jusante da estação de estudo (Vauchel, 2011).

1.4.2 Medição de vazão

A vazão é o volume de água que flui através de uma seção transversal em uma determina unidade de tempo. A vazão expressa-se em (m^3/s; l/s; l/h). As primeiras medições de vazão nos rios amazônicos do Brasil foram feitas com molinete hidrométrico, equipamento que permite medir a velocidade pontual da água em diferentes profundidades em vários perfis verticais distribuídos ao longo da seção transversal de medição. A vazão era calculada pela integração da velocidade e a área da seção. As duas técnicas mais utilizadas para medir a vazão com molinete hidrométrico em grandes rios, na Amazônia são:

1. Método de Medição de Grandes Rios (Oltman, 1964; Jaccon e Cudo, 1984; OMM, 1994)

2. Método do Barco ancorado (Chevallier, 1993; OMM, 1994)

A primeira técnica consiste em determinar a velocidade de um perfil em dois pontos (20 e 80%) ou mais (20 40, 60 e 80%) da profundidade total. A trajetória do barco é monitorada desde a margem com ajuda de três estações topográficas fixas que corrigem a direção por posicionamento triangular. A segunda técnica consiste em colocar o barco ancorado em diferentes pontos da seção e medir a velocidade a dois pontos (20 e 80%) ou 3 pontos (20 40 e 80%) da profundidade total. Estes métodos têm a desvantagem de que para sua realização, precisa-se de um ou dois dias de trabalho para medir larguras

[1] a barragem natural é o impedimento da curso natural de um tributário devido a cheia do rio principal

maiores a 2 km, tempo no qual o nível da água pode mudar aumentando as incertezas na medição de vazão (Gomes e Santos, 1999). Outra desvantagem no método do barco ancorado é o aumento do grau de risco quando ultrapassa-se os 2 m s^{-1} de velocidade em profundidades maiores que 30 m.

1.4.2.1 Medição de vazão com ADCP

No Brasil desde 1994 implementou-se na Amazônia a técnica acústica para medir a vazão através de um correntômetro acústico denominado ADCP (*Acustic Doppler Current Profiler*), técnica experimentada por Guyot et al. (1995),Guimarães et al. (1997) e Filizola et al. (1999, 2009). Atualmente, este equipamento faz parte da rotina de medições das instituições nacionais (ANA e CPRM). O ADCP é um equipamento cujo principio de funcionamento está baseado no efeito *Doppler*. Mede as componentes de velocidade da água em diferentes camadas da coluna d'água e, calcula em tempo real a vazão em função da posição com referência ao fundo (Fig.1.12). O ADCP emite uma onda acústica por cada um dos quatro transdutores de cerâmica que ele possui. Este sinal é refletido pelas partículas em suspensão que encontram-se na corrente de água, as quais se supõem terem a mesma velocidade que a corrente (Instruments, 1996; Le Coz et al., 2008). A velocidade radial é calculada pela diferença de frequências, uma emitida pelo aparelho e a outra de retorno apôs reflexão pelas partículas. A descarga é calculada a partir da integração dos valores de velocidade de cada célula de área predeterminada na qual se divide a seção durante a medição. Uma medição de vazão é validada, depois de ter sido realizado um mínimo de dois trajetos completos de ida e volta ao longo da seção transversal do rio, e calculado um erro de desvio padrão menor que 4.5% (Oberg, 2002).

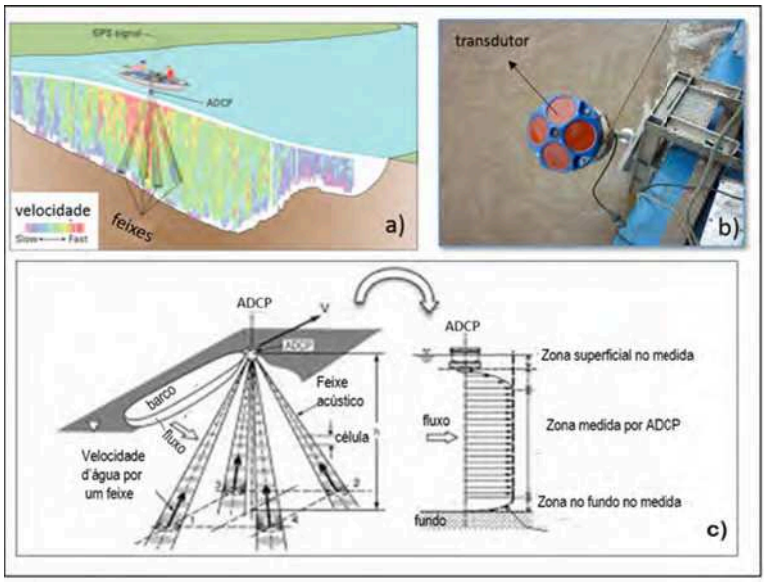

Figura 1.12: *a) Esquema de medição com ADCP (Gotvald e Oberg, 2009), b) Montagem do ADCP no rio Amazonas Fonte: Observatório ORE-HYBAM, c) Representação dos feixes acústicos e zonas de medição com o ADCP. Adaptado de: http:// www.wmo.int*

.

Embora a utilização de ADCP tenha sido um avanço nas medições de vazão, sobre tudo na Amazônia, exitem problemas e limitações: *i*) O ADCP não realiza uma medida pontual de velocidade, o valor da velocidade é o resultado da média das velocidades projetadas por 3 dos 4 feixes. Este resultado é válido se as velocidades forem homogêneas. *ii*) A configuração dos feixes (ângulo de 20°) faz com que a superfície de medida se incremente com a profundidade, o que significa que à grandes profundidades também haverão grandes zonas de medida, por exemplo em um profundidade de 20 m a superfície de medida no fundo é de 100 m^2. Deve-se considerar que existe uma superposição de áreas a cada segundo de medida ja que o barco esta em movimento. *iii*) Outra limitação corresponde às zonas que não são medidas pelo ADCP, uma destas zonas são as células do fundo, o que limita o cálculo da velocidade de cisalhamento. O valor desta zona é obtido por regressão de um perfil de velocidades em uma extensão de 6% da profundidade total ao fundo.

1.5 Perfil de velocidade e concentração de sedimentos em suspensão

O transporte de sedimentos no curso de água depende das características: do fluido (velocidade e viscosidade), do escoamento (declividade e profundidade) e propriedades dos sedimentos (granulometria, densidade e composição). O esforço tangencial (força/área), resultado da interação entre as camadas do fluido e estas com as paredes do leito, se conhece como tensão de corte ou cisalhamento. Segundo a lei de Reynolds, no fluido permanente, uniforme e bidimensional (planos x-horizontal, z-vertical), a expressão de tensão de cisalhamento em toda a coluna d'água é o resultado de dois componentes: *i*) um esforço de corte turbulento e, *ii*) um esforço de corte laminar (Equação 1.2). A suspensão das partículas é causada pelo cisalhamento turbulento e o movimento da matéria no fundo se deve ao cisalhamento laminar ou turbulento. Na camada laminar a tensão de corte é originada pela existência de um gradiente de velocidade e pela viscosidade do fluido. A camada turbulenta é caracterizada por vórtices onde o cisalhamento laminar é nulo. Entre estas duas camadas existe uma zona de transição onde ocorre a combinação das duas forças (Laguionie, 2006). Nas proximidades do fundo, a camada gerada puramente por forças viscosas em escoamento laminar é conhecida como camada limite, mas se o escoamento for turbulento a camada laminar, é na verdade, uma subcamada da camada limite(Fig.1.13).

$$\underbrace{\tau_{(z)} = -\rho_w * (u')_{(z)} * w'_{(z)}}_{\text{Cisalhamento turbulento}} \quad + \quad \underbrace{\mu * \frac{\delta_u}{\delta z}}_{\text{Cisalhamento laminar}} \tag{1.2}$$

onde:
$\tau_{(z)}$= força de cisalhamento no nível z,
ρ_w= massa por unidade de volume d'água ($kg.m^{-3}$),
u' = componente de velocidade horizontal instantânea no nível z,
$w'_{(z)}$= componente de velocidade vertical instantânea no nível z,

μ= viscosidade dinâmica do fluido, $\mu = \nu * \rho_w$,
ν= viscosidade cinemática

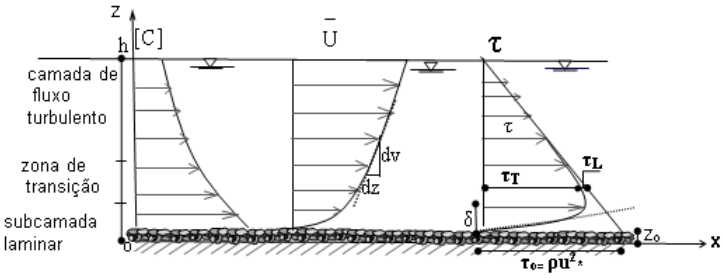

Figura 1.13: *Representação gráfica de um perfil de concentração [C], velocidade média (U) e esforço de fricção (τ) , z= eixo vertical, z_o= camada de atrito, δ_v/δ_z= gradiente de velocidade em direção do fluxo, τ_L= esforço de cisalhamento laminar, τ_T= esforço de cisalhamento turbulento, τ_o=esforço de corte no fundo e u^*= velocidade de corte*

.

1.5.1 Camada laminar

Na camada laminar ou viscosa, o fluido exerce uma tensão de cisalhamento ligada a um gradiente de velocidade próximo à parede dado por:

$$\tau_v = \frac{\delta_u}{\delta z} = \tau_o = (1 - \frac{z}{h}) \tag{1.3}$$

se z<< h :

$$\tau_v = \tau_o = \frac{\delta_u}{\delta z}$$

No fundo a tensão de cisalhamento (τ_o) é expressa também em termos de velocidade de corte (μ^* em ms^{-1}) onde ρ_w é a massa volumétrica d'água (kg.m^{-3}) (Equação 1.4). Esta velocidade de corte não é uma velocidade mensurável, mas é um modelo que permite expressar a cortante de cisalhamento ou força tangencial em unidades diferentes.

$$\tau_o = \rho_w(\mu^*)^2 \tag{1.4}$$

1.5.2 Camada turbulenta

Na camada turbulenta fora da camada laminar, Reynolds definiu a tensão de cisalhamento em função ρ_w,u',w'. Prandtl (1925) propôs relacionar u' e w' a um gradiente de velocidade (δ_u/δ_z). Ele caracterizou a turbulência através de um modelo de comprimento de mistura (ℓ), a qual supõe-se idêntica nas duas direções do escoamento. Ou seja, considera-se que as flutuações turbulentas da velocidade instantânea horizontal (u') têm a mesma magnitude que as flutuações da velocidade vertical (w') (Equação 1.5).

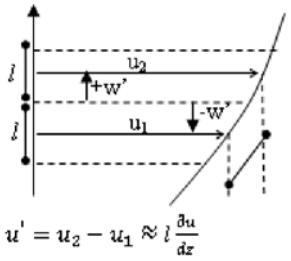

$$u' \approx \ell \frac{\delta_u}{\delta_z} \qquad w' \approx \ell \frac{\delta_u}{\delta_z} \tag{1.5}$$
$$\tau_t = \rho_w l^2 (u^*)^2$$

Schlichting (1955) propôs a hipótese de que o comprimento da zona de mistura é proporcional à distância (z) nas proximidades do leito. Dessa forma, $\ell = kz$, onde κ é a constante de von Kármán= 0.40 para águas claras (Marcarenhas et al., 2003).

$$\tau = \rho_w \kappa^2 \left(\frac{\delta_u}{\delta_z} \right)^2 \tag{1.6}$$

teremos que

$$\left(\frac{\delta_u}{\delta_z} \right)^2 = \sqrt{\tau / \rho_w}$$

Utilizando a aproximação de Boussinesq, que considera a tensão tangencial constante, temos:

$$\tau_t = \rho_w \nu \frac{\delta_u}{\delta_z} \tag{1.7}$$
$$\nu = \ell^2 \frac{\delta_u}{\delta_z}$$

Se a relação se aplica fora da camada laminar, mas muito perto onde τ varia em relação a z, para τ_o, teremos:

$$\frac{\delta_u}{\delta_z} = \frac{u^*}{\kappa z}, \quad ou\ seja \qquad \frac{u}{u^*} = \frac{1}{\kappa} \ln \left(\frac{u^* z}{\nu} \right) \tag{1.8}$$

Integrando a expressão anterior, tem-se a lei da Parede uo Lei de Prandtl-Karman :

$$\frac{u}{u^*} = \frac{1}{\kappa} \ln \left(\frac{z}{z_o} \right); \tag{1.9}$$

onde z_o é a distancia em que u=0, conhecida como comprimento de rugosidade do escoamento. A Equação 1.9 também pode ser expressa em termos dos coeficientes:

$$a = \frac{u^*}{\kappa} \qquad b = -u^* \left(\frac{1}{\kappa} \ln z_o \right) \tag{1.10}$$

O coeficiente a pode ser determinado através de um ajuste logarítmico do perfil de velocidade média que pode ser medido na lâmina d'água, o que permite calcular a velocidade de cisalhamento.

1.5.3 Repartição da concentração de sedimentos na coluna de água- Perfil de Rouse

O precursor na análise e modelagem da distribuição dos sedimentos em suspensão foi Hunter Rouse (1937), através do uso de modelo físico que descreve a distribuição vertical da concentração de sedimentos em suspensão a partir de um nível de referência perto do leito. Esta fórmula considera a concentração de sedimentos em suspensão em um estado estável para uma determinada profundidade, ou seja, admite que existe um equilíbrio entre a sedimentação das partículas em suspensão e a re-suspensão devido à difusão turbulenta (Equação 1.11 e Fig.1.14). Se o coeficiente de Rouse (W) é alto, significa que existe um incremento na concentração de sedimentos em suspensão na profundidade, mas se o coeficiente for baixo significa que a concentração de sedimentos é quase constante com a profundidade (Bouchez et al., 2011b).

$$\frac{C_{(z)}}{C_{ref}} = \left(\frac{H - z}{z} . \frac{z_{ref}}{H - z_{ref}} \right)^{W} \tag{1.11}$$

Onde: $C_{(z)}$ é a concentração de sedimentos em suspensão no nível z; C_{ref} é a concentração de sedimentos em suspensão de referência na profundidade próximo ao leito, z é a profundidade próximo ao leito, z_{ref} é a profundidade desejada com referência ao fundo, H profundidade total, W número de Rouse, definido por $\frac{ws}{\kappa . u^*}$ onde ws é velocidade de sedimentação, κ é a constante de Von Kármán (0.41) e u^* é a velocidade de cisalhamento. Pelo fato de ser um modelo físico, o modelo de Rouse tem sido utilizado

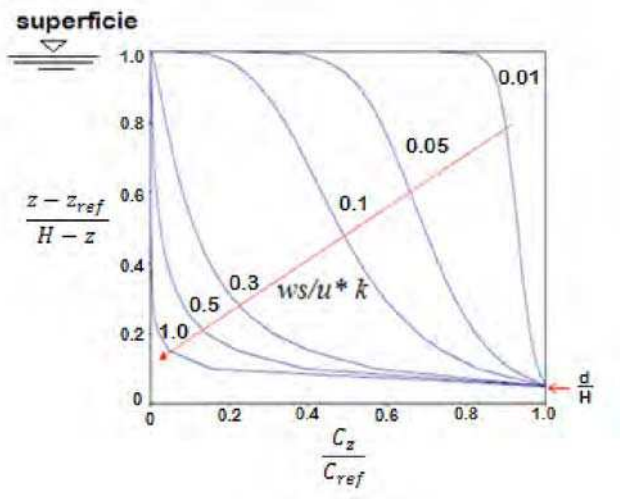

Figura 1.14: *Esquema dos diferentes tipos de Perfil de Rouse em função do Número de Rouse Adaptado: (ASCE, 1977)*

em vários estudos para caracterizar perfis verticais de concentração de sedimentos em suspensão. Na Amazônia, Vanoni (1979) mostrou a aplicação do perfil de Rouse em função da granulometria. Bouchez et al. (2011b) um estudo realizado nos principais cursos d'água da Amazônia (Madeira, Solimões, Amazonas) indicaram que não existe um perfil

de Rouse único característico para uma só secção, e que os parâmetros de Rouse têm variação no espaço e no tempo. E para o qual são necessários maiores estudos para entender os processos de distribuição vertical.

1.5.4 Velocidade de sedimentação

A velocidade de sedimentação é um parâmetro importante na modelagem do transporte do material em suspensão. Este parâmetro depende tanto da forma quanto do tamanho da partícula. A velocidade de sedimentação de uma partícula pode ser calculada a partir do equilíbrio entre as forças de gravidade e as forças de resistência, sendo que a determinação do coeficiente de resistência ainda está em estudo (Camenen, 2007). Stokes (1851) mostrou que o coeficiente de resistência é inversamente proporcional ao número de Reynolds (R_*). O número de Reynolds é definido como a relação entre as forças de inercia e as forças de viscosidade presentes no escoamento. Se R_* é baixo (< 1). R_*=$\omega_s\ d/\nu$ onde ω_s=velocidade de sedimentação; d=diâmetro da partícula e ν=viscosidade cinemática. Se $R_* > 10^5$, o coeficiente é constante. Camenen (2007) indicou uma fórmula semi-empírica (Equação 1.12) que toma em conta as características da partícula.Esta equação considera 3 coeficientes para os dois comportamentos assintóticos do coeficiente de resistência. Os três coeficientes da equação foram ajustados para diferentes tipos de partículas em quanto a forma e tamanho e densidade. Utiliza-se o coeficiente A para um alto número de Reynolds e o coeficiente B para um baixo número de Reynolds e o exponente m para vincular estes dois comportamentos. A (Tabela 1.3), indica para varios tipos de material os valores dos coeficientes A, B e m, e também os valores de csf e P que corresponde a forma e redondez da partícula respectivamente.

$$\omega_s = \frac{\nu}{\delta} R_* = \frac{\nu}{\delta}\left[\sqrt{\frac{1}{4}\left(\frac{A}{B}\right)^{\frac{2}{m}} + \left(\frac{4}{3}\frac{d_*^3}{B}\right)^{\frac{1}{m}}} - \frac{1}{2}\left(\frac{A}{B}\right)^{\frac{1}{m}}\right] \tag{1.12}$$

onde

$$d_* = \left(\frac{(s-1)g}{den\nu^2}\right)^{\frac{1}{3}} d$$

Tabela 1.3: Valores dos coeficientes A,B e m da equação de Camenen (2007), csf e P correspondem aos fatores da forma das partículas, cfs= forma plana e P= forma aredondada

Material	csf	P	A	B	m
Spherical particles	1	6	24	0.39	1.92
Smooth cobbles	0.7	5	24.5	0.62	1.71
Natural sand	0.7	3.5	24.6	0.96	1.53
Crushed sand	0.7	2	24.7	1.36	1.36
Long cylinders	0.4	5	36	1.51	1.4
Silt, cohesive particle	0.4	2	38	3.55	1.12
Flocs	0.6	1	26.8	2.11	1.19

Droppo (2004) indicou que para águas naturais a fórmula de Stokes (Equação 1.13) pode ser uma boa alternativa para determinar a velocidade de sedimentação. Na Amazô-

nia brasileira Bouchez et al. (2011b) e Vanoni (1979) utilizaram também a fórmula de Stokes para seus estudos.

$$w_s = \frac{g}{18}.\frac{(\rho_s - \rho_w)}{\rho_w}.\frac{\phi^2}{\nu} \tag{1.13}$$

onde: w_s: velocidade de sedimentação (cm s^{-1}); g:aceleração da gravidade = 9.81 (m s^{-2}); ρ_s: densidade da partícula = 2650 (kg m^3); ρ_w: densidade do fluido = 997 (kg m^3); ϕ: diâmetro da partícula (μm); ν: viscosidade cinemática do fluído= $8.54* 10^{-7}$ (m^2 s^{-1}).

Le Roux (2005) sugeriu fazer correções da densidade e viscosidade da água em função da sua temperatura. Medidas com a técnica do ADCP indicam que a temperatura média no Solimões/Amazonas é de 27°C nessa condição as equações de ajuste da densidade e viscosidade do fluído são as seguintes:

$$\rho_w = -5*10^{-10}.^oC^4+8*10^{-8}.^oC^3-9*10^{-6}.^oC^2+7*10^{-5}.^oC+0.9995; para(26 <^o C < 40) \tag{1.14}$$

$$\mu = 4 * 10^{-6}.^oC^2 - 4 * 10^{-4}.^oC + 0.0164; para(20 <^o C < 30) \tag{1.15}$$

μ= viscosidade dinâmica da água ν=viscosidade cinemática = $\mu/$ ρ_w=densidade da água

Capítulo 2

Materiais e Métodos

A metodologia deste trabalho baseou-se em amostragens pontuais que complementaram a base de dados já constituída e, que serve para determinar os fluxos de sedimentos nas estações de Tamshiyacu no Peru e de Óbidos no Brasil. Além das coletas este trabalho coloca em evidencia a utilização de métodos indiretos, como a turbidez, para determinar a concentração de sedimentos em suspensão. Escolheu-se a turbidez, face ao fato de a sonda medição ser de alta frequência quanto à adquisição de dados, o que permite caracterizar melhor a distribuição espacial e temporal dos sedimentos em suspensão na seção.

A (Fig.2.1) esquematiza a metodologia seguida neste trabalho, onde pode-se destacar três etapas: *i*) a primeira etapa que corresponde as amostragens. Este trabalho se apoia em coletas de amostras, medições de turbidez e granulometria nas estações escolhidas (no apêndice mostra-se como realizar a calibração da turbidez e o processo para determinar a granulometria); *ii*) a segunda etapa corresponde a analises de dados coletados nas medições de campo e no laboratório, onde se fez a separação de sedimentos finos $[C_f]$ e areias $[C_c]$. Esta distinção foi feita para poder identificar as diferenças entre a distribuição vertical e horizontal destes dois tipos de sedimentos durante o período hidrológico. Igualmente, foi feito no laboratório a calibração da turbidez também em função da granulometria. foram traçadas curvas de calibração para sedimentos finos e areias. Também é mostrado o processo para utilizar a turbidez e determinar a concentração de sedimentos baseada na granulometria. Este método utiliza o Modelo de Rouse para separar o sinal dos sedimentos finos das areias; *iii*) os resultados correspondem a quantificação dos fluxos sedimentários no rio Amazonas, na saída do Peru e na estação de Óbidos a 870 km antes da desembocadura.

Tem-se ressaltar que uma grade parte do tempo durante o doutorado foi dedicado a coleta, testes no campo para consolidar a base de dados, além dos testes no laboratório. Como o projeto faz parte do Observatório ORE-Hybam foi dedicado um tempo no monitoramento regular das estações que formam parte do programa, com capacitação aos observadores e estudantes.

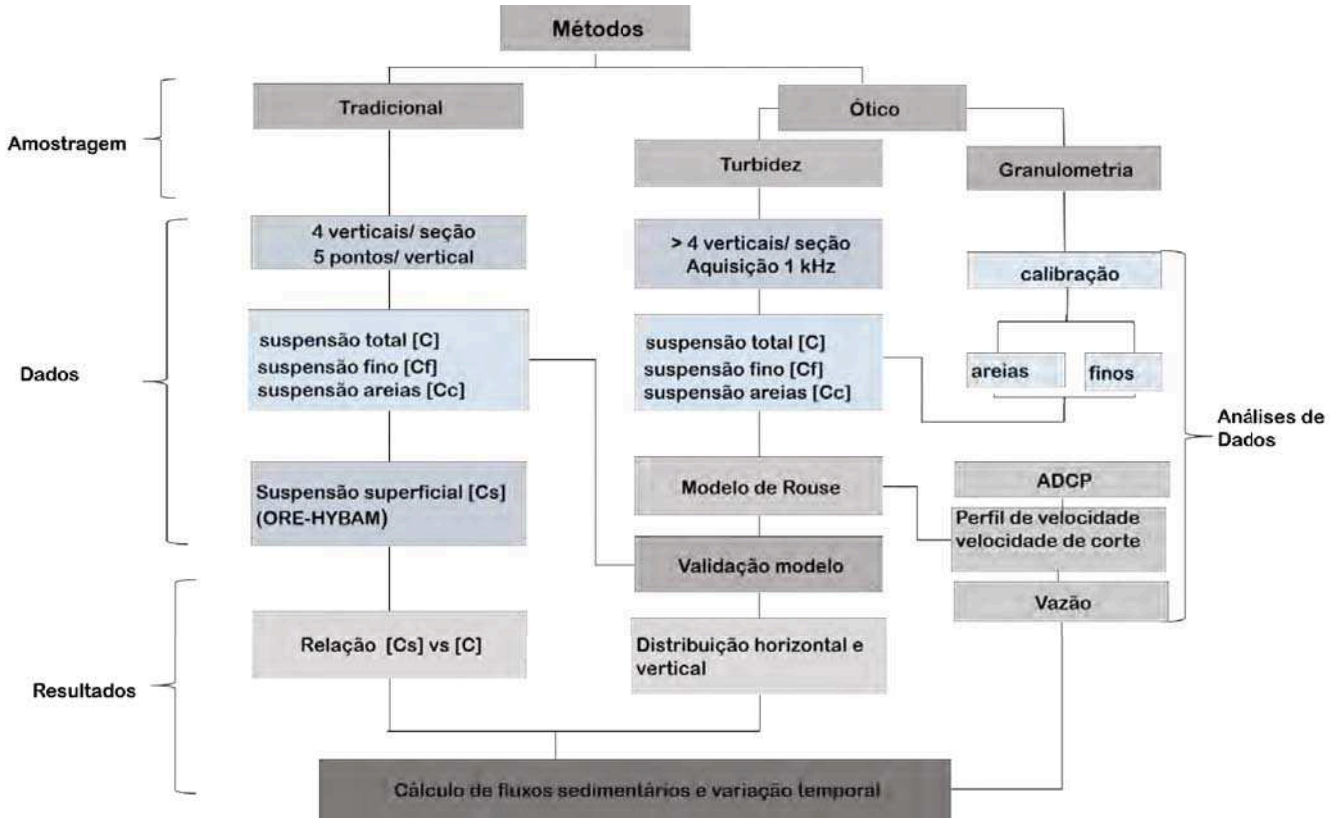

Figura 2.1: *Esquema da metodolgia*

2.1 Área de Estudo

Para determinar as características hidrológicas e sedimentares, faz-se necessário utilizar uma rede de estações de monitoramento que permita o acompanhamento em longo prazo das fontes de água e sedimentos. No Brasil, o monitoramento hidrométrico sistemático em escala nacional iniciou em 1967, com o DNAEE (Departamento Nacional de Águas e Energia Elétrica) que depois (1996-1997) passou a chamar-se ANEEL (Agência Nacional de Energia Elétrica). Atualmente o monitoramento é feito pela ANA (Agência Nacional de Águas) através do Serviço Geológico do Brasil (CPRM). No Peru, o SENAMHI (Servicio Nacional de Meteorologia e Hidrologia) iniciou o monitoramento do nível do rio em estações da Amazônia em 1984, e a medição de vazão iniciou-se em 2001 com a colaboração do Programa ORE-HYBAM.

No presente estudo face aos objetivos que se destina, escolheu-se 14 estações, sendo que 7 estão localizadas ao Peru e 7 no Brasil, estas estações foram escolhidas primeiro por su localização estratégica, e segundo porque são estações com continuo monitoramento (Fig.2.2,Tabela 2.1).

No Peru o período de estudo foi a partir 2001 até 2010 e no Brasil o período de estudo é 1995-2013, consequência dos diferentes períodos de coleta.

No Peru o objetivo foi implantar um sistema de amostragem que permita calcu-

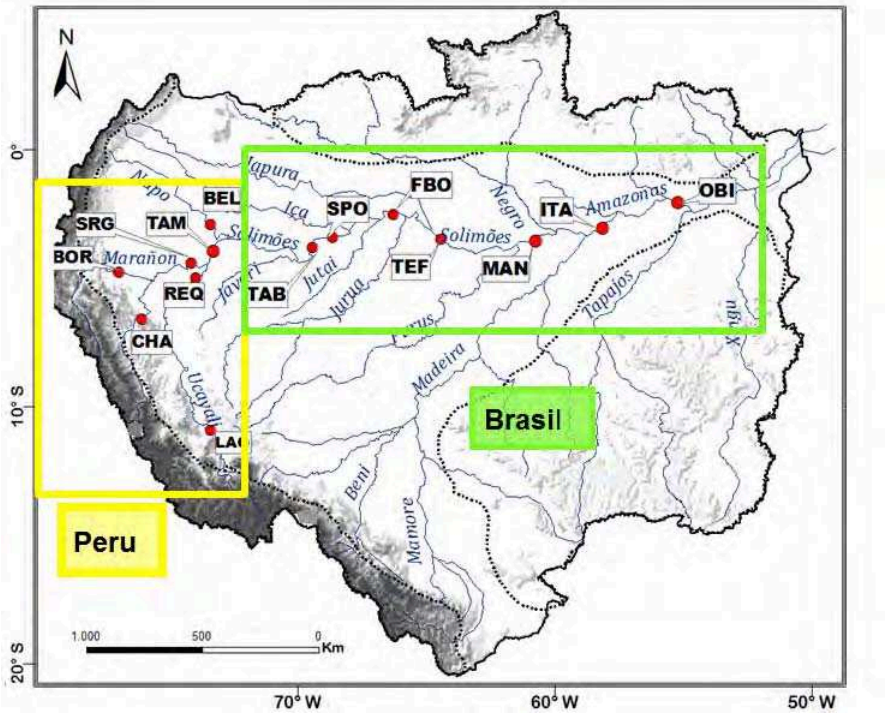

Figura 2.2: *Estações de estudo: Peru: BOR= Borja, CHA=Chazuta, LAG=Lagarto, SRG= San Regis, REQ= Requena,TAM= Tamshiyacu, BEL= Bellavita, TAB= Tabatinga, SPO= São Paulo de Olivença, FBO= Fonte Boa, TEF= Tefé, MAN= Manacapuru, ITA= Itacoatiara e OBI=Óbidos*

lar o balance sedimentar na bacia amazônica do Peru, já no Brasil onde o sistema de amostragem já faz parte do monitoramento regular, os objetivos foram realizar analises granulométricos, analisar a concentração de material em suspensão em função da granulometria, realizar um balanço sedimentário na planície amazônica Brasileira, Incorporar a utilização de um sensor ótico para determinar concentração de sedimentos em suspensão e aplicar o Modelo de Rouse para determinar o gradiente vertical de concentração, todas estas atividades permitiram cumprir com os objetivos propostos neste estudo. Por tal motivo que o trabalho está dividido em artigos:

No primeiro artigo é apresentado o estudo enfocando-se só no Peru, onde são calculados os fluxos líquidos e sólidos, considerando 3 estações Sub-Andinas localizadas sobre rio Marañón (BOR), Huallaga (CHZ), Ucayali (LAG) e na planície peruana consideramos 4 estações também sobre os rios Maraón (SRG), Ucayali (REQ), Amazonas (TAM) e Napo (BEL).

No segundo artigo enfoca-se na estação de Óbidos localizada a 870 km antes da desembocadura e é considerada como estação que monitora a maior vazão do mundo. Neste estudo determinou-se os fluxos de sedimentos em suspensão.

No terceiro artigo são consideradas 4 estações de planície desde Peru ate Brasil:Tamshiyacu (TAM), Manacapuru (MAN), Itacoatiara (ITA) e Óbidos (OBI). A estação de Tamshiyacu (TAM), localiza-se na planície peruana, e recebe os aportes de água

Tabela 2.1: Lista das estações monitoradas, dados de localização,medição de vazão das estações de estudo e período de dados de vazão

Código	Estação	Rio	LAT ° S	LON ° W	AREA Km2	Vazão (m3 s-1)	Período
BOR	Borja	Marañón	4.4704	77.5482	114,280	5,000	2004-2010
CHA	Chazuta	Huallaga	6.5704	76.1193	68,720	2,980	2004-2010
LAG	Lagarto	Ucayali	10.6081	73.8709	190,810	6,540	2009-2010
REQ	Requena	Ucayali	4.9027	73.6721	346,600	11,400	2004-2010
SRG	San Regis	Marañón	4.5100	73.9500	361,880	16,170	2004-2010
TAM	Tamshiyacu	Amazonas	4.0033	73.1600	719,640	28,000	2001-2010
BEL	Bellavista	Napo	3.4800	73.0800	100,030	6,600	2004-2010
TAB	Tabatinga	Amazonas	4.2347	69.9447	890,000	37,900	1990-2014
SPO	Saõ Paulo de Olivença	Solimões	3.5167	69.0167	940,000	47,600	1974-2014
FBO	Fonte Boa	Solimões	2.4914	66.0617	1,159,000	57,000	1978-2014
TFE	Tefé	Solimões	3.7667	64.9500	1,500,000	84,600	1996-2010
MAN	Manacapuru	Solimões	3.3083	60.6094	2,147,730	104,000	1963-2014
ITA	Itacotiara	Amazonas	4.0333	58.4833	435,000	150,300	1978-2014
OBI	Óbidos	Amazonas	1.9187	55.5134	4,680,000	181,700	1968-2014

e sedimento dos Andes peruanos e equatorianos. A estação de Manacapuru (MAN), localizada amontante da foz do rio Negro, recebe os aportes líquidos e sólidos do alto Solimões que proveem dos Andes peruanos, equatorianos e colombianos bem como os da planície. Itacoatiara (ITA), estação localizada depois da confluência do rio Madeira com o rio Amazonas, recebe os aportes ricos em sedimentos do rio Madeira que proveem dos Andes bolivianos e peruanos em como aqueles do rio Solimões, além dos fluxos pobres em sedimentos que veem do escudo Guianês como são os do rio Negro. Foram consideradas unicamente as 4 estações porque o objetivo de este terceiro artigo é mostrar a metologia para o cálculo de concentrações utilizando turbidez e o modelo de Rouse. No entanto, tem-se previso um próximo estudo comiserando os dados de turbidez coletados durante o período de doutorado nas estações do Alto Solimões: Tabatinga (TAB), Saõ Paulo de Olivença (SPO), Fonte Boa (FBO) e Tefé (TEF).

2.2 Dados

Neste estudo durante o período 2011-2014 fizeram-se medições de vazão líquida, coletas para determinação de vazão sólida, perfis de turbidez e coletas para realizar análise de granulometria. O resumo dos dados utilizado são descritos na Tabela 2.2.

Tabela 2.2: Quantidade de dados utilizados neste estudo

Tipo de Dado	Quantidade
coletas de material em suspensão(vazão sólida)	1480 amostras
medidas de turbidez	329 perfies
medidas de granulometria	352 análises
aforos líquidos	160 medições

2.3 Coleta de dados

2.3.1 Nível d'água e Medição de vazão

O nível d'água encontra-se a cargo das Intuições Nacionais dO Peru e Brasil. Em cada estação são feitas duas leituras por dia. O valor diário corresponde à media das duas leituras, cujo calculo é feito através do programa HYDRACCESS (http://www.ore-hybam.org/index.php/por/Software).

A medição de vazão é feita com o Acustic Doppler Current Profiler (ADCP). Campanhas de medição de vazão e manutenção das réguas dos níveis d'água são planejadas a cada três meses para as estações de Tamshiyacu e Óbidos. São de responsabilidade das respetivas instituições encarregadas, sendo, no Peru o SENAMHI junto com ORE-HYBAM, e no Brasil a ANA através da CPRM do Pará. As estações de Manacapuru e Itacoatiara pertencem ao projeto de Eventos Extremos no Estado do Amazonas comandado pela CPRM do Amazonas. Nestas estações as medições de vazão são realizadas cada mês.

Jaccon e Cudo (1987, 1989); Meade et al. (1991), indicam que as estações da planície amazônica mostram uma curva não univoca na relação nível d'água e vazão. Este comportamento deve-se ao fato de que, em certos períodos, pode-se observar a inversão do escoamento devido à baixa inclinação e aos barramentos naturais criados pelo rio principal, que impedem a saída dos afluentes. Neste caso, Vauchel (2011) propõe utilizar a fórmula de Mannin-Stricker (Equação 1) para o cálculo de vazões diárias.Os valores do coeficiente n encontrados estão entre 0.028 e 0.056, valores semelhantes aos obtidos por Strasser et al. (2005).

2.3.2 Perfil de velocidade média

O perfil logarítmico de velocidades está caracterizado por dois coeficientes, a e b, detalhado no Capitulo I, Equação 1.10. Determina-se o perfil de velocidade média com o objeto de calcular o coeficiente a que é diretamente ligado a velocidade de cisalhamento, velocidade requerida para determinar o coeficiente do modelo de Rouse. Para determinar os coeficientes, utiliza-se os dados de velocidade instantânea obtidas das medidas do ADCP. No entanto, a velocidade instantânea, mostra oscilações na direção vertical que dificulta o traçado do perfil logarítmico. Portanto, utiliza-se uma média entre vários perfis. Têm-se dois critérios a serem avaliados: variação temporal e variação espacial. Foi colocado como referência o fundo antes da analise de dados de velocidade (Fig.2.3).

Na superfície e no fundo da seção são zonas que o ADCP não consegue medir. pelo que utilizou-se a função "*inpaint nans*"deselvovida por John D'Ericcoque permite interpolar as velocidades nestas zonas sim dados. Os dados do ADCP foram exportados e analisados no Matlab através do código VMT (Velocity Mapping Toolbox) disponibilizado pela USGS (Serviço Geológico dos Estados Unidos) criado inicialmente por Dan Pearson (Univer. of Hull, UK) e Jon Czuba (USGS Washington, WSC). O programa encontra-se disponível no sitio da USGS: https://hydroacoustics.usgs.gov/movingboat/VMT/VMT.shtml. Uma vez lidos os dados no matlab, aplica-se a função "*inpaint nans*".

Depois pode-se proceder à determinação do perfil de velocidades.

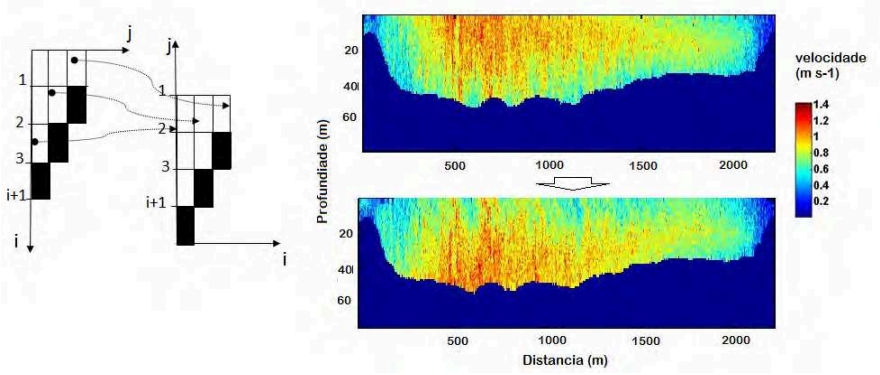

Figura 2.3: *Esquema da troca de referência com respeito ao fundo*

2.3.2.1 Variação temporal

Este método permite conhecer quanto tempo é necessário para ter um valor estável dos coeficientes que descrevem o perfil logarítmico. Realizou-se dois casos: medição em ponto fixo e outro no barco na deriva, considerando que mesmo que seria melhor realizar medições em ponto fixo as dificuldades e o risco de segurança não lho permitem por isso que as coletas são realizadas com barco a deriva. (Fig.2.4a,b). O teste foi feito para: 1 segundo, 1, 3, 5 e 7 minutos. Observa-se que o perfil toma uma forma logarítmica no minuto 1 quando o barco está em ponto fixo e aos 3 minutos quando o barco está a deriva. Decidiu-se que o tempo mínimo de adquisição dos dados para fazer a média é de 3 minutos.

2.3.2.2 Variação espacial

Neste caso, na vertical de escolhida para coleta, considera-se uma zona de influencia que servirá para realizar a média da velocidade. A zona de influência é determinada a partir da adição de perfis verticais da velocidade até obter-se um perfil logarítmico. O teste indica que depois de 20 perfis obteve-se um traçado logarítmico (Fig.2.4c).

2.3.2.3 Cálculo de incertezas do coeficiente a do perfil logarítmico de velocidades

A incerteza do coeficiente a provêm principalmente do armazenamento de vários perfis de velocidade até encontrar a estabilidade do coeficiente. Outra fonte de incerteza é o traçado da regressão para determinar um perfil logarítmico, e a incerteza que provêm do fato de não se realizar medições com barco em ponto fixo. Para determinar as incertezas de flutuações utilizou-se 40 perfis das diferentes campanhas realizadas entre 2011 até 2013, considerou-se as flutuações como uma distribuição retangular, e no caso do traçado da regressão utilizou-se o intervalo de confiança de 95%. Para o cálculo de incertezas de comparação entre os métodos de barco fixo e a deriva, fizeram-se 3

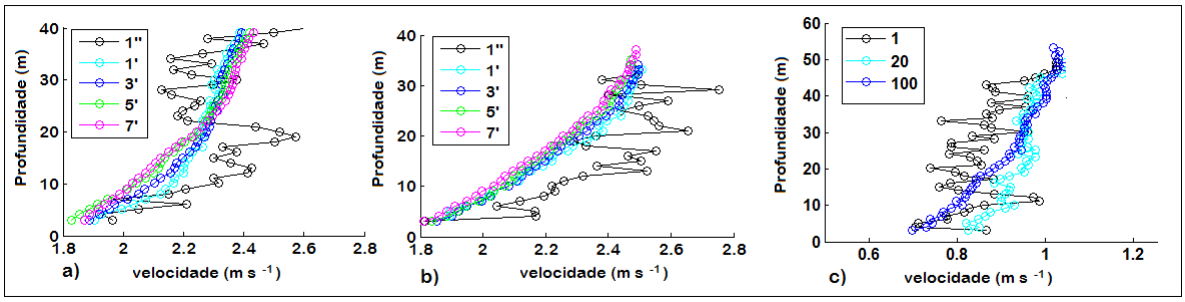

Figura 2.4: *Perfil logarítmico de velocidade,Vertical 2 estação de Óbidos em 09/06/2013 variação temporal a) barco em ponto fixo; b) barco a deriva e c) Estação Itacoatiara em 10/12/2012-variação espacial*

campanhas pontuais, realizadas em dezembro de 2011, maio de 2012 e junho de 2013. O resumo de incertezas se detalha na (Fig.2.5). O acumulo destas incertezas tem como resultado um 32%.

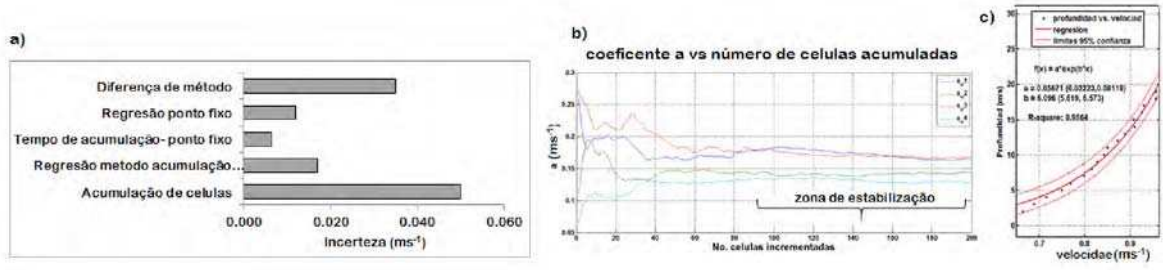

Figura 2.5: *a) Cálculo de incerteza do coeficiente a,b) Flutuação do coeficiente a nas 4 diferentes verticais distanciadas en referencia na margem esquerda da estação de Óbidos 18-12-2011, (av1= 590 m, av2= 1130 m, av3= 1670 m e av4 = 2200 m distancia da margem esquerda), c) tração da regressão, Óbidos vertical 4 de 18-12-2011*

2.3.3 Amostragem de água e sedimentos em suspensão

No Peru, as medições de vazão são acompanhadas por coletas para determinação de concentração de sedimentos em suspensão da seção. No Brasil são organizados campos pontuais para as amostragens, tentando abranger o regime hidrológico. A metodologia de amostragem deste trabalho está baseada no método de amostragem instituído pelo Observatório ORE-HYBAM a partir de 1995 (Guyot et al., 1999; Filizola e Guyot, 2004).

Devido às diferenças de grandeza e logísticas entre as estações peruanas e brasileiras, existe uma modificação do volume d'água coletado durante as campanhas, no entanto, a metologia de amostragem e filtração é a mesma. O volume d'água coletado é de 500 ml no Peru e 7 L no Brasil (Fig.2.6). O procedimento para determinar a concentração de sedimentos em suspensão é o seguinte:

1. *separação de finos e areias*, a amostra coletada passa por uma peneira de 63 µm do tamanho da malha para a separação de material grosseiro. As areias são recuperadas em um filtro de 45 µm de porosidade para logo ser levado à estufa.
2. *material fino*, a amostra restante que passou pela peneira é homogenizada para separar 1000 ml dos quais 300 ml são filtrados através de um filtro de 45 µm de porosidade. No Peru é filtrada toda amostra que foi coletada.
3. *secagem*, os filtros são secados por 60 minutos a 105 °C no Brasil no laboratório da UFAM-LAPA (Laboratório de Potamologia da Amazônia) e no Peru no Laboratório da UNALM (Universidad Agraria La Molina).
4. *determinação da concentração*, por diferença de pesos e dividindo pelo volume, calcula-se a concentração de sedimentos tanto de finos como de grosseiros para cada ponto amostrado.

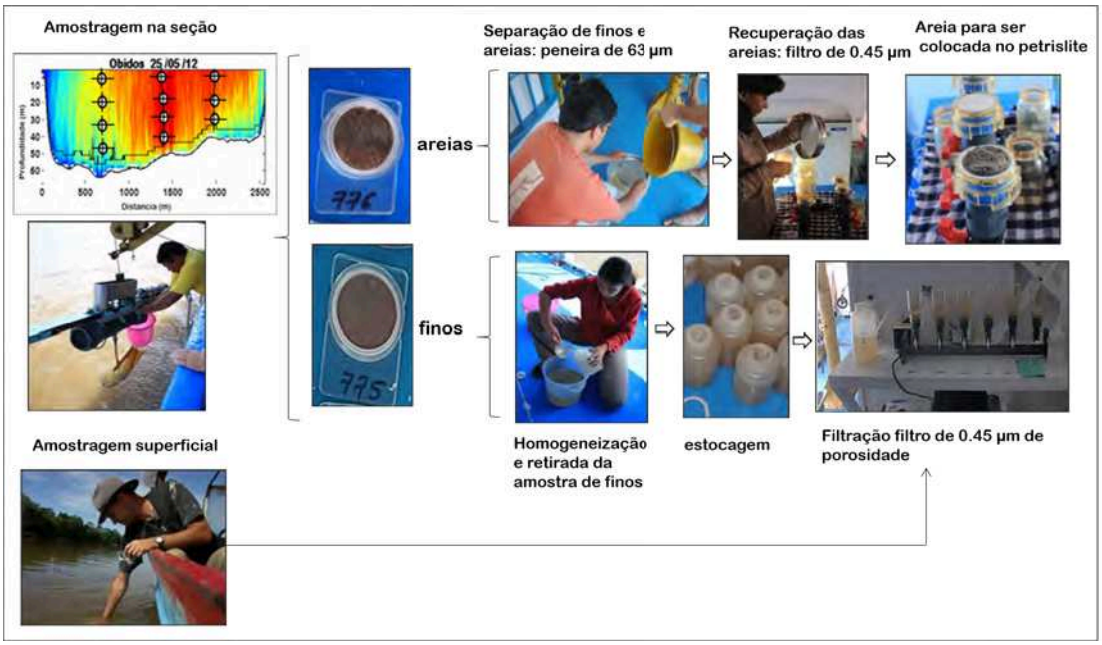

Figura 2.6: *esquematização do processo de coleta e filtração em campo e amostragem superficial a cada dez dias*

As estações escolhidas, com exceção de Itacoatiara, fazem parte do Observatório ORE-HYBAM que realiza o monitoramento das seções, assim como o seguimento da evolução dos sedimentos no tempo, através de coletadas de 500 ml de amostra a cada dez dias, retiradas do meio do rio em uma profundidade de 20 cm da superfície.

2.3.4 Medição de turbidez

Antes de ser utilizada a sonda no campo, fez-se testes no laboratório para saber sobre a influência da luz e a linearidade do sensor, realizando assim a calibração da mesma.

2.3.4.1 Testes de turbidez

A totalidade do trabalho aqui proposto foi feito com uma sonda YSI V2 6600, nefelômetro infravermelho de alta definição com resolução de 0.1 NTU, precisão de ± 2% de leitura ou 0.3 NTU e longitude de onda de 860 nm (ISSO 7027). O primeiro teste consistiu em determinar a influência da luz exterior no aparelho. Para esta incógnita, fizeram-se medições em ambientes externos e em laboratório, utilizando uma proteção no dispositivo de medida. O segundo teste foi para determinar a linearidade do sinal, para isso utilizou-se leite por ser uma solução homogênea. No anexo A encontra-se bem descrito o procedimento e resultados destes testes, que formaram parte do trabalho de mestrado (Grillot, 2011).

2.3.4.2 Calibração da Turbidez

A medida da turbidez é sensível ao tamanho da partícula, e esta sensibilidade diminui quando o tamanho da partícula aumenta (Baker e Lavelle, 1984; Pavanelli e Bigi, 2005). A metodologia empregada consiste em medir a Turbidez específica (Ts) que é a sensibilidade da medida da turbidez para uma concentração de material em suspensão de granulometria estabelecida (Campbell e Spinrad, 1987).

$$Ts = \frac{Turbidez}{[C] * \phi} \tag{2.1}$$

Para a calibração, foi elaborado um sistema que consta de um cilindro plástico transparente de 20 cm de diâmetro, 40 cm de altura e 2 L de volume, colocado sobre um agitador magnético para manter a homogenização da mistura água sedimento. A calibração consiste em variar as concentrações conhecidas de sedimentos de uma determinada granulometria e medir a respectiva turbidez. O sedimento tipo areia corresponde ao leito das estações estudadas, que foram previamente secado e separado por peneiramento, e, para granulometrias finas (silte e argila) utilizou-se a própria água do rio separando o sedimento grosseiro, e por diluição obteve-se a curva de calibração. A concentração foi obtida por filtração através de um filtro de 0.45 µm. A granulometria de todos os pontos de calibração é determinada com o granulômetro à laser (Fig. 2.7).

2.3.4.3 Propriedade de decomposição do sinal ótico

No caso do Solimões/Amazonas exite a presença de dois tipos de granulometrias predominantes, partículas finas de diâmetro de 10-20 µm e areias entre 100-180 µm. Para determinar se o sinal da turbidez é o resultado do sinal de cada grupo de partículas presentes em uma amostra, fez-se o seguinte teste: Em uma quantidade conhecida de material fino (12 µm) agregou-se, progressivamente concentrações conhecidas de areias (278 µm). As curvas indicam uma inclinação similar, o que mostra que efetivamente o sinal ótico consegue detectar separadamente uma mistura de material fino e areias. Este resultado permite utilizar a granulometria e as curvas de calibração conhecidas para dissociar o sinal de turbidez (Fig.2.8).

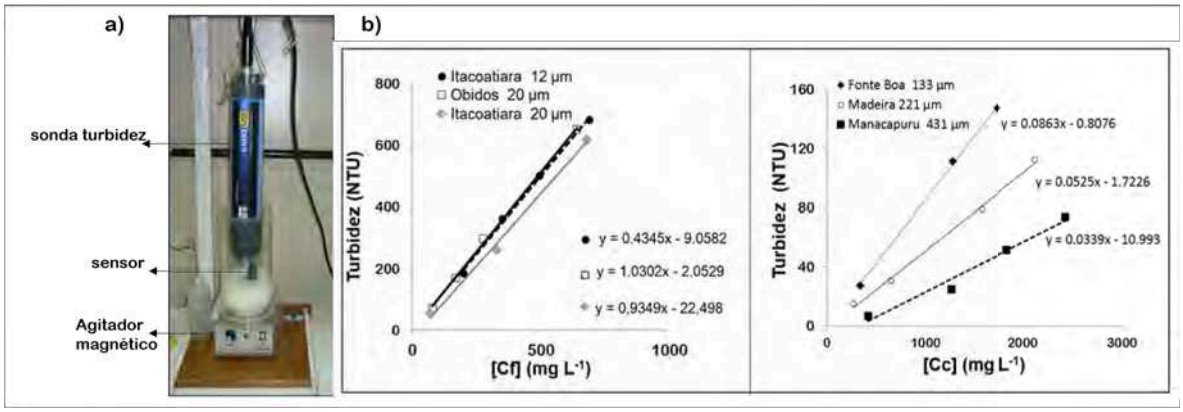

Figura 2.7: *a) sistema de calibração da turbidez, b) curvas de calibração para finos e areias*

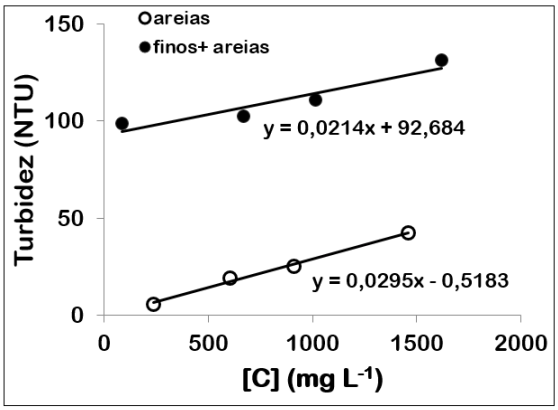

Figura 2.8: *Teste de separação do sinal de turbidez para finos e areias.*

2.3.4.4 Adquisição de dados de turbidez no campo

Em campo, instalou-se a sonda de turbidez YSI V2 6600 no mesmo dispositivo que o amostrador, deste modo obteve-se dados no mesmo tempo que as amostragens. A sonda é programada para uma aquisição a cada 1 kHz. O perfil médio corresponde as média dos perfis de baixada e de subida do amostrador, o que significa que cada ponto de turbidez corresponde à média de valores a cada 50 cm. A profundidade é controlada através do sensor de pressão da sonda (Fig.2.9). As fontes de incertezas correspondem: uma incerteza composta dada pela profundidade e a turbidez para obter o perfil médio, esta incerteza corresponde a 7%.

2.3.5 Medição da granulometria

Utilizou-se para este trabalho um granulômetro Malvem Mastersizer 2000 cuja faixa de medida é de 0.02 µm e 2000 µm do laboratório da CPRM (Manaus). Antes de implantar uma metodologia de determinação de granulometria foram realizados os seguintes testes:

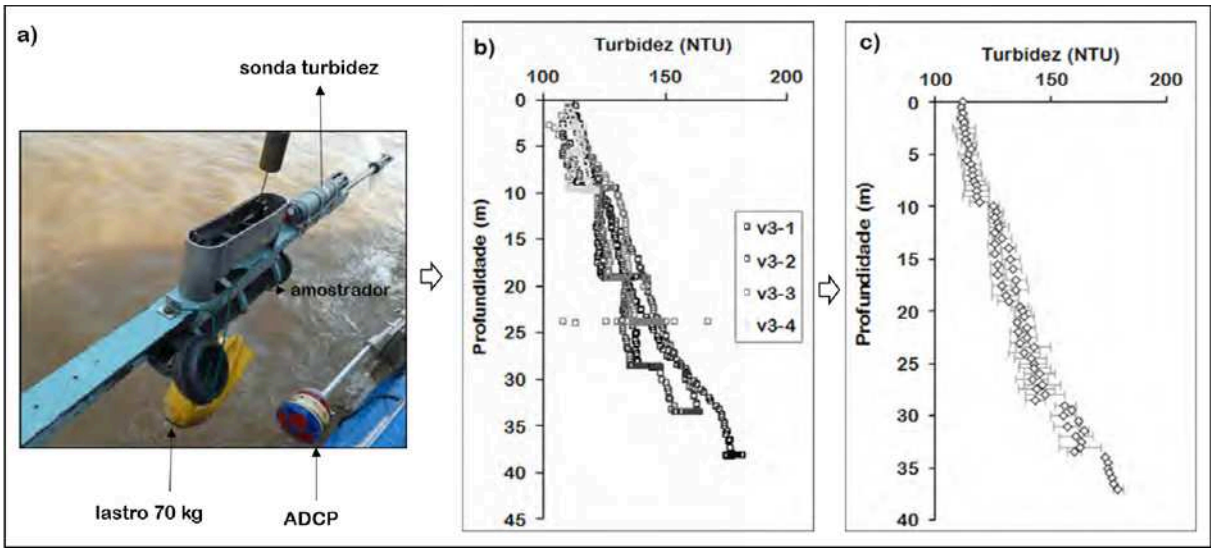

Figura 2.9: *a) Instalação da sonda de turbidez no dispositivo de amostragem,b) Exemplo da aquisição de perfis para cada ponto de amostragem Exemplo vertical 3 em Óbidos no 17-12-2005, c) Perfil médio da vertical 3.*

- A velocidade e tempo de mistura da amostra sem causar rompimento dos grãos ou flocos naturais;
- A representatividade do volume coletado para as análises;
- A utilização de ultrasson;
- O tempo que a amostra pode ficar no laboratório antes de ser analisada, sem ter a formação de flocos.

A metologia e resultados destes testes encontra-se no Anexo B

Para determinar a granulometria, fez-se coletas de amostras em campo que foram posteriormente analisadas em laboratório. Em cada ponto de amostragem dos 7 litros da medição tradicional foram retirados 500 ml para medir a granulometria, tomando-se o cuidado na homogeneização da amostra. Estas amostras foram colocadas diretamente no granulômetro laser. No Peru, foram duplicadas as amostragens, sendo uma para concentração de sedimentos e outra para granulometria.

2.3.5.1 Diâmetro da partícula

A distribuição granulométrica de uma amostra homogênea, geralmente é representada por uma lei log-normal onde o diâmetro representativo é o d_{50}. No entanto, a granulometria do Solimões/ Amazonas é representada por dois tipos o modas se sedimentos característicos (com excepção da superfície onde a granulometria é definida por um só tipo de partículas finas). Ou seja se expressamos o diâmetro em log D, a distribuição granulométrica é o resultado da mistura de duas distribuições normais com parâmetros de μ e σ. Utilizou-se a função "*findepeaks* "no Matlab para poder separar

cada lei normal da distribuição granulométrica expressada em volume (Fig.2.10). Por definição da lei normal o 95% da população situa-se no intervalo de $\mu - 2\sigma, \mu + 2\sigma$.

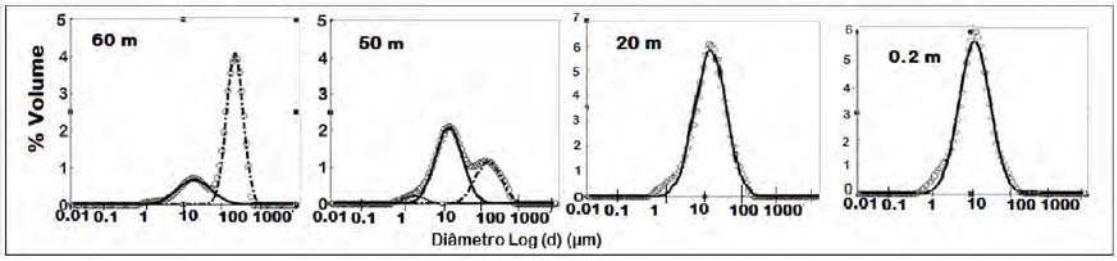

Figura 2.10: *Perfil granulométrico e descomposição da distribuição normal de cada moda presente em cada ponto medido- Estação de Itacoatiara- maio 2012*

2.4 Cálculo de vazão sólida

O cálculo da vazão sólida foi feito utilizando o programa HYDROMESAD, desenvolvido por (Vauchel, 2009), inspirado em MESAD (Cochonneau 2004). Este programa determina a concentração média da seção através da ponderação da concentração pela vazão. A zona de influencia é determinada em cada seção considerando como limite vertical a distancia média entre uma amostra e outra e como limite horizontal se aplica o porcentagem da profundidade medida (Fig.2.11).

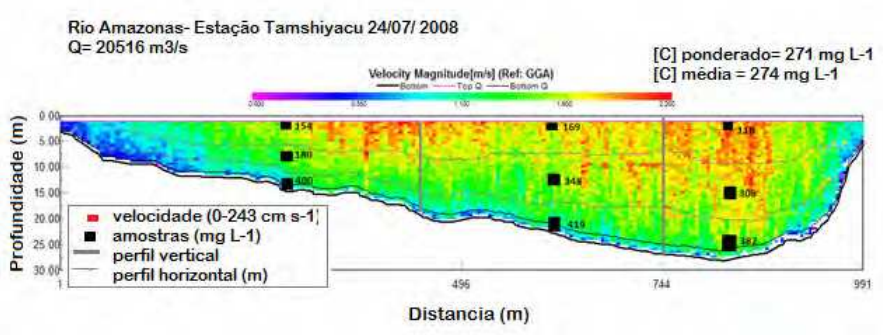

Figura 2.11: *Esquema gráfico da medição de vazão dada pelo ADCP na seção de Tamshiyacu-Peru e método de ponderação para determinar a concentração média da seção*

Capítulo 3

Dinâmica dos sedimentos em suspensão do rio Amazonas no Peru

Journal of South American Earth Sciences xxx (2012) 1–10

Contents lists available at SciVerse ScienceDirect

Journal of South American Earth Sciences

journal homepage: www.elsevier.com/locate/jsames

Suspended sediment dynamics in the Amazon River of Peru

Elisa Armijos [a], Alain Crave [b,c,*], Philippe Vauchel [d], Pascal Fraizy [d], William Santini [d], Jean-Sèbastien Moquet [e], Nore Arevalo [f], Jorge Carranza [g], Jean-Loup Guyot [h]

[a] LBA, Instituto Nacional de Pesquisas da Amazônia (INPA), Universidade do Estado do Amazonas (UEA), Av. André Araújo, 2936, Aleixo, CEP 69060-001, Manaus, Brazil
[b] Géoscience Rennes, CNRS/INSU UMR 6118, Campus de Beaulieu, 35042 Rennes, France
[c] Université de Rennes 1, Campus de Beaulieu, 35042 Rennes, France
[d] GET (CNRS, IRD, OMP, Université de Toulouse), 14 Avenue Edouard Belin, 31400 Toulouse, France
[e] Universidade de São Paulo, Instituto de Geociencias, Rua do lago, 562, cidade Universitária São Paulo, São Paulo, Brazil
[f] UNALM, Universidad Nacional Agraria La Molina, Facultad de Ingeniería Agrícola, Avenida La Molina s/n, Lima 12, Peru
[g] SENAMHI – DGH Servicio Nacional de Meteorología e Hidrología, Dirección General de Hidrología, Casilla 11-1308, Lima 11, Peru
[h] GET (CNRS, IRD, OMP, Université de Toulouse), IRD, CP 7091 Lago Sul, CEP 71635-971 Brasília, DF, Brazil

Resumo

No Peru a bacia Amazônica abrange uma área de 977.920 km^2, se entende desde os Andes ($\approx$ 6000 m.s.n.m) até a planície ($\approx$ 100 m.sn.m). Está composta por duas principais sub-bacias, a bacia do rio Marañón composta principalmente por afluentes do norte e a bacia do rio Ucayali com afluentes do sul. A confluência entre estes dois rios forma o Amazonas cujo monitoramento é realizado na estação de Tamshiyacu.

A bacia amazônica peruana apresenta contrastes fisiográficos e climáticos entre os Andes que inclui as sub-bacias Andinas e a planície. No entanto, estes contrastes também são observados entre o norte e sul da Bacia. Estes contrastes tem influência nos fluxos sedimentares. Neste contexto, o objetivo deste estudo foi determinar a variabilidade temporal do fluxos de água e sedimentos em suspensão nas sub-bacias andinas e na planície amazônica peruana.

A partir de 2003 o Observatório ORE-HYBAM (IRD-SENAMHI-UNALM) inicia o monitoramento de água e sedimentos nas estações peruanas. Neste estudo foram consideradas 8 estações localizadas nos principais rios amazônicos. Três estações localizadas na parte sub-Andina e cinco estações na planície peruana. No período 2003-2010, em cada uma das estações, foram feitas coletas de sedimentos em suspensão a cada dez dias e as medições de vazão líquida e sólida a cada três meses.

Na parte Andina observam-se altas variações de descarga como resposta instantânea da precipitação, enquanto que na planície estas variações são de baixa frequência. Os meses de cheia nas sub-bacias Andinas são de dezembro até maio e os meses de estiagem encontram-se entre julho e setembro. Já na planície os meses de cheia acontecem em abril e maio e de estiagem entre julho e setembro. Ao se comparar as bacias do Marañón e Ucayali, a bacia do Marañón (16.175 m^3 s^{-1} bacia do norte) tem maior aporte de descarga líquida quanto a comparamos com a bacia do Ucayali (11.415 m^3 s^{-1} bacia do sul).

Os rios Andinos apresentam uma relação entre concentração de sedimentos em suspensão e vazão, no entanto, quanto mais nos aproximamos na planície, esta relação toma uma configuração de *loop*, o que impede sua utilização. Este fenômeno de histerese pode ser causado pela diferença entre o regime sedimentar e a vazão. Para contornar este problema de variabilidade temporal realizou-se coletas regulares de água e sedimento durante o regime hidrológico. O fato que a concentração de sedimentos superficiais a cada dez dias apresentam uma boa relação com a concentração média de sedimentos da seção (r^2=0.72), é possível quantificar o fluxo de sedimentos a partir desta relação. Na região Andina observa-se uma alta variação dos sedimentos em suspensão en quanto na planície o regime estacional é mais marcado. Em contrapartida a sub-bacia do Ucayali tem um maior aporte de fluxo de sedimentos aproximadamente 360 Mt year^{-1}, enanto a bacia do Marañón tem um aporte de 144 Mt year^{-1}. O que significa que o fluxo que ingressa no Brasil é aproximandamente 540 Mt year^{-1}.

Résumé

Au Pérou le bassin Amazonien représente une superficie de 977.920 km^2 qui s'étend depuis les Andes ($\approx$ 6000 m.s.n.m) jusqu'à la plaine du même nom ($\approx$ 100 m.s.n.m). Il comprend deux sous-bassins principaux, le bassin du Marañon constitué principalement par des affluents venus du nord et du bassin de l'Ucayali issu de formateurs venant du sud. La confluence de ces deux fleuves forme l'Amazone dont la station de Tamshiyacu assure le suivi.

Le bassin Amazonien au Pérou présente des contrastes physiographiques et climatiques entre les sous bassins andins et la plaine. Mais l'on observe également de tels contrastes entre le sud et le nord du bassin. Ces contrastes vont influencer fortement les flux sédimentaires. L'objectif de cette étude sera de déterminer la variabilité temporelle dans un tel contexe des flux d'eau et de sédiments en suspension dans les sous bassins andins ainsi que dans la plaine amazonienne péruvienne.

A partir de 2003 l'Observatoire ORE-HYBAM (IRD-SENAMHI-UNALM) a inicié le suivi hydrologique et sédimentaire des stations péruviennes. On a considéré dans cette étude 8 stations situées sur les principaux fleuves Amazoniens dont trois dans la partie sub-andine et cinq dans la plaine. Sur la période 2003-2010, et sur chacune de ces stations, on a prélevé tous les dix jours des échantillons en surface de sédiments en suspension et réalisé tous les trois mois des mesures de débit liquide et solide sur la section totale.

Dans la partie andine, on observe de fortes variations de débit en réponse instantanée aux précipitations alors que dans la plaine ces variations s'atténuent. Dans les sous bassins Andins les crues ont lieu de décembre à mai et l´étiage de juillet à septembre. Dans la plaine la période de crue arrive en avril-mai, celle d'étiage s'étalant aussi de juillet á septembre. On remarquera que le bassin du Marañon apporte un débit liquide supérieur á celui de l'Ucayali, 16,175 m^3 s^{-1} pour le Marañon contre 11,415 m^3 s^{-1} pour l'Ucayali.

Dans les cours d'eau Andins on peut établir une relation directe entre concentration de sédiments en suspension et débit liquide alors qu'au fur et à mesure que l'on avance dans la plaine cette relation tend à prendre une forme de *loop* qui empêche un calcul direct du flux solide. Ce phénomène d'hystérésis peut provenir du déphasage entre les flux sédimentaires et liquides et l'on doit donc contourner ce problème de variation temporelle en réalisant un échantillonnage continu tout au long du cycle hydrologique.

En effet, la concentration de sédiments de superficie des échantillons présente une bonne relation avec la concentration moyenne dans la section (r^2=0.72) et l'on peut arriver á calculer le flux solide en se basant sur cette relation.

Dans la partie andine on observe comme pour les débits une très forte variation des

valeurs de concentration en materiel en suspension alors que dans la plaine le régime saisonnier est plus marqué. En revanche, c´est cette fois le bassin de l´Ucayali qui amène le plus gros flux sédimentaire avec approximativement 360 Mt an^{-1} quand dans le même temps on obtient 144 Mt an^{-1} pour le Marañon. Au final se sont 540 Mt an^{-1} qui transitent par l'Amazone à la frontière péruano-brésilienne.

Suspended sediment dynamics in the Amazon River of Peru

Elisa Armijos[1], Alain Crave[2,3], Philippe Vauchel[4], Pascal Fraizy[4], William Santini[4], Jean Sebastian Moquet[5], Nore Arevalo[6], Jorge Carranza[7],Jean Loup Guyot[8].

1 – LBA, Instituto Nacional de Pesquisas da Amazônia (INPA)- Universidade do Estado do Amazonas (UEA). Av. André Araújo, 2936, Aleixo, CEP 69060-001, Manaus- Brazil .
2 – Géoscience Rennes, CNRS/INSU UMR 6118, Campus de Beaulieu, 35042 Rennes, France.
3 – Université de Rennes 1, Campus de Beaulieu, 35042 Rennes, France.
4 – GET (CNRS, IRD, OMP, Université de Toulouse), 14 Avenue Edouard Belin, 31400 Toulouse, France.
5 – Universidade de São Paulo -Instituto de Geociencias Rua do lago, 562 - cidade Universitária São Paulo, São Paulo – Brazil.
6 – UNALM, Universidad Nacional Agraria La Molina – Facultad de Ingeniería Agrícola, Avenida La Molina s/n, Lima 12, Perú.
7 – SENAMHI – DGH Servicio Nacional de Meteorología e Hidrología – Dirección General de Hidrología, Casilla 11-1308, Lima 11, Perú
– GET (CNRS, IRD, OMP, Université de Toulouse), IRD, CP 7091 Lago Sul, CEP 71635-971 Brasília, DF, Brazil.

Abstract

The erosion and transport of sediments allow us to understand many activities of significance such, as crust evolution, climate change, uplift rates, continental processes, the biogeochemical cycling of pollutants and nutrients. The Amazon basin of Peru has contrasting physiographic and climatic characteristics between the Andean piedmont and the plains and between the north and south of the basin which is why there are why 8 gauging stations located along the principal rivers of the Andean piedmont (Marañón, Huallaga, Ucayali) and the plain (Marañón, Tigre, Napo, Ucayali and Amazon rivers). Since 2003, the ORE-Hybam (IRD-SENAMHI-UNALM) observatory has performed regular measurements at strategic points of the Amazon basin to understand and model the systems behavior and their long-term dynamics. On the Andean piedmont, the suspended yields are governed by a simple model with a relationship between the river discharge and the sediment concentration. In the plain, the dilution effect of the concentrations can create hysteresis in this relationship on a monthly basis. The Amazon basin of Peru has sediments yield of $541 * 10^6$ t year $^{-1}$, 70% of which comes from the southern basin.
KEY WORDS: hydrology, sedimentation, erosion, Andes, sediment transport, Andean piedmont.

Introduction

Erosion and transport processes are key factors for understanding the dynamics of natural systems of different scales. Among other factors, the influence of erosion processes on mountain range dynamics is one of the crucial points for understanding

climate and tectonic feedback (Willett, 1999; Molnar, 2003). How earth materials transit from mountain ranges to oceans in terms of mass and time is still an open question. Erosive processes are sensitive to many factors, such as temperature, rainfall, runoff, landscape characteristics, lithology, and, significantly anthropogenic activities (Walling, 2006). The challenge is to understand the respective effects of these factors on erosion rates at different scales.

The Suspended sediment load in rivers integrates the upstream to downstream balance of all erosion processes in the hydrological basin. Therefore, suspended sediment loads provide information on present-day mean catchment denudation rates and on the dynamic response to climate inputs under specific geological and anthropogenic contexts (Dadson et al., 2003; Walling, 2006). However, suspended sediment load is a complex signal resulting from numerous factors. Currently, there is no evidence of the relative dominance of each factor. Climate and tectonic factors are the relevant parameters at large spatial and temporal scales because they fix the potential of mass that can be eroded and the amount of water needed to transport the sediments. Therefore, mountain ranges with high climatic gradients are interesting contexts within which to interpret suspended sediment loads in terms of transport efficiency.

The Amazon basin in Peru presents has several advantages for studying erosion-transport processes. Firstly, the Andes, which cover the upstream part of the basin, are one of the world's highest mountain ranges, with an average elevation of 4000 m (m asl). Second, there are pluviometric contrasts between the southern tropical and equatorial hydrological regimes (Espinoza et al., 2009b). Third, there is a low rate of erosion due to anthropogenic activity. Since 2003, the observatory ORE-Hybam (IRD-SENAMHI-UNALM) has been performing out regular measurements in strategic points of the Amazon Basin with the objective of providing the research community with high quality scientific data needed to understand and model systems behavior and their long-term dynamics. A previous study (Guyot et al., 2007a) presented preliminary results on sediments fluxes for the Marañón, Napo and Ucayali rivers with a 2 years dataset. Due to the lack of data, however, the sediment and erosion rates of the piedmont between the Andes and the Amazon plain remain an open question. This paper develops a more complete analysis of a seven years dataset for the Peruvian Amazon gauging station network. New and more precise estimates are presented with a focus on the temporal variability of the sediment load for the principal rivers of the upper Amazon basin in Peru. Different sediment load dynamics between the Andes and the basin's plains show how the main climatic regimes in this part of the Amazon basin may control the production and the transport of sediment.

Area of study

Peru's Amazonian river basin spreads out over 977 920 km^2, stretching from the Andes (6000 m asl) to the eastern plains (100 m asl). Seventy- six percent of Peruvian the territory and 98% of its water resources are in the Amazonian region (DGAS in 1995), but it is home to only 2% of the population (Figure 1). The precipitation regime

is classified as humid tropical, however, it is characterized by geographic variability (Laraque et al., 2007; Espinoza et al., 2006). The average annual precipitation over the region is 1600 mm. Precipitation in the Andean region varies significantly, both spatially and seasonally, in contrast to the homogenous precipitation distribution on the plains. In the south, the mountainous part of the Huallaga and Ucayali basins is characterized by an intense period of rain from December to May. This phenomenon is more intense at lower altitudes and to the north, leading to higher precipitation values and a shorter dry season (June to August). In the north, the mountainous part of the Marañón basin experiences an intermediate rainfall regime, with a rainy season from January to April. On the windward slopes of the Andes, near the equatorial latitudes, a long rainy season (February to July) is observed and a dry season is entirely absent. A more uniform precipitation regime is observed on the plains at the foot of the Andes basin (Espinoza et al., 2009a). The type of flora depends on the altitude, ranging from "Paramo" at over 3000 m to the tropical rainforests in the lowlands (Kvist and Nebel, 2000).

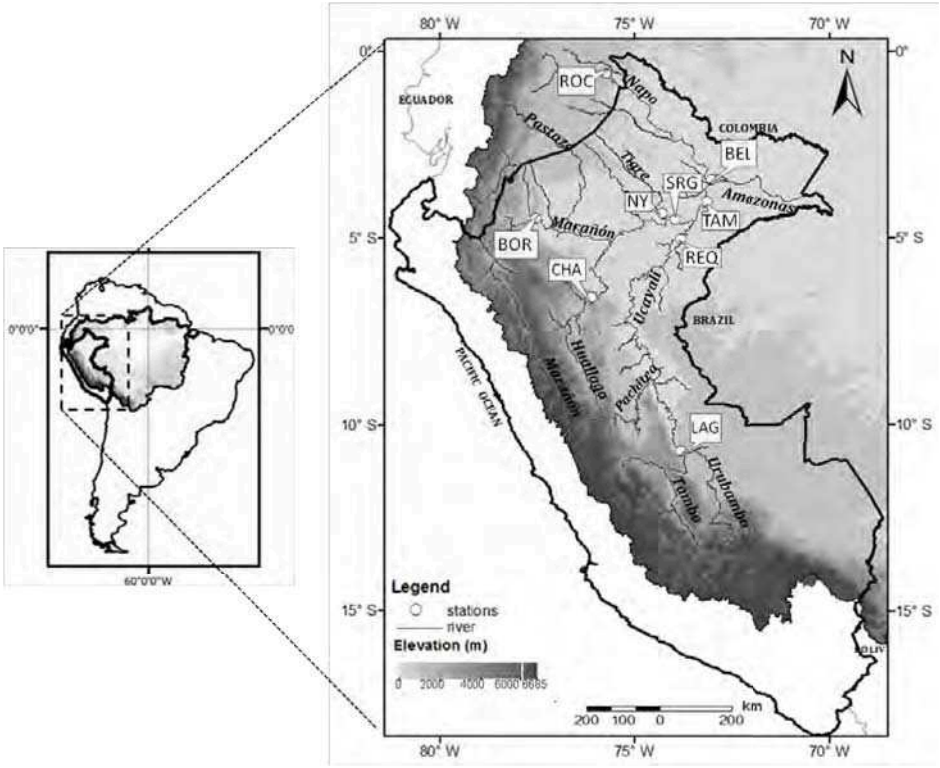

Figure 1. *Location the Peruvian Amazon basin and the reference hydrological stations mentioned in the text. Digital Model SRTM-resolution, 90m (Rabus et al., 2003).*

Geologically, the western part of Peru is divided into sectors that have experienced uplift or subsidence during the Quaternary. The plains of the Ucayali basin, between the Arc de Fitzcarraldo to the south and Contamana to the north, are located on top of a horizontal segment of a subduction zone formed during the Pliocene, favoring sediment accumulation (Roddaz et al., 2006). Some terraces of the high Ucayali basin are most likely the result of this uplifting. In northern Peru, the Marañón basin during the same

period suffered subsidence that continues in the Pastaza River depression and in the inter-river zones of the Marañón and Ucayali Rivers (Dumont et al., 1992). The Arc de Fitzcarraldo, perpendicular to the Andes' axis, is the result of the horizontal subduction of the Nazca fault. The Pastaza alluvial cone, one of the world's largest, is described as an extremely active zone in terms of erosion dynamics (Bernal et al., 2011).

Data and methods

Data collection

Hydrological data from nine gauging stations (Table 1, Figure 1) are presented: three Hybam stations located in Peru (CHA, LAG, NY), one Hybam station located in Ecuador (Rocafuerte) and five SENAMHI gauging stations in Peru (BEL, BOR, SRG, REQ, TAM). ROC, BOR, CHA and LAG monitor the outlet of the Andean part of the Napo, Marañón, Huallaga and Ucayali rivers, respectively. The total water balance and sediment discharge are monitored for the Napo (BEL), Marañón (SRG) and Ucayali (REQ) rivers. TAM is the first gauging station of the Amazon River mainstream after the confluence of the Marañón and Ucayali rivers. Note that the Amazon River at TAM collects inputs from both Marañón and Ucayali with few transversal inputs at the confluence (Figure1). The starting date of the regular water discharge and sediment concentration monitoring depends on the specific station (Table 1). This study concerns only the period during which regular monitoring for both water discharge and concentration are available. The LAG gauging station is relatively new with two years of measurements.

Table 1. The network of gauging stations in the Amazon basin of Peru. Superficial sampling= samples made by one person every 10 days (observer samples). Sediment samples = mean concentrations of the cross section (sampling of the different depths)

STATION CODE	GAUGING STATION	RIVER	LAT (deg.) S	LON (deg.) W	AREA Km2	NUMBER OF GAUGING	SEDIMENT SAMPLES	SURFACIAL SAMPLES	PERIOD
BOR	Borja	Marañón	4.47	77.55	114 280	20	119	305	2004-2010
CHA	Chazuta	Huallaga	6.57	76.12	68 720	12	70	249	2004-2010
NY	Nva. York	El Tigre	4.32	74.29	42 170	10	74	122	2006-20009
LAG	Lagarto	Ucayali	10.61	73.87	190 810	30	256	197	2009-2010
REQ	Requena	Ucayali	4.9	73.67	346 600	40	283	80	2006-2010
SRG	San Regis	Marañón	4.51	73.95	361 880	36	245	191	2004-2010
TAM	Tamshiyacu	Amazonas	4	73.16	719 640	58	441	191	2004-2010
ROC*	Nvo.Rocafuerte	Napo	0.92	75.39	27 390	32	207	291	2001-2010
BEL	Bellavista	Napo	3.48	73.08	100 030	20	96	168	2004-2010

*Armijos et al.,2013

Water discharge measurement

For all gauging stations, the HYBAM and SENAMHI observers have measured staff gauges twice daily since 1986 for the oldest stations (TAM, SRG, REQ, BOR) and since 2006 for the more recent ones (NY). Field river gauging is performed regularly to match all water discharge ranges and to calibrate the rating curves between the water discharge and water level at each gauging station. To date, an average of 30 campaigns per station have been performed. Stream water discharges are measured with a 600 kHz Acoustic Doppler Current Profiler (ADCP) with a GPS positioning protocol to avoid any error of water velocity measurement induced by moving river bottoms (Mueller and Wagner, 2009). Daily water discharges are calculated using the HYDRACCESS software (http://www.orehybam.org/index.php/eng/Sofware/Hydraccess). We estimate the range of cumulative uncertainties (ninetieth percentile) on daily water discharge values between ± 2% and ± 5% depending on the gauging station (Vauchel, 2009).

TSS measurement

At each gauging station, observers took a 500 ml sample from the middle reach of the river every 10 days. These samples were filtered through a cellulose acetate filter with a pore diameter of 0.45 µm. Samples were also collected at different depths of the river cross section during field campaigns in to define an empirical rating curve between surface concentration and Total Solid Suspension concentration ($[TSS]$). The former rating curve helped us estimate $[TSS]$ from the 10-day sampling period. During a few field campaigns, we repeated the complete procedure of $[TSS]$ measurement several times and attempted to monitor the $[TSS]$ gradient near the river bottom at a resolution of 50 cm.

From this specific set of data, we estimated the standard deviation of $[TSS]$ values considering the after the entire sampling properties, field measurements and method of calculation. For stable hydrologic conditions, the standard deviations of concentrations were 15% and 36% of the mean value for samples taken at the surface and at less than 1 m from the bottom, respectively. To take into account the spatial variation of the water velocity gradient on the gauging section, HYDRACCESS applies a water discharge-weighted average to calculate $[TSS]$ for each gauging operation. Actually, the large concentration variability near river bottom does not have a strong effect on average $[TSS]$ estimation because the vertical velocity profile decreases from the surface to the riverbed. The maximum standard deviation of the average $[TSS]$ is 20% for gauging campaigns. To estimate $[TSS]$ from the 10-day surface sample, we employed an empirical linear fit (Figure 2) to the rating curve between $[TSS]$ and surface concentration.

All station data of gauging campaigns are combined to achieve statistical significance. Actually, all station data sets present the same increasing dispersion with increasing surface concentration. The dispersion of the values results from both measurement

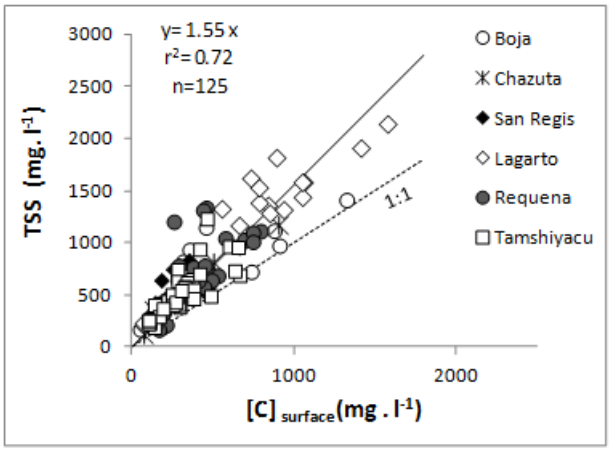

Figure 2. *Relationship between surface [C] and mean [TSS] concentrations in the mean cross-sectional area for all gauging stations (mg. l^{-1}). The coefficient of the linear regression is 1.55, with a standard deviation of 5%. Period 2004-2010. 125 samples.*

errors and the selective mobilization of sand in the water column during flooding. Presently, given our data we are limited to employing this relationship between $[TSS]$ and surface concentration. The linear trend proposed in this study is a first approximation to estimate $[TSS]$ from the sampling protocol with local observers. The coefficient of the linear regression is 1.55 with a relative standard deviation of 5%.

Data processing

Biases and imprecision in the $[TSS]$ average and water discharge depend on the regular (sampling frequency)/(variability water discharge frequency) ratio and the method used to average the data (Phillips et al., 1999; Moatar et al., 2006). Because our dataset presents a large spectrum of hydrological regimes, we applied different methods to estimate the inter-annual average and uncertainties of the monthly mean Total Suspended Sediment concentration ($[TSS]_m$) and fluxes (QS_m). Three methods were employed:

Method M1 is the standard method used for the Hybam project. M1 is described in detail in (http://www.ore-hybam.org/index.php/eng/Sofware/Hydraccess). The main assumption of M1 is that daily [TSS] variation follows a linear interpolation between two 10-day in-situ concentration values. Average monthly and annual values of solid discharge are calculated by multiplying the daily water discharge by the daily concentration. This method is reliable for estimating the real concentration with low uncertainty when the daily concentration variability is low, as in the Amazon plain. When the daily concentration variability is high, like in the Andean range, M1 corresponds to a complex discharge-weighted average method.

Method M2 estimates QS_m by multiplying the inter-annual monthly mean water discharge (Q_m) and concentration ($[TSS]_m$). Q_m is calculated directly from the daily discharge values with Eq(1):

$$Q_m = \frac{1}{n} \sum Q_{mi}$$

where $Q_m i$ is the water discharge for the mith observation and n is the total number of observations for the month m for the entire dataset range. $[TSS]_m$ is calculated with a discharge-weighted mean concentration method, Eq(2):

$$TSS_M = \frac{\sum TSS_{mi} * Q_{mi}}{Q_{mi}}$$

where $[TSS]_{mi}$ is the total suspended sediment concentration for the mith observation for month m for the entire dataset range. For each month, we suppose that the density distribution probability of gauging water discharges and daily water discharge are the same which is a necessary condition to obtain significant means

Method M3 is a rating curve method applied to derive $[TSS]_m$ with Q_m when these variables present a univocal trend. For this study, M3 is used mainly to calculate annual water and sediment fluxes. All methods only estimate the true values of $[TSS]$ with uncertainty related to the in-situ measurement protocol, daily hydrological variability and calculation method. We assumed there is no systematic bias of concentration value in our dataset. The confidence intervals in the following text integrate all uncertainties of all steps of the process. To test the reliability of M1 and M2, we controlled the sediment mass balance budget at the confluence between the Marañón and Ucayali rivers with time-series of SRG, REQ and TAM. Note that this test corresponds only to a hydrologic regime with low daily water discharge variability

Results

All figures with monthly mean water discharge, concentrations and sediment fluxes present values calculated with the M2 method because this method is the most widely used in the literature and does not introduce any assumptions. However, M1 gives similar results at monthly and annual scales.

Hydrology

In what follows, we present the principle results on the hydrology regime characteristics of the study region. For a more complete analysis of the hydrology of Peruvian rivers see, Espinoza et al.,(2006,2011). and . Daily water discharges (Q) are displayed in Figure 3 for the 2006-2010 series. The Andean stations (BOR, CHA, ROC) demonstrate high frequency variability superimposed on a low frequency annual cycle. On the plains, the hydrologic regime at SRG, REQ, TAM, and BEL reveals only a low frequency annual cycle. Several factors may act as low-pass filters for the hydrologic signal. First, diffusive processes on flood wave propagation over more than 1000 km

decrease water level fluctuations downstream (Trigg et al., 2009). Second, the shallow topographic slope of the Amazon plain decreases the contribution of the short-term hydrologic response to river water discharge (Beighley et al., 2009).

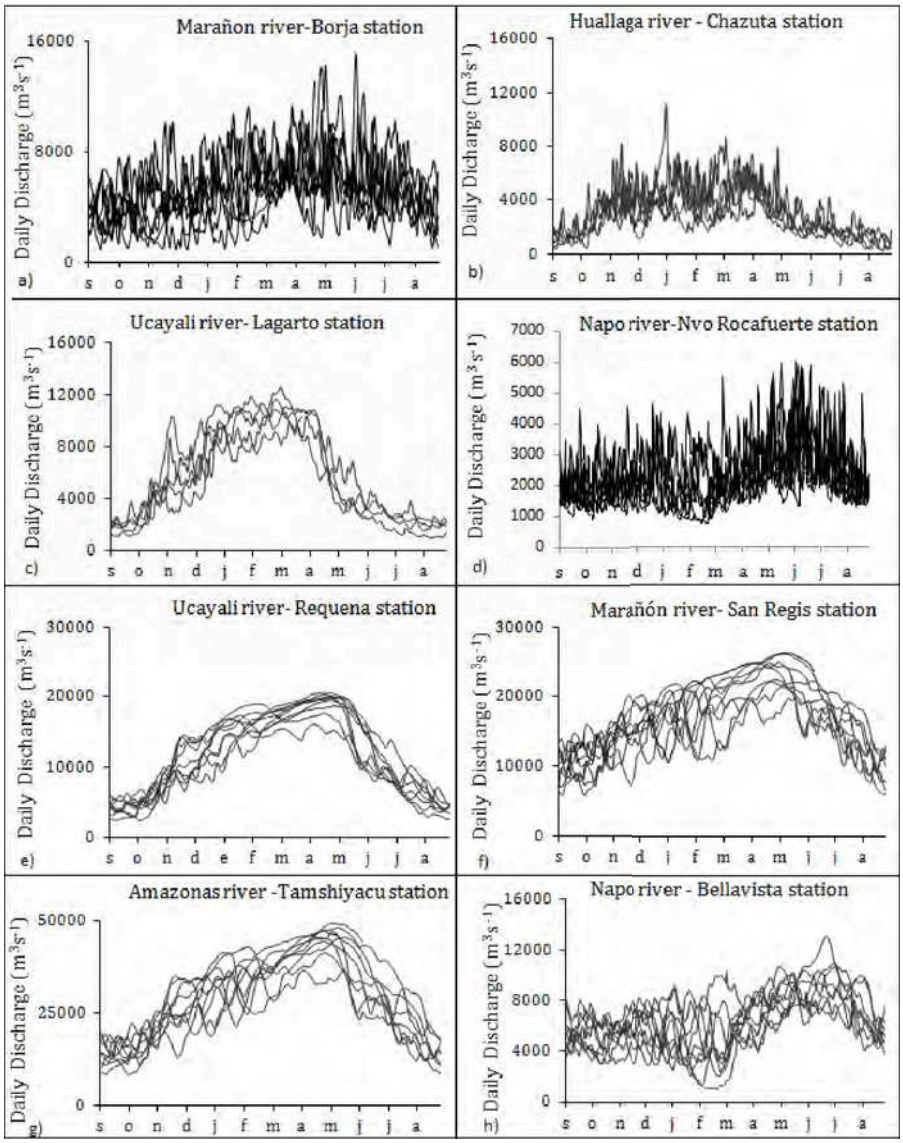

Figure 3. *Daily discharge period 2006-2010 for all gauging stations (m^3 s^{-1}).a) Marañón River-BOR, b) Huallaga River-CHA, c) Ucayali River-LAG, d) Napo River- ROC, e) Ucayali River- REQ, f) Marañón River-SRG, g) Amazon River-TAM, h) Napo River-BEL.*

The flood amplitude at the Andean stations is equivalent to the amplitude of the annual low frequency fluctuation. The Q_m annual fluctuations (Figure 4) reflect the climatic context of the southern tropical regime for the Ucayali River and the equatorial regime for the Marañón and Napo rivers (Espinoza et al., 2006; Espinoza et al., 2009a; Espinoza et al., 2011;). High water discharges occur from December to February in the southern part of the Ucayali River (LAG), from January to March in the southern region of the Marañón River (CHA), and from May to July in the Napo River (ROC and BEL). At BOR, the Marañón River drains an area from 2°S to 7°S latitude therefore, Q_m experiences smooth annual variability as a combination of the southern tropical and

equatorial hydrological regimes. On the Peruvian Amazon plain (REQ, SRG, TAM), Q_m reveals a regular unimodal annual fluctuation with maximum discharges during March and May. Balances between upstream and downstream runoff for each river provide information about the hydrological regime of areas lacking monitoring (Figure 4).

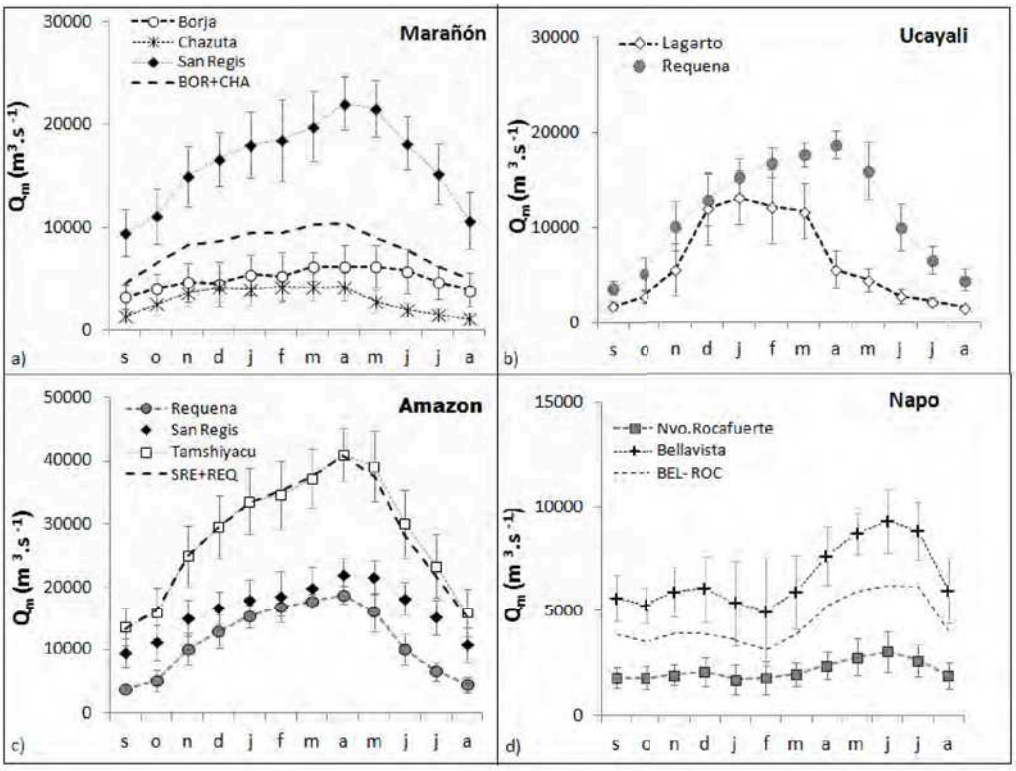

Figure 4. *Monthly flow balance downstream–upstream to basins: a) Marañón, b) Ucayali, c) Amazon and d) Napo. Error bars refer to standard deviation.*

The hydrology of non-monitored areas exhibits runoff variability at the monthly scale for the Ucayali, Marañón and Napo rivers, with a similar trend to the equatorial hydrological regime, with a high water discharge period during April to July. However, for non-monitored areas, the maximum water discharge period shifts from April to June for the Ucayali and Napo rivers, respectively. This area marks the south to north transition from the southern tropical to equatorial climatic regimes (Espinoza et al., 2009a). Q_m exhibits a negative (October to March) and positive (April to September) budget at the confluence of the Ucayali and Marañón rivers (Figure 5). Such cyclic change is correlated to the cyclic filling and erosion of the floodplain between the Marañón and Ucayali rivers.

The mean annual water discharges are listed in Table 2. The contributions of the Marañón, Ucayali and Napo rivers to the Amazon water discharge are 47%, 33% and 19%, respectively. These results compliment previous results on water discharge for the same area (Guyot et al., 2007a).

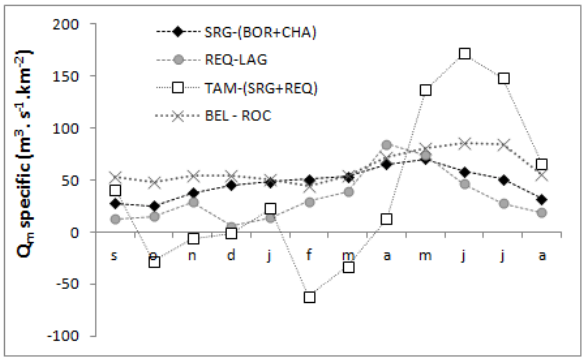

Figure 5. *Variability of runoff of the non-monitored areas at a monthly scale, values normalized for the surface basins for the Amazon (TAM-(SRG-REQ)) Ucayali (REQ-LAG), Marañón (SRG-(BOR-CHA) and Napo (BEL-ROC) basins.*

TSS and sediment fluxes

For water discharge, the daily $[TSS]$ variability exhibits low and high-frequency fluctuations on the plains and in the Andean region, respectively (Figure 6).

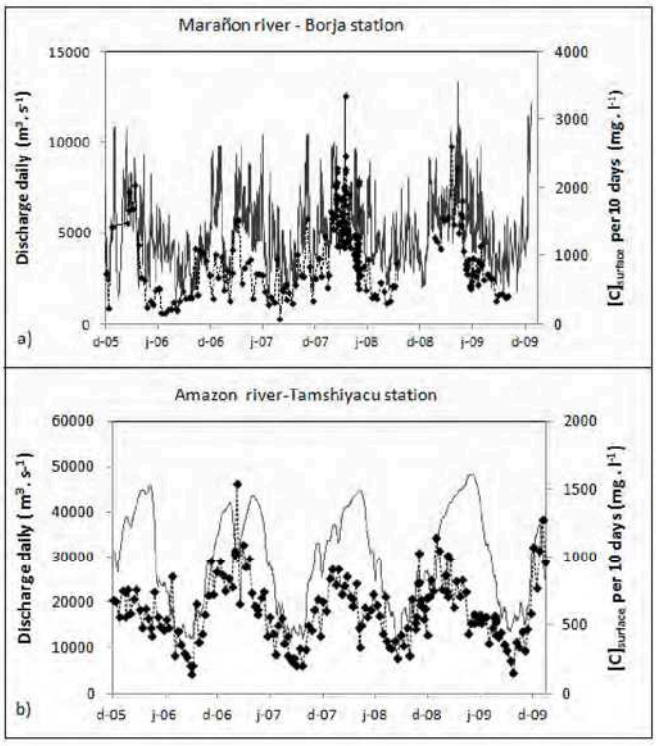

Figure 6. *Daily discharge and surface sediment concentrations per every 10 days for two stations a) the Marañón River (Borja) on the Andean piedmont , b) the Amazon River (Tamshiyacu) on the plain. Period: December 2005 to December 2007.*

To test the significance of daily $[TSS]$ reconstitution with M1 for Andean rivers, we performed high-frequency sampling during a two-month flood period in 2008 at BOR and applied a Nash criterion between the observed values and M1's values. A Nash

criterion of 0.26 invalidates the daily $[TSS]$ values between the two 10-day sampling periods calculated with M1 for rivers with high-frequency water discharge. Therefore, the daily $[TSS]$ interpolated with M1 has no physical meaning. However, M1 should be considered as a daily water discharge weighted averaging procedure for the Andean context. For a low-frequency water discharge regime, M1 $[TSS]$ daily values may have a physical significance because of the low temporal variability of $[TSS]$ (Filizola and Guyot, 2009). As a result, daily $[TSS]$ reconstitution with M1 presents a discrepancy in physical significance between Andean and Amazon plain contexts. The relationship between the [TSS] collected during field campaigns and the water discharge shows a large dispersion around a hypothetical average rating curve for any station of our dataset (Figure 7). Such a rating curve regression model has too large of a confidence interval to be attractive for daily $[TSS]$ estimation. Without any reliable methods to model daily $[TSS]$, we do not delve into the analysis of $[TSS]$ on a daily scale.

At a monthly scale, $[TSS]_m$ is related to Q_m for Andean and plain rivers following two types of trends (Figure 7). $[TSS]_m$ in Andean rivers (BOR, CHA, LAG, ROC) exhibits a unique linear rating curve with Q_m (r^2= 0.86) (Figure 8a), which suggests that M3 is reliable for estimating $[TSS]_m$ from Q_m. The $[TSS]_m$ in Amazon plain rivers (NY, BEL, SRG, REQ, TAM) exhibit hysteresis with respect to water discharge seasonality and drainage area (Figure 7). All rivers mainly controlled by an equatorial climatic regime (NY, BEL, SRG, TAM) follow the same main linear $[TSS]_m$ trend for different Q_m ranges (Figure 8b). The Ucayali River at REQ exhibits a larger hysteresis loop with $[TSS]_m$ four times larger than that for the Marañón and Napo rivers. M3 cannot be applied to the Amazon plain rivers because of this hysteresis.

The monthly mean sediment flux (Qs_m) is derived from $[TSS]_m$ and Q_m to calculate the mass balance variability between the Andeans and Amazon plain sediment fluxes (Figure 9). The Qs_m for the Andean rivers follows the Q_m time variations with an amplification factor, as the linear rating curve between $[TSS]_m$ and Qm suggests. At the downstream point of the Marañón River (SRG), Qs_m exhibits the same relative dynamic as that at the BOR station, but with a smaller fluctuation. Only half the upstream Qs_m passes through the Marañón River to reach the Amazon River during the highest flow period (March to May). For the Ucayali River, the Qs_m balance between REQ and LAG shows a negative budget during November to March and a positive budget during April to October, which indicates that the non-monitored area in the Ucayali basin provides sediment flux at least during March to October. Along the Napo River, Qs_m exhibits a unique dynamic from upstream (ROC) to downstream (BEL), with a positive mass balance budget between BEL and ROC during the entire hydrological cycle. The Qs_m in the Amazon River (TAM) almost balances the Marañón (SRG) and Ucayali (REQ) inputs and is mainly controlled by the large seasonal fluctuations of Qsm from the Ucayali River.

$[TSS]$ yields the monthly mass balance differences between upstream and downstream Qs_m, providing information on erosion and deposition rates for non-monitored

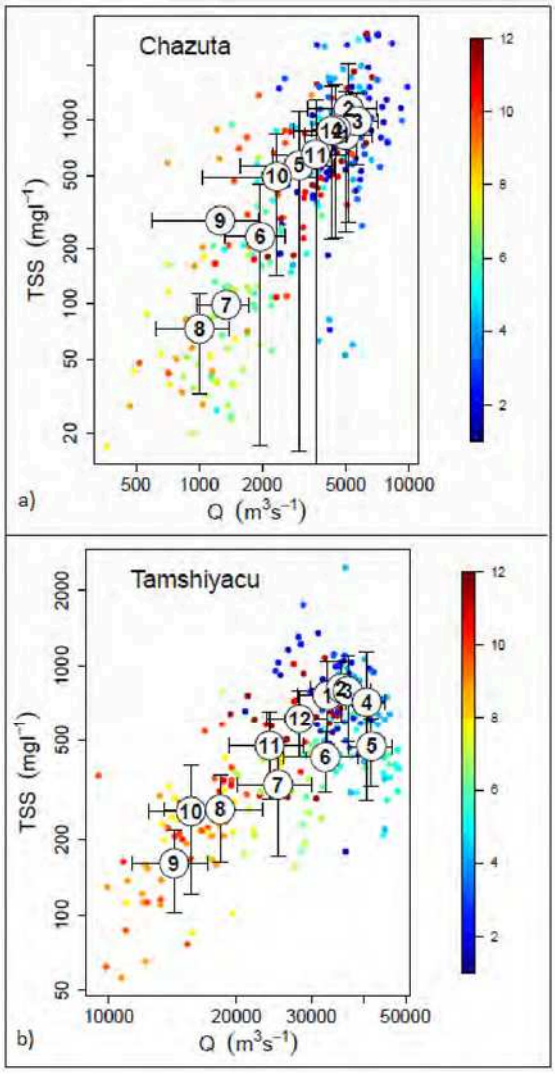

Figure 7. *Relation [TSS] vs Q. The small points with different colorS represent the daily values each month of the year and the circles represent the monthly mean value. The number written on the circle corresponds to the number of the month of the year. a) the Huallaga River (Chazuta) on the Andean piedmont, b) the Amazon river (Tamshiyacu) on the plain.*

areas. On the flood plain between SRG, REQ and TAM, the deposition and erosion rates are cyclic and are ten times greater than for the other parts of the study area (Figure 10).

To estimate the dynamic of non-monitored TSS sources, the positive mass balance between upstream and downstream areas is divided by the corresponding Q_m to obtain an equivalent monthly mean $[TSS]_m$ for non-monitored areas ($[TSS]_m$*). The $[TSS]_m$* for the Ucayali, Marañón and Napo rivers are nearly constant during the annual cycle, with values ten times larger for the Ucayali River than for the Marañón and Napo rivers (Figure 11).

Table 2 displays the annual TSS flux estimation with M1 and M2 for all gauging stations and M3 for Andean gauging stations. The differences among the M1, M2 and

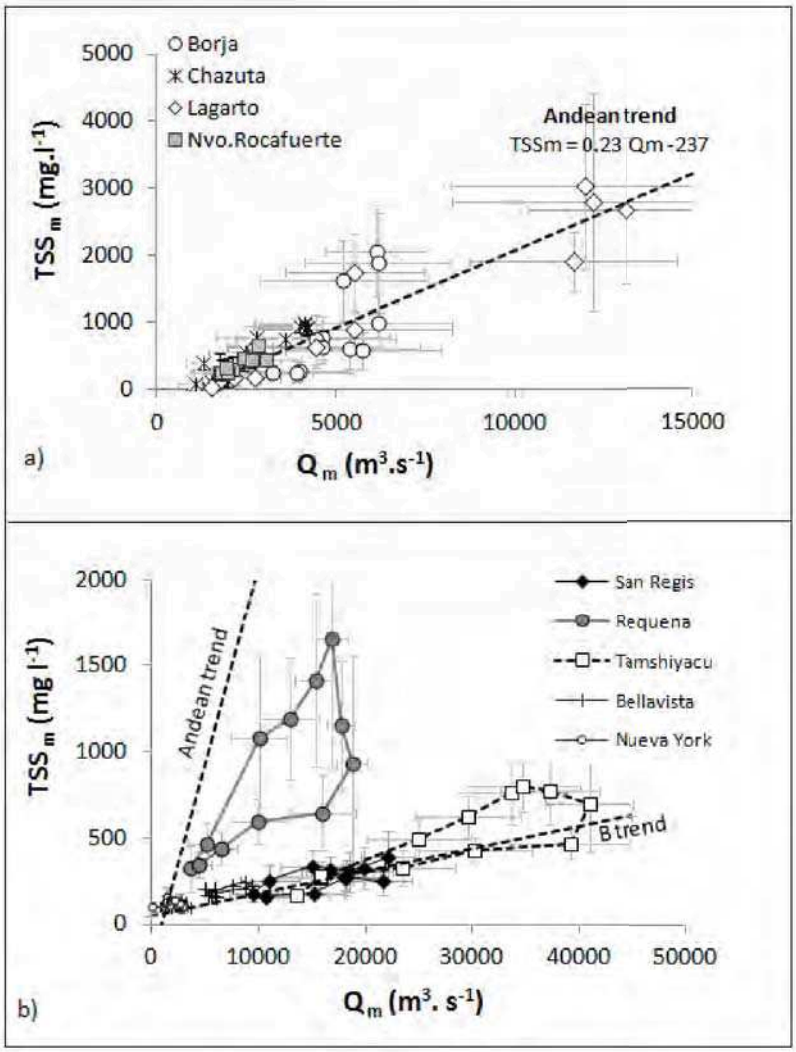

Figure 8. *Relation $[TSS]_m$ vs Q_m for a) Andean piedmont stations and b) plain stations. Errors bars represent the standard deviation.*

M3 results are within a range of ± 10% of the average values and within a range of ± 30% of upper and lower deciles. The results with M3 are intrinsically on the same order as those with M2, M3 is deduced from a linear regression fit on M2 results. If M3 is not appropriate when the dataset includes $[TSS]$ monitoring, it could be very helpful to estimate $[TSS]_m$ for time series without concentration monitoring. Note that both M1 and M2 satisfy annual mass conservation at the confluence between the Ucayali and Marañón rivers.

More than 540 million tons of sediments are transported each year in the upstream part of the Amazon River. Two-thirds of the TSS fluxes of Amazon come from the Ucayali River, 27% from the Marañón River and 8% from Napo River. Along the Napo River, suspended yield increases from Rocafuerte to Bellevista and provides evidence of another sediment source. Along the Marañón River, the combined suspended yield of BOR and CHA is significantly larger than the suspended yield at San Regis (120% with

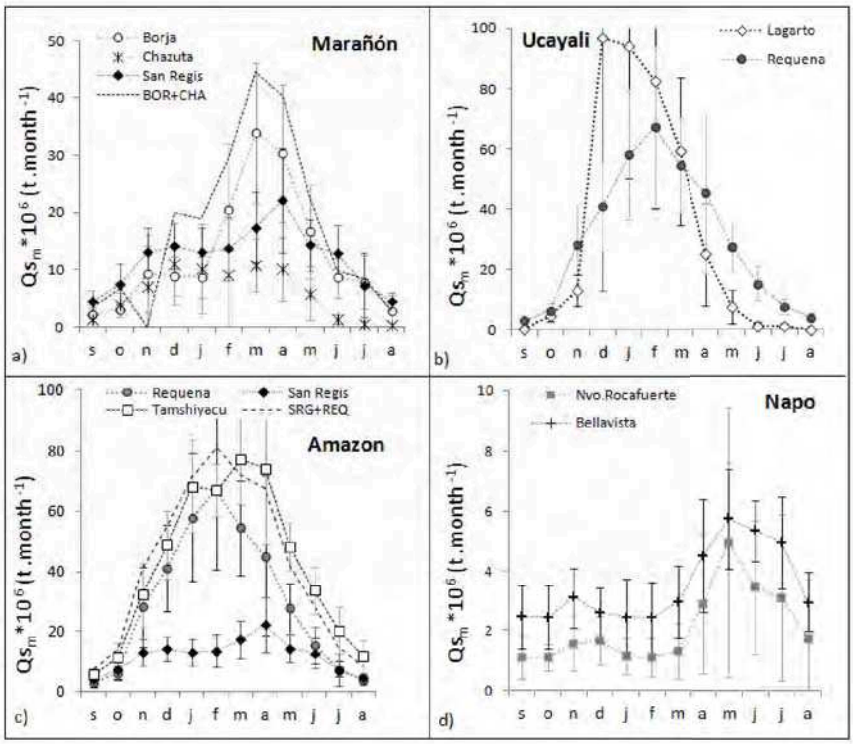

Figure 9. *Relation $[TSS]_m$ vs Q_m for a) Andean piedmont stations and b) plain stations. Errors bars represent the standard deviation.*

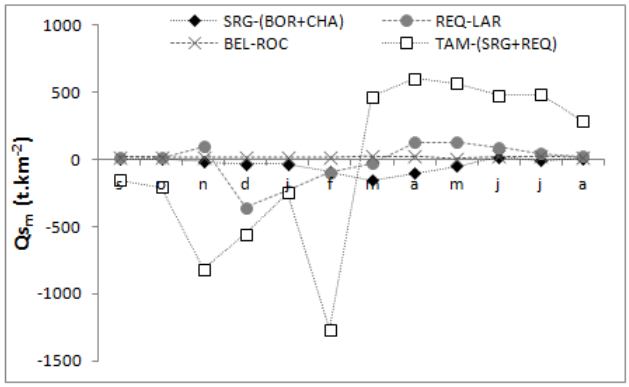

Figure 10. *Variability-specific sediment yields of the non-monitored areas at the monthly scale, values normalized by the surface basins for: the Amazon (TAM-(SRG-REQ)), Ucayali (REQ-LAG), Marañón (SRG-(BOR-CHA) and Napo (BEL-ROC) basins.*

M1 and 150% with M2), indicating a non-negligible sedimentation rate in the Marañón plain. For the Ucayali River, annual suspended yield between Lagarto and Requena does not show significant differences.

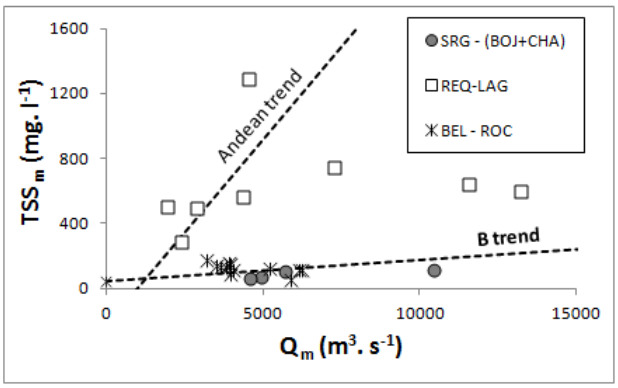

Figure 11. *Erosion and deposition rates of the non-monitored areas of the Marañón, Ucayali and Napo rivers. B trend = 0.013+48.62, r2=0.88.*

Table 2. Mean annual water discharges and comparison of the yields suspended sediments for three methods. Percentage contribution to total output ratio of Peru basin.

COD	Discharge			Yield Suspended Sediments					
				M1		M2			M3
	$m^3\ s^{-1}$	%	l $year^{-1}$ km^2	$*10^6$ t $year^{-1}$	%	$*10^6$ t $year^{-1}$	%	t $year^{-1}$ km^2	$*10^6$ t $year^{-1}$
BOR	5 018	14	44	132	22	153	28	1335	149
CHA	2 984	9	43	73	12	71	13	1037	51
NY	2 187	6	52	9	2	7	1	176	-
LAG	6 544	19	34	400	67	386	71	2024	378
REQ	11 415	33	33	395	66	359	66	1036	-
SRE	16 175	47	45	173	29	144	27	399	-
TAM	28 090	81	39	556	93	499	92	694	-
BEL	6 609	19	66	45	7	42	8	419	-
ROC	2 226	6	81	21*	3	25	5	920	19
BEL+TAM	**34 699**	**100**	**42**	**601**	**100**	**541**	**100**	**660**	

*Armijos et al.,2013

Discussion

The univocal trend between $[TSS]_m$ and Qm for Andean tributaries suggests that erosion processes in Andes are transport limited at the monthly scale, meaning mainly controlled by water flow (sediments are available and sediments flux depends only on the transport capacity of the river). This has been already observed in other mountain ranges(Dadson et al., 2003), where the combined effects of intensive rainfall, steep topography and seismicity provide sufficient material to rivers. The observation of a unique monthly rating curve is an original result for a basin of such size and for the north-to-south expanse area. A simple linear rating curve could be applied to Andean tributaries to deduce $[TSS]_m$ and Qm despite different climatic, vegetation, soil and lithology contexts.

Further analysis on the $[TSS]_m$ of Bolivian and Ecuadorian Andean tributaries are necessary to confirm this important result. On the plain, the $[TSS]_m$ vs Q_m relati-

onship appears to depend on the climatic regime. On the Napo and Marañón plains, the $[TSS]_m$ exhibits an average linear rating curve with a coefficient ten times lower than that for Andean tributaries, despite weak dispersion induced by modest hysteresis effects. Taking into account **i)** the low sediment production of the Tiger River, **ii)** the low constant $[TSS]_m{}^*$ value and **iii)** the water discharge at ROC, BOR and CHA which corresponds to half the total water discharge measured on the plain, areas lacking monitoring of the Napo and Marañón basins act as a constant rate dilution process for any Q_m range.

Therefore, the coefficient of the linear rating curve decreases along the Napo and Marañón rivers. Note that all areas lacking monitoring in the Marañón and Napo basins are between 1°S and 4°S latitude with the same equatorial climatic regime, which explains the synchronous variability of the water discharge for both monitored and non-monitored areas in this part of the Amazon basin. The Ucayali River presents a different scheme with a well-developed hysteresis between $[TSS]_m$ and Q_m. For this river, the $[TSS]_m{}^*$ are constant and smaller than at the upstream part of the Ucayali basin (LAG). However Q_m^* shows a phase difference of two months with Q_m at LAG, induced by non-synchronous rainfall rate variability between the south tropical and equatorial climates (Espinoza et al., 2006). This phase difference in water discharge dynamics causes a seasonal dilution rate that decreases the $[TSS]_m$ value as part of the annual cycle and generates a hysteresis trend between $[TSS]_m$ and Q_m. Because more than 60% of the $[TSS]$ from the Amazon River comes from the Ucayali River, this hysteresis is also observed in this river, but with lesser amplitude due to relatively constant $[TSS]$ inputs from the Marañón River.

Except for the hysteresis dynamic process, the monthly sediment production Qs_m in the upper Amazon basin in Peru may correspond to a simple scheme with two types of sediment sources or processes. One dominant process is in the Andes with a quadratic relationship with Q_m and a second dominant process is in the plains with a linear relationship with Q_m. Currently there are no sufficient observations to define these processes. Based on the non-negligible erosion and deposition rates observed at the confluence between the Marañón and the Ucayali rivers, we may assume that the wide floodplains of these two rivers play a regulatory role in Amazon River sediment production. Indeed, in this floodplain, topography, vegetation, slopes and hydraulic conditions are very different than those in Andes and can be the place of specific erosion and, above all, deposition processes. Annual mass balance budgets reveal erosion in the non-monitored area of the Napo River, significant sedimentation in the Marañón floodplain and neither erosion nor sedimentation in the Ucayali floodplain. Note that inputs from other Andean non-gauged tributaries such as the Morona, Pastaza, and Patchitea rivers, may increase our sedimentation rate estimation inside the Marañón and Ucayali basins.

The annual erosion rates do not exhibit a particular relationship with specific water discharge (Table 2), which demonstrates that another variable exists that controls the

rate of erosion apart from the variable annual flow. Presently, there are no data that allow us to understand this observation. A greater spatial and temporal resolution precipitation data set (including rainfall intensity) in addition to a more detailed analysis of the local topography and seismicity would be necessary.

Conclusion

The data collected by the Hybam project have allowed this study to be realized, which is a contribution to the scientific knowledge of the Amazonian Peruvian basin, where few studies have been conducted on sediment yields. A quantification of the discharge and sediment yields has been performed out on a monthly and yearly basis for the upper and lower basins of the Peruvian Amazonian region. A contribution of this work has is the demonstration of a simple relationship between $[TSS]$ and discharge for the stations in the Andean region. On the plains, the dilution effect of the concentrations can create hysteresis in this relationship on a monthly basis, which means that a gap exists between the discharge sources and sediment yields for the same basin.

The major part of the sediment yield is from the Andes, and the plain can act as a diffuse source or, more importantly, as a zone of sedimentation of approximately 20 to 50% of the charge coming from the Andes. The same figures were found by Guyot et al. (1994) in the high basin of the Mamore River in Bolivia. Comparing the results found in a first estimation in 2007 by Guyot et al., we can say with more confidence that the Marañón Plain is a zone of sedimentation rather than an erosion plain. To estimate the real sedimentation rate, the suspended sediment yield coming through the Pastaza and Morona rivers needs to be quantified.

The annual rate of sedimentary flux that comes from the Peruvian basin is 541 $*10^6$ t year $^{-1}$ which corresponds to 660 t year^{-1} km^{-2} ; with 70% coming from the southern region of the basin.

Acknowledgements This study was performed with support from the Servicio Nacional de Meteorología e Hidrología del Perú (SENAMHI) and the Institut de Recherche pour le Dèveloppement (IRD). We would like to thank participants in the ORE-HYBAM project from Peru (UNALM) and each of the observers of the gauging stations for his daily work and France (GET Toulouse).

Bibliography

Armijos, E., Laraque, A., Barba, S., Bourrel, L.,Ceron, C., Lagane, C., Magat, P., Moquet, J.S., Pombosa, R., Sondag, F., Vera, A. Guyot , J.L. submitted. Yields of suspended sediment and dissolved solids from the Andean basins of Ecuador. Hydrological Sciences Journal HSJ-2011-0219.

Beighley, R. E., Eggert, K. G., Dunne, T., He, Y., Gummadi, V., Verdin, K. L. Simulating hydrologic and hydraulic processes throughout the Amazon River Basin. Hydrological Processes.Vol.23, Issue 8, pages 1221–1235, 15 April 2009.

Bernal, C., Christophoul, F., Darrozes, J., Soula, J.C., Baby, P., Burgos, J. Late Glacial and Holocene avulsions of the Rio Pastaza Megafan (Ecuador–Peru): frequency and controlling factors. International Journal of Earth Sciences. Geol Rundsch .2011. 100:1759–1782.DOI 10.1007/s00531-010-0555-9.

Dadson, S., Hovius, N.,Chen, H., Dade, W., Hsieh, M.L.,Willett, S., Hu, J.C., Horng, M.J., Chen, M.C., Stark,C., Laguel, D., Lin, J-C. 2003. Links between erosion, runoff variability and seismicity in the Taiwan orogen. Nature. Vol. 426. 6967.pag. 648-51.

DGAS (Dirección General de Aguas y Suelos).1995 Hacia una gestión integrada de los recursos hídricos en el Perú. Ministerio de Agricultura, Perú.

Dumont, J.F., Garcia, F., Fournier, M., 1992. Registros de cambios climáticos por los depósitos y morfologías fluviales en la Amazonia occidental. Paleo ENSO Records. Internalcional Symposium. Lima March 1992. In Ortlieb Macharé (Eds). Orstom-Concytec. Lima 1992, p. 87-92.

Espinoza, J.C., Fraizy, P., Guyot, J.L., Ordoñez, J., Pombosa, R., Ronchail, J. 2006. La variabilité des débits du rio Amazonas au Pérou. In: IAHS (Editor), Fifth FRIEND World Conference held Climate Variability and Change–Hydrological Impacts. Vol 308, La Havana, Cuba, pp. 424-429.

Espinoza, J.C., Ronchail, J., Guyot, J.L., Cocheneau, G., Filizola, N., Lavado, W., De Oliveira, E., Pombosa, R., Vauchel, P. 2009a. Spatio-temporal rainfall variability in the Amazon Basin Countries (Brazil, Peru, Bolivia, Colombia and Ecuador). International Journal of Climatology, 29, 1574-1594.

Espinoza, J.C., Guyot, J.L., Ronchail, J., Cochonneau, G., Filizola, N., Fraizy, P., De Oliveira, E., Ordoñez, J., Vauchel, P. 2009b.Contrasting regional discharge evolutions in the Amazon Basin (1974–2004). J Hydrol 375:297–311.

Espinoza, J.C ., Lengaigne, M., Ronchail, J., Janicot, S. 2011. Large-scale circulation patterns and related rainfall in the Amazon Basin: a neuronal networks approach. Earth and Environmental Science. Climate Dynamics. DOI 10.1007/s00382-011-1010-8.

Filizola, N., Guyot, J.L. 2009. Suspended sediment yields in the Amazon basin: an assessment using the Brazilian national data set. Hydrological Processes 23, 3207–3215. DOI: 10.1002/hyp.7394

Guyot, J.L., Bourges J., Cortez J., 1994. Sediment transport in the Rio Grande, an Andean river of the Bolivian Amazon drainage basin. IAHS Publ n° 224 (Proceedings of the Camberra Symposium).

Guyot, J.L., Bazan, H., Fraizy, P., Ordonez, J., Armijos. E., Laraque. A. 2007. Suspended sediment yields in the Amazon basin of Peru, a first estimation.. HS2005 -Water quality and sediment behaviour of the future: Predictions.

Kvist, L.P.,Nebel, G. 2000.Bosque de la llanura aluvial del Perú: Ecosistemas, habitantes y uso de los recursos. Folia Amazónica. Vol 10. Instituto de Investigaciones de la Amazonia Peruana.

Laraque, A., Ronchail, J., Cochonneau, G., Pombosa, R., Guyot, J.L. 2007.Heterogeneous distribution of rainfall and discharge regimes in the Ecuadorian Amazon basin. Journal of Hydrometeorology 8:1364–1381.

Molnar, P. 2003. Nature, nurture and landscape Geomorphology.Nature.Vol 426 .11 December 2003.

Moatar, F., Person, G., Meybeck, M., Coynel, A., Etcheber, H., Crouzet, P.H. 2006. The influence of contrasting suspended particulate matter transport regimes on the bias and precision of flux estimates . Science of the Total Environment .370 : 515-531.

Mueller, D.S., Wagner, C.R. 2009. Measuring Discharge with Acoustic Doppler Current Profilers from a Moving Boat. USGS Techniques and Methods 3- A22.

Phillips, J.M., Webb, B.W., Walling, D.E., Leeks, G.J.L.1999. Estimating the suspended sediment loads of rivers in the LOIS study area using infrequent samples. Hydrological Processes. Special Issue: River Basin Sediment Dynamics.Vol. 13, Issue 7, pages 1035–1050. May 1999.

Rabus, B., Eineder, M., Roth, A., Bamler, R. 2003. The Shuttle Radar Topography Mission a new class of digital elevation models acquired by spaceborne radar. Photo and Rem. Sen. 57, 241-262.

Roddaz, M., Brusset, S., Baby, P.,Hérail, G., 2006. Miocene tidal-influenced sedimentation to continental Pliocene sedimentation in the forebulge-backbulge depozones of the Beni-Mamore foreland Basin (northern Bolivia). Journal of South 1290 American Earth Sciences, 20(4), 351-368.

Trigg, M., Wilson, M.D., Batesa, P.D., Horritt, M.S., Alsdorf, D.E., Forsberg, B.R., Vega, M.C. 2009. Amazon flood wave hydraulics. Journal of Hydrology. Vol. 374, Issues 1-2, 30 July 2009, Pages 92-105 doi:10.1016/j.jhydrol.2009.06.

Vauchel, P. 2009. Hidromesad: Logiciel de gestión y tratamiento de datos hidrológicos y de sedimentos. Informe Técnico Proyecto Hybam Lima-Perú.

Walling, D. E. 2006. Human impact on land–ocean sediment transfer by the world's rivers. Geomorphology. Vol.79, Issues 3-4, 30 September 2006, Pages 192-216.37th Binghamton Geomorphology Symposium.

Willet, S. 1999. Orogeny and orography: The effects of erosion on the structure of mountain belts. Journal of Geophysical Research. Vol 104.No.B12 pages 28,957-28981, December 10, 1999.

Capítulo 4

Nova estimação do fluxo sedimentário no rio Amazonas

New estimates of suspended sediment flux in the Amazon River link coarse sediment flux to climate variability

Resumo

A biodiversidade e produtividade ecológica e da floresta das várzeas na bacia Amazônica esta baseada em nutrientes e matéria orgânica associada aos sedimentos em suspensão. Neste contexto, destaca-se a importância de quantificar os sedimentos em suspensão no rio Amazonas. As analises de 586 amostras obtidas durante o período 1995-2013 indicam que os sedimentos em suspensão do baixo Amazonas estão compostos de dois tipos de sedimentos em função de sua granulometria: sedimentos finos (15 µm) e sedimentos grosseiros de (150 µm), e cada tipo de sedimento apresenta uma diferente taxa de transporte durante o ano hidrológico. O fluxo de sedimentos no baixo Amazonas é de 1100 Mt ano^{-1} $\pm$ 25%, dos quais 60% correspondem ao fluxo de sedimentos finos e 40% correspondem ao fluxo de sedimentos grosseiros. Existem evidencias da sensibilidade dos sedimentos frente a variabilidade climática, mas esta depende da distribuição espacial e sazonal das precipitações. Pode-se observar que existe um incremento dos sedimentos finos durante os anos El Niño assim como também um aumento de sedimentos grosseiros durante os anos La Niña e em episodios do dipolo do Altlântico Tropical.

Résumé

La biodiversité et la productivité de la forêt amazonienne dans la plaine d'inondation est basée sur les nutriments et la matière organique associés aux sédiments en suspension. Dans ce contexte, nous mettons en lumiére l'importance d'une quantification des sédiments en suspension de l'Amazone. L'analyse de 586 échantillons collectés entre 1995 et 2013 montre que la concentration de sédiments en suspension sur la basse Amazone est composée de deux populations de sédiments de tailles différentes : sédiments fins (10 µm) et grossiers (250 µm). Chaque population présente un taux de transport différent tout au long de l'année hydrologique. Le flux de sédiments en suspension de la basse Amazone est estimé à 1100 Mt an^{-1} $\pm$ 25%, dont 60% est constitué du flux de sédiments fins et 40% de celui des grossiers. Nous mettons en évidence la sensibilité du flux sédimentaire à la variabilité climatique quoique cette sensibilité dépende du type de sédiment, et de la distribution spatiale des précipitations sur le bassin et de leur saisonnalité. De fait, le flux de sédiments grossiers augmente lors des années caractérisées par des épisodes froids dans la zone du Pacifique central équatorien (La Niña) et pendant les annés do dipole do Atlantique Tropical.

New estimates of suspended sediment flux in the Amazon River link coarse sediment flux to climate variability

E. Armijos[1,2*], N. Filizola[3], A. Crave[4], J.C. Espinoza[5], P. Fraizy[6], P. Vauchel,[6], R. Espinoza[7], J.M. Martinez[6], P. Ribeiro [1], R.A. Dos Santos [3,8], G. Cochonneau [6], P. Fonseca[1], E. De Oliveira[9], W. Santini[6] and J.L. Guyot[6].

1 – Programa de Pós-graduação CLIAMB, Instituto Nacional de Pesquisas da Amazônia (INPA), Universidade do Estado do Amazonas (UEA), Manaus, Brasil.
2 – Université Paul Sabatier, Toulouse, France.
3 – Universidade Federal do Amazonas (UFAM), Manaus, Brasil.
4 – Géoscience Rennes, CNRS UMR 6118, Rennes, France.
5 – Subdirección de ciencias de la atmósfera e hidrósfera-Instituto Geofísico del Perú (IGP), Lima, Perú.
6 – Géoscience Environnement Toulouse (GET- CNRS, IRD, Université de Toulouse), Toulouse,France.
7 – Géoscience Environnement Toulouse (IRD/GET), Toulouse, France.
8 – Universidad Nacional Mayor de San Marcos, Lima, Perú.
9 – Serviço Geológico do Brasil (CPRM), Manaus,Brasil.
10 – Agência Nacional da Agua (ANA), Brasília, Brasil.

Abstract

The biodiversity and productivity of the Amazon floodplain depend on nutrients and organic matter transported with suspended sediments *(1)*. However, there are still fundamental unknowns about how hydrological and climatic variability influence sediment flux in the Amazon River. To address this gap we analyzed sediment samples collected every ten days from 1995-2014. We found a bimodal distribution of sediment sizes, with distinct fine (15 µm) and coarse sediments (150 µm), which followed contrasting seasonal and long-term patterns. By taking these dynamics into account, we estimate the suspended sediment flux of the lower Amazon River is 1100 Mt year^{-1} ±25%, of which 60% is fine and flux and 40% is coarse suspended flux. We establish that suspended sediment flux is linked to climate, with higher coarse suspended sediment flux during cool episodes in the central equatorial Pacific (La Niña) and the warm phase of the Tropical South Atlantic.

The Amazon River accounts for almost of fifth of global freshwater discharge *(2)* and supplies the majority of the Atlantic Ocean's sediment *(3, 4)*. The water and sediment flowing through Amazon carry carbon and nutrients that fuel productivity on the immense Amazon floodplain resulting in globally relevant fluxes of organic carbon *(5)*, water vapor *(6, 7)*, and CO2 *(8)*. The expansion of hydropower and agriculture has put severe pressure on the Amazon basin, altering discharge and sediment flux *(9, 10)*. Indeed, 151 new dams are currently planned on five major Andean tributaries *(11)*. As such, the Amazon Basin is a critical and strategic zone for studying the effects of climate change and direct human disturbance on water, sediment, and biogeochemical

fluxes.

The Amazon Basin includes regions with contrasting topography, climate, and hydrology, sediment flux depends on the timing and amount of regional discharge and the availability of sediment sources. Tributaries from the Andes supply the majority of sediments, nutrients, and organic matter to the main stem of the Amazon *(1 and 12-16)*. As the Amazon nears the ocean, it receives influx from the Peruvian, Colombian and Ecuadorian Andes in the Solimões River (contributing 60% of annual average discharge), the Peruvian and Bolivian Andes in the Madeira River (15% of discharge), and the Guyana shield in the Negro River (14% of discharge; *17*). The Solimões and Madeira rivers are rich in suspended sediment, while the Negro River is largely sediment-free. Peak rainfall occurs from March to May in the northern region (the Negro basin), and from December to February in the southern and western regions *(7)*. These differences in rainfall produce a flood period on the main stem from May to June, and a low water period from September to November.

Previous studies have shown that Amazon River discharge is related to climate variability *(18-19)*, however, the relationship between the interannual climate variability and sediment flux in the Amazon is unknown. There has been an intensification of extreme hydrological events in the Amazon basin during the last decades linked to anomalies in the surface temperature of the Pacific and Atlantic Oceans. El Niño conditions (1998, 2003) or warm episodes in the Tropical North Atlantic (2005, 2010) have been associated with extreme droughts, while La Niña or warm conditions in the Tropical South Atlantic (1999, 2009, 2012) are related to extreme floods *(20-29)*.

Sediment flux in the Amazon is poorly constrained with current estimates of sediment flux varying by a factor of two (600 to 1300 Mt year^{-1}) at the most downstream Óbidos gauging station *(30-34)*. The difference in the estimates is the difficulty in performing measurements with the traditional methods due to the large scale of the cross section and also high cost for monitoring in long-term. To explore the possible link between climate and sediment flux, we used samples obtained every ten days during twenty years of sediment monitoring at the Óbidos gauging station from 1995 to 2014 (Fig 1A,1C). This dataset of 622 samples provides unprecedented temporal resolution and enables improved estimates of sediment load and the identification of climatic controls. One of our main findings is that the suspended sediment at Óbidos has two

well-defined sediment size fractions (fine sediment of 15 µm and coarse sediment of 150 µm), which show contrasting transport dynamics throughout the hydrological year (Fig. 1B).

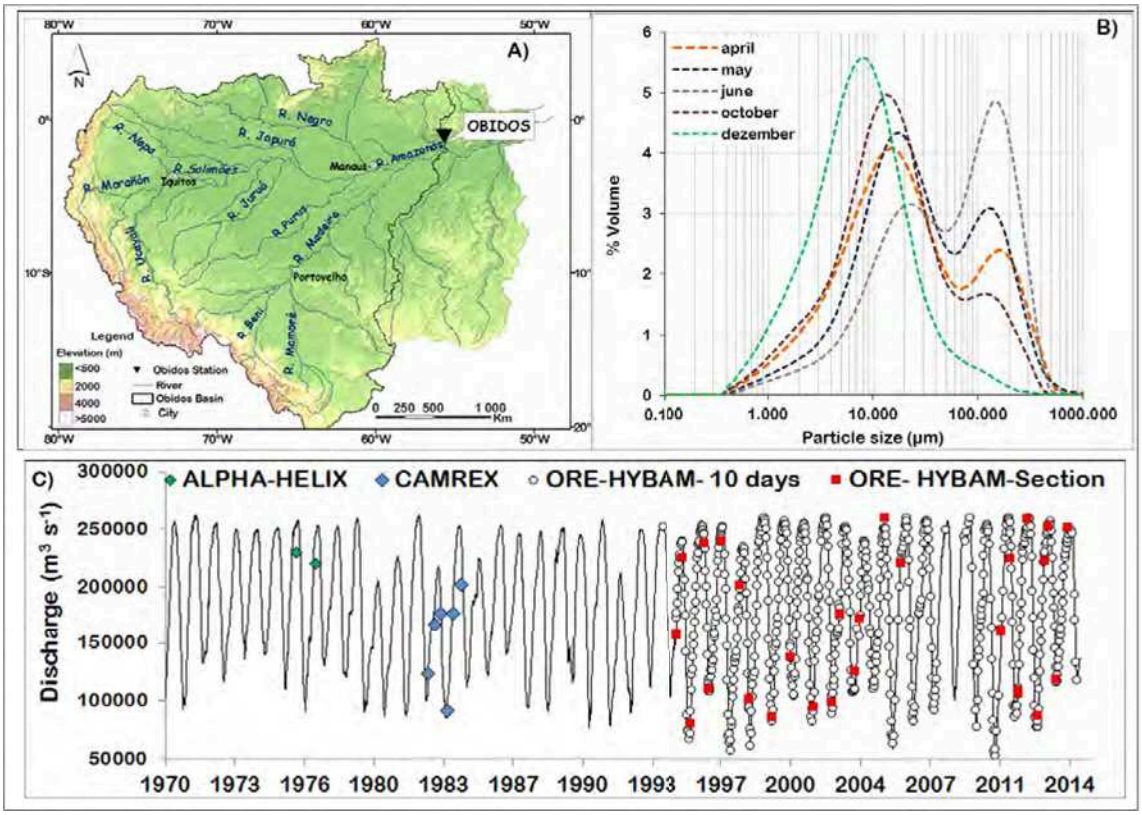

Figure 1. *A*) Amazon basin and Óbidos station gauging location; *B*) Particle size at Óbidos gauging station for different months of the hydrologic regime and *C*) Temporal records of the measured suspended sediment load at Óbidos gauging station: green diamond = ALPHA HELIX project (1976-1977); blue diamond = CAMREX project (1982-1984). White circles are surface suspended sediments and red squares are suspended sediment measurement in cross section = SO-HYBAM observatory (1995-2014). .

This observation substantially changes the manner of quantifying sediment fluxes and elucidates how sediment yield in the Amazon River responds to annual and interannual variability in rainfall and discharge.

Typically, to calculate suspended sediment flux, the empirical relationship between sediment concentration and water discharge is used. For the Amazon River at the Óbidos gauging station, this relationship shows a clockwise hysteresis *(33-35)* meaning sediment concentration is higher during the rising limb of the hydrograph than at the equivalent discharge during the falling limb. By analyzing the monthly average of the fine and coarse sediment concentrations separately, we found that this hysteresis

is caused by variability in fine sediment load, while the coarse sediment load follows a simpler power law trend (Fig. 2 A,B,C). Two phenomena control the degree of hysteresis in fine sediment flux. First, peak sediment flux from the Madeira and Solimões rivers occurs during the rising limb (February-March) approximately three months before peak discharge in these rivers. Second, influx of the sediment-free water from the Negro River in May-June dilutes total suspended sediment concentration during the falling limb.

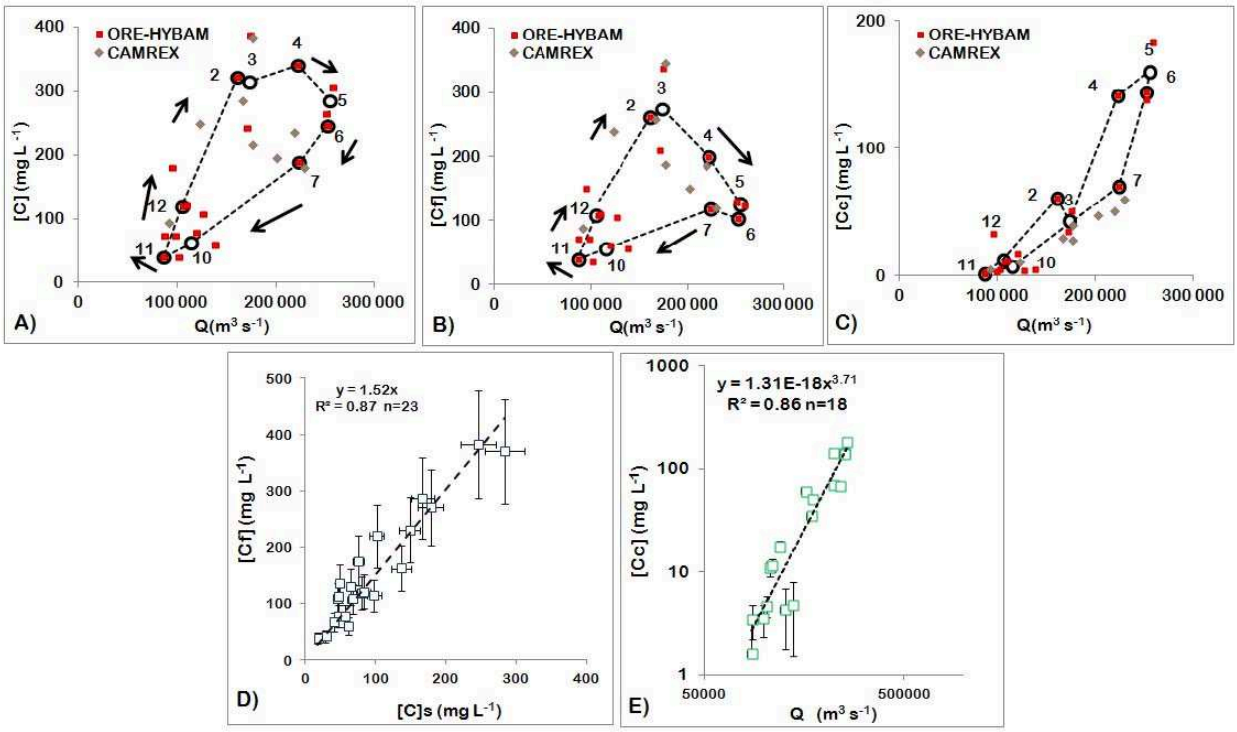

Figure 2. Relationship between mean monthly suspended sediments and discharge (black circles) at Óbidos: A) Total suspended sediments ([C]); B) Fine suspended sediments ([Cf]); C) Coarse suspended sediments ([Cf]); red square-measure of SO-Hybam observatory and brown diamonds measure of CAMREX Project; D) Relationship between fine suspended sediment ([Cf]) and surface suspended sediment ([Cs]); E) Relationship between coarse suspended sediment ([Cc]) and discharge measure, uncertainty bar more small that of symbol.

Given these differences in fine and coarse sediment transport, we propose a new approach to calculate the suspended sediment flux in the Amazon. First, we find that fine sediment concentration in the river cross section is strongly correlated with total suspended sediment concentration at the water surface (r = 0.87, σ = 12%; Fig. 2D), allowing the estimation of fine sediment flux from easily collected surface samples and discharge *(33)*. Because the Óbidos watershed is so large, changes in fine sediment con-

centration are slow on a percentage per day basis, meaning linear interpolation between measurements every 10 days introduces little error. The strong correlation between coarse sediment flux and discharge allows us to calculate the coarse sediment flux using the empirical rating curve (r = 0.9, σ = 16%; Fig. 2E). The sum of the fine and coarse fluxes gives a total sediment flux at Óbidos of 1100 ±25% MT year^{-1}, of which 60% is fine suspended sediment flux and 40% is sandy suspended sediment flux (Table 1).

Table 1. Suspended sediments flux at Óbidos gauging station. Qs_f and Qs_c = fine and coarse suspended sediments flux respectively

Discharge * 10^3 m^3 s^{-1}	Surface * 10^3 km^2	Sediment flux * 10^6 t year $^{-1}$			Specify Sediment flux t $km^{-}2$ $year^{-1}$		
		Qsf	Qsc	Qs	Qsf	Qsc	Qs
180	4667	650	450	1100	139	96	235

Using this method, we found that fine and coarse fluxes have very different seasonal signals, with fine sediment flux peaking from February to March and highest coarse sediment flux from April to June. As expected, the bulk of suspended sediment load comes from the Madeira and Solimões Rivers, though the input of sand in the flood period from the Negro River cannot be discounted (Fig. 3A).

These new estimates reveal three regimes of suspended sediment transport on the Amazon. First, from December to March there are high concentrations of both fine and coarse sediments due to rainfall in the Andean sub-basins (the Solimões and Madeira basins; Fig. 3B). Second, there is a period of predominantly coarse suspended sediment flux during the flood period from April to June due to re-suspension of the coarse particles from the riverbed, and dilution from the sediment-poor Negro River. Third, suspended sediment flux is low during the low-flow period from August to October (Fig. 3B).

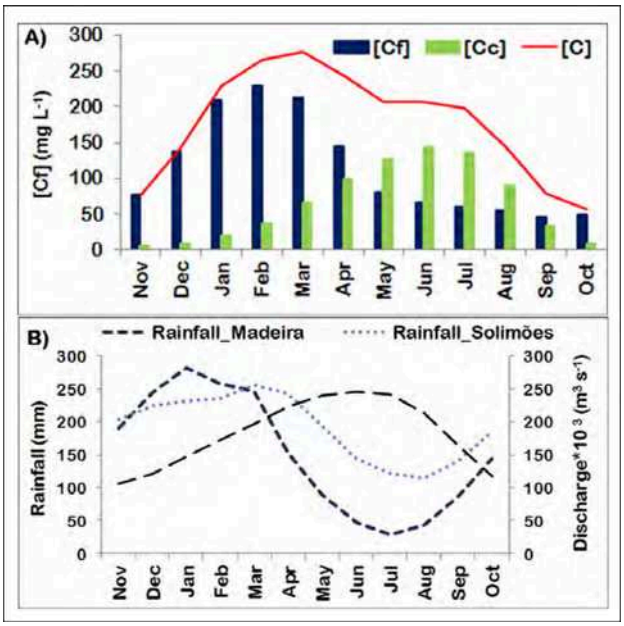

Figure 3. A) Mean monthly rainfall in Solimões basin (1978-2004; No.stations=281) and Madeira basin (1978-2004; No.station=209) and mean monthly discharge of Amazon basin at Óbidos gauging station (1968-2014) adapted from reference (2); B) Temporal suspended sediment concentration of [Cf] and [Cc] and [C].

We also found that coarse and fine sediment transport is related in different ways with regional climate. Based on correlation analysis between sea surface temperature *(36)* and coarse sediment flux, we found that higher coarse sediment flux occurs during cool conditions in the central equatorial Pacific (La Niña events). In addition, an increase of 38% in the coarse sediments flux was also observed in 2009 (Fig. 4A), a year characterized by extreme floods related to warm episodes in the Tropical South Atlantic *(29, 30)*. On the other hand, a decrease of up to 40% of the coarse sediments flux was recorded during warm conditions in the central equatorial Pacific (El Niño years, Fig. 4A). The significant negative relationship between the sea surface temperature in the central equatorial Pacific and coarse sediment fluxes ($r = -0.70$, $p<0.001$, Fig. 4B) suggests that increased discharge from cooler Pacific temperature leads to an increase in the hydraulic capacity to transport coarse sediment.

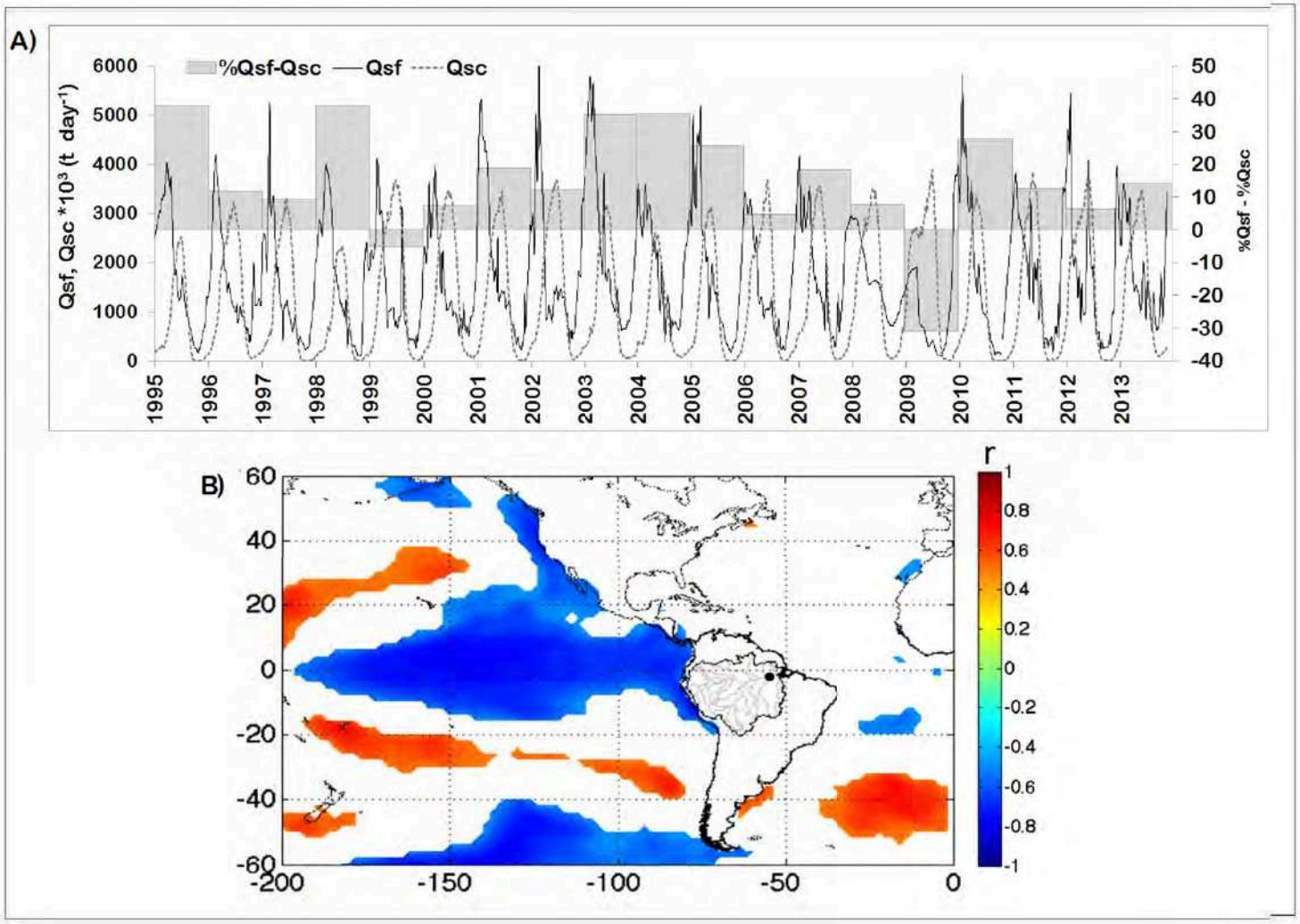

Figure 4. A) Daily sediments flux: black line corresponds to fine suspended sediments flux, gray dashed line corresponds to the coarse sediments flux and the gray bars correspond to the percentage of fine sediments flux in relation to coarse sediments flux. B) Coefficient of correlation between SST and coarse sediments flux for the 1995-2014 period computed for the January-December. Only values with $p<0.05$ are plotted. The Amazon basin and the location of Óbidos station are indicated whith a black line and a black dot, respectively

Based on our dataset (1995-2014), we found no relationship between the maximum and minimum fine sediments flux and the extreme hydrological events (r = 0.11 and 0.02). This results could be due to differences in rainfall regime and the different forcing act separately in the main tributaries of Amazon River (Solimões, Madeira and Negro Rives). Indeed, 2005 and 2010 droughts had different effects, while 2005 was more intense in southwestern Amazonia while 2010 was stronger in central and eastern Amazonia *(37)*. However in locale scale e.g. in the Bolivian Amazon, for instance (Beni and Mamoré rivers), it is observed the accumulation of fine sediments during the floods associated with La Niña events *(38)*.

In summary, the suspended sediment flux in the Amazon River at Óbidos shows a bimodal size distribution, with fine sediments near 15 µm accounting for 60% of annual sediment load and coarse sediments of 150 µm accounting for 40%. Coarse sediment flux was strongly related with discharge, meaning that this part of the sediment flux is correlated with the climatic oceanic indices that control Amazon basin hydrology. The relationship between the fine sediment flux sediment and discharge presents a more complex hysteresis trend related to the different production phases of the main fine sediment sources over the Amazon basin. To answer the question of what controls fine sediment flux in the Amazon, accurate time and spatial monitoring of the fine sediment on the Amazon mainstem and major sub-basins are required. We suggest that the methodology from this study be applied in the Andean rivers of the Amazon basin, namely the separation of the granulometric mode to explore the relationships with hydrology and climatic indices.

References and Notes

1. M. McClain, R. Naiman., Andean influences on the biogeochemistry and ecology of the Amazon River.*BioScience*. **58**, 325-338 (2008).

2. J. Callède, et al., Les apports en eau de l'Amazone à l'Océan Atlantique. *Revue des sciences de l'eau/Journal of Water Science*. **23**, 247-273 (2010).

3. J. P. Syvitski, S. D. Peckham, R. Hilberman, T. Mulder, Predicting the terrestrial flux of sediment to the global ocean: a planetary perspective. *Sedimentary Geology*. **162**, 5-24 (2003).

4. J. D. Milliman, K. L. Farnsworth, River discharge to the coastal ocean: *a global synthesis* (Cambridge University Press, 2011).

5. P. Moreira ˘ Turcq, et al., Exportation of organic carbon from the Amazon River and its main tributaries. *Hydrological Processes*. **17**, 1329-1344. (2003).

6. E. Salati, P. B. Vose, Amazon basin: a system in equilibrium. *Science*. **225** (1984).

7. J.C. Espinoza, et al., Spatio temporal rainfall variability in the Amazon basin countries (Brazil, Peru, Bolivia, Colombia, and Ecuador). *International Journal of Climatology*. **29**, 1574-1594 (2009).

8. G. Abril, et al., Amazon River carbon dioxide outgassing fuelled by wetlands. *Nature*. **505**, 395-398 (2013).

9. E. A. Davidson, et al., The Amazon basin in transition, *Nature*. **481**, 321-328 (2012).

10. J. Ferreira, et al., Brazil's environmental leadership at risk, *Science*. **346**, 706-707 (2014).

11. M. Finer, C. Jenkis, Proliferation of hydroelectric dams in the Andean Amazon and implications for Andes-Amazon connectivity, *Plos one*. **7**, e35126 (2012).

12. E. Armijos, et al., Suspended sediment dynamics in the Amazon River of Peru.*Journal of South American Earth Sciences*. **44**, 75-84 (2013).

13. E. Armijos, et al., Yields of suspended sediment and dissolved solids from the Andean basins of Ecuador. *Hydrological Sciences Journal*. **58**, 1478-1494 (2013).

14. R. Espinoza Villar, et al., A study of sediment transport in the Madeira River, Brazil, using MODIS remote-sensing images. *Journal of South American Earth Sciences*. **44**, 45-54 (2013).

15. J. S. Moquet, et al., Cl and Na Fluxes in an Andean Foreland Basin of the Peruvian Amazon: An Anthropogenic Impact Evidence. *Aquatic Geochemistry*. **20**, 613-637 (2014).

16. W. Santini et al., Sediment budget in the Ucayali River basin, an Andean tributary of the Amazon River. *IAHS Publ*. **367** (2014).

17. N. Filizola, J.L. Guyot, Suspended sediment yields in the Amazon basin: an assessment using the Brazilian national data set. *Hydrological Processes*. **23**, 3207-3215 (2009).

18. J. C. Espinoza, et al., Contrasting regional discharge evolutions in the Amazon basin (1974–2004). *Journal of Hydrology*. **375**, 297-311 (2009).

19. J. Callède, et al., Evolution du débit de l'Amazone à Óbidos de 1903 à 1999. *Hydrological Sciences Journal.***49**, 85-97 (2004).

20. J. C. Espinoza, et al., Climate variability and extreme drought in the upper Solimões River (western Amazon Basin): Understanding the exceptional 2010 drought. *Geophysical Research Letters.* **38** (2011).

21. M. Gloor, et al., Intensification of the Amazon hydrological cycle over the last two decades. *Geophysical Research Letters.* **40**, 1729-1733 (2013).

22. J. A. Marengo, J. A, et al. Two Contrasting Severe Seasonal Extremes in Tropical South America in 2012: Flood in Amazonia and Drought in Northeast Brazil. *Journal of Climate.* **26**, 9137-9154 (2013).

23. J.C. Espinoza, et al., From drought to flooding: understanding the abrupt 2010-11 hydrological annual cycle in the Amazonas River and tributaries. *Environmental Research Letters.* **7**, 024008 (2012).

24. J. A. Marengo, J. Tomasella, W. R. Soares, L. M. Alves, C. A. Nobre, Extreme climatic events in the Amazon basin. *Theoretical and Applied Climatology.* **107**, 73-85 (2012).

25. J.A. Marengo, J.C.Espinoza, Extreme seasonal droughts and floods in Amazonia: causes, trends and impacts. *International Journal of Climatology.* **1097**, (2015).

26. J. A. Marengo, et al., The drought of Amazonia in 2005. *Journal of Climate.* **21**, 495-516 (2008).

27. J. A. Marengo, et al., The drought of 2010 in the context of historical droughts in the Amazon region. *Geophysical Research Letters.* **38**, L12703 (2011).

28. J. C. Espinoza, et al., Climate variability and extreme drought in the upper Solimões River (western Amazon Basin): Understanding the exceptional 2010 drought. *Geophysical Research Letters.* **38** (2011).

29. J. A. Marengo, J. Tomasella, W. R. Soares, L. M. Alves, C. A. Nobre, Extreme climatic events in the Amazon basin. *Theoretical and Applied Climatology.* **107**, 73-85 (2012).

30. J.A. Marengo, J.C. Espinoza, Extreme seasonal droughts and floods in Amazonia: causes, trends and impacts. *International Journal of Climatology.* **1097**, (2015).

31. R. J. Gibbs, Amazon River: Environmental factors that control its dissolved and suspended load. *Science.* **156**, 1734-1737 (1967).

32. R. H. Meade, et al., Sediment loads in the Amazon River. *Nature.* **278**, 161-163 (1979).

33. R. H. Meade, T. Dune, J.E. Richey, U. Santos, E. Salati, Storage and remobilization of suspended sediment in the lower Amazon River of Brazil. *Science.* **228**, 488-490 (1985).

34. J. L. Guyot, N. Filizola, A. Laraque, Régime et bilan du flux sédimentaire de l'Amazone à Óbidos (Pará, Brésil) de 1995 à 2003. Sediments Budgets 1. *IAHS Publ.* **291**, 347-354 (2005).

35. J.M. Martinez, et al., Increase in suspended sediment discharge of the Amazon River assessed by monitoring network and satellite data. *Catena.* **79**, 257-264 (2009).

36. T. Dunne et al., Exchanges of sediment between the flood plain and channel of the Amazon River in Brazil. *Geological Society of America Bulletin.* **110**, 450-467 (1998). 37. T.M. Smith, R.W. Reynolds, Extended Reconstruction of Global Sea Surface Temperatures Based on COADS Data (1854-1997). *Journal of Climate.* **16**, 1495-1510 (2003).

37. J.A. Marengo, J.C. Espinoza. Extreme seasonal droughts and floods in Amazonia: causes, trends and impacts. *International Journal of Climatology.* (2015).

38. R. Aalto, et al., Episodic sediment accumulation on Amazonian flood plains influenced by El Nino/Southern Oscillation.*Nature.* **425**, 493-497 (2003).

Acknowledgement

The SO-HYBAM (The Observation Service geodynamical, hydrological and biogeochemical control of erosion/alteration and material transport in the Amazon basin, supported by IRD- Institute for Research and Development, France) together the National Water Agency (ANA) and Geological Survey of Brazil (CPRM) and the Amazon Potamology Laboratory of Amazon Federal University (UFAM), Brazil. We tanks of Bosco Alfenas. The especially reconnaissance to Pascal Fraizy and Philippe Vauchel. We tanks of National Institute of Amazonian Research (INPA) and Estate University of Amazon (UEA) and the Climate and Environmental Program (CLIAM), especially Dr. Luis Cândido and Dra. Rita Valeria Andreoli.

Supplementary Materials

Since 1995, in the context of the SO-HYBAM program, 548 measures of discharge were made using a Rio Grande 600 kHz RDI Acoustic Doppler Current Profiler (ADCP) monitored by a global positioning system (GPS) to account for the river's moving bed. The Óbidos gauging station presents non-unique rating curve between the stage and discharge. Continuous measurement during 36 hours has showed that the non-unique rating curve is due to the influence of the tide, as well as the low slope and floodplains with regular hydrological regimes, flood and low flood period. For this case, the option is to calculate the daily discharge from the Manning-Strickler formula*(1)*. The daily surface water slope is calculated between the Óbidos and Santarém downstream gauging station. Manning's roughness coefficient is between 0.028 and 0.052, where high values correspond to low levels of the main channel and low values include the flood plains channel control. The calculated discharge is overestimated by 4% compared with the measured discharge. From 1995-2013, we made 26 measurements of the Óbidos cross section with 586 samples during different periods of the annual hydrological cycle. At the beginning of the project, there was no separation of fine and coarse sediments, therefore, there were fewer samples for the coarse sediments. To collect suspended sediment, we use the same sampling protocol used by the SO-HYBAM observatory *(2-6)*. Discrete water samples of 7 L were collected at different depths for several profiles with samples at less than 1m from the riverbed. The spatial location of the profiles in the cross section depends on the acoustic backscatter signal of the ADCP and the moving bottom estimation. For each sample, the coarse and fine sediments are separated using a 63 µm sieve. A 300 mL sample of the fine sediments is filtered through a 0.45 µm cellulose filter. Repeated measurements revealed an uncertainty of 10% for surface concentrations and 25% for the concentrations near the river bottom. The dates of both the discharge and the suspended sediments are stored and processed by the software HYDRACCESS (http://www.ore-hybam.org/index.php/eng/Software/Hydraccess). The grain size distributions were defined using a Malvern Mastersizer 2000 laser granulometer at the CPRM Laboratory in Manaus. The laser diffraction results are reported on a volume basis. Eighty-six samples were made in different periods of the hydrologic year and at several points of cross-section for measurements of the particle size. The particle size obtained in this study is similar to that found by (6). These authors show that the source of the fine and coarse sediments are the Andean Chain. In this study, the oceanic features were analyzed using NOAA Extended Reconstructed SST V3b data available at 2° resolution from the NOAA-CPC *(7)*. This information is freely available

at: http://www.esrl.noaa.gov/psd/data/gridded/data.noaa.ersst.html.

References

1. P. Kosuth, *et al.*, Sea tide effects on flows in the lower reaches of the Amazon River. *Hydrol. Process.* **23** , 3141-3150 (2009).

2. J. L. Guyot, N. Filizola, A. Laraque, Régime et bilan du flux sédimentaire de l'Amazone à Óbidos (Pará, Brésil) de 1995 à 2003. Sediments Budgets 1. *IAHS Publ.* **291**, 347-354 (2005).

3. N. Filizola, J.L. Guyot, Suspended sediment yields in the Amazon basin: an assessment using the Brazilian national data set. *Hydrological Processes.***23**, 3207-3215 (2009).

4. N. Filizola, J. L Guyot, The use of Doppler technology for suspended sediment discharge determination in the River Amazon. *Hydrological Sciences Journal.* **49**, 143-153 (2004).

5. J.M. Martinez, *et al.*, Increase in suspended sediment discharge of the Amazon River assessed by monitoring network and satellite data. *Catena* . **79**, 257-264 (2009).

6. T.M. Smith, and R.W. Reynolds, Extended Reconstruction of Global Sea Surface Temperatures Based on COADS Data (1854-1997). *Journal of Climate.* **16**, 1495-1510 (2003).

Capítulo 5

Estudo do gradiente vertical do sedimentos

Measuring and modeling vertical gradients in the suspended sediments in the Amazon River

Resumo

Estimar a denudação dos continentes para os oceanos é um dos desafios nas últimas décadas. A bacia Amazônica é uma das principais fontes de sedimentos no mundo. As primeiras estimativas do fluxo de sedimentos no rio Solimões/Amazonas data do final da década de sessenta. Desde então, baseados em amostragens tradicionais vários são os trabalhos que apresentaram diferentes resultados. Se bem a amostragem é uma medida direita da concentração de sedimentos em suspensão, porém tem um alto custo econômico e limitações em termos de resolução espacial e temporal, devido a que estas técnicas precisam de 4-6 de horas de trabalho para poder realizar entre 4 ao 9 perfis em seções de 2 a 4 km entre uma margem e outra, com profundidades de 20 a 60 m. Outra das desvantagem dos métodos tradicionais em rios de grande porte é o alto grau de perigo que se apresenta ao realizar as coletas no caso do uso de um barco ancorado.

Desde alguns anos observa-se o aumento na utilização de métodos indiretos para determinar a concentração de sedimentos em suspensão ($[C]$), este aumento deve-se à técnicas indiretas que permitem caracterizar a variabilidade espacial e temporal da $[C]$ com menor custo e tempo. A turbidez é uma medida indireta da $[C]$ em função da granulometria e precisa de calibração previa. Para o rio Solimões/Amazonas a calibração

foi feita para os dois tipos preponderantes de granulometria: partículas finas 10-20 µm e areias 100-200 µm.

Este trabalho descreve um método para realizar medidas de sedimentos em suspensão no rio Solimões/Amazonas utilizando a turbidez. Este método baseia-se na aplicação do modelo de Rouse para predizer perfies de $[C]$ ao longo da seção transversal em função da granulometria e finalmente calcular o fluxo de sedimentos em suspensão com uma melhor resolução. Para cumprir os objetivos propostos fizeram-se medições em dois períodos hidrológicos (enchente e cheia) em quatro estações hidrológicas distribuídas ao longo do rio Solimões/Amazonas localizadas entre as planícies amazônicas peruana e brasileira. Em cada uma das seções de medição fizeram-se 3 a 4 perfies e em cada perfil coletou-se amostras concentração de sedimentos finos $[C_f]$ concentração de areias $[C_c]$, granulometria e medições de turbidez.

Ensaios no laboratório indicam que o sinal resultante da turbidez em uma amostra é o resultado da soma dos sinais de turbidez de cada uma das partículas presentes nessa amostra. Utilizou-se o modelo de Rouse para separar o sinal de turbidez, resultado das dois classificações de sedimentos. O modelo de Rouse é definido por dois parâmetros, um coeficiente (que corresponde à concentração de sedimentos de referencia com respeito ao fundo) e um exponente (que relaciona a velocidade de sedimentação com a velocidade de cisalhamento). Observações no campo mostram que sedimentos finos são predominantes no primeiro terço superior de cada perfil. Baseando-se na calibração feita no laboratório para sedimentos finos, transforma-se este primeiro terço em $[C_f]$ para logo ajustar o perfil de Rouse nesta fração do perfil e este resultado é estendido em toda a profundidade. Conhecida a $[C_f]$ pode-se conhecer a turbidez das areias por subtração da turbidez total e utilizando a curva de calibração das areias feita no laboratório converte-se em $[C_c]$. A soma de $[C_f]$ e $[C_c]$ corresponde a $[C]$.

A validação do método foi feita a partir da comparação do diâmetro da partícula medido no laboratório e o diâmetro modelado no perfil de Rouse. Os resultados indicam que o tamanho da partícula é duas vezes maior que o medido no granulômetro à laser. Acredita-se que esta diferença deve-se as incertezas introduzidas no cálculo do exponente de Rouse: O fato de utilizar a fórmula de sedimentação de Stocks que calcula o diâmetro considerando que as partículas são esféricas e também o fato de considerar a densidade da sílica como a densidade das partículas. Outra fonte de incerteza decorre

da determinação na velocidade de cisalhamento a qual obtêm-se à partir da média de vários perfis de velocidade até obter um perfil logarítmico. Outra hipóteses para a diferença entre os resultados é o fracionamento da partícula no momento da medição com o granulômetro à laser, onde a velocidade de mistura difere das condições naturais. Observa-se que em uma mesma seção, os perfis de Rouse para sedimentos finos têm os mesmos parâmetros. Não entanto, os perfis de Rouse para areias mostram variações no coeficiente de um perfil para outro, isso deve-se à heterogeneidade nas condições hidráulicas em uma mesma seção. Utilizar um mesmo coeficiente para toda a seção implica em uma sensibilidade de até o $\pm$ 29% no fluxo de areias. O analise temporal mostra a variação dos coeficientes de Rouse. Na época da enchente é predominante $[C_f]$ e na época de cheia a $[C_c]$ joga um papel preponderante. Consequentemente, o coeficiente de Rouse de finos é maior na época da enchente que na época de cheia e vice-versa para o coeficiente de Rouse das areias.

As concentrações calculadas com o método de separação do sinal de turbidez são comparáveis com as concentrações medidas o que indica que a aplicação do modelo de Rouse em função da turbidez e granulometria é uma opção para determinar a concentração de sedimentos em suspensão.

Résumé

Estimer les apports de l'érosion des continents à l'océan est un des défis de ces dix dernières années. Le bassin Amazonien est l'une des principales sources de sédiments au monde. Les premières estimations du flux de sédiments du Solimões/Amazone datent de la fin des années soixante-dix. Depuis lors, basées sur des échantillonnages traditionnels, de nombreuses études ont donné des résultats différents. Bien que l'échantillonnage soit une mesure directe de la concentration de sédiments en suspension, il reste d'un coût élevé et présente des limitations en terme de résolution spatio-temporelle dues à ce que ces techniques demandent 4 à 6 heures de travail pour pouvoir réaliser entre 4 et 9 profils sur des sections de 2 à 4 km de large et de 20 à 60 m de profondeur. Un autre désavantage de ces méthodes traditionnelles appliquées aux grands fleuves réside dans les risques importants encourus à devoir échantillonner à partir d'un bateau á l'ancre.

Depuis quelques années on voit augmenter le nombre de méthodes indirectes pour déterminer la concentration de sédiments en suspension ($[C]$), permettant, outre une économie de temps et de moyens, une meilleure caractérisation de la variabilité spatio temporelle de $[C]$. L'une d'entre elles utilise la turbidité en fonction de la granulométrie et requiert une calibration préalable. Cette calibration a été réalisée pour les deux types de granulométrie prépondérantes dans le Río Solimoes/Amazone : les particules fines (10-20 µm) et les sables (100-200 µm).

Cette étude décrit une méthode basée sur l'application du modèle de Rouse permettant de prédire des profils de $[C]$ dans une section transversale en fonction de la granulométrie et finalement de calculer le flux de sédiment avec une meilleure résolution. Pour atteindre ces objectifs, les mesures ont été réalisées à deux periodes du cycle hydrologique (montée de crue et pic de crue) sur quatre stations hydrométriques distribuées le long du Rio Solimões/Amazone entre les plaines Amazoniennes du Pérou et du Brésil. Sur chacune de ces sections ont été réalisé 3 à 4 profils verticaux et sur chacun d'entre eux on a échantillonné la concentration de sédiments fins $[C_f]$, la concentration en sable $[C_c]$, déterminé la granulométrie et mesuré en continu la turbidité. Des essais en laboratoire ont montré que le signal de turbidité pour un échantillon est le résultat de la somme des signaux de turbidité de chacun des deux types de particules présentes dans cet échantillon.

On a utilisé le modèle de Rouse pour différencier le signal de turbidité résultant des

deux classes de sédiments en présence. Ce modèle requiert la détermination de deux paramétres, un coefficient (la concentration de sédiments prise comme référence pour le fond) et un exposant qui relie la vitesse de sédimentation à la vitesse de cisaillement. Les observations de terrain montrent que les sédiments fins prédominent dans le premier tiers supérieur de chaque profil. En se basant sur une calibration faite en laboratoire pour les sédiments fins, on transforme en $[C_f]$ ce premier tiers avant que d'ajuster le profil de Rouse á cette fraction du profil, pour ensuite étendre le résultat obtenu à la profondeur totale. Connaissant $[C_f]$ et la turbidité totale, on peut déduire par soustraction la turbidité due aux sables et, en utilisant cette fois une calibration pour les sables faite en laboratoire, on la traduit en $[C_c]$. La somme de $[C_f]$ et $[C_c]$ correspond alors à $[C]$.

La validation de la méthode a été faite á partir de la comparaison du diamétre des particules mesuré en laboratoire avec le diamétre modélisé par le profil de Rouse. Les résultats indiquent que la taille de la particule obtenue est deux fois plus grande que celle mesurée au granulomètre laser. Nous pensons que cette différence est due aux incertitudes introduites par le calcul de l'exposant de Rouse : En effet, celui-ci fait intervenir la formule de sédimentation de Stocks qui calcule le diamètre en assimilant la particules á une sphère et utilise comme valeur de densité celle couramment admise pour la silice. Enfin, dans ce calcul, la vitesse de cisaillement a été obtenue en prenant la moyenne de plusieurs profils de vitesse jusqu' à obtenir un profil logarithmique. Autre hypothèse pouvant expliquer cette différence: un fractionnement des particules au moment de la mesure au granulomètre laser car la vitesse de mélange dans l'appareil diffère des conditions naturelles.

Nous avons observé que dans une même section, les profils de Rouse pour les sédiments fins ont les mêmes paramètres. Cependant, les profils de Rouse pour les sables montrent des variations du coefficient d'un profil à l'autre dues pet être à l'hétérogénéité des conditions hydrauliques dans une même section. Utiliser un même coefficient pour toute la section entraine une sensibilité pouvant affecter jusqu'à $\pm$ 29% le flux de grossiéres. L'analyse dans le temps montre des variations des coefficients de Rouse, car pendant la période de montée de crue c'est la concentration de fines qui prédomine, mais durant la crue les sables deviennent prépondérants. D'où un coefficient pour les fines plus fort en montée de crue qu'en pic de crue, respectivement plus faible pour les sables.

Les concentrations calculées en scindant en deux le signal de turbidité sont néanmoins comparables aux concentration mesurées, montrant ainsi que l'application du

modèle de Rouse en fonction de la turbidité et de la granulométrie reste une bonne option pour la détermination des flux de sédiments.

Measuring and modeling vertical gradients in the suspended sediments in the Amazon River

E. Armijos[1,2*], A. Crave[3,4], J.L. Guyot[5], A.L.M.R. Dos Santos[6,9], F. Sampaio[1], P. Fraizy[5] E. De Oliveira[7], R. Espinoza[8], , W. Santini[5], J.M. Martinez[5], P. Autin[5,9], N.Pantoja[6], M.Oliveira[6] and N. Filizola[9].

1 – CLIAMB, Instituto Nacional de Pesquisas da Amazônia (INPA), Universidade do Estado do Amazonas (UEA), Av. André Araújo, 2936, Aleixo, CEP 69060-001, Manaus, Brasil.
2 – Université de Toulouse 3 Paul Sabatier, 118 Route de Narbonne, 31062 Toulouse, France.
3 – Géoscience Rennes, CNRS/INSU UMR 6118, Campus de Beaulieu, 35042 Rennes, France.
4 – Université de Rennes 1, Campus de Beaulieu, 35042 Rennes, France.
5 – Géoscience Environnement Toulouse (CNRS, IRD, OMP, Université de Toulouse),14 Av. Edouard Belin, 31400 Toulouse, France.
6 – Servicio Geológico do Brasil (CPRM), Av. André Araújo, 2160, CEP: 69060-000 Manaus-Brasil.
7 – Agência Nacional da Agua (ANA), Setor Policial, área 5, Quadra 3, Blocos "B","L","M"e "T".
8 – Universidad Nacional Mayor de San Marcos, Calle Germán Amézaga N° 375 Lima, Perú..
9 – Universidade Federal do Amazonas (UFAM), Av. General Rodrigo Octávio, 6200, Coroado I,CEP: 69077-000, Manaus, Brasil.

**Corresponding author.* Tel:+55 92 931 64734-Fax:+55 92 364 3625. E-mail: armijos.elisa@gmail.com

Abstract

Accurately measuring sediment flux in large rivers remains a challenge due to the cross-sectional spatial and temporal variability of suspended sediment concentration in conjunction with sampling procedures that fail accurately quantify those differences. This study presents a better protocol for field campaign can be proposed to improve the measurement of suspended sediment concentration field of the Amazon River or similar large river using of a turbidimeter and Rouse model. Profiles of vertical concentrations of fine (9-24 µm) and coarse (65-326 µm) sediment are defined separately at a high spatial resolution using a careful calibration procedure for turbidity. In situ measurements of suspended-sediment concentration profiles at gauging stations over 3,000-km during low water and flood periods indicate that the Rouse model and its underlying theory are relevant to modeling concentration variability with depth in the Amazon River. Sediment flux of fine and coarse are calculated separately by combining the ADCP velocity field and the concentration field derived from the calibrated Rouse models.

keywords

suspended sediments, turbidity, Rouse model, Amazon River, in situ concentration measurement, sediment flux monitoring.

1 Introduction

It has been estimated that the denudation of the continents and the transfer of sediment to the oceans by rivers is between 13 to 51 Gt year^{-1} (Syvitski, 2003). The difference in these estimates is mainly due to differences in data quality, which is a result of varying measurement techniques during long periods of observation, and uncertainties associated with the sampling procedures (Milliman and Meade, 1983). The Amazon River makes an important contribution to the global sediment flux. Gibbs (1967a),provided the first estimate at Óbidos, the last gauging station before the mouth (500-600 Mt^{-1}); Subsequently, Meade (1994) obtained a different value (1100-1300 MT $^{-1}$) based on fieldwork that examined depth-integrated samples in several profiles (Richey et al., 1986; Meade et al., 1985). Later, Filizola (2003) and Guyot et al. (2005) calculated that the Amazon River provides 800 MT year^{-1} to the Atlantic Ocean. This estimation considers point samples measurements from cross-sections and temporal variability in the hydrological regime. The variability of these estimates comes from the different datasets and calculation protocols.
In the Amazon River, the uncertainty in the sediment flux calculation stems from the difficulty of monitoring and integrating the lateral and vertical gradients in suspended sediment concentrations $[C]$ in time and space. The suspended sediment concentration is not directly correlated with discharge, and the sediment peak occurs three months before the flood. Similar observations were made in the Peruvian and Brazilian lowlands (Armijos et al., 2013a; Guyot et al., 2005).

Two main protocols are applied in the field. One is related to the use of depth-integrating samplers and is recommended by the USGS (Edwards e Glysson, 1988). The main advantage of a depth-integrating sampler is that it samples along an entire vertical profile Meade (1994). However, the sampler must maintain a constant downward velocity and must stay at a fixed point in the stream to respect the isokinetic conditions at the sampler mouth. Both conditions are very hard to achieve due the power of the Amazon River flow and, above all, due to the large vertical gradient in flow velocity from the surface to the bottom, which changes the isokinetic conditions. The main disadvantage of this method is that there is no information about the vertical gradients in $[C]$, which can help to model transport processes. The second protocol consists of collecting water samples from discrete depths in different profiles in a cross-section (Filizola, 2003; Guyot et al., 2005). The main advantage of this method is that it

assesses the vertical gradient in $[C]$ with a spatial resolution that depends on the number of samples. Discrete-depth water sampling is a more time-consuming method than the previous one. Usually 3 or 5 samples per profile are collected to allows the exploration of 3 or 4 vertical profiles in the river cross-section during one day in the Amazon River context.

The physical model of Rouse has been proposed to describe the vertical distribution of suspended sediment in a river channel (Rouse, 1938). One of the main assumptions of this model is that there is equilibrium between the settling velocity and the vertical mixing of sediments. Vanoni (1980) and Bouchez et al. (2011a, 2011b) used the Rouse model to predict for various grain sizes of sediment the vertical concentration profiles in the Solimões River. These studies consider either a median sediment size or deduce the sediment size from in situ concentration profiles obtained with a discrete water sampling method. Guyot (1993), Dunne et al. (1998), and Filizola (2003) observed that the suspended sediment in Amazonian rivers are composed of fine sediments $[C_f]$ (clay and silt) and coarse sediments $[C_c]$ (sand), which exhibit different concentrations depending on the hydrological regime and on the contributions of the tributaries. Thus, the following question arises: What is the best way to take into account different sediment sizes in the calibration of the Rouse model parameters to reduce the uncertainty in the use of the Rouse model?.

The methods to quantify sediment concentrations have evolved with technological advances. Wren et al. (2000) conducted a comparative study of different field techniques for suspended sediment measurements and listed the advantages and disadvantages of each method. They stated that the method selection depends on both the river and purpose. The exploration of indirect methods to estimate suspended sediments has greatly evolved in recent years (Martinez et al., 2009). Traditional methods, such as discrete-depth water samples, are expensive, time-consuming, and limited in terms of spatial and temporal resolutions, particularly in large rivers, and should be improved with new technologies.

This paper describes how turbidity sensors can significantly improve the assessment of the suspended sediment concentration field and consequently the sediment flux monitoring for large rivers, such as the Amazon River. A new methodology is developed to take into account different suspended sediment size modes for the interpretation of the turbidity signal. In this manner, each sediment type can be analyzed separately with different physical models to reproduced spatial gradient of concentrations. Applying this methodology to the Amazon River field leads to a better spatial monitoring of

sediment concentration and understanding of temporal sediment flux variability than previous studies. The main purpose of the paper is to describe step by step this original methodology, the relative assumptions and their validation with data with Amazon River. Finally, an efficient field protocol is proposed to monitor the sediment concentration field of the Amazon River or similarly large rivers

2 Methodology

2.1 Study site

The Amazon basin drains an area of 5,961,000 km^2 (Callède et al., 2010). The basin comprises four main geomorphological zones: **1)** the Andes, which includes the sub-Andes zone characterized by steep slopes and high erosion; **2)** the foreland basin, which is a transitional zone between the Andes and the floodplains formed by recent erosion of the Andes; **3)** the Amazon floodplain, which is composed of an accumulation of sediments from the Andes; and **4)** the Guyana and Brazilian shields, which are two well-eroded Precambrian basements in the northern and southern parts of the basin (De Brito Neves and Cordani, 1991; Roddaz et al., 2005). The Amazon River is formed by the confluence of the Ucayali and Marañón in Peru. The river's name changes to Rio Solimões as it enters Brazil, and it is called the Amazon River after its confluence with the Rio Negro (Fig. 1). The Madeira River and Solimões River are the main tributaries that transport sediment from the Andes. Although the Negro River contributes to 14% of the Amazon River's total discharge, it is poor in suspended sediment (Molinier et al., 1995).

The Amazon River has an average flow of 210 $\times 10^3$ m^3 s^{-1} (Callède et al., 2010). This study uses data from four gauging stations at both the Solimões and Amazon Rivers because they have been monitored for several decades: Tamshiyacu (TAM), located in the Amazon River at the Peruvian Amazon plain; Manacapuru (MAN), located in the Solimões River; Itacoatiara (ITA), located in the Amazon River downstream of confluence with the Negro and Madeira Rivers; and Obidos (OBI), the last gauging station in the Amazon River 870 km before it reaches the sea. The data were collected in 2011 and 2012 during flow and sediment concentration peaks: February (TAM) and May (Brazilian stations) and November-December which correspond to the rising suspended sediment concentrations at the Brazilian stations (Table 1).

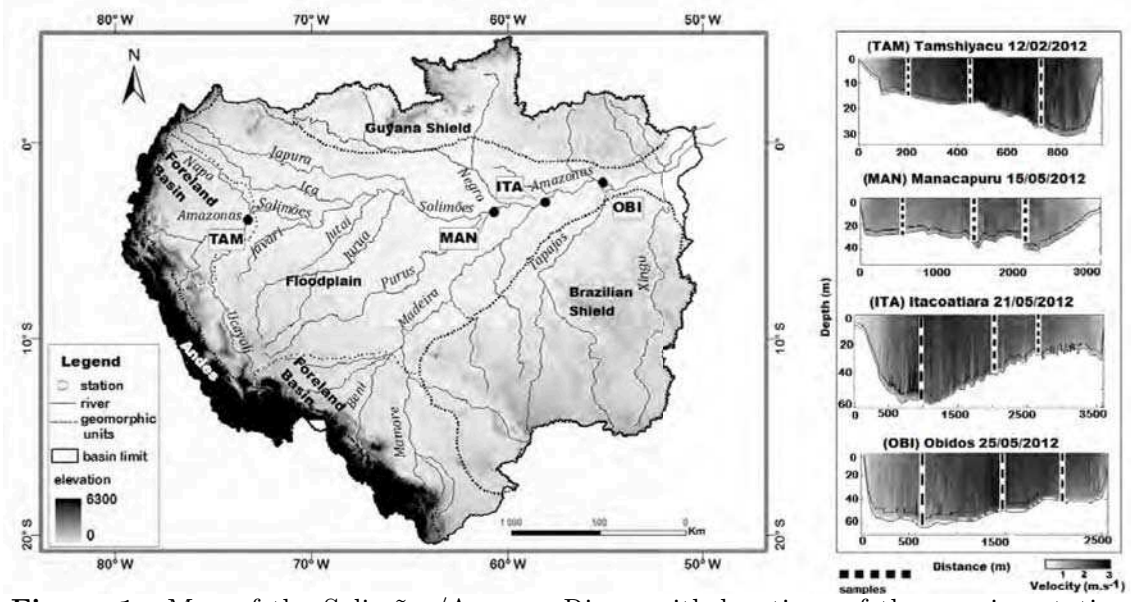

Figure 1. Map of the Solimões/Amazon River, with locations of the gauging stations and sampling sites..

Table 1. Gauging stations on the Solimões and Amazon River.

COD	Station	River	Date	Profile	Distance LB* (m)	Total Depth (m)	Latitude $^o(S)$	Longitude $^o(W)$	Discharge (m^3s^{-1})
TAM	Tamshiyacu	Amazon	21/11/2011	P1	238	12	4.00727	73.16676	23370
				P2	478	17	4.00572	73.16617	
				P3	718	26	4.00416	73.16360	
			12/02/2012	P1	273	16	4.00867	73.16612	45400
				P2	542	22	4.00662	73.16467	
				P3	789	31	4.00476	73.16332	
MAN	Manacapuru	Solimões	11/12/2011	P1	600	17	3.31832	60.55399	67260
				P2	1600	23	3.32666	60.55311	
				P3	2400	27	3.33415	60.55329	
			12/05/2012	P1	700	27	3.31816	60.55358	145700
				P2	1400	35	3.32645	60.55254	
				P3	2200	38	3.33416	60.55280	
ITA	Itacoatiara	Amazon	15/12/2011	P1	400	46	3.15954	58.41147	106400
				P2	900	53	3.16402	58.41050	
				P3	1600	30	3.16950	58.41029	
				P4	2400	22	3.17637	58.40856	
			22/05/2012	P1	900	61	3.16334	58.41067	237700
				P2	1700	40	3.17144	58.40842	
				P3	2600	27	3.17789	58.40774	
OBI	Óbidos	Amazon	17/12/2011	P1	500	54	1.93772	55.49478	106900
				P2	1130	56	1.94217	55.49762	
				P3	1670	41	1.94592	55.50078	
				P4	2200	34	1.94960	55.50429	
			27/05/2012	P1	700	62	1.93930	55.49612	259200
				P2	1500	49	1.94552	55.49687	
				P3	2100	43	1.94928	55.50449	

*LB=Distance of Left bank

2.2 Field monitoring

We use the same methodology for sampling and flow measurement as the Observatory Environmental Research Observatory of geodynamical, hydrological and bioge-

ochemical control of erosion/alteration and material transport in the Amazon, Orinoco and Congo basins (SO-HYBAM). The flow at each of the gauging stations is measured using a Rio Grande 600 kHz RDI Acoustic Doppler Current Profiler (ADCP) monitored by a global positioning system (GPS).

Along with the flow measurements, 7-L discrete water samples are collected with a horizontal water sampler at different depths along selected profiles across the section. To ensure that the sample is obtained at a given vertical profile, the sampler is tied to a 70-kg weight. The location of the profile is chosen by considering two criteria: the spatial distribution of the acoustic backscatter signal of the ADCP and a moving-bottom estimation. For each sample, the coarse and fine sediments is separated using a 63 µm sieve. A 300 mL sample of fine sediments is filtered through a 0.45 µm cellulose filter. The samples of fine and coarse sediments are then taken to the Amazon Potamology Laboratory (LAPA−UFAM) to be dried at a 100^oC for an hour. Repeat measurements revealed an uncertainty of ± 10% for surface concentrations and ±25% for concentrations near the river bottom.

A high-definition YSI V2 6600 infrared (860-nm wavelength) nephelometer (0.1 NTU resolution, 2% accuracy, and 90° angle detection) turbidity sensor, coupled with a pressure detector is attached to the sampler and records turbidity during sampler lowering, with a data acquisition frequency of 1 Hz. Thus, a high-resolution turbidity profile is captured along a given vertical profile. Each value of turbidity (T) corresponds to the average signal over a height of 50 cm, and the maximum uncertainty of this measurement is ± 7%.

2.3 Determination of suspended sediment concentration profile using turbidity measurements

Turbidity represents the transparency reduction of water due to the presence of suspended matter, such as sand, clay, or organic matter (ASTM, 2003). Turbidity can be measured by a turbidity-meter, whose sensor detects the portion of light that is scattered by suspended particles (Anderson, 2004). Turbidity is an optical measurement technique to estimate $[C]$ without interfering the sediment (Bunt et al., 1999; Pavanelli e Bigi, 2005; Restrepo e Pierini, 2012; Landers, 2011). One of its main advantages is that it provides the opportunity to obtain values at high frequency with portable probes. However, this procedure requires calibration to account for sediment granulometry, nature and color (Ludwig e Hanes, 1990; Butt et al., 2002; Minella et al., 2008; Thollet et al., 2013). For example, the assumption of a single representative diameter is not appropriate

and can leads to large uncertainty in the calculation of $[C]$. Indeed, turbidity is the addition of the turbidity signal relative to each granulometric mode and depends on the sediment concentration in each mode (see section 2.3.1). Interpreting turbidity as a concentration requires identifying the turbidity intensity relative to each mode and applying appropriate calibration curves relative to each mode.

The 65 samples collected during the field campaigns show that the sediment particle sizes at the four gauging stations are between 9 and 24 µm for fine sediments and between 65 and 156 µm for coarse sediments (Table 2). Note the exception for coarse sediments at MAN during the high water period (326 µm on average). This simple configuration of granulometry over thousands of kilometers from Tamshiyacu to Óbidos offers the opportunity to use turbidity as an efficient signal to measure the concentration of both sediment modes. However, this requires developing a new methodology to analyze turbidity data. The main difficulty is taking into account the mass partition between the two modes, which may vary vertically with the river depth. To develop an adequate methodology, we first evaluate several properties of turbidity in the laboratory using suspended Amazon River sediment to define specific calibration curves. Second, we develop a sequential method to extract the concentration profiles of both modes from in situ turbidity profiles knowing the size modes of the suspended sediment.

Table 2. Samples of fine and coarse sediment data of particle size measure with laser granulometer for Solimões and Amazon River.
T_f=Turbidity of fine sediment; T_c= Turbidity of coarse sediments; $[C]$=Total suspended sediments; $[C_f]$= Concentration of fine sediments; $[C_c]$= Concentration of coarse sediments; $\%[C_f]$ and $\%[C_c]$= % of fine coarse sediments; ϕ_f= diameter of fine sediments; ϕ_c= diameter of coarse sediments; σ_f and σ_c= standard deviation

.

Station	River	Date	Profile	Depth(m)	Turbidity		Suspended Sediments					Laser Granulometry			
					Tf (NTU)	Tc (NTU)	[C] (mg L^{-1})	$[C_f]$ (mg L^{-1})	$[C_c]$ (mg L^{-1})	$\%[C_f]$ %	$\%[C_c]$ %	ϕ_f (μm)	σ_f	ϕ_c (μm)	σ_c
Tamshiyacu	Amazonas	21/11/2011	P1	0.2	218		245	234	11	96	4	10	0.82		
				3	271	8	544	378	166	69	31	11	0.82		
				6	279	37	487	376	112	77	23	9	0.34	35	0.50
				9	287	42	784	461	323	59	41	10	0.52	73	0.31
				11	296	34	886	413	473	47	53	15	0.80	126	0.30
			P2	0.2	206		200	200	0.3	100	0	7	0.47		
				4	268	23	408	351	57	86	14	10	0.54	47	0.54
				9	278	103	416	302	114	73	27	13	0.60	65	0.37
				13	286	61	589	432	157	73	27	10	0.54	107	0.28
				17	303	83	1236	555	681	45	55	13	0.56	125	0.26
			P3	0.2	356		359	323	36	90	10				
				7	398	39	412	342	71	83	17				
				13	405	10	470	377	93	80	20				
				20	415	20	390	340	50	87	13				
				24	432	130	604	373	231	62	38				
		12/02/2012	P1	0.2	325		311	310	2	99	1				
				4	403	51	870	618	252	71	29				
				8	415	38	898	619	279	69	31				
				11	424	51	1919	1225	694	64	36				
				15	444	82	1645	722	923	44	56				
			P2	0.2	400		416	385	31	93	7				
				5	410	18	791	548	243	69	31				
				10	422	29	674	521	153	77	23				
				15	435	33	1261	574	686	46	54				
				19	454	18	854	523	330	61	39				
			P3	0.2	384		690	519	171	75	25				
				7	384	68	713	549	164	77	23				
				15	389	17	695	510	186	73	27				
				22	394	16	735	534	201	73	27				
				26	403	51	1000	498	502	50	50				

Table 2.(*continued*)

Station	River	Date	Profile	Depth(m)	Turbidity		Suspended Sediments					Laser Granulometrie			
					Tf (NTU)	Tc (NTU)	[C] (mgL^{-1})	$[C_f]$ (mgL^{-1})	$[C_c]$ (mgL^{-1})	$\%[C_f]$ %	$\%[C_c]$ %	ϕ_f (μm)	σ_f	ϕ_c (μm)	σ_c
Manacapuru	Solimões	11/12/2011	P1	0.2	197		166	160	6	97	3				
				7	216	22	222	197	25	89	11				
				14	229	6	244	221	23	91	9				
				15	236	6	249	222	27	89	11				
			P2	0.2	200		209	196	13	94	6				
				6	203	5	232	204	28	88	12				
				11	205	4	214	196	17	92	8				
				17	212	20	270	215	56	79	21				
			P3	0.2	180		220	220	0.4	99	1	7	0.53		
				7	214	16	273	238	35	87	13	12	0.53		
				15	228	47	362	250	112	69	31	18	0.53	45	0.49
				22	246	65	846	500	346	59	41	19	0.51	76	0.26
				25	273	120	699	410	289	59	41	20	0.51	76	0.46
		12/05/2012	P1	0.2	41		23	20	3	88	12				
				9	45	4	116	44	71	38	62				
				18	46	9	237	48	189	20	80				
				23	47	8	541	72	468	13	87				
				25	48	14	363	55	308	15	85				
			P2	0.2	60		52	44	9	84	16	14	0.77		
				11	54	13	205	67	138	33	67	21	0.71	258	0.33
				22	54	12	555	69	486	12	88	28	0.82	307	0.28
				28	54	14	426	59	367	14	86	23	0.77	330	0.28
				31	55	11	548	69	479	13	87	27	0.79	310	0.29
			P3	0.2	31		19	19	0.1	99	1	15	0.50		
				19	51	15	48	38	10	80	20	19	0.48	77	0.39
				26	52	18	98	58	40	59	41	19	0.48	77	0.39
				33	52	124	980	100	881	10	90	19	0.50	172	0.18
				36	53	169	1223	123	1200	10	98	19	0.51	186	0.18

Table 2.(*continued*)

Station	River	Date	Profile	Depth(m)	Turbidity		Suspended Sediments					Laser Granulometrie			
					Tf (NTU)	Tc (NTU)	[C] (mgL^{-1})	$[C_f]$ (mgL^{-1})	$[C_c]$ (mgL^{-1})	$\%[C_f]$ %	$\%[C_c]$ %	ϕ_f (μm)	σ_f	ϕ_c (μm)	σ_c
Itacoatiara	Amazon	15/12/2011	P1	0.2	122		91	90	1	99	1	7	0.46		
				9	125	11	114	111	3	97	3	8	0.52		
				19	126	3	107	102	5	95	5	9	0.52		
				29	127	6	103	99	4	96	4	9	0.50		
				38	128	5	130	113	17	87	13	11	0.77	65	0.34
				43	131	1	120	110	10	92	8	11	0.70	80	0.37
			P2	0.2	124		86	85	1	99	1				
				14	136		159	150	9	94	6				
				33	145	18	262	226	36	86	14				
				45	152	3	388	366	21	94	6				
				49	163	30	262	204	58	78	22				
			P3	0.2	125		86	86	0.4	100	0				
				14	136	8	129	123	6	95	5				
				24	140	13	168	151	17	90	10				
				33	148	53	620	495	125	80	20				
				35	156	42	382	300	82	78	22				
			P4	0.2	125		103	102	0.4	100	0	7	0.38		
				6	126	10	97	96	1	99	1	9	0.42		
				11	130	7	121	117	4	97	3	9	0.50	31	0.30
				17	136	104	264	247	17	94	6	12	0.54	60	0.20
				20	144	216	482	431	51	89	11	12	0.54	80	0.40
		22/05/2012	P1	0.2	59		44	40	4	91	9	12	0.57		
				23	57	10	123	64	59	52	48	14	0.48	69	0.26
				54	61	19	1477	69	1408	5	95	14	0.51	157	0.48
				58	63	34	714	74	640	10	90	20	0.64	232	0.31
			P2	0.2	59		47	47	0.4	99	1				
				26	78	20	228	92	137	40	60				
				38	84	50	830	109	721	13	87				
			P3	0.2	29		48	47	1	98	2	13	0.41		
				15	99	11	267	122	144	46	54	20	0.58	116	0.29
				26	107	138	821	221	600	27	73	22	0.54	137	0.19

Table 2.(*continued*)

Station	River	Date	Profile	Depth(m)	Turbidity		Suspended Sediments					Laser Granulometrie			
					Tf (NTU)	Tc (NTU)	[C] (mgL^{-1})	$[C_f]$ (mgL^{-1})	$[C_c]$ (mgL^{-1})	$\%[C_f]$ %	$\%[C_c]$ %	ϕ_f (μm)	σ_f	ϕ_c (μm)	σ_c
Óbidos	Amazon	17/12/2011	P1	0.2	110		88	88	1	99	1				
				11	117	2	93	91	2	98	2				
				33	121	12	112	95	18	84	16				
				46	125	7	124	102	22	82	18				
				50	131	8	180	111	69	62	38				
			P2	0.2	105		78	78	0.3	99	1				
				14	114	13	103	99	4	96	4				
				29	117	10	128	121	7	95	5				
				43	122	10	108	102	6	94	6				
				48	128	18	137	118	19	86	14				
			P3	0.2	112		76	75	0.3	100	0	8	0.44		
				10	126		94	91	2	97	3	10	0.42		
				24	130	12	224	192	32	86	14	15	0.52	40	0.25
				34	134	26	174	143	31	82	18	14	0.51	80	0.35
				38	140	39	219	163	56	75	25	14	0.52	87	0.42
			P4	0.2	107		81	81	0.1	100	0				
				10	128		100	99	1	99	1				
				18	130	8	104	100	5	96	4				
				26	133	7	182	172	11	94	6				
				31	140	8	294	246	48	84	16				
		27/05/2012	P1	0.2	58		60	56	4	93	7	15	0.59		
				20	84		131	89	42	68	32	20	0.74	48	0.30
				40	86	26	420	138	282	33	67	20	0.56	142	0.31
				55	89	34	667	131	536	20	80	20	0.59	171	0.37
			P2	0.2	70		47	45	2	96	4	15	0.48		
				17	73		156	101	56	64	36	15	0.56	30	0.30
				30	74	20	334	131	202	39	61	21	0.52	153	0.19
				40	76	30	270	119	151	44	56	20	0.51	131	0.20
				50	81	93	1152	184	968	16	84	20	0.54	162	0.20
			P3	0.2	89		40	40	0.4	99	1	13	0.46		
				12	128		196	132	64	67	33				
				26	132	39	257	147	110	57	43	20	0.54	40	0.40
				36	136	99	681	345	337	51	49	24	0.29	103	0.17
				42	143	174	831	323	508	39	61	24	0.70	128	0.30

2.3.1 Turbidity tests and $[C]$ measurement

- *Measurement of granulometry*

  The grain size distributions in each sample were measured using a Malvern Mastersizer 2000 laser granulometer at the CPRM laboratory in Manaus. Laser diffraction results are reported on a volume basis. Several laboratory tests were conducted to optimize **i)** the blending speed (at 2,350 rpm, the mixture is homogeneous without bubbles), **ii)** the storage time (measurements were gradually recorded during six weeks of storage, beyond which similar results were obtained), and **iii)** the ultrasound tests, which were conducted with different ultrasound frequencies for 30 seconds (the results were similar to tests made without ultrasonication). For remote sampling locations, we added a few drops of chlorine prior to

storage in a dark location to avoid the growth of organic matter.

To define each grain size distribution curve, we use a Gaussian mixture distribution and obtain the particle size mode (ϕ) and the standard deviation for each distribution.

- *T vs. [C] calibration*

  The laboratory calibration consists of measuring the turbidity of a known concentration and granulometry. This methodology has been explained by Sternberg et al. (1991) and Merten et al. (2013). A sample of water with fine sediments was placed in a transparent plastic cylinder with a diameter of 20 cm and a height of 40 cm and is stirred at a constant velocity to maintain a homogeneous suspension. A calibration curve was obtained by successive dilutions starting at 1,000 mg L^{-1}. For the coarse sediments, the bed load material from the different gauging stations, distributed along the Solimões and Amazon rivers, was similarly processed, except that the concentration was gradually increased to obtain the calibration curve (Fig. 2). All calibration curves show linear trends for the suspended sediment concentration range that are effective in the Amazon context. Each calibration curve is defined by a sensitivity factor, called "specific turbidity", ($T/[C]$).

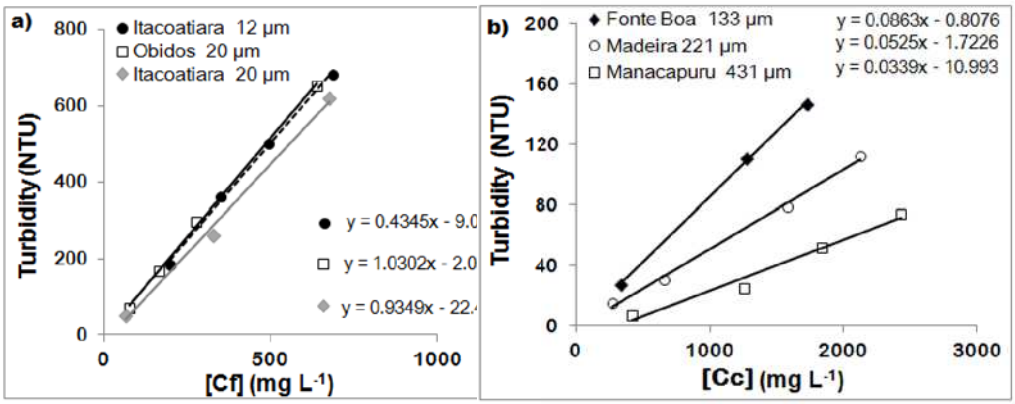

Figure 2. Calibration of turbidity to concentration using water samples from each gauging station. a) Fine sediment and b) coarse sediment.

The $T/[C]$ variability is explored in the laboratory using different fine and coarse sediment types. The results show that $T/[C]$ follows a linear trend with the size modes of the sediment types and has error bars that can be reduced if fine and coarse sediment cases are split into two groups of data (Fig. 3). The $T/[C]$ decreases with increasing sediment size by a factor of 18 and 13 for fine and coarse sediment types, respectively. Note that for this sensor, $T/[C]$ is 18 times higher for

20-µm sediment than for 200-µm sediment. This observation supports our decision to neglect the turbidity induced by coarse sediment when the concentration of coarse sediment is ten times lower than the concentration of fine sediment.

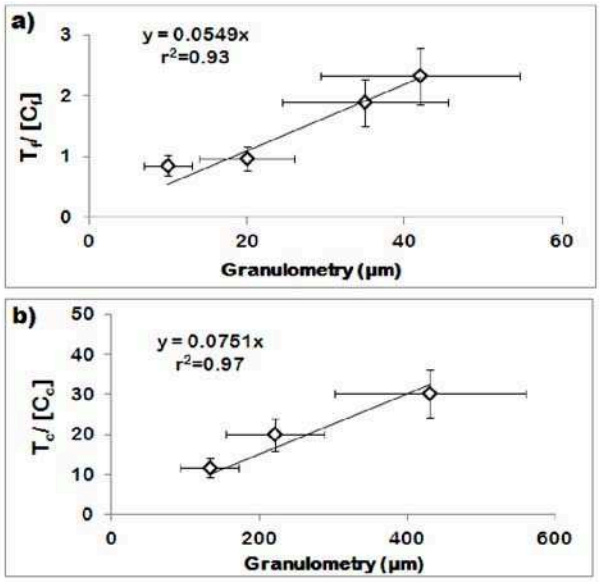

Figure 3. Relationship between specific turbidity and particle size: a) fine sediment $[T_f]/[C_f]$=0.0549ϕ_f; b) coarse sediment $[T_c]/[C_c]$=0.0751ϕ_c.

- *Testing sensor response to fine and coarse sediment mixing*

  Based on laboratory work, we find that the optical responses of fine and coarse sediment of the Amazon follow an additive pattern. For verification, an experiment was conducted (Fig. 4). Starting with a solution of a known concentration of fine sediment (12-µm), known concentrations of coarse sediment (278-µm) were gradually added to the mixture, and the turbidity was recorded. The same procedure was performed without the only coarse material. The results show that the gradients of both curves are similar, with a gap in turbidity that corresponds to the presence of fine sediment. This demonstrates that the resulting turbidity of the solution is a combination of the turbidity induced by the fine and coarse sediment concentrations. The relative parts induced by fine and coarse sediment depend on both concentration and $T/[C]$ values.

2.3.2 Method used to extract a concentration profile from a turbidity profile

The turbidity profile is the result of the granulometric distribution and the relative vertical concentration gradient for each sediment size mode. In this study, we take advantage of the fact that suspended sediment in the Amazon River exhibits only two

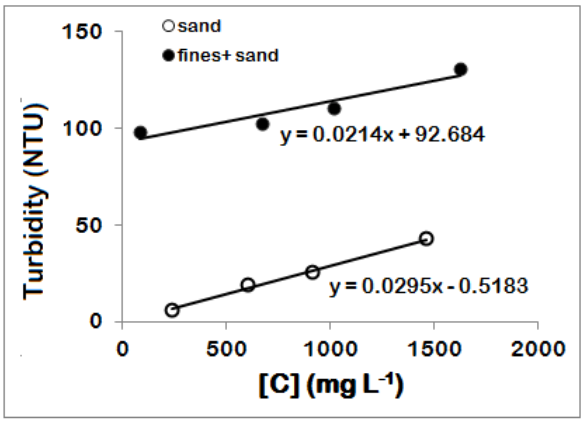

Figure 4. Additive property of turbidity as a function of concentration.

well-defined granulometric modes corresponding to well-defined $T/[C]$ factors. However, it is necessary to use a method based on the separation of sediment types. The Rouse model is considered to be a tool for separating the turbidity signal, for which it is necessary to account for hypotheses that were demonstrated in laboratory experiments. The study followed the methodology below (Fig. 5).

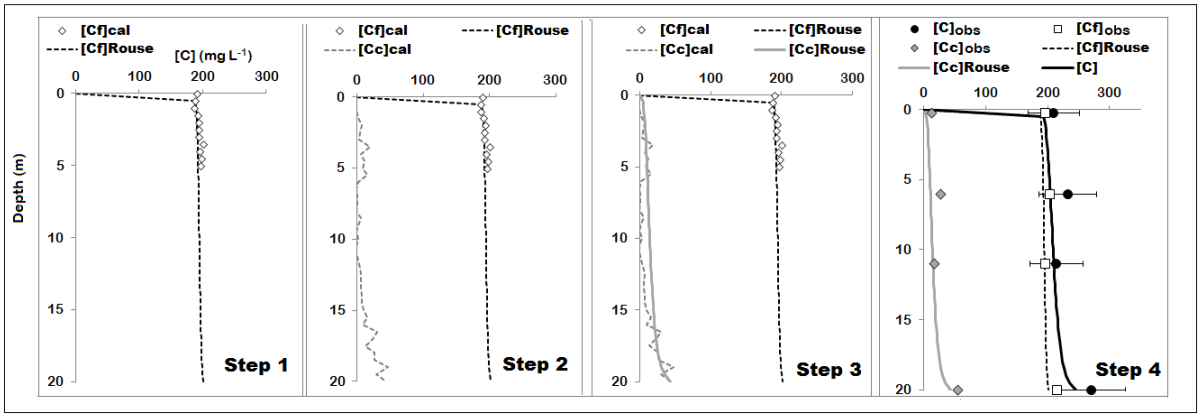

Figure 5. Methodology used to transform the turbidity profiles into concentration profiles.

Step 1. Turbidity profiles were measured in each location where samples of water and sediment were collected. Because the upper third of the suspended sediments vertical concentration profile is mostly composed of fine particles (Table 2, Fig. 6), T for this upper part is relevant for the fine sediment concentration $[C_f]$ gradient. The first one-third of $([C_f]_{cal})$ is calculated by applying the $T/[C]$ factor of the fine sediment mode.

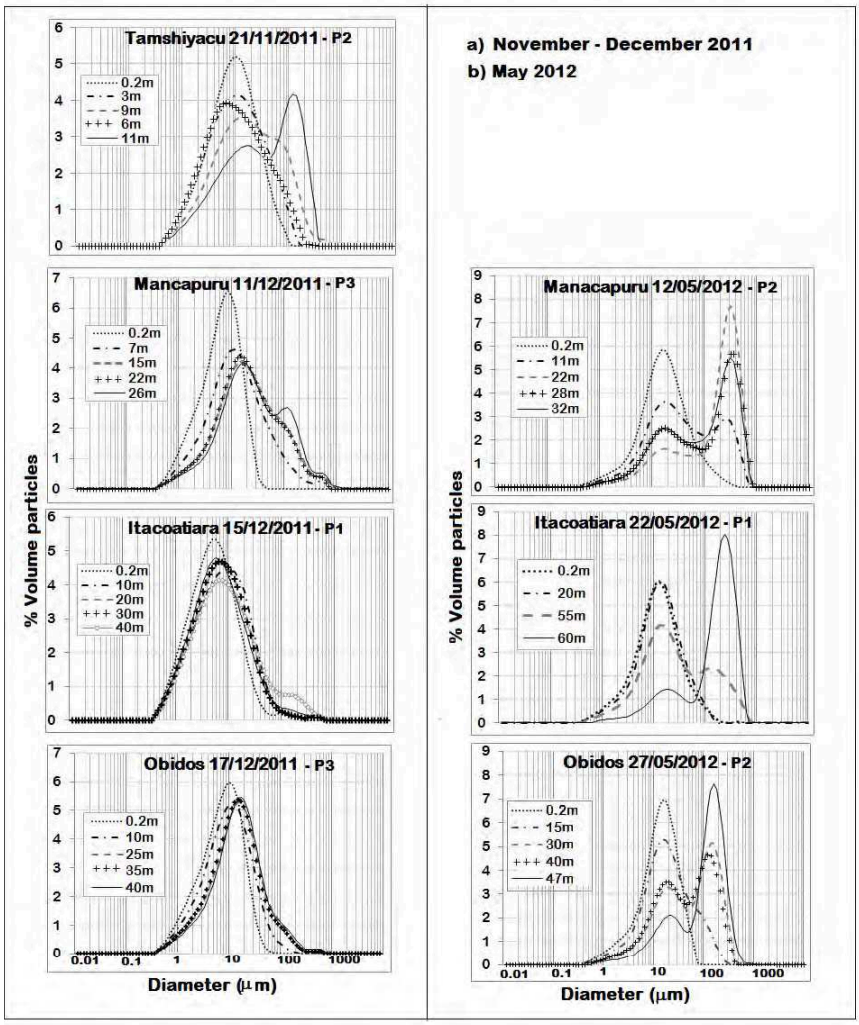

Figure 6. Grain size distributions for all the gauging stations in periods of a) high water and b) low water for one profile.

Step 2. Over the entire depth profile, we calculate the best Rouse fine sediment concentration profile, $[C_f]_{Rouse}$, that fit $[C_f]_{cal}$ calculated in step 1. From $[C_f]_{Rouse}$, the vertical turbidity for fine sediment (Tf_{Rouse}) is deduced from the inverse value of $T/[C]$ for fine sediment. Then, the turbidity profile for coarse sediment (Tc) is derived by subtracting TfRouse from T at each depth, based on the additive properties of the turbidity signal. $[C_c]_{cal}$ is calculated based on Tc by applying the $T/[C]$ factor of the coarse sediment mode.

Spet 3. We fit a Rouse profile ($[C_f]_{Rouse}$) to the $[C_c]_{cal}$ profile obtained in step 2.

Step 4. Finally, we obtain two concentration profiles: one for fine sediments ($[C_f]_{Rouse}$) and one for coarse sediments ($[C_c]_{Rouse}$). The sum of both profiles corresponds to the total concentration profile of the suspended sediment $[C]$.

2.4 Rouse profile calibration and validation

The Rouse profile aims to describe the vertical distribution of suspended sediment under steady state conditions when downward settling is balanced by upward transport processes of sediment. It predicts that the suspended sediment concentration follows the following equation:

$$\frac{C_{(z)}}{C_{(ref)}} = \left(\frac{H-d}{d}.\frac{z}{H-z}\right)^{W} \tag{5.1}$$

where: $[C_{(z)}]$ is the sediment concentration at level z, $[C_{(ref)}]$ is the reference concentration at distance $z = d$ ($d = 0.03{*}H$, which corresponds to the minimum distance between the turbidity sensor and bed), H is the total depth, W is the Rouse number, which is defined as $\frac{w_s}{\kappa.u^*}$ where w_s is the settling velocity, κ is the Von Kármán constant (0.41) and u^* is the shear velocity.In a steady, turbulent and uniform flow, the velocity distribution is well represented by the law of the wall:

$$\frac{\bar{u}}{u^*} = \frac{1}{\kappa}.\ln\left(\frac{z}{z_o}\right) \tag{5.2}$$

Where $\bar{u}$ is the time-averaged flow velocity at a distance z; z_o is the bed roughness length. Equation 2 can also be written as follows:

$$\bar{u} = a.\ln(z) + b \tag{5.3}$$

where: $u^* = a \times \kappa$; $z_o = \exp\left(\frac{-b}{a}\right)$.

The coefficients of a and b were estimated by fitting the average of various ADCP velocity profiles. Because data are collected using an ADCP in motion, it is necessary to obtain the average of various profiles to correctly describe a logarithmic profile. Nystrom et al. (2007) conducted laboratory experiments showing that ADCPs are capable of correctly reproducing the logarithmic profile of velocity predicted by the law of the wall. However, during field measurements, it is necessary to average several vertical profiles to obtain such logarithmic profiles of velocity Stone e Hotchkiss (2007). We found that with the high velocities (>2 m s^{-1}) and large width (>2 km) of the Solimões/Amazon River, the number of velocity profiles needed to obtain a significant u^* value depends on the stability of the coefficient a. Generally, stable values were reached using approximately 50 to 60 ADCP velocity profiles, corresponding to a spatial average of 150 m (i.e., 10% of the total width of the section) in the cross-section direction. The uncertainty of u^* is ± 33%. This uncertainty includes the fact that velocity profiles are registered during the drift of the boat instead of the fixed-point protocol.

To validate the application of the Rouse model theory to the vertical concentration profile for fine and coarse sediment, two criteria are checked. The first one is the coherency between the sample concentrations and concentrations calculated from the Rouse profiles. The second criterion is the coherency between the sediment size mode calculated from the W and ws values and the particle size mode measured with the laser granulometer. The settling velocity (w_s) is a function of particle size following Stoke's law.

2.5 Estimation of suspended sediment flux

The instantaneous suspended-sediment flux (Qs_i) in each ADCP cell is calculated as:

$$Qs_i = Q_i \ * \ [C_i] \tag{5.4}$$

where Q_i is the instantaneous water discharge of the ADCP cell in $m^3\ s^{-1}$ and $[C_i]$ is the suspended sediment concentration ($[C_f] + [C_c]$) in mg L^{-1}. The total sediment flux is calculated by summing all Qsi values in the section in kg s^{-1}. To test the sensitivity of Qs_i to each parameter of the Rouse model, W is fixed and $[C]_{(ref)}$ is varied, and vice versa, for both fine and coarse sediment cases.

3. Results

Fig. 7 shows a good coherence between the fine and coarse concentrations obtained from turbidity and the discrete fine and coarse samples, with $r^2 = 0.71$. The main disparities depend on the coarse sediment concentration near the river bottom.

The W_f (fine-sediment Rouse number) and W_c (coarse-sediment Rouse number) values are in range of 0.01 to 0.03 and 0.25 to 0.60, respectively (Table 3). For a single cross-section W_f, W_c and the coefficient $[C_f]_{ref}$ show a lateral variation that is within the range of the uncertainties, and $[C_c]_{ref}$ varies with the vertical location. Again, careful calculation or measurement of $[C_c]_{ref}$ must be performed to significantly reduce uncertainty in the concentration prediction. For flux estimations of fine sediments, a linear interpolation is valid to fix the Rouse model for unmeasured vertical profiles. For coarse sediments, the variation in $[C_c]_{ref}$ from one vertical profile to another is significant, suggesting the importance of the local hydraulic conditions. This variation can present an uncertainty of up to ±36% in the estimates of the solid coarse sediment flux.

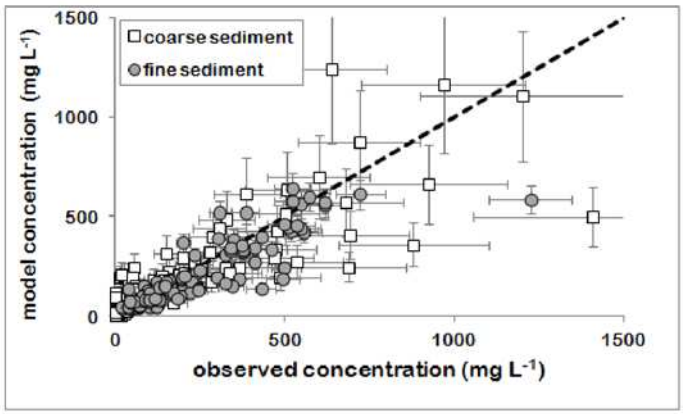

Figure 7. Rouse model concentration *vs* observed concentration; gray circle for fine sediments and white square for coarse sediments, $r^2 = 0.72$.

Although the uncertainty in the coarse sediment flow calculation is important, the uncertainty decreases to ±25% for the total suspended sediment flux estimation because of the homogeneity of the fine sediment concentration across the entire section.

This methodology produces data on concentration fields with better spatial resolution throughout the cross-section of the river. Instead of averaging ADCP velocity data for a number of surfaces that correspond to the number of samples conducted during the field campaign, a concentration field is modeled at the same resolution as the field of water velocity measured with the ADCP. The resulting total sediment discharge integrates all products of water discharge with concentration at the best resolution scale for the observations. This is the most accurate manner to take into account the non-linear gradients in velocity and concentration in the calculation for the cross-section. This method can be applied for each sediment size mode. For the Amazon River, our results, obtained from only a low number of vertical profiles, notably improve our understanding of the sediment flux dynamics. The error in the calculation of total sediment flux depends on the relative amplitude of the coarse sediment flux. This error varies from ±17 to ∓29% during the high-water period and from ±12 to ±14% during the low-water period.

Table 4 summarizes the sediment flux calculations applying Rouse profiles for each ADCP vertical profiles. The fine sediment flux is twice the coarse sediment flux in the low-water period. This ratio is reversed during the flood period. The sensitivity of the sediment flux estimate is assessed by exploring the range of values for each parameter. The sensitivity range is ±12% and ±36% for fine and coarse sediments, respectively, and is mainly controlled by the $[C_f]_{ref}$ and $[C_c]_{ref}$ variability.

Table 3. Parameters of the Rouse model for the Solimões and Amazon River: Distance above the bed (d),shear velocity (u^*). To fine sediments: Reference concentration ($[C_f]_{ref}$, Rouse's number(W_f) and settling velocity (w_{sf}). To coarse sediments: Reference concentration ($[C_c]_{ref}$, Rouse's number(W_c) and settling velocity (w_{sc})

Station	River	Date	Profile	u^*	d	Rouse fine sediment			Rouse coarse sediment		
						W_f	$[C_f]_{ref}$	w_{sf}	W_c	$[C_c]_{ref}$	w_{sc}
				(m s^{-1})	(m)		(mg L^{-1})	(m s^{-1})		(mg L^{-1})	(m s^{-1})
Tamshiyacu	Amazon	21/11/2011	P1	0.082	0.8	0.02	420	0.0006	0.30	450	0.0096
			P2	0.115	0.9	0.02	420	0.0009	0.50	600	0.0224
			P3	0.074	1.2	0.02	350	0.0005	0.30	200	0.0086
		12/02/2012	P1	0.082	0.8	0.03	620	0.0009	0.30	800	0.0096
			P2	0.074	1.0	0.03	630	0.0008	0.25	400	0.0072
			P3	0.094	1.3	0.01	460	0.0004	0.25	400	0.0092
Manacapuru	Solimões	11/12/2011	P1	0.037	0.8	0.03	210	0.0004	0.30	35	0.0043
			P2	0.052	1.0	0.01	200	0.0002	0.30	35	0.0061
			P3	0.062	1.3	0.05	260	0.0012	0.30	300	0.0072
		12/05/2012	P1	0.062	1.3	0.02	45	0.0004	0.25	350	0.0060
			P2	0.114	1.6	0.01	52	0.0002	0.25	320	0.0111
			P3	0.089	1.8	0.01	50	0.0003	0.60	500	0.0208
Itacoatiara	Amazon	15/12/2011	P1	0.051	2.2	0.01	110	0.0002	0.20	10	0.0040
			P2	0.059	2.5	0.03	190	0.0007	0.20	55	0.0046
			P3	0.081	1.8	0.03	190	0.0010	0.30	75	0.0095
			P4	0.081	1.0	0.02	140	0.0006	0.60	90	0.0190
		22/05/2012	P1	0.089	2.9	0.02	55	0.0007	0.40	600	0.0140
			P2	0.050	2.0	0.02	80	0.0004	0.40	500	0.0078
			P3	0.091	1.3	0.02	115	0.0007	0.40	400	0.0141
Óbidos	Amazon	17/12/2011	P1	0.055	2.5	0.02	95	0.0004	0.35	40	0.0075
			P2	0.055	2.4	0.02	95	0.0004	0.30	20	0.0065
			P3	0.064	1.9	0.02	109	0.0005	0.30	60	0.0075
			P4	0.054	1.6	0.03	125	0.0006	0.30	60	0.0063
		27/05/2012	P1	0.074	3.1	0.02	90	0.0006	0.30	350	0.0086
			P2	0.205	2.5	0.02	90	0.0016	0.40	600	0.0320
			P3	0.123	2.1	0.02	160	0.0010	0.40	350	0.0192

4. Discussion

Splitting each turbidity vertical profile into two profiles relative to fine and coarse sediment is possible because of the additive properties of the sediment mode size and mass concentration near the Amazon riverbed and by assuming a model of the vertical profile. The methodology proposed in this study allows the extraction of concentration profiles for each size mode with less uncertainty than without size mode consideration. The results demonstrate that careful interpretation of turbidity significantly reduces this dispersion and the corresponding errors in the concentration values. This leads to a much better definition of vertical profiles with high spatial resolution and the opportunity to fit a physical model to interpret vertical concentration gradients. In this study, we propose the use of the Rouse profile as a tool for the splitting methodology

Table 4. Suspended sediments flux.

COD	Station	River	Date	Dicharge (m^3 s^{-1})	Sediment Flux Qs (kg s^{-1}) Fine	Coarse	Total
TAM	Tamshiyacu	Amazon	11/11/2011	23370	9323	4087	13410
			12/02/2012	45387	25602	13377	38979
MAN	Manacapuru	Solimões	11/12/2011	66337	13144	3766	16910
			12/05/2012	145740	6832	21830	28662
ITA	Itacoatiara	Amazon	15/12/2011	105841	12532	4397	16929
			22/05/2012	236542	18538	56543	75082
OBI	Óbidos	Amazon	17/12/2011	107892	9569	3212	12781
			27/05/2012	259076	26129	48836	74967

and as the basic model relevant for the Amazon River for a large range of sediment sizes (1 µm – 300 µm). The coherency between the particle size of the measured particles and the particle size of the particles modeled with the Rouse exponent calibration is acceptable. The particle diameter modeled with the Rouse profile is twice as large as that measured with the laser granulometer (Fig. 8), which is a good result considering all the sources of uncertainties for sediment size definition: flocculation processes occurring during transportation and laboratory storage, fragmentation during the measurement process with the laser granulometer, skewness in the mode pikes and calculating the particle size diameter from W, which is linked to u^* uncertainty and biases introduced by the use of Stoke's law to model w_s.

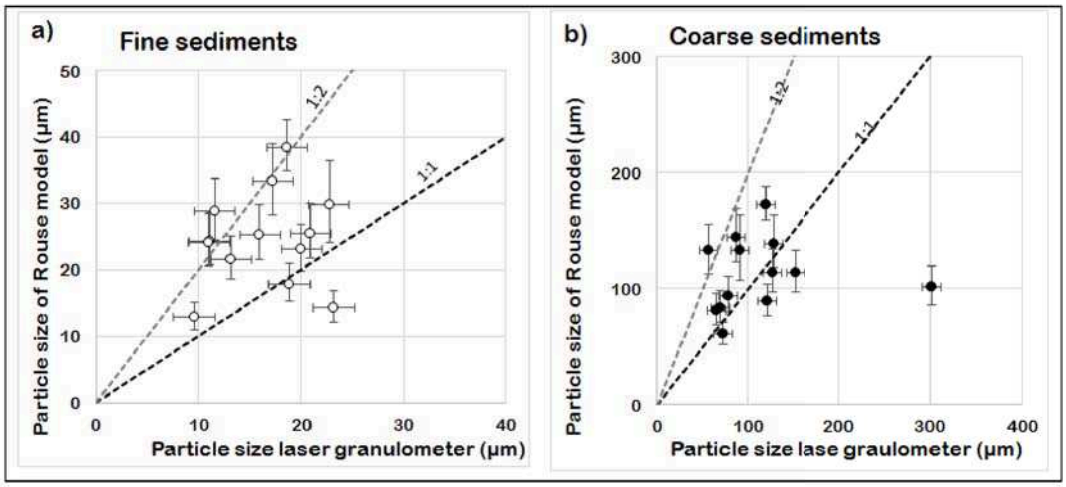

Figure 8. Particle size measurement via laser granulometry (m) *vs* particle size of the Rouse model (m) for fine and coarse sediments.

The Rouse model has already been proposed by authors for the Amazon River based

on in situ data (Vanoni, 1979, Bouchez et al., 2011a). However, the previous studies consider one sediment size mode per vertical profile of samples or for the entire gauging station. Our results show that the Rouse profile theory can be defined per sediment size mode when a combination of different size modes is present. This notably improves the use of the Rouse model to predict vertical concentration gradients and defines the main source of uncertainty as the calibration of $[C_c]_{ref}$.

5. Conclusion

This study demonstrates that turbidity sensors can greatly enhance suspended sediment monitoring of large rivers. Consequently, it can reduce logistical constraints and significantly improve the accuracy of the results. The methodology proposed in this study leads to a much better definition of the concentration gradients in the river section because it considers a mix of particle sizes. Each mode can be modeled independently from one another to fit a Rouse model, which is relevant for every suspended sediment size mode.

Therefore, traditional methods of sediment flux monitoring along the Amazon River can be updated using optical technologies and an adapted sampling strategy. Fine sediment concentration profiles can be simply monitored using samples from the surface and/or MODIS satellite images (Martinez et al., 2009). Then, from these data on the fine sediment concentration at the surface of the stream, we can apply a Rouse model with an average exponent of 0.02. Coarse sediment concentration profile monitoring requires determining the concentration gradient near the river bottom. For this, one profile with a turbidimeter probe and one sample, preferably at less than 1 m from the bottom, are enough to fit a Rouse model. This protocol notably improves **1)** the accuracy of the concentration profile that is multiplied by the ADCP velocity field and consequently the sediment flux assessment and **2)** the efficiency of the field campaign in terms of time and logistics.

The Rouse model helps to describe vertical gradients in the suspended sediment concentration. It reduces the problematic aspects of vertical concentration profile prediction by calculating the two main parameters of this model for each sediment size mode. If the sediment size modes are known, the Rouse exponents can be calculated directly using the ADCP data. The main difficulty remains obtaining samples near the bedform for each vertical profile to calibrate $[C_c]_{ref}$ because the lateral gradient of $[C_c]_{ref}$ along the river cross-section is the main source of uncertainty in the sediment flux profile

calculation. Collecting samples near the bottom of large rivers is sometimes a challenge and requires a good knowledge of the bottom and synchronization between the team members in the Amazon context. If the sediment size modes are unknown, this protocol must be adapted to capture the gradient of concentration where the values are larger, meaning the bottom third of the river. Finally, three samples are needed to describe the trend of concentration near the river bottom, and we recommend sampling at z equal to 5, 10, and 20 percent of the total depth H.

One of the main findings of this study is that a field campaign protocol has been proposed to improve the measurement of suspended.

Acknowledgement

This study was conducted with support from the Agencia Nacional de Aguas (ANA), Serviço Geológico do Brasil (CPRM), the Institut de Recherche pour le Dèveloppement (IRD), and Servicio Nacional de Meterología e Hidrología (SENAMHI-Perú). We would like to thank the participants in the Laboratorio de Potamologia da Amazônia (LAPA) and the entire crew of Janes Jose IV, especially Captains Jose and Baxinho and Bosco Alfanes for all the support during the field days. We also thank the Laboratory of CPRM, especially Paulo Melo and Magda Ferreira. The authors of this article are listed sequentially according to their contribution to this work. The last author is the coordinator, who is responsible for the publication. The authors would like to thank J. Bouchez and an anonymous reviewer for their critical comments, which greatly improved the manuscript.

I Appendice-Notacion

$[C]$	total suspended sediment concentration (mg L^{-1})
$[C_f]$	fine suspended sediment concentration (mg L^{-1})
$[C_c]$	coarse suspended sediment concentration (mg L^{-1})
$[C_f]_{cal}$	fine suspended sediment concentration using a fine calibration curve (mg L^{-1})
$[C_c]_{cal}$	coarse suspended sediment concentration using a coarse calibration curve (mg L^{-1})
$[C_f]_{Rouse}$	fine suspended sediment concentration modeled by Rouse model (mg L^{-1})
$[C_c]_{Rouse}$	coarse suspended sediment concentration modeled by Rouse model (mg L^{-1})
$[C_z]$	suspended sediment concentration at level z (mg L^{-1})
$[C]_{ref}$	reference suspended sediment concentration a above the bed (mgL^{-1})
$[C_f]_{ref}$	fine reference suspended sediment concentration a above the bed (mg L^{-1})
$[C_c]_{ref}$	coarse reference suspended sediment concentration a above the bed (mg L^{-1})
W	Rouse number
W_f	fine Rouse number
W_c	coarse Rouse number
u^*	shear velocity (m s^{-1})
w_s	settling velocity (m s^{-1})
T	turbidity (NTU)
$T/[C]$	specific turbidity
Tf_{Rouse}	fine sediments turbidity obtained by Rouse model (NTU)
Tc	coarse sediments turbidity (NTU)
ϕ_f	fine size particle (μm)
ϕ_c	coarse size particle (μm)

Bibliography

Anderson, C.,2004. Turbidity,(version 2): Us geological survey techniques of water-resources investigations, book 9, chap, A6, section 6.

Armijos, E., Crave, A., Vauchel, P., Fraizy, P., Santini, W., Moquet, J.-S., Arevalo, N., Carranza, J. and Guyot, J.-L.,2013. Suspended sediment dynamics in the Amazon River of Peru, Journal of South American Earth Sciences 44, 75–84.

ASTM International, a.,2003. D1889–00-Standard test method for turbidity of water, Annual Book of ASTM Standards,Water and Environmental Technology.

Bouchez, J., Metivier, F., Lupker, M., Maurice, L., Perez, M., Gaillardet, J. and France-Lanord, C.,2011. Prediction of depth-integrated fluxes of suspended sediment in the Amazon River: Particle aggregation as a complicating factor, Hydrological processes 25(5), 778–794.

Bouchez, J., Lupker, M., Gaillardet, J., France-Lanord, C. and Maurice, L., 2011b. How important is it to integrate riverine suspended sediment chemical composition with depth? clues from amazon river depth-profiles, Geochimica et Cosmochimica Acta 75(22), 6955–6970.

Bunt, J. A., Larcombe, P. and Jago, C. F.,1999. Quantifying the response of optical backscatter devices and transmissometers to variations in suspended particulate matter, Continental shelf research 19(9), 1199–1220.

Butt, T., Miles, J., Ganderton, P. and Russell, P.,2002. A simple method for calibrating optical backscatter sensors in high concentrations of non-cohesive sediments, Marine Geology 192(4), 419–424.

Callède, J., Cochonneau, G., Alves, F.V., Guyot, J.-L., Guimaraes, V. S. and De Oliveira, E.,2010. Les apports en eau de l'Amazone à l'Océan Atlantique, Revue des sciences de l'eau/Journal of Water Science 23(3), 247–273.

De Brito Neves, B. B. and Cordani, U. G.,1991. Tectonic evolution of South America during the late proterozoic, Precambrian Research 53(1), 23–40.

Dunne, T., Mertes, L. A., Meade, R. H., Richey, J. E. and Forsberg, B. R.,1998. Exchanges of sediment between the flood plain and channel of the amazon river in brazil, Geological Society of America Bulletin 110(4), 450–467.

Edwards, T. K., Glysson, G. D. 1988. Field methods for measurement of fluvial sediment (pp. 9-32). Department of the Interior, US Geological Survey
.

Filizola, N.,2003. Transfert sédimentaire actuel par les fleuves Amazoniens, PhD thesis, Université Paul Sabatier.

Filizola, N. and Guyot, J.L.,2004. The use of doppler technology for suspended sediment discharge determination in the river Amazon/l'utilisation des techniques doppler pour la détermination du transport solide de l'Amazone, Hydrological Sciences Journal 49(1), 143–153.

García, M.,2008. Sediment Transport and Morphodynamics. In Sedimentation Engineering: Pro- cesses, Measurements, Modeling and Practice, chapter 2, pp. 21–163.

Gibbs, R.J.,1967. Amazon rivers: Environmental factors that control its dissolved and suspended load, Science 156, 3.

Guyot, J.-L.,1993. Hydrogéochimie des fleuves de l'Amazonie Bolivienne, PhD thesis, Université de Bordeaux 1, Talence,France.

Guyot, J.-L. and Called, H.,1990. Utilisation de mesures journalières de la turbidité pour l'estimation des flux de matières en suspension. l'exemple des fleuves Andins de Bolivie, in 'Proceeding of two Lausanne Symposia", August 1990, IAHS Publ. No 193, 1990. Disponible en la Biblioteca del IRD en La Paz, Bolivia'.

Guyot, J.L., Filizola, N. and Laraque, A., 2005. Régime et bilan du flux sédimentaire de l'Amazone à Obidos (Pará, Brésil) de 1995 à 2003, Sediments Budgets 1. IAHS Publ (291), 347.

Landers, M. N.,2011. Fluvial suspended sediment characteristics by high-resolution, surrogate metrics of turbidity, laser-diffraction, acoustic backscatter, and acoustic attenuation, PhD thesis, Georgia Institute of Technology.

Le Roux, J.,2005. Grains in motion: A review, Sedimentary Geology 178(3), 285–313.

Ludwig, K. A. and Hanes, D. M.,1990. A laboratory evaluation of optical backscatterance suspended solids sensors exposed to sand-mud mixtures, Marine Geology 94(1), 173–179.

Martinez, J.-M., Guyot, J.-L., Filizola, N. and Sondag, F.,2009. Increase in suspended sediment discharge of the Amazon River assessed by monitoring network and satellite data, Catena 79(3), 257–264.

Meade, R. H.,1994. Suspended sediments of the modern Amazon and Orinoco rivers, Quaternary International 21, 29–39.

Meade, R. H., Dunne, T., Richey, J. E., Santos, U. d. M. and Salati, E.,1985. Storage and remobilization of suspended sediment in the lower Amazon River of Brazil, Science 228(4698), 488–490.

Merten, G. H., Capel, P. D. and Minella, J. P.,2013. Effects of suspended sediment concentration and grain size on three optical turbidity sensors, Journal of Soils and Sediments pp. 1–7.

Milliman, J. D. and Meade, R. H.,1983. World-wide delivery of river sediment to the oceans, The Journal of Geology pp. 1–21.

Minella, J. P., Merten, G. H., Reichert, J. M. and Clarke, R. T.,2008. Estimating suspended sediment concentrations from turbidity measurements and the calibration problem, Hydrological processes 22(12), 1819–1830.

Molinier, M., Guyot, J.-L., De Oliveira, E., Guimaraes, V., Chaves, A., Olivry, J. and Boulègue, J.,1995. Hydrologie du bassin de l'Amazone, Proc. Grands Bassins Fluviaux P´eri-atlantiques 1, 335–344.

Nystrom, E. A., Rehmann, C. R. and Oberg, K. A.,2007. Evaluation of mean velocity and turbulence measurements with adcps, Journal of hydraulic engineering 133(12), 1310–1318.

Pavanelli, D. and Bigi, A.,2005. Indirect methods to estimate suspended sediment concentration: Reliability and relationship of turbidity and settleable solids, Biosystems engineering 90(1), 75–83.

Phillips, J. and Walling, D.,1995. An assessment of the effects of sample collection, storage and resuspension on the representativeness of measurements of the effective particle size distribution of fluvial suspended sediment, Water Research 29(11), 2498–2508.

Restrepo, J.C. and Pierini, J. O.,2012. Medición de la concentración de sedimentos en suspension mediante dispositivos opticos y acústicos: aplicación en sistemas tropicales (delta del Río Mira, Colombia), Latin American Journal of Aquatic Research 40(1), 153–168.

Richey, J. E., Meade, R. H., Salati, E., Devol, A. H., Nordin, C. F. and Santos, U. D.,1986. Water discharge and suspended sediment concentrations in the Amazon River: 1982–1984, Water Resources Research 22(5), 756–764.

Roddaz, M., Viers, J., Brusset, S., Baby, P. and Hérail, G.,2005. Sediment provenances and drainage evolution of the neogene Amazonian foreland basin, Earth and Planetary Science Letters 239(1), 57–78.

Rouse, H.,1938. Nomogram for the settling velocity of spheres, National Research Council, Division of Geology and Geography.

Sternberg, R., Kineke, G. and Johnson, R.,1991. An instrument system for profiling suspended sediment, fluid, and flow conditions in shallow marine environments, Continental Shelf Re- search 11(2), 109–122.

Stone, M. C. and Hotchkiss, R. H.,2007. Evaluating velocity measurement techniques in shallow streams, Journal of Hydraulic Research 45(6), 752–762.

Syvitski, J. P., Peckham, S. D., Hilberman, R. and Mulder, T.,2003. Predicting the terrestrial flux of sediment to the global ocean: a planetary perspective, Sedimentary Geology 162(1), 5-24.

Thollet, F., Le Coz, J., Antoine, G., Fran¸cois, P., Saguintaah, L., Launay, M. and Camenen, B.,2013. Influence de la granulométrie des particules sur la mesure par turbidimétrie des flux de mati‘eres en suspension dans les cours d'eau, La Houille Blanche (4), 50–56.

Vanoni, V. A., 1979. Sediment studies in the Brazilian Amazon River basin.

Vanoni, V. A., 1980. Sediment studies in the Brazilian Amazon River basin, Report KH-P-168, W.M. Keck Laboratory of Hydraulic and Water Resources.

Wren, D., Barkdoll, B., Kuhnle, R. and Derrow, R.,2000. Field techniques for suspended- sediment measurement, Journal of Hydraulic Engineering 126(2), 97–104.

Capítulo 6

Conclusões

O contínuo monitoramento feito por o Observatório SO-HYBAM junto com a parceria das Instituições Nacionais, SENAMHI no Peru e ANA-CPRM no Brasil, permitiu determinar os fluxos de sedimentos em suspensão nos principais rios da bacia amazônica peruana (Marañón, Huayllaga, Ucayali e Amazonas) e no Amazonas na estação de Óbidos. Além este estudo mostra a distribuição vertical dos sedimentos em suspensão na seção na calha principal do Rio Solimões/Amazonas.

As bacias sub-Andinas apresentam uma variabilidade hidrológica de alta frequência acompanhada pelos fluxos de sedimentos em suspensão, no entanto, esta variabilidade diminui em frequência na planície e os fluxos sedimentários tem um adianto no pico de sedimentos de até 3 meses em comparação com o pico da cheia. Atribuímos este comportamento às diferenças entre os regimes do norte e sul da Bacia, além do ingresso das águas pretas que são pobres em sedimentos. No entanto, ainda restam os questionamentos sobre a compreensão da histerese, que deve ser entendida.

A distinção dos dois tipos de sedimentos presentes no rio Solimões/Amazonas e sua diferenciada presença durante o regime hidrológico é um passo a mais na compreensão dos processos de transporte no rio Amazonas.
Graças a este analise foi possível de calcular os fluxos de sedimentos na estação de Óbidos, considerada como a estação que monitora a maior bacia do mundo e ate agora foi motivo de discussão en quanto as diferencias nas estimativas.

Este estudo deu uma pauta na sensibilidade dos fluxos sedimentários frente às variabilidades climáticas, colocando em evidência que em anos El Niño a porcentagem de fluxos de sedimentos grosseiros tem um decréscimo, e em de eventos La Niña são observados altas porcentagens de fluxos de areias. A positiva correlação entre o resfriamento da temperatura da superfície de mar do Pacífico com os fluxos de sedimentos de areias, coloca aos fluxos de sedimentos como indicadores da variabilidade climática, no entanto, ainda precisa-se aprofundar-se no tema e continuar com as análises, já que a bacia Amazônica é a maior do mundo com características continentais.

A utilização de técnicas indiretas com é a turbidez, pode ser utilizada no rio Solimões/Amazonas, este estudo descreve a metodologia a ser empregada para o uso em grandes rios. Apresenta-se uma calibração em função da granulometria, permitindo ter uma calibração para material fino e outra para areias. Mostrou-se que medições de alta frequência descrevem melhor a distribuição espacial na seção.

Mostrou-se também que não existe um perfil característico de concentração em cada seção, no entanto, a distribuição de sedimentos finos é mais homogênea na seção, tendo sempre um gradiente vertical na época de enchente e este gradiente decresce na época de cheia. Já para as areias o comportamento é contrário, em que perfis verticais são observados na época de enchente e gradientes marcados na época de cheia. A forma dos perfis verticais tem variação espacial para as areias, e a distribuição é heterogênea, indicando que são as condições hidráulicas que regem este comportamento.

Este estudo mostra que no rio Amazonas é factível a utilização de um modelo de concentração como é o modelo de Rouse junto com a turbidez, sempre e quando se faça a distinção dos tipos de sedimentos, finos e areias. Este é um passo também na predição de perfis de concentração com um equipamento mas versátil.

Um dos próximos passos é entender variabilidade espacial a nivel da bacia no Alto Solimões utilizando ferramentas como imagens MODIS acoplados aos resultado obtidos neste estudo, achamos que esta junção de ferramentas pode ser utilizado também na compreensão das histereses.

Finalmente, podemos concluir que cada inovação ao estudo feito na maior Bacia do mundo é um passo na compressão de processos de erosão e transporte de sedimentos, no entanto, faz-se necessário um monitoramento contínuo.

Referências Bibliográficas

Aalto, R., Maurice-Bourgoin, L., Dunne, T., Montgomery, D. R., Nittrouer, C. A., e Guyot, J.-L. (2003). Episodic sediment accumulation on Amazonian flood plains influenced by El Nino/Southern Oscillation. *Nature*, 425(6957):493–497.

Abril, G., Martinez, J.-M., Artigas, L. F., Moreira-Turcq, P., Benedetti, M. F., Vidal, L., Meziane, T., Kim, J.-H., Bernardes, M. C., Savoye, N., et al. (2014). Amazon river carbon dioxide outgassing fuelled by wetlands. *Nature*, 505(7483):395–398.

Anderson, C. (2004). Turbidity,(version 2): US Geological Survey techniques of Water-resources Investigations, book 9, chap. *A6, section*, 6.

Anderson, C. (2005). Turbidity. . *S. Geological Survey Techniques of Water Resources Investigations Book, Chapter A6, Section 6.7*, 9.

Armijos, E., Crave, A., Vauchel, P., Fraizy, P., Santini, W., Moquet, J.-S., Arevalo, N., Carranza, J., e Guyot, J.-L. (2013a). Suspended sediment dynamics in the Amazon River of Peru. *Journal of South American Earth Sciences*, 44:75–84.

Armijos, E., Laraque, A., Barba, S., Bourrel, L., Ceron, C., Lagane, C., Magat, P., Moquet, J. S., Pombosa, R., Sondag, F., et al. (2013b). Yields of suspended sediment and dissolved solids from the Andean basins of Ecuador. *Hydrological Sciences Journal*, 58(7):1478–1494.

ASCE (1977). *American Society of Civil Engineer, Manual Sedimentation Engineering*, volume 54. 10017, New York, n.y.10017.

ASTM, S. (2003). Standard test method for dynamic young's modulus, shear modulus, and poisson's ratio by impulse excitation of vibration. *West Conshohocken: ASTM International*, pgs. 1876–1878.

Baker, E. T. e Lavelle, J. W. (1984). The effect of particle size on the light attenuation coefficient of natural suspensions. *Journal of Geophysical Research: Oceans (1978–2012)*, 89(C5):8197–8203.

Beighley, R., Eggert, K., Dunne, T., He, Y., Gummadi, V., e Verdin, K. (2009). Simulating hydrologic and hydraulic processes throughout the amazon river basin. *Hydrological Processes*, 23(8):1221–1235.

Bernal, C., Christophoul, F., Darrozes, J., Soula, J.-C., Baby, P., e Burgos, J. (2011). Late glacial and holocene avulsions of the rio pastaza megafan (ecuador–peru): frequency and controlling factors. *International Journal of Earth Sciences*, 100(7):1759–1782.

Bernal, I. e Tavera, H. (2002). Geodinámica, sismicidad y energía sísmica en Perú. *Monografía, IGP, Lima-Perú*.

Bordas, M., Semmelmann, F., e TUCCI, C. (2004). Elementos de engenharia de sedimentos. *Hidrologia. Ciência e Aplicação. Porto Alegre: Editora da UFRGS/ABRH,*.

Bouchez, J., Lupker, M., Gaillardet, J., France-Lanord, C., e Maurice, L. (2011a). How important is it to integrate riverine suspended sediment chemical composition with depth? clues from amazon river depth-profiles. *Geochimica et Cosmochimica Acta*, 75(22):6955–6970.

Bouchez, J., Metivier, F., Lupker, M., Maurice, L., Perez, M., Gaillardet, J., e France-Lanord, C. (2011b). Prediction of depth-integrated fluxes of suspended sediment in the Amazon River: Particle aggregation as a complicating factor. *Hydrological processes*, 25(5):778–794.

Bunt, J. A., Larcombe, P., e Jago, C. F. (1999). Quantifying the response of optical backscatter devices and transmissometers to variations in suspended particulate matter. *Continental shelf research*, 19(9):1199–1220.

Butt, T., Miles, J., Ganderton, P., e Russell, P. (2002). A simple method for calibrating optical backscatter sensors in high concentrations of non-cohesive sediments. *Marine Geology*, 192(4):419–424.

Callède, J., Cochonneau, G., Alves, F. V., Guyot, J.-L., Guimarães, V. S., e De Oliveira, E. (2010). Les apports en eau de l'Amazone à l'océan Atlantique. *Revue des sciences de l'eau/Journal of Water Science*, 23(3):247–273.

Callède, J., Guyot, J. L., Ronchail, J., L'Hôte, Y., Niel, H., e de Oliveira, E. (2004). Evolution du débit de l'Amazone à óbidos de 1903 à 1999/Evolution of the River Amazon's discharge at óbidos from 1903 to 1999. *Hydrological Sciences Journal*, 49(1):85–97.

Callède, J., Kosuth, P., e DE OLIVEIRA, E. (2001). Etablissement de la relation hauteur-débit de l'Amazone à óbidos: méthode de la dénivelée normale à "géométrie variable". *Hydrological sciences journal*, 46(3):451–463.

Camenen, B. (2007). Simple and general formula for the settling velocity of particles. *Journal of Hydraulic Engineering*, 133(2):229–233.

Campbell, D. E. e Spinrad, R. W. (1987). The relationship between light attenuation and particle characteristics in a turbid estuary. *Estuarine, Coastal and Shelf Science*, 25(1):53–65.

Carvalho, L. M., Jones, C., e Liebmann, B. (2004). The South Atlantic convergence zone: Intensity, form, persistence, and relationships with intraseasonal to interannual activity and extreme rainfall. *Journal of Climate*, 17(1):88–108.

Chakrapani, G. (2005). Factors controlling variations in river. *Current Science*, 88(4).

Chevallier, P. (1993). Aquisição e processamento de dados. *Hidrologia (Org. Tucci, CEM)*, 2.

Constantine, J. A., Dunne, T., Ahmed, J., Legleiter, C., e Lazarus, E. D. (2014). Sediment supply as a driver of river meandering and floodplain evolution in the Amazon Basin. *Nature Geoscience*, 7(12):899–903.

Coynel, A. (2005). *Erosion mécanique des sols et transferts géochimiques dans le bassin Adour-Garonne*. PhD thesis, Université de Bordeaux 1.

Dadson, S. J., Hovius, N., Chen, H., Dade, W. B., Hsieh, M.-L., Willett, S. D., Hu, J.-C., Horng, M.-J., Chen, M.-C., Stark, C. P., et al. (2003). Links between erosion, runoff variability and seismicity in the taiwan orogen. *Nature*, 426(6967):648–651.

Davidson, E. A., de Araújo, A. C., Artaxo, P., Balch, J. K., Brown, I. F., Bustamante, M. M., Coe, M. T., DeFries, R. S., Keller, M., Longo, M., et al. (2012). The Amazon basin in transition. *Nature*, 481(7381):321–328.

De Almeida, F. F., Hasui, Y., e Neves, B. B. d. B. (1976). The upper Precambrian of South America. *Boletim IG-USP*, 7:45–80.

De Brito Neves, B. B. e Cordani, U. G. (1991). Tectonic evolution of South America during the late Proterozoic. *Precambrian Research*, 53(1):23–40.

De Oliveira Carvalho, N. (1994). *Hidrossedimentologia prática*. CPRM.

De Oliveira Carvalho, N., Filizola Pantoja, Júnior, N., Dos Santos Coutinho, P. M., e Lima, Furquim Werneck, J. E. (2000). *Guia de práticas sedimentométricas*. Aneel.

Diplas, P., Kuhnle, R., Gray, J., Glysson, D., e Edwards, T. (2008). Sediment transport measurements. *Sedimentation Engineering: Theories, Measurements, Modeling, and Practice. ASCE Manuals and Reports on Engineering Practice*, (110):165–252.

Droppo, I. G. (2004). Structural controls on floc strength and transport. *Canadian Journal of Civil Engineering*, 31(4):569–578.

Dubreuil, P., Lamagat, J., e Vuillaume, G. (1970). Tarage et calcul des débits des stations hydrométriqu non univoque.

Dumont, J.-F., Garcia, F., e Fournier, M. (1992). Registros de cambios climaticos por los depositos y morfologias fluviales en la amazonia occidental. Em *International Symposium on Former ENSO Phenomena in Western South America: Records of El Niño Events. Paleo-ENSO records international symposium. Extended abstracts. Lima*, pgs. 87–92.

Dunne, T., Mertes, L. A., Meade, R. H., Richey, J. E., e Forsberg, B. R. (1998). Exchanges of sediment between the flood plain and channel of the Amazon River in Brazil. *Geological Society of America Bulletin*, 110(4):450–467.

Edwards, T. K. e Glysson, G. D. (1988). *Field methods for measurement of fluvial sediment*. Department of the Interior, US Geological Survey.

Espinoza, J., Fraizy, P., Guyot, J., Ordoñez, J., Pombosa, R., e Ronchail, J. (2006). La variabilité des débits du rio amazonas au pérou. *IAHS publication*, pgs. 424–429.

Espinoza, J. C., Guyot, J. L., Ronchail, J., Cochonneau, G., Filizola, N., Fraizy, P., Labat, D., de Oliveira, E., Ordoñez, J. J., e Vauchel, P. (2009a). Contrasting regional discharge evolutions in the Amazon basin (1974–2004). *Journal of Hydrology*, 375(3):297–311.

Espinoza, J. C., Ronchail, J., Frappart, F., Lavado, W., Santini, W., e Guyot, J. L. (2013). The Major Floods in the Amazonas River and Tributaries (Western Amazon Basin) during the 1970–2012 period: A Focus on the 2012 Flood. *Journal of Hydrometeorology*, 14(3):1000–1008.

Espinoza, J. C., Ronchail, J., Guyot, J. L., Cochonneau, G., Filizola, N., Lavado, W., De Oliveira, E., Pombosa, R., e Vauchel, P. (2009b). Spatio-temporal rainfall variability in the Amazon basin countries (Brazil, Peru, Bolivia, Colombia, and Ecuador). *International Journal of Climatology*, 29(11):1574–1594.

Espinoza, J. C., Ronchail, J., Guyot, J. L., Junquas, C., Drapeau, G., Martinez, J. M., Santini, W., Vauchel, P., Lavado, W., Ordoñez, J., et al. (2012). From drought to flooding: understanding the abrupt 2010–11 hydrological annual cycle in the amazonas river and tributaries. *Environmental Research Letters*, 7(2):024008.

Espinoza, J. C., Ronchail, J., Guyot, J. L., Junquas, C., Vauchel, P., Lavado, W., Drapeau, G., e Pombosa, R. (2011). Climate variability and extreme drought in the upper Solimões River (western Amazon Basin): Understanding the exceptional 2010 drought. *Geophysical Research Letters*, 38(13).

Espinoza Villar, R., Martinez, J.-M., Guyot, J.-L., Fraizy, P., Armijos, E., Crave, A., Bazán, H., Vauchel, P., e Lavado, W. (2012). The integration of field measurements and satellite observations to determine river solid loads in poorly monitored basins. *Journal of Hydrology*, 444:221–228.

Espurt, N., Brusset, S., Baby, P., Hermoza, W., Bolaños, R., Uyen, D., e Déramond, J. (2008). Paleozoic structural controls on shortening transfer in the Subandean foreland thrust system, and southern Ucayali basins, Peru. *Tectonics*, 27(3).

Ferreira, J., Aragão, L., Barlow, J., Barreto, P., Berenguer, E., Bustamante, M., Gardner, T., Lees, A., Lima, A., Louzada, J., et al. (2014). Brazil's environmental leadership at risk. *Science*, 346(6210):706–707.

Filizola, N. (2003). *Transfert sédimentaire actuel par les fleuves Amazoniens*. PhD thesis, Université Paul Sabatier.

Filizola, N., Guimarães, V., e Guyot, J. L. (1999). Medição de vazão em grandes rios com o uso do perfilador doppleracustico de corrente. Em *Manaus' 99 international symposium-Hydrological and Geochemical processes in large scale river basins. Manaus, Brasil*.

Filizola, N. e Guyot, J. L. (2004). The use of Doppler technology for suspended sediment discharge determination in the River Amazon. L'utilisation des techniques Doppler pour la détermination du transport solide de l' Amazone. *Hydrological Sciences Journal*, 49(1):143–153.

Filizola, N. e Guyot, J. L. (2009). Suspended sediment yields in the Amazon basin: an assessment using the Brazilian national data set. *Hydrological Processes*, 23(22):3207–3215.

Filizola, N. e Guyot, J. L. (2011). Fluxo de sedimentos em suspensão nos rios da Amazônia. *Revista Brasileira de Geociências*, 41(4):566–576.

Filizola, N., Guyot, J. L., e Guimarães, V. (2009). Measuring the discharge of the Amazon river using doppler technology (Manacapuru, Amazonas, Brazil). *Hydrological processes*, 23(22):3151–3156.

Finer, M. e Jenkins, C. N. (2012). Proliferation of hydroelectric dams in the Andean Amazon and implications for Andes-Amazon connectivity. *Plos one*, 7(4):e35126.

Fisch, G., Marengo, J. A., e Nobre, C. A. (1998). The climate of amazonia-a review. *Acta Amazonica*, 28(2):101–101.

Florencio, R. e Selmo, S. (2006). Estudo comparativo de granulometria a laser para finos da reciclagem de resíduos de construção e demolição. *17 CBECIMat-Congresso Brasileiro deEngenharia e Ciência dos Materiais*, 15.

Fu, R., Yin, L., Li, W., Arias, P. A., Dickinson, R. E., Huang, L., Chakraborty, S., Fernandes, K., Liebmann, B., Fisher, R., et al. (2013). Increased dry-season length over southern amazonia in recent decades and its implication for future climate projection. *Proceedings of the National Academy of Sciences*, 110(45):18110–18115.

Gardi, C., Angelini, M., Barceló, S., Comerma, J., Cruz Gaistardo, C., Encina Rojas, A., Jones, A., Krasilnikov, P., Mendonça Santos Brefin, M., Montanarella, L., Muñiz Ugarte, O., Schad, P., Vara Rodríguez, M., e Vargas, R. e. (2014). *Atlas de suelos de América Latina y el Caribe*. Comisión Europea - Oficina de Publicaciones de la Unión Europea, L-2995 Luxembourg, 176 pp.

Gibbs, R. J. (1967a). Amazon River: Environmental factors that control its dissolved and suspended load. *Science*, 156(3783):1734–1737.

Gibbs, R. J. (1967b). Amazon River: Environmental factors that control its dissolved and suspended load. *Science*, 156(3783):1734–1737.

Gibbs, R. J. (1981). Sites of river-derived sedimentation in the ocean. *Geology*, 9(2):77–80.

Gloor, M., Brienen, R., Galbraith, D., Feldpausch, T., Schöngart, J., Guyot, J.-L., Espinoza, J., Lloyd, J., e Phillips, O. (2013). Intensification of the amazon hydrological cycle over the last two decades. *Geophysical Research Letters*, 40(9):1729–1733.

Gomes, J. e Santos, I. d. (1999). Análise comparativa de campanhas de medição de descarga líquida pelos métodos convencional e acústico. *Simpósio Brasileiro de Recursos Hídricos*, 13.

Gotvald, A. J. e Oberg, K. A. (2009). Acoustic Doppler Current Profiler Applications used in Rivers and Estuaries by the US Geological Survey.

Grillot, N. (2011). Flux solides sur le bassin amazonien. Master 2, UM2. Université de Montpellier 2.

Guimarães, V., Guyot, J., Filizola, N., e Oliveira, E. (1997). O uso do ADCP (correntômetro de perfilagem acústico por efeito Doppler) para medição de vazão e estimativa do fluxo de sedimentos nos grandes rios da bacia Amazônica (l'emploi de l'ADCP pour la mesure du débit et l'estimation du flux de sédiments dans les grands fleuves du bassin amazonien). *XII Simpósio Brasileiro de Recursos Hídricos*, 1:545–552.

Guimaraes, V. e Jaccon, G. (1983). Calibragem em estações fluviométricas da bacia amazônica. aplicação do método gradiente linimétrico. *5to Simpósio Brasileiro de Hidrologia e Recursos Hídricos,*, (1).

Guimberteau, M., Ronchail, J., Espinoza, J., Lengaigne, M., Sultan, B., Polcher, J., Drapeau, G., Guyot, J.-L., Ducharne, A., e Ciais, P. (2013). Future changes in precipitation and impacts on extreme streamflow over amazonian sub-basins. *Environmental Research Letters*, 8(1):014035.

Guyot, J. (1993). *Hydrogéochimie des fleuves de l'Amazonie bolivienne*. PhD thesis, Université de Bordeaux 1, Talence, FRANCE.

Guyot, J., Conceiçô, S., Guimarâes, V., Dos Santos, J., e Longuinhos, R. (1995). Mediçâo de vazâo com adcp—primeiros resultados na bacia amazônica (mesures de débits avec l'adcp—premiers résultats dans le bassin amazonien, en portugais). *A Âgua em Revista*, 3(4):26–30.

Guyot, J. L., Bazan, H., Fraizy, P., Ordonez, J. J., Armijos, E., e Laraque, A. (2007a). Suspended sediment yields in the Amazon basin of Peru: a first estimation. *IAHS publication*, 314:3.

Guyot, J. L., Bourges, J., e Cortez, J. (1994). Sediment transport in the rio grande, an andean river of the bolivian amazon drainage basin. *IAHS Publications-Series of Proceedings and Reports-Intern Assoc Hydrological Sciences*, 224:223–232.

Guyot, J. L., Filizola, N., e Laraque, A. (2005). Régime et bilan du flux sédimentaire de l'Amazone à óbidos (Pará, Brésil) de 1995 à 2003. *Sediments Budgets 1. IAHS Publ*, (291):347.

Guyot, J. L., Filizola, N., Laraque, A., e Seyler, P. (1999). La variabilité saisonnière des flux sédimentaires dans le bassin de l'Amazone. Em *Conference on Hydrological and Geochemical Processes in Large-scale River Basins, Manaus, Brazil*.

Guyot, J.-L., Jouanneau, J., Soares, L., Boaventura, G., Maillet, N., e Lagane, C. (2007b). Clay mineral composition of river sediments in the amazon basin. *Catena*, 71(2):340–356.

Herschy, R. W. (1995). *Streamflow measurement*. CRCPress.

Instruments, R. D. (1996). Acoustic doppler current profilers principles of operation: A practical primer. *RD Instruments, San Diego*, 36.

Jaccon, G. e Cudo, K. (1984). Curso sobre tecnicas de mediçao de descarga liquida em grandes rios: Manaus, 04 a 09 de junho de 1984.

Jaccon, G. e Cudo, K. (1987). Calibragem de posto fluviométrico : roteiro, cuidados e recomendações. *7to Simpósio Brasileiro de Hidrologia e Recursos Hídricos,*, (1).

Jaccon, G. e Cudo, K. (1989). Hidrologia : Curva-chave, análise e traçado. *DNAEE-ORSTOM.*, (1).

Jaccon, G. e Guimaraes, V. (1985). Pesquisas hidrológicas no rio solimões. *6to Simpósio Brasileiro de Hidrologia e Recursos Hídricos,*, (1).

Kvist, L. P. e Nebel, G. (2000). Bosque de la llanura aluvial del perú: Ecosistemas, habitantes y uso de los recursos. *Folia Amazónica*, 10(1-2):5–56.

Laguionie, P. (2006). *Mesures in situ et modelisation du transport des sediments en riviere. Applicacation au bssin versant de la Velaine*. PhD thesis, Université de Rennes 1.

Landers, M. N. (2011). *Fluvial suspended sediment characteristics by high-resolution, surrogate metrics of turbidity, laser-diffraction, acoustic backscatter, and acoustic attenuation*. PhD thesis, Georgia Institute of Technology.

Laraque, A., Ronchail, J., Cochonneau, G., Pombosa, R., e Guyot, J. L. (2007). Heterogeneous distribution of rainfall and discharge regimes in the ecuadorian amazon basin. *Journal of hydrometeorology*, 8(6):1364–1381.

Lawler, D. M. (2005). Spectrophotometry: turbidimetry and nephelometry. Em *Encyclopedia of Analytical Science, Elsevier, 2nd ed, 10 volumes, 343-351.*, pgs. 343–351.

Le Coz, J., Marchand, P., Brochot, J.-F., Pierrefeu, G., Le Coz, J., e Saysset, G. (2008). *Mesures hydrologiques par profileur Doppler*. Editions Quae.

Le Roux, J. (2005). Grains in motion: A review. *Sedimentary Geology*, 178(3):285–313.

Leite, N. K., Krusche, A. V., Ballester, M. V., Victoria, R. L., Richey, J. E., e Gomes, B. M. (2011). Intra and interannual variability in the madeira river water chemistry and sediment load. *Biogeochemistry*, 105(1-3):37–51.

Ludwig, K. A. e Hanes, D. M. (1990). A laboratory evaluation of optical backscatterance suspended solids sensors exposed to sand-mud mixtures. *Marine Geology*, 94(1):173–179.

Marcarenhas, F., Miguez, M., e Silva, R. (2003). *Hidráulica fluvial*, volume 1. Rio de Janeiro: COPPE/UFRJ.

Maréchal, A. (2000). *Relations entre caractéristiques de la pollution particulaire et paramètres optiques dans les eaux résiduaires urbaines*. PhD thesis.

Marengo, J. A., Alves, L. M., Soares, W. R., Rodriguez, D. A., Camargo, H., Riveros, M. P., e Pabló, A. D. (2013). Two contrasting severe seasonal extremes in tropical south america in 2012: flood in amazonia and drought in northeast brazil. *Journal of Climate*, 26(22):9137–9154.

Marengo, J. A., Nobre, C. A., Tomasella, J., Oyama, M. D., Sampaio de Oliveira, G., De Oliveira, R., Camargo, H., Alves, L. M., e Brown, I. F. (2008). The drought of Amazonia in 2005. *Journal of Climate*, 21(3):495–516.

Marengo, J. A., Tomasella, J., Alves, L. M., Soares, W. R., e Rodriguez, D. A. (2011). The drought of 2010 in the context of historical droughts in the Amazon region. *Geophysical Research Letters*, 38(12).

Marengo, J. A., Tomasella, J., Soares, W. R., Alves, L. M., e Nobre, C. A. (2012). Extreme climatic events in the Amazon basin. *Theoretical and Applied Climatology*, 107(1-2):73–85.

Martinelli, L. A., Victoria, R. L., Dematte, J. L. I., Richey, J., e Devol, A. (1993). Chemical and mineralogical composition of Amazon River floodplain sediments, Brazil. *Applied Geochemistry*, 8(4):391–402.

Martinez, J.-M., Guyot, J.-L., Filizola, N., e Sondag, F. (2009). Increase in suspended sediment discharge of the Amazon River assessed by monitoring network and satellite data. *Catena*, 79(3):257–264.

McClain, M. E. e Naiman, R. J. (2008). Andean influences on the biogeochemistry and ecology of the Amazon River. *BioScience*, 58(4):325–338.

Meade, R. H. (1994). Suspended sediments of the modern Amazon and Orinoco rivers. *Quaternary International*, 21:29–39.

Meade, R. H., Dunne, T., Richey, J. E., Santos, U. d. M., e Salati, E. (1985). Storage and remobilization of suspended sediment in the lower Amazon River of Brazil. *Science*, 228(4698):488–490.

Meade, R. H., Nordin, C. F., Curtis, W. F., RODRIGUES, F. M. C., DO VALE, C. M., e EDMOND, J. M. (1979). Sediment loads in the amazon river.

Meade, R. H., Rayol, J. M., Da Conceicão, S. C., e Natividade, J. R. (1991). Backwater effects in the amazon river basin of brazil. *Environmental Geology and Water Sciences*, 18(2):105–114.

Melack, J. e Forsberg, B. (2001). Biogeochemistry of amazon floodplain lakes and associated wetlands. *The biogeochemistry of the Amazon basin and its role in a changing world*, pgs. 235–276.

Merten, G. H., Capel, P. D., e Minella, J. P. (2013). Effects of suspended sediment concentration and grain size on three optical turbidity sensors. *Journal of Soils and Sediments*, pgs. 1–7.

Mertes, L. A. e Meade, R. H. (1985). *Particle sizes of sands collected from the bed of the Amazon River and its tributaries in Brazil during 1982-84*. US Department of the Interior, Geological Survey.

Milliman, J., Farnsworth, K., Jones, P., Xu, K., e Smith, L. (2008). Climatic and anthropogenic factors affecting river discharge to the global ocean, 1951–2000. *Global and planetary change*, 62(3):187–194.

Milliman, J. D. e Farnsworth, K. L. (2011). *River discharge to the coastal ocean: a global synthesis*. Cambridge University Press.

Milliman, J. D. e Meade, R. H. (1983). World-wide delivery of river sediment to the oceans. *The Journal of Geology*, pgs. 1–21.

Minella, J. P., Merten, G. H., Reichert, J. M., e Clarke, R. T. (2008). Estimating suspended sediment concentrations from turbidity measurements and the calibration problem. *Hydrological processes*, 22(12):1819–1830.

Moatar, F., Person, G., Meybeck, M., Coynel, A., Etcheber, H., e Crouzet, P. (2006). The influence of contrasting suspended particulate matter transport regimes on the bias and precision of flux estimates. *Science of the Total Environment*, 370(2):515–531.

Molinier, M., Guyot, J.-L., De Oliveira, E., Guimarães, V., Chaves, A., Olivry, J., e Boulègue, J. (1995). Hydrologie du bassin de l'Amazone. *Proc. Grands Bassins Fluviaux Péri-atlantiques*, 1:335–344.

Molnar, P. (2003). Geomorphology: Nature, nurture and landscape. *Nature*, 426(6967):612–614.

Moore, S. (2012). Monitoring flow and fluxes of suspended sediment in rivers using side-looking acoustic Doppler current profilers. *University of Grenoble, Grenoble*.

Moquet, J.-S., Maurice, L., Crave, A., Viers, J., Arevalo, N., Lagane, C., Lavado-Casimiro, W., e Guyot, J.-L. (2014). Cl and na fluxes in an andean foreland basin of the peruvian amazon: An anthropogenic impact evidence. *Aquatic Geochemistry*, 20(6):613–637.

Mora, A., Baby, P., Roddaz, M., Parra, M., Brusset, S., Hermoza, W., e Espurt, N. (2010). Tectonic history of the Andes and sub-Andean zones: implications for the development of the Amazon drainage basin. *Amazonia, Landscape and Species Evolution, a Look into the Past (Hoorn, C.*

Moreira-Turcq, P., Seyler, P., Guyot, J. L., e Etcheber, H. (2003). Exportation of organic carbon from the amazon river and its main tributaries. *Hydrological Processes*, 17(7):1329–1344.

Mueller, D. S., Wagner, C. R., Rehmel, M. S., Oberg, K. A., e Rainville, F. (2009). *Measuring discharge with acoustic Doppler current profilers from a moving boat*. US Department of the Interior, US Geological Survey.

Niño, Y. (2004). Hidráulica Fluvial y Transporte de Sedimentos. *Universidad de Chile*.

Nordin, C., Cranston, C., e Mjia, A. (1983). New technology for measuring water and suspended-sediment discharge of Large Rivers. Em *Proceedings of the Second International Symposium on River Sedimentation*, pgs. 1145–1158. Water Resources and Electric Power Press Beijing.

Nystrom, E. A., Rehmann, C. R., e Oberg, K. A. (2007). Evaluation of mean velocity and turbulence measurements with adcps. *Journal of hydraulic engineering*.

Oberg, K. (2002). In search of easy-to-use methods for calibrating ADCPs for velocity and discharge methods in Conference of Hydraulic Measurements and Experimental Methods, Estes Park, Colorado, 2002. *Proceedings: Environmental and Water Resources Institute of the American Society of Civil Engineers*.

Oltman, R. E. (1964). *Amazon River Investigations: Reconnaissance Measurements of July, 1963*. Geological Survey.

OMM, O. M. M. (1994). Guia de prácticas hidrológicas- adquisición y proceso de datos, análisis, medición y otras aplicaciones.

Pavanelli, D. e Bigi, A. (2005). Indirect methods to estimate suspended sediment concentration: reliability and relationship of turbidity and settleable solids. *Biosystems engineering*, 90(1):75–83.

Phillips, J. e Walling, D. (1995). An assessment of the effects of sample collection, storage and resuspension on the representativeness of measurements of the effective particle size distribution of fluvial suspended sediment. *Water Research*, 29(11):2498–2508.

Phillips, J., Webb, B., Walling, D., e Leeks, G. (1999). Estimating the suspended sediment loads of rivers in the lois study area using infrequent samples. *Hydrological processes*, 13(7):1035–1050.

Pinter, N. e Brandon, M. (2002). *Como a Erosão constrói montanhas*. In: Scientific American Brasil,São Paulo, Duetto, edição especial. 20.

Pouilly, M., Beck, S., Moraes, R., Ibanez, C., et al. (2004). *Diversidad biológica en la llanura de inundación del Río Mamoré: importancia ecológica de la dinámica fluvial*.

Quesada, C., Lloyd, J., Anderson, L., Fyllas, N., Schwarz, M., e Czimczik, C. (2011). Soils of Amazonia with particular reference to the RAINFOR sites. *Biogeosciences*, 8(6).

Restrepo, J. C. e Pierini, J. O. (2012). Medición de la concentración de sedimentos en suspensión mediante dispositivos ópticos y acústicos: aplicación en sistemas tropicales (delta del río Mira, Colombia). *Latin American Journal of Aquatic Research*, 40(1):153–168.

Restrepo, J. D., Kjerfve, B., Hermelin, M., e Restrepo, J. C. (2006). Factors controlling sediment yield in a major South American drainage basin: the Magdalena River, Colombia. *Journal of Hydrology*, 316(1):213–232.

Richey, J. E., Meade, R. H., Salati, E., Devol, A. H., Nordin, C. F., e Santos, U. D. (1986). Water discharge and suspended sediment concentrations in the Amazon River: 1982–1984. *Water Resources Research*, 22(5):756–764.

Roddaz, M., Brusset, S., Baby, P., e Hérail, G. (2006). Miocene tidal-influenced sedimentation to continental pliocene sedimentation in the forebulge–backbulge depozones of the beni–mamore foreland basin (northern bolivia). *Journal of South American Earth Sciences*, 20(4):351–368.

Roddaz, M., Viers, J., Brusset, S., Baby, P., e Hérail, G. (2005). Sediment provenances and drainage evolution of the neogene Amazonian foreland basin. *Earth and Planetary Science Letters*, 239(1):57–78.

Rouse, H. (1938). *Nomogram for the settling velocity of spheres*. National Research Council, Division of Geology and Geography.

Salati, E., Marques, J., e Molion, L. (1978). Origem e distribuição das chuvas na Amazônia. *Interciencia*.

Santini, W., Martínez, J.-M., Espinoza-Villar, R., Cochonneu, G., Vauchel, P., Moquet, J.-S., Baby, P., Espinoza, J.-C., Lavado, W., Carranza, J., et al. (2014). Sediment budget in the Ucayali River basin, an Andean tributary of the Amazon River.

Smith, T. M. e Reynolds, R. W. (2003). Extended reconstruction of global sea surface temperatures based on coads data (1854-1997). *Journal of Climate*, 16(10):1495–1510.

Sternberg, R., Kineke, G., e Johnson, R. (1991). An instrument system for profiling suspended sediment, fluid, and flow conditions in shallow marine environments. *Continental Shelf Research*, 11(2):109–122.

Stone, M. C. e Hotchkiss, R. H. (2007). Evaluating velocity measurement techniques in shallow streams. *Journal of Hydraulic Research*, 45(6):752–762.

Strasser, M. A., Ribeiro Neto, A., Silva, R., e Mascarnhas, F. (2005). Estudo da variação do coeficiente de rugosidade de Manning em rios da Bacia Amazônica por meio de modelagem hidrodinâmica. *XVI Simpósio Brasileiro de Recursos Hídricos*.

Syvitski, J. P. (2003). Supply and flux of sediment along hydrological pathways: research for the 21st century. *Global and Planetary Change*, 39(1):1–11.

Syvitski, J. P., Peckham, S. D., Hilberman, R., e Mulder, T. (2003). Predicting the terrestrial flux of sediment to the global ocean: a planetary perspective. *Sedimentary Geology*, 162(1):5–24.

Tessier, C. (2006). *Caractérisation et dynamique des turbidités en zone côtière: l'exemple de la région marine Bretagne Sud*. PhD thesis, Université de Bordeaux 1.

Thollet, F., Le Coz, J., Antoine, G., François, P., Saguintaah, L., Launay, M., e Camenen, B. (2013). Influence de la granulométrie des particules sur la mesure par turbidimétrie des flux de matières en suspension dans les cours d'eau. *La Houille Blanche*, (4):50–56.

Trigg, M. A., Wilson, M. D., Bates, P. D., Horritt, M. S., Alsdorf, D. E., Forsberg, B. R., e Vega, M. C. (2009). Amazon flood wave hydraulics. *Journal of Hydrology*, 374(1):92–105.

Vanoni, V. A. (1979). Sediment studies in the Brazilian Amazon River basin. *World Meteorological Organization*.

Vanoni, V. A. (1980). Sediment studies in the Brazilian Amazon River basin. *Report KH-P-168, W.M. Keck Laboratory of Hydraulic and Water Resources.*

Vauchel, P. (2009). Hidromesad,logiciel de gestión y tratamiento de datos hidrológicos y de sedimentos. Informe Técnico. Technical report, IRD-GET- France, Hybam Lima-Peru.

Vauchel, P. (2011). Première analyse des données- Internal Report. Technical report, IRD-GET- France.

Villar, R. E., Martinez, J.-M., Le Texier, M., Guyot, J.-L., Fraizy, P., Meneses, P. R., e de Oliveira, E. (2013). A study of sediment transport in the madeira river, brazil, using modis remote-sensing images. *Journal of South American Earth Sciences*, 44:45–54.

Walling, D. (2005). Tracing suspended sediment sources in catchments and river systems. *Science of the total environment*, 344(1):159–184.

Walling, D. (2006). Human impact on land–ocean sediment transfer by the world's rivers. *Geomorphology*, 79(3):192–216.

Walling, D. e Collins, A. (2000). *Integrated assessment of catchment sediment budgets: A technical manual*. School of Geography and Archaeology, University of Exeter.

Walling, D., Owens, P., Carter, J., Leeks, G., Lewis, S., Meharg, A., e Wright, J. (2003). Storage of sediment-associated nutrients and contaminants in river channel and floodplain systems. *Applied Geochemistry*, 18(2):195–220.

Walling, D. e Webb, B. (1987). Suspended load in gravel-bed rivers: Uk experience. *Sediment Transfer in Gravel-Bed Rivers. John Wiley & Sons New York. 1987. p 691-723, 8 tab, 11 fig, 54 ref.*

Walling, D. e Webb, B. (1988). The reliability of rating curve estimates of suspended sediment yield: some further comments. *IN: Sediment Budgets. IAHS Publication*, (174).

Wedd, M. W. (2003). Determination of particle size distributions using laser diffraction. *Educational Resources for Particle Technology*, 4(1):1–4.

Willett, S. D. (1999). Orogeny and orography: The effects of erosion on the structure of mountain belts. *Journal of Geophysical Research: Solid Earth (1978–2012)*, 104(B12):28957–28981.

Williamson, T. N. e Crawford, C. G. (2011). Estimation of suspended-sediment concentration from total suspended solids and turbidity data for Kentucky, 1978-19951. *JAWRA Journal of the American Water Resources Association*, 47(4):739–749.

Wittmann, H. (2008). *New applications to in situ-produced cosmogenic nuclides in river sediment: High mountain belt denudation in the Swiss Alps and Bolivian Andes and sediment transfer and storage in the Amazon basin*. PhD thesis.

Wolf, A. T., Natharius, J. A., Danielson, J. J., Ward, B. S., e Pender, J. K. (1999). International river basins of the world. *International Journal of Water Resources Development*, 15(4):387–427.

Wren, D., Barkdoll, B., Kuhnle, R., e Derrow, R. (2000). Field techniques for suspended-sediment measurement. *Journal of Hydraulic Engineering*, 126(2):97–104.

Apêndice A

Calibração Turbidez

A.1 Características das sondas de turbidez

A turbidez (T) é uma técnica indireta para determinar a concentração de sedimentos em suspensão ([C]). Logo, eis a importância de conhecer em detalhes as vantagens e limitações do equipamento que mede a turbidez. Com este objetivo, fez-se necessário que antes do inicio das medições fossem realizados testes com três sondas YSI, de diferentes modelos, que permitiram compreender o funcionamento do equipamento e as incertezas no momento da medida.

A.1.1 Princípio do funcionamento do equipamento

Uma sonda de turbidez é composta do « corpo da sonda » e um « sensor de turbidez »,de forma que, estas duas partes devem ser compatíveis para poderem ser utilizadas (Figura.A.1). As sondas utilizadas foram cedidas pelo IRD e pela ANA exclusivamente para a realização dos testes, cujas características técnicas são resumidas na (Tabela.A.1):

Figura A.1: *Sonda de turbidez 6820 V2*

Para saber se a tradução do sinal elétrico em sinal ótico depende do sensor do corpo da sonda, foram realizados testes com duas sondas, cujos sensores são compatíveis (Sonda 2 e Sonda 3). O teste foi realizado com duas concentrações diferentes de sedimento fino das estações de Óbidos e Foz do Madeira. A (Fig.A.2) mostra os resultados da estação da Foz do Madeira, onde i) apresenta a relação de [C] e T para

Tabela A.1: Características técnicas das sondas

	Sonda 1	Sonda 2	Sonda 3
Modelo de sonda	YSI 6920	YSI 6820 V2	YSI 6600 V2
Modelo do sensor	YSI 6136	YSI 6136	YSI 6026
ótico	Lot. No. 03B1251	S/N 09A131280	s/N Y3310
Longitude onda	infravermelho	infravermelho	infravermelho
Incerteza (NTU)	0,3	0,3	0,3
Origem	IRD	ANA	IRD

as sondas 2 e 3 com sus próprios sensores e *ii*) apresenta a relação de [C] e T para as mesmas sondas 2 e 3 mas trocando seus sensores. O resultado indica que é o corpo da sonda quem transforma o sinal elétrico em sinal de turbidez. No entanto, os sensores podem também influir nas medidas. Por isso, a recomendação é utilizar o mesmo sensor e corpo de sonda com os quais foi feita a calibração.

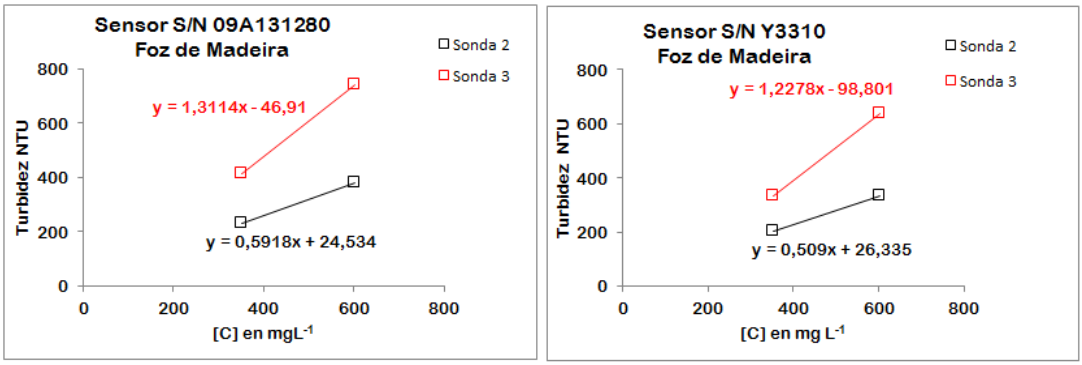

Figura A.2: *Resposta do sensor de turbidez, i) Sondas 2 e 3 com seus próprios sensores, ii) troca de sensores*

A.1.2 Impactos do meio exterior sobre a medida

Para conhecer o grau de interferência que pode ter a luz na medida da turbidez, foram realizados testes empregando o mesmo material, mas mudando os ambientes (Fig.A.3):

- ao exterior com a luz do sol,
- dentro do laboratório com luz artificial e
- na ausência de luz (escuro), envolvendo o dispositivo com papel alumínio

A.1.2.1 Procedimento

Neste teste utilizou-se: água destilada e as 3 sondas, com a proteção e sem proteção. A (Tabela.A.2) sintetiza o equipamento, material utilizado e as hipóteses feitas sobre o parâmetro luz.

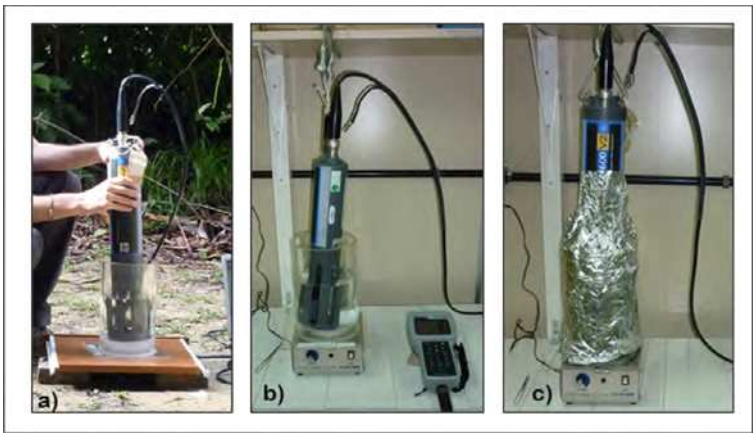

Figura A.3: *Teste de luz a) no exterior, b) luz artificial- laboratório, c) escuro*

Tabela A.2: Impacto da luz sobre a turbidez registrada

		Exterior	Laboratório	Escuro
Equipamento e Material	Contendo	A	A	A
	Volume da água destilada (L)	2	2	2
	Agitação	Não	Não	Não
	Papel alumínio	Não	Não	Sim
	Data logger externo	Unicamente para a sonda 2		
Hipóteses	Intensidade luminosa	Variável	Constante	Nulo
	Presença de luz	Importante	Insignificante a nulo	Nulo
Sonda	Pré-aquecimento (min.)	5	5	5
	Tempo de medida (min.)	3	3	3

A.1.2.2 No exterior

Ao que parece, quando se coloca a proteção do sensor, cria-se uma espécie de tela sobre os raios luminosos, tornando o sinal mais estável (Fig.A.4). No entanto, na ausência desta tela, as grandes variações do sinal são atribuídas às variações da quantidade de raios infravermelhos emitidos pela luz do sol, e que não são absorvidos ou refletidos pela água (proporcionalmente). Este mesmo comportamento foi observado para as 3 sondas.

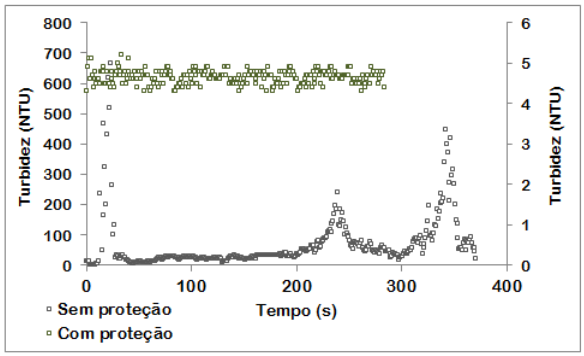

Figura A.4: *Sinal de turbidez da sonda 2 com e sem proteção no exterior*

A.1.2.3 No laboratório

Dentro do laboratório, independente da sonda utilizada, o sinal registrado foi considerado estável, e a variação da medida esteve dentro da gama de incerteza (Fig.A.5). Igualmente como o observado no caso anterior, quando se coloca a proteção, os valores de turbidez diminuíram. Achamos que esta proteção cumpre a função de bloquear as interferências que podem ser ocasionadas pela luz do meio exterior. Porém, em condições de laboratório, a diferença entre medida com e sem proteção foi considerada insignificante.

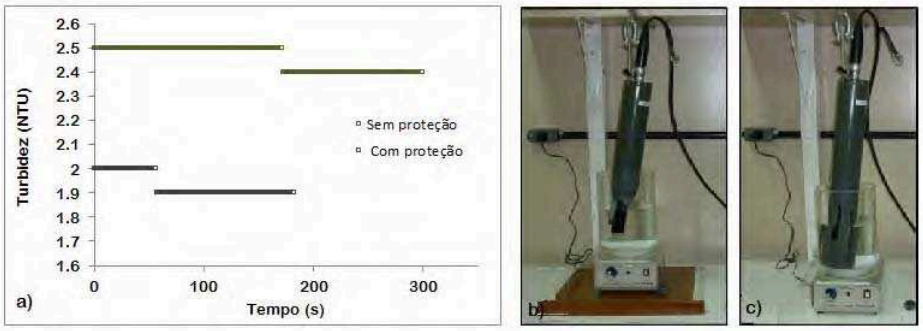

Figura A.5: *a) Sinal de turbidez da sonda 2 b) com e c)s em proteção*

A.1.2.4 Em ambiente escuro

Foram observadas as mesmas constatações que o caso anterior para as 3 sondas (Fig.A.6). E do mesmo modo quando a proteção foi utilizada, registraram-se valores ligeiramente menores.

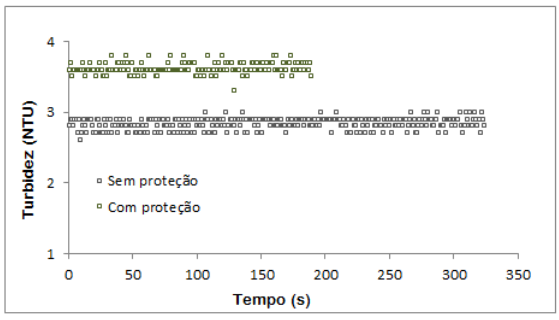

Figura A.6: *Sinal de turbidez da sonda com e sem proteção no escuro*

Foi observado que o sinal de turbidez varia com ou sem proteção quando o sensor se encontra no ambiente exterior. Mostrando que quando o sensor se encontra em um lugar fechado (laboratório ou na ausência de luz), a diferença é insignificante. Na prática quando se utiliza a sonda em um meio natural, o fabricante (YSI) aconselha mergulhar o sensor no mínimo a 70 cm de profundidade para evitar interferência causada pela absorção da água de raios infravermelhos do sol.

A.1.3 Teste de linearidade do sinal de turbidez

A hipótese principal, e sem duvida a mais importante em uma calibração no laboratório, é a linearidade do sinal e a proporcionalidade do sinal de T em função da [C] . Para verificar estas hipóteses foi realizado o teste com leite, como alternativa para não utilizar uma solução NTU. Para efeito, foi adicionado a um volume d'água constante, uma quantidade de leite que foi aumentando gradualmente até chegar ao ponto de saturação. Para manter a homogenização da solução utilizou-se um agitador magnético e um imã. Os resultados mostraram que o sinal de turbidez é linear para as 3 sondas (Fig.A.7).

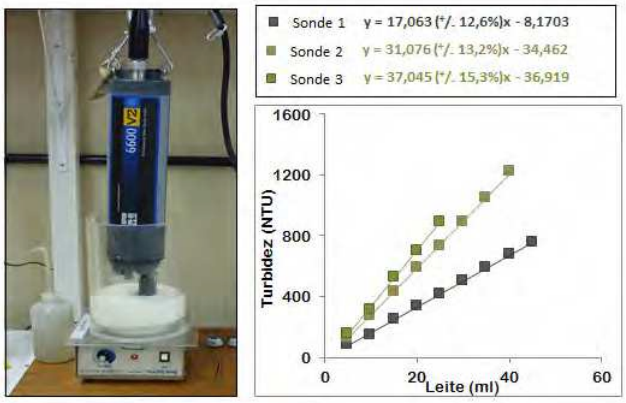

Figura A.7: *Dispositivo para a calibração do leite e teste de linearidade para as 3 sondas*

Podemos concluir que é importante conhecer o equipamento e suas limitações nas condições ambientais que será requerido. Os resultados indicam que cada sonda tem suas características de forma que a calibração é própria para cada sonda(corpo + sensor). No campo, é importante evitar a influência da luz solar que pode criar interferências nas medidas pelo menos 70 cm baixo o espelho d'águas. E por último o sinal de turbidez é linear, propriedade que simplifica a calibração e utilização.

Apêndice B

Granulometria

B.1 Determinação granulométrica em amostras dos Rios da bacia Amazônica

O transporte e depositação dos sedimentos nos sistemas fluviais é seletivo. Guyot et al. (1999) encontraram que para o rio Madeira na Bolívia, as partículas mais grosseiras depositam-se no pie de monte, no entanto, que as partículas finas podem ser transportadas até a desembocadura do rio. Conhecer as características geomorfológicas dos sistemas fluviais ajuda a compreender a dinâmica fluvial, entender o funcionamento ecológico, e estimar as taxas de erosão das bacias de drenagem (Walling e Webb, 1987; Guyot et al., 2005; Wittmann, 2008). Do ponto de vista técnico, esta informação pode ser valiosa para aplicações na engenharia civil (vida útil dos reservatórios, construção de pontes, etc). Este trabalho está dirigido a estabelecer uma metodologia tanto no campo (amostra representativa) como no laboratório (granulometro laser) afim poder realizar análises com resultados comparáveis.

B.2 Fundamentos da Granulometria Laser

A técnica do espalhamento de luz é cada vez mais utilizadapor permitir que partículas com tamanhos nanométricos ou até milimétricos sejam medias. No mais, é simples operacionalmente e permite a reprodutibilidade dos resultados em pouco tempo. A granulometria laser é deduzida a partir da interação entre um conjunto de partículas e um feixe de luz incidente, mediante uma analises da difração do feixe de luz (Fig.B.1). Quando um feixe de luz monocromático é colimado de gás hélio (He) ou néon (Ne), atinge uma quantidade de partículas, parte desta luz é submetida a um espalhamento, parte é absorvida e parte é transmitida. No espalhamento, a luz pode ser difratada, refratada e refletida. O granulômetro laser utiliza a difração, um conjunto de lentes, detectores foto-elétricos e um microprocessador que captam a intensidade da energia espalhada e transformá-la em distribuição volumétrica das partículas, assumindo-se, o princípio que as partículas têm formato esférico (Florencio e Selmo, 2006). O espalhamento pode ocorrer no meio seco(ar) ou úmido como água, álcool ou outros líquidos orgânicos.

O princípio da granulometria laser está baseado em duas teorias, de Fraunhofer e Mie. Quando o tamanho da partícula é maior que o comprimento de onda incidente,

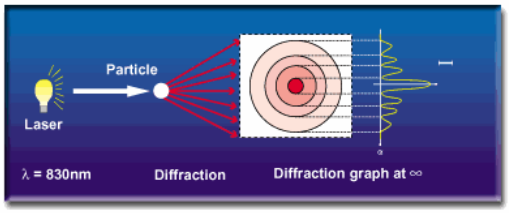

Figura B.1: *Tecnica de medição do granulométro laser. Fonte: http : //www.cilas.com/laser − diffraction − particle − size − analysis − principles.htm*

ou quando o material é muito absorvente, o efeito da borda das partículas contribui com uma parte importante na intensidade total difusa. A interferência que proveem principalmente do contorno da partícula é a difração criada pela curvatura da luz à interface. Neste caso, o modelo matemático para o cálculo da curva granulométrica é a teoria de Fraunhofer. Este modelo tem a vantagem de eliminar totalmente as propriedades ópticas da amostra e do meio portador, não sendo necessário conhecer os índices de refração. Em contraste, quando o tamanho de partícula é próximo do comprimento de onda incidente, a teoria Fraunhofer já não é adequada para descrever a difusão, porque estão envolvidos os fenômenos de reflexão e refração, sendo uma parte significativa na intensidade espalhada. Neste caso aplica-se a teoria de Mie, que leva em conta os índices de refração da amostra e do meio portador (Fig.B.2).

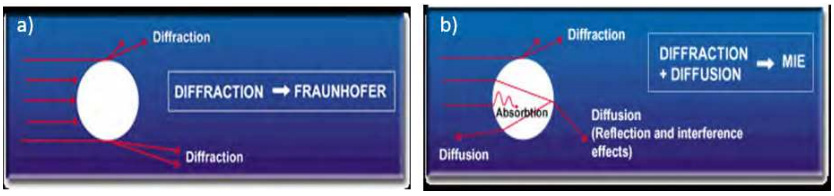

Figura B.2: *a) teoria do Fraunhofer, b) teoria de Mie*

O resultado dado pelo granulômetro laser é a repartição do volume da população (amostra), isto é, a repartição de esferas equivalentes que ocupam o mesmo volume que a amostra medida e conduz ao mesmo espectro. Os resultados são apresentados em forma numérica e gráfica através de histogramas de repartição de classes ou curva acumulada.

B.3 Metodologia-Técnica de medição

Utilizou-se um equipamento tipo Mastersizer 2000, Malvern cuja gama de média é de 0.02 µm e 2000 µm. O principal interesse para realizar estas análises é encontrar o melhor método de amostragem que permita obter o diâmetro dos rios Amazônicos. Para alcançar este objetivo, temos dois enfoques a serem seguidos: i) a parte de coleta, na qual são considerados três tipos de amostras, que estão em função do volume do amostrador de 7L, considerando que para o granulômetro laser precisa-se somente de 800 - 900 ml. Os testes foram realizados sobre amostras de 5L em estado seco e em forma aquosa, e em amostras de água com menor volume. ii) O outro enfoque é determinar

no laboratório o método de execução, ou seja, a velocidade de mistura e aplicação de ultrasson.

B.3.1 Amostras de 5 L em fase seca

Tipo de amostra: em pó Estação: Manacapuru
Rio: Solimões Data: 16-02-2011
Identificacão: Amostra em superfície V5

B.3.1.1 Procedimento

O procedimento com estas amostras foi o seguinte:

- Coletar 5 L de amostra em superfície e levar para o laboratório,
- Decantar,
- Levar na estufa, secar o material que decantou, e obter um pó
- Escolher uma porção pequena o mais representativa possível da amostra e colocar em 800 ml de água.
- Análises 1. Velocidade da bomba 2300 rpm, sem ultrasson,
- Análises 2. Velocidade da bomba 4000 rpm por 60 segundos. Velocidade da bomba de medida 2300 rpm,
- Análises 3. velocidade da bomba 4000 rpm por 60 segundos. Ultrassom 8 micra por 30 segundos. Velocidade da bomba de medida: 2300 rpm.
- Análises 4. Comparar os resultados obtidos com os resultados do Laboratório do CNRS- Rennes onde não foi utilizado ultrasson mas também a amostra não foi secada.

B.3.1.2 Resultados

No momento da secagem a amostra aglomera-se formando partículas maiores que as originais como o indica a (Fig.B.3) e (Tabela. B.1). Observa-se uma alta variação do diâmetro representativo. Temos que lembrar que as amostras de superfície nesta estação e neste período não contém material grosseiro. Para este tipo de amostras, deveria ser feito a metodologia do tipo A3 aumentando o tempo de ultrasson, e ainda assim teria que ser com reservas, devido a que o tipo de material não sempre o mesmo.

Tabela B.1: Resultado das análises com amostra em pó- Volume 5L

Tipo de Metodologia de Análises	Volume %	Diâmetro μm	Obscuração %
A1	5.7	120.2	6
A2	6	91.2	9.3
A3	4.9	22.9	16.1
A4	4.1	15	

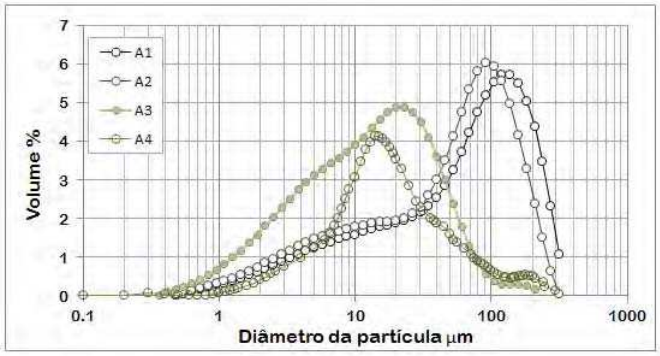

Figura B.3: *Amostra de Manacapuru- 16-02-2011. Amostra em pó- utilizando diferentes cenários: A1.- velocidade da bomba 2300 rpm. A2. Adicionando ultrasson 400 rpm por 60 segundos. A3.- Mistura por 60 segundos mais ultrasson por 30 segundos. A4. Analises realizado na França*

B.3.2 Amostras de 5 L em fase aquosa

Esta fase realizou-se com uma mesma amostra, na qual, foi-se modificando a quantidade de amostra para observar a representatividade dela em fase aquosa.

Tipo de amostra : fase aquosa — Estação: Manacapuru
Rio : Solimões — Data: 25-07-2011
Identificação : Amostra em superfície

B.3.2.1 Procedimento

O procedimento é:

- Decantar as amostras de 5 litros, até obter uma substância aquosa,
- Colocar no agitador magnético e com ajuda da pipeta escolher de 10 a 20 ml de amostra e cno bécher com 800 ml de água,
- Fazer a medição de granulométrica,
- Análises 1. Quantidade de amostra 20 ml,
- Análises 2. Quantidade de amostra 30 ml,

B.3.2.2 Resultados

A FiguraB.4 e a Tabela B.2, indicam que os valores são reprodutíveis mesmo se utilizarmos uma maior concentração, mostrando que, o importante é ter uma amostra representativa. No entanto, como a amostra tem que ficar algum tempo em decantação, pode ocorrer o problema de agregamento das partículas.

Tabela B.2: Resultado das análises com amostra em solução aquosa provenientes do Volume 5L

Tipo de Metodologia de Análise	Volume	Diâmetro	Obscuração
	%	μm	%
A1	4.8	20	8.4
A2	4.9	20	11.3

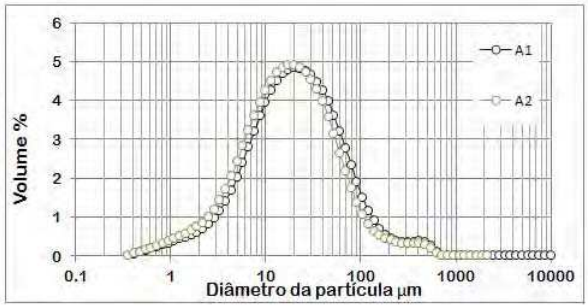

Figura B.4: *Amostra superficial de Manacapuru- 25-07-2011. Amostra em fase aquosa- utilizando diferentes quantidades de amostra: A1=20 ml e A2=30 ml*

B.3.3 Amostras menores a 1000 ml em fase líquida

Nesta análise, utilizou-se uma amostra de superfície para obter a quantidade de volume necessária para realizar a granulometria. inicia-se com uma amostra completa de 800 ml e depois segue-se fazendo diluições.

Tipo de amostra: líquida Estação: Itacoatiara
Rio: Amazonas Data: 20-02-2011
Data
Identificação: Amostra em superfície V3

B.3.3.1 Procedimento

O procedimento é:

- Colocar toda a amostra no bécher de 800 ml, se a obscuração for maior deverá ser feita a diluição,
- Determinar o mínimo de amostra para as análises de granulometria realizando as seguintes análises:
- Análise 1. Quantidade de amostra 800 ml e 0 ml de água,
- Análise 2. Quantidade de amostra 300 ml e 500 ml de água,
- Análise 3. Quantidade de amostra 200 ml e 600 ml de água,
- Análise 4. Quantidade de amostra 100 ml e 700 ml de água,
- Análise 5. Quantidade de amostra 100 ml e 700 ml de água,
- Análise 6. Quantidade de amostra 100 ml e 700 ml de água,
- Análise 7. Amostra feita na França.

B.3.3.2 Resultados

Os Resultados indicam que quando a amostra é muito carregada, a obscuração também é muito alta, fazendo-se necessário uma diluição da amostra. As diferentes diluições indicam porcentagem de volumeis que estão entre os diâmetros de 8.71 e 10 µm, tendo uma diferença de 0.2%, mostrando que se poderia escolher entre um ou outro volume.. Em relação à amostra da França, existe uma diferença que pode estar ligada ao tipo de aparelho e ao método de medição, como a diferença de velocidade da bomba.

Tabela B.3: Resultado das análises com amostra em fase líquida

Tipo de Metodologia de Análise	Volume	Diâmetro	Obscuração
	%	μm	%
A1			49
A2	5.5	10	13
A3	5.8	8.7	8.2
A4	6.3	10	4.2
A5	6.3	10	4.2
A6	6.2	8.7	4.1
A7	5	13	

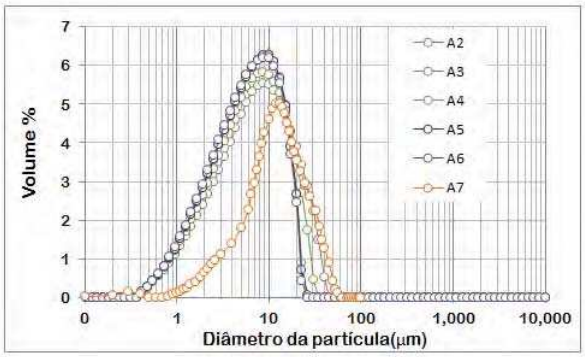

Figura B.5: *Amostra superficial de Itacoatiara- 20-02-2011. Amostra em fase líquida- utilizando diferentes volumeis de diluição*

B.3.4 Conclusões

- As amostras em fase líquida indicam reprodutibilidade, sendo esta a coleta mais adaptada. Na questão de representatividade, é suficiente com ter uma amostra bem homogeneizada, ja que a granulometria mede a distribuição de volume. Este teste foi aplicado também para amostras em profundidade e os resultados foram similares.
- O volume adequado seria de 1 Litro, lembrando que assim pode-se ter amostra suficiente para repetir as análises. No entanto, se houver dificuldade de obter este volume, pode-se fazer a análise com uma amostra de até 100 ml. Contudo, recomenda-se que as análises não sejam feitas com um volume menor a 300 ml, pois as concentrações podem ser baixas dependendo do período do ciclo hidrológico.
- Importante observar se as amostras contem matéria orgânica, porque pois podem influenciar nas análises granulométrico..
- Para as amostras que já foram coletadas em galão de 5 Litros, o melhor é que elas fiquem em condição aquosa.
- Como recomendação, deve-se observar que o volume no becker não seja menor que 800 ml.

Apêndice C

Sedimentos em suspensão e material dissolvido dos Andes do Equador

Yields of suspended sediments and dissolved solids from the Andean basins of Ecuador

Hydrological Sciences Journal
Publication details, including instructions for authors and subscription information:
http://www.tandfonline.com/loi/thsj20

Yields of suspended sediment and dissolved solids from the Andean basins of Ecuador

Elisa Armijos[ab], Alain Laraque[c], Sonia Barba[d], Luc Bourrel[c], Catalina Ceron[e], Christelle Lagane[c], Philippe Magat[c], Jean Sebastien Moquet[c], Rodrigo Pombosa[a], Francis Sondag[cf], Philippe Vauchel[c], Andrea Vera[e] & Jean Loup Guyot[cf]

[a] Instituto Nacional de Meteorología e Hidrología (INAMHI), Iñaquito N36-14 y Correa, Quito, Ecuador

[b] Instituto Nacional de Pesquisas da Amazônia (INPA), LBA-CLIAMB, Universidade do Estado do Amazonas, 2936 Aleixo, CEP 69060-001, Manaus, Brazil

[c] GET (CNRS, IRD, OMP, Université de Toulouse), 14 Avenue Edouard Belin, F-31400, Toulouse, France

[d] Universidad Politécnica Nacional (EPN), Ladrón de Guevara E11, 253, Quito, Ecuador

[e] Universidad Central del Ecuador (UCE), Ciudadela Universitaria, Avenida América, Quito, Ecuador

[f] IRD,

Published online: 15 Oct 2013.

To cite this article: Elisa Armijos, Alain Laraque, Sonia Barba, Luc Bourrel, Catalina Ceron, Christelle Lagane, Philippe Magat, Jean Sebastien Moquet, Rodrigo Pombosa, Francis Sondag, Philippe Vauchel, Andrea Vera & Jean Loup Guyot (2013) Yields of suspended sediment and dissolved solids from the Andean basins of Ecuador, Hydrological Sciences Journal, 58:7, 1478-1494, DOI: 10.1080/02626667.2013.826359

To link to this article: http://dx.doi.org/10.1080/02626667.2013.826359

http://dx.doi.org/10.1080/02626667.2013.826359

Yields of suspended sediment and dissolved solids from the Andean basins of Ecuador

Elisa Armijos[1,2], Alain Laraque[3], Sonia Barba[4], Luc Bourrel[3], Catalina Ceron[5], Christelle Lagane[3], Philippe Magat[3], Jean Sebastien Moquet[3], Rodrigo Pombosa[1], Francis Sondag[3,6], Philippe Vauchel[3], Andrea Vera[5] and Jean Loup Guyot[3,6]

[1]*Instituto Nacional de Meteorología e Hidrología (INAMHI), Iñaquito N36-14 y Correa, Quito, Ecuador*
armijos.elisa@gmail.com

[2]*Instituto Nacional de Pesquisas da Amazônia (INPA), LBA-CLIAMB, Universidade do Estado do Amazonas, 2936 Aleixo, CEP 69060-001, Manaus, Brazil*

[3]*GET (CNRS, IRD, OMP, Université de Toulouse), 14 Avenue Edouard Belin, F-31400 Toulouse, France*

[4]*Universidad Politécnica Nacional (EPN), Ladrón de Guevara E11, 253 Quito, Ecuador*

[5]*Universidad Central del Ecuador (UCE), Ciudadela Universitaria, Avenida América, Quito, Ecuador*

[6]*IRD, CP 7091 Lago Sul, CEP 71635-971 Brasília, DF, Brazil*

Received 9 July 2012; accepted 10 January 2013; open for discussion until 1 April 2014

Editor Z.W. Kundzewicz

Citation Armijos, E., Laraque, A., Barba, S., Bourrel, L., Ceron, C., Lagane, C., Magat, P., Moquet, J.-S., Pombosa, R., Sondag, F., Vauchel, P., Vera, A., and Guyot, J.L., 2013. Yields of suspended sediment and dissolved solids from the Andean basins of Ecuador. *Hydrological Sciences Journal*, 58 (7), 1478–1494.

Abstract Water discharge and suspended and dissolved sediment data from three rivers (Napo, Pastaza and Santiago) in the Ecuadorian Amazon basin and a river in the Pacific basin (Esmeraldas) over a 9-year period, are presented. This data set allows us to present: (a) the chemical weathering rates; (b) the erosion rates, calculated from the suspended sediment from the Andean basin; (c) the spatio-temporal variability of the two regions; and (d) the relationship between this variability and the precipitation, topography, lithology and seismic activity of the area. The dissolved solids load from the Esmeraldas basin was 2×10^6 t year^{-1}, whereas for the Napo, Pastaza and Santiago basins, it was 4, 2 and 3×10^6 t year^{-1}, respectively. For stations in the Andean piedmont of Ecuador, the relationship between surface sediment and the total sediment concentration was found to be close to one. This is due to minimal stratification of the suspended sediment in the vertical profile, which is attributed to turbulence and high vertical water speeds. However, during the dry season, when the water speed decreases, sediment stratification appears, but this effect can be neglected in the sediment flux calculations due to low concentration rates. The suspended sediment load in the Pacific basin was 6×10^6 t year^{-1}, and the total for the three Amazon basins was 47×10^6 t year^{-1}. The difference between these contributions of the suspended sediment load is likely due to the tectonic uplift and the seismic and volcanic dynamics that occur on the Amazon side.

Key words hydrology; erosion; Andes; chemical weathering; Amazon basin; Pacific basin

Apports de matières en suspension et de solides dissous des les bassins andins de l'Equateur

Résumé Cet article présente un ensemble de données concernant l'exportation d'eau et de matières en suspension et dissoutes de trois rivières (Napo, Pastaza et Santiago) du bassin de l'Amazonie équatorienne et d'une rivière du bassin du Pacifique (Esmeraldas) sur une période de neuf ans. Cet ensemble de données nous permet de d'appréhender : (a) le taux d'altération chimique; (b) les taux d'érosion, calculés à partir des sédiments en suspension dans le bassin andin; (c) la variabilité spatio-temporelle des deux régions; et (d) les relations entre la variabilité et l'activité des précipitations, la topographie, la lithologie et l'activité sismique de la zone. La charge de solides dissous dans le bassin Esmeraldas était de 2×10^6 t an^{-1}, alors que pour le bassin du Napo, Pastaza et de Santiago, elle était respectivement de 4, 2 et 3×10^6 t an^{-1} Pour les stations du piémont andin de l'Equateur,

le rapport entre la concentration des sédiments en surface et la concentration totale de sédiments a été trouvé proche de 1. Cela est dû à la stratification minimale des sédiments en suspension selon le profil vertical, qui est attribuée à la turbulence et à des vitesses élevées de déplacement vertical de l'eau. Cependant, pendant la saison sèche, lorsque la vitesse de l'eau diminue, la stratification des sédiments apparaît mais cet effet peut être négligé dans les calculs de flux de sédiments en raison des faibles taux de concentration. La charge sédimentaire dans le bassin du Pacifique était de 6×10^6 t an^{-1}, et le total pour les trois bassins de l'Amazone était de 47×10^6 t an^{-1}. La différence entre ces apports de sédiments en suspension est probablement due à la surrection tectonique et à la dynamique sismique et volcanique qui se produisent sur le versant amazonien.

Mots clefs hydrologie; érosion; Andes; altération chimique; bassin de l'Amazone; bassin du Pacifique

INTRODUCTION

The Andes represent 11% of the 6.1×10^6 km^2 Amazon Basin (Goulding *et al.* 2003), and are the most important source of sediment from the South American continent and the third largest source of sediment in the world, after the Ganges-Brahmaputra and Yellow rivers (Degens *et al.* 1991). The Amazon River discharges 6500×10^9 m^3 year^{-1} of water (Callède *et al.* 2010), approx. 800×10^6 t year^{-1} of suspended sediments (Guyot *et al.* 2005, Martinez *et al.* 2009) and approx. 270×10^6 t year^{-1} of dissolved elements (Mortatti and Probst 2003, Moquet 2011) into the Atlantic Ocean.

Research on the processes of erosion and weathering and the spatio-temporal variability of the Amazon Basin has been ongoing for several decades (Gibbs 1967, Meade *et al*. 1979, 1985, Dunne *et al*. 1998, Filizola and Guyot 2004, 2009, Guyot *et al*. 1996, 2005, 2007, Moquet *et al*. 2011). The Andean drainage basins of Bolivia produce dissolved sediment load of 10×10^6 t year^{-1} as they leave the Andes (Beni River at Angosto del Bala and Grande River at Abapo) because of the high solubility of the rocks (Guyot 1993, Moquet *et al*. 2011), which gives a chemical weathering rate of 44 t year^{-1} km^{-2}. At the same stations, the mechanical erosion rates are 3140 t year^{-1} km^{-2} for the Beni River and 2130 t year^{-1} km^{-2} for the Grande River (Guyot *et al*. 1996). In Peru, 76% of the total area of the country is in the Amazon basin (977 900 km^2), and 53% of that is Andean. The results presented by Guyot *et al.* (2007) and Armijos (2010) demonstrate that the sediment flux through the Amazon River in Peru is 570×10^6 t year^{-1} (approx. 550 t year^{-1} km^{-2}).

Geologically, Ecuador is located in a transition zone of the subducting Nazca Plate and is also affected by the Carnegie Ridge collision. This position is responsible for the high volcanic and seismic activity (Legrand *et al*. 2005). Furthermore, Ecuador has a spatially variable rainfall distribution (Laraque *et al*. 2007, Espinoza *et al*. 2009), which directly influences the quality and quantity of the dissolved and suspended sediments.

Few studies have been performed on the quantification of fluxes in Ecuador due to the difficulty and cost of data collection; most have concentrated on the Napo River basin. Armijos (2002), Cerón (2004) and Laraque *et al.* (2004) presented the first data on water discharge and sediment fluxes in Amazon basins. Vanacker *et al.* (2007) worked in mountain basins in the Upper Santiago basin (Paute basin) and showed that small basins have high values of sediment concentration mainly due to landslides and not because of human influence. However, Molina *et al*. (2008) found basins in the Andean Páramo (Upper Santiago basin) where human activity can be an indirect cause of erosion in the sense of opening roads that leave the soil exposed. Hence the importance of regular monitoring of sediment concentration, especially in small basins that have quick response to changes in environment. Melo (2010) mapped risk areas for erosion in the Esmeraldas and Guyas basins. Narvaez and Vera (2007) and Galeas and Melo (2007) performed a comparative characterization of the major dissolved elements and suspended sediment yields in both the eastern and western basins (Napo and Esmeraldas) and showed that the waters of Ecuador are calcium bicarbonate type with a predominance of Na^{2+}, Mg^{2+} and K^+. Moquet (2011) presented factors that influence weathering in the Andean region of the Amazon basin. Laraque *et al.* (2009) identified significant erosive processes in the Andes and the plains of the Napo basin in Ecuador and Peru, for 2001–2005 and 2004–2005, respectively.

We complement this work by providing a data set for the Ecuadorian Andean basins and new estimates for: (a) chemical weathering rates; (b) erosion rates calculated from suspended sediments; (c) the spatio-temporal variability of the two regions; and (d) the relationships between this variability and precipitation, topography, lithology and seismic

activity. The sediment load data set was collected over nine years (2001–2009), and the dissolved solids data set ranges over eight years (2001–2008). The study area covers six gauging stations in Amazonian basins (Napo, Pastaza and Santiago) and two gauging stations in the Esmeraldas basin in the Pacific region. These stations were monitored by the ORE (Environmental Research Observatory) of the HYBAM (Geodynamical, hydrological and biogeochemical control of erosion/alteration and material transport in the Amazon basin) programme in Ecuador (INAMHI–IRD collaboration).

STUDY AREA

Ecuador is located in South America and extends along both sides of the Equator (La Condamine 1751) between latitudes 1°30′ N and 5°00′ S and longitudes 75°20′ E and 81°0′ W, occupying an area of 248 406 km^2. The Andes comprise the central third of Ecuador, stretching from north to south and forming two belts approximately 645 km long and 15–65 km wide (DINAGE 1997). There are about 50 volcanoes, 25% of which are still active (Monzier and Robin 1995). The Cordillera, which is covered by glaciers, has peaks of 4000 to 6000 m (Aspiazu and Luna 1993), divides Ecuador into two regions (west and east) and forms the water divide between basins. Most of the rivers have their origin in the Andean glaciers, from where they flow west to the Pacific Ocean, or east to become part of the Amazon basin.

This study covers the three major basins in the Amazonian region—from north to south, the Napo, Pastaza and Santiago rivers—and the Esmeraldas River basin, whose waters flow to the Pacific Ocean (Fig. 1 and Table 1).

The eastern or Amazonian region accounts for 50% of the total area of Ecuador and includes a third, non-continuous, 50-km-wide cordillera formed by the Galeras (Napo basin), Cutucú and Condor (Santiago basin) mountain ranges, where volcanoes, such as Reventador (3485 m) and Sumaco (3900 m), are located. This landscape is known as the Upper East, whereas the Lower East is characterized by flat topography (ECORAE 2002). The topography of both the Pacific and Atlantic basins includes steep slopes of 40 to 70% in the Andes that gradually become plains at lower elevations (Winckell 1997). Ecuador is an area with much seismic activity due to its location in a subduction zone, i.e. where the Nazca oceanic plate is beneath the continental plate of South America (Gutscher *et al*. 1999, Legrand *et al*. 2005), the presence of geological faults that cross the territory, and the associated volcanic activity (*Servicio Nacional de Sismologia y Vulcanoligia*; http://www.igepn.edu.ec). In the Amazon region, the Andean foothills present two areas of uplift, Santiago and Napo, separated by a deep depression known as the Cone of Pastaza (Bès de Berc *et al*. 2005). A summary of the lithology and seismic activity is provided in Table 2.

The vegetation in the Pacific and Amazonian regions is diverse and depends on the orography, changing from "wastelands" above 3000 m altitude to marshes of humid, natural forest in the lowlands. The two zones have a human presence with cultivation of short-cycle crops; greater human impacts are seen in the Pacific region where the agriculture is more industrialized (Neil 1997). Information on land use and cover was taken from the map data of the MAG IICA CLIRSEN Project, updated in 2001, scale 1:25 000. The coverage and land use in the Esmeraldas basin showed higher incidence of cropping (27% of cocoa, coffee, banana and African oil palm plantations, 18% of cultivated pasture and 11% of the short-cycle crops). The Napo, Pastaza and Santiago basins are less disturbed, but the human presence has begun to expand. The areas of cultivated pasture are 18, 15 and 12% respectively, and of natural forest 55, 13 and 46%. In the Pastaza basin, 17% of the area is used for short-cycle crops. In the Santiago basin, 20% of the area is under logged forest. In the Esmeraldas basin, urban area covers 1% the total basin area.

Ecuador has contrasting climates in the Andes and the plains. In the Amazon region, annual precipitation ranges from 500 to 4000 mm year^{-1}, varying primarily with altitude (Heredia and Pombosa 1999). The upper part of the eastern basins receives intense rainfall, both unimodal and bimodal, with maximum values in March–April and in October, and a minimum in June–August (Laraque *et al*. 2007). The rainfall decreases from north to south (Moreno and Tapia 2001) without clear seasonality, and rains are persistent throughout the year (Fig. 1). According to Laraque *et al*. (2007), the annual precipitation is approx. 3100 mm year^{-1} in the Napo basin, 2300 mm year^{-1} in the Pastaza basin and 2000 mm year^{-1} in the Santiago basin.

The western basin also has a complex spatial rainfall distribution and precipitation ranges from 300 to 6000 mm year^{-1}; the highest recorded annual precipitation is in the Cordillera foothills, which are characterized by a warm, humid climate. Long-duration, low-intensity rainfall occurs in the upper

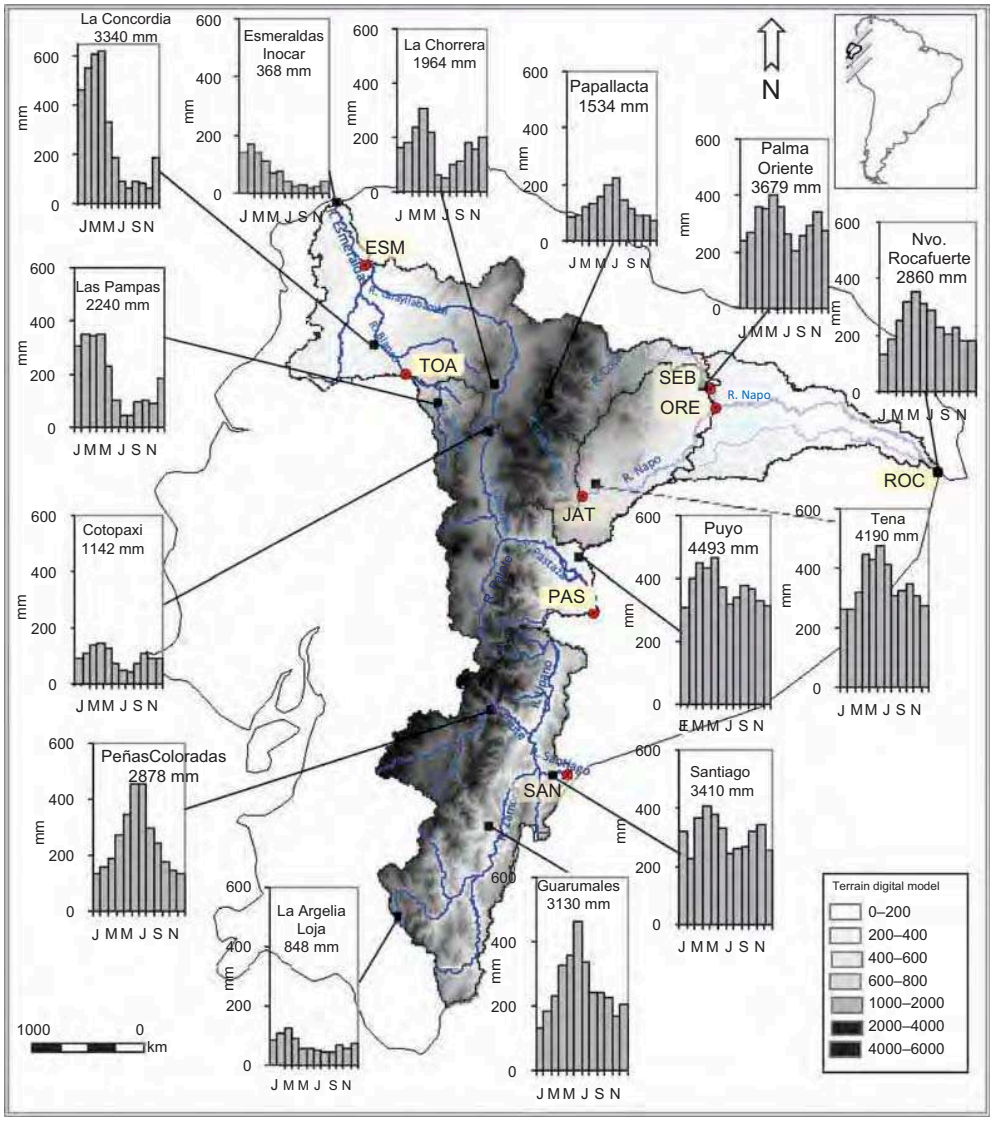

Fig. 1 Topographic map (from SRTM data) of the Napo, Pastaza, Santiago and Esmeraldas river basins (Ecuador) and the monthly rainfall regime (January–December) for 14 INAMHI climatic stations. The annual rainfall value after the station name is for the 1970–2002 period, except for the Santiago River, which represents 1985–1994. See Table 1 for the station codes.

parts of the mountains. In the inter-Andean valleys, precipitation is a function of relief; in valleys rainfall is <300 mm year^{-1} increasing to 1200–1400 mm year^{-1} in the mountains (Fig. 1). The influence of air from the Pacific Ocean defines two periods: a rainy winter from January to May, and a summer or dry season from June to November (Galeas and Melo 2007).

DATA AND METHODS

Under the HYBAM Environmental Research Observatory (http://www.ore-hybam.org)—through an agreement between the IRD (Institut de recherche pour le développement, France) and the INAMHI (*Instituto Nacional de Meteorología e Hidrología* of Ecuador)—monitoring of the network of hydrological and sediment stations in Ecuador began in 2001 (Pombosa *et al*. 2001–2010).

To identify and quantify suspended sediment and dissolved solids yields in the Amazon basin of Ecuador, five gauging stations (SEB, ORE, ROC, PAS, SAN, see Table 1) were installed in an area of 115 600 km^2 (Fig. 1), completing the INAMHI network in this region (JAT, Jatunyacu station, has been operated by INAMHI since 1966). To compare the

Table 1 The gauging station network in the Amazonian and Pacific drainage basins of Ecuador.

Basin	River	Station	Code	Coordinates		Station altitude (m a.s.l.)	Basin area (km^2)	% Andes area >500 m a.s.l.	Equipment
				Latitude	Longitude				
Amazonian									
Napo	Jatunyacu	DJ Iloculín	JAT	01° 98722S	77° 91917 W	570	3130	100	Gauge
	Coca	San Sebastián	SEB	00° 57444S	77° 00694 W	290	5330	92	Limnigraph
	Napo	Fco Orellana	ORE	00° 47083S	76° 99028 W	262	12400	69	Limnigraph
	Napo	Nvo. Rocafuerte	ROC	00° 91686S	75° 39639 W	189	27390	49	Limnigraph
Pastaza	Pastaza	La Unión	PAS	01° 90690S	77° 82073 W	663	12700	100	Gauge
Santiago	Santiago	Pto Santiago	SAN	03° 04435S	78° 01449 W	320	23880	98	Limnigraph
Pacific									
Esmeraldas	Toachi	Sto Domingo	TOA	00° 24500S	79° 12778 W	535	2380	100	Gauge
	Esmeraldas	DJ Sade	ESM	00° 52333N	79° 41528 W	110	19650	58	Gauge

Table 2 Slope, lithology and seismology. Data sources: SRTM (Rabus *et al*. 2003) with 90-m resolution; 1/1 000 000 maps of IGGM (*Dirección General de Geologia y Minas*, Moquet 2011, *Servicio Nacional de Sismologia y Vulcanologia, Escuela Politécnica Nacional*, EPN).

Code	Basin slope (%)	Lithology (%)				Volcanic and seismic activity, ≥4.8 Mw and ≤5.5 Mw							
		Sedimentary clastic	Igneous-felsic		Meta-morphic	1995–2000	2002	2003	2005	2006	2007	2008	2009
			Volcanic	Plutonic									
JAT	39	3	30	29	38								
SEB	34	31	6	35	28	1	1●		1				
ORE	22	73	8	10	10	1			1				
ROC	18	59	5	11	10								1
PAS	28	10	61	9	19	10			1	3	2	2	2
SAN	33	57	4	6	32	52 (2*)		2		1	1*	1	2
TOA	28	0	100	0	0	1							
ESM	22	21	71	0	1	1*					1		

Notes: *Earthquake >5.6 Mw; ●Volcanic eruption.

processes on both sides of the Andes, two INAMHI gauging stations in the Pacific zone on the Esmeraldas River (TOA and ESM) were sampled. The study period covers nine years (2001–2009), except for stations Pastaza in La Union (PAS) and Toachi in Santo Domingo (TOA), where monitoring ceased in 2005.

In the Andean Emeraldas basin, we have a data set for Toachi station, which represents 26% of the total Andean surface (8900 km^2 at elevations above 500 m a.s.l.). For the dissolved and suspended solids calculation we used a weighting based on the following rationale: the isohyets map shows a north–south orientation of precipitation (Melo 2010). The slope is similar along the observed cross-section in the slope map (Galeas and Melo 2007; scale: 1:2 500 000, DEM resolution: 90 m). In the Andean Esmeraldas basin, land cover is linked to the altitudinal level. One source of the dissolved sediments could be anthropogenic (cities and agriculture); the indicators are the increase of Cl^-, SO_4^{2-} and Na^+ (Moquet 2011). Narvaes and Vera (2007) analysed these ions in the Esmeraldas basin and observed that there is no difference between the Toachi and Esmeraldas stations; they concluded that the higher percentage of anions and cations in the Esmeraldas River come from alteration of the underlying rocks, and that the increase in K^+ may be a consequence of human presence.

The methodologies for both gauging and sampling were the same as those adopted in Brazil and Bolivia, which is where the ORE-HYBAM work began (Guyot *et al*. 2005). The cumulative uncertainty calculation was determined from a series of experimental observations of the variables involved in the sampling and in laboratory processes. Ten samples were taken at the surface and at less than 1 m from the river bed bottom. To calculate the uncertainty of the solid load, two measurements were made in the same section. These tests were performed in the HYBAM Observatory (Guyot *et al*. 1994, Vauchel 2009, Moquet 2011, Armijos *et al*. 2013).

The geographic extent of the watershed and the river network were estimated using the Shuttle Radar Topography Mission (SRTM) digital elevation model (Rabus *et al*. 2003) with a resolution of 3 arc sec (90 m), and the Hydrological Modeling and PrePro2002 (Olivera *et al*. 2002) ArcGIS extensions.

The description of the lithology of the study area is primarily based on the 1:1 000 000 maps of the *Dirección General Geología y Minas* (DGGM; Baldock 1982). The seismic and volcanism data were obtained from the *Servicio Nacional de Sismologia e Vulcanologia* (Institute of Geophysics Escuela Politécnica Nacional, http://www.igepn.edu.ec).

Water levels and discharge measurements

Because of the rapid variability over time of this type of Andean river, in addition to the two daily stage level readings taken by an observer, an automatic stage recorder was installed at several gauging stations; these sensors were programmed to record every hour.

Discharge was measured with a 1200-KHz ADCP (Acoustic Doppler Current Profiler; RDI 1999), which measured the water velocity in different layers of the water column and calculated the discharge in real time using a bottom-tracking positioning method that is well-suited for this type of river (Filizola and Guyot 2004).

Every three months, field measurements were taken at each of the gauging stations to verify and complete the rating curve. The discharge value corresponds to a minimum of four measurements or transects—two steps and back. The value of discharge is accepted if the maximum error between the measurements is 4%. During the nine years, 145 discharge measurements, representing 696 transects, were taken at the five gauging stations installed by the HYBAM Observatory and 385 measurements were taken at the three stations operated by INAMHI since 1966.

Total dissolved solids (TDS)

In the TDS analysis, we used water collected and filtered *in situ* (0.45-μm filter) on the 10th day of each month. Water samples were sent to the laboratory at Géosciences Environnement Toulouse (GET, Toulouse, France) for determination of concentrations of the major elements (Ca^{2+}, Mg^{2+}, Na^+, K^+, Cl^-, NO_3^-, SO_4^{2-}, HCO_3^-) and silica. Cation concentrations were measured using an ICP-AES atomic absorption spectrophotometer, and anion concentrations using an IC-HPLC high-pressure ion chromatograph, and a continuous flow spectrocolorimeter was used to measure silica concentrations. The total concentration of dissolved solids was the sum of the concentrations of the major elements plus silica (SiO_2). The quantity of the dissolved solids transported by the river, expressed in t d^{-1}, was determined by multiplying the concentration of the dissolved solids by the instantaneous discharge. The uncertainties of the dissolved material data are explained in Moquet (2011);

note that the error in the calculation of the dissolved flux is 20% for the monthly sampling.

Total suspended sediment (TSS)

To determine the concentration of the suspended sediment at each gauging station, a 500-ml surface sample was collected in the middle of the river every 10 days (on the 1st, 10th and 20th day of each month). At the INAMHI laboratory in Quito, the samples were filtered through a 0.45-μm cellulose acetate filter. This sampling frequency allowed better observation of the temporal variability of sediment fluxes.

To provide a broader picture of the suspended sediment in the water column in each stream, samples were taken every three months along three representative vertical profiles of the river section. A manual vertical sampler was used at three positions: surface (20 cm), intermediate and 50–100 cm above the bottom, for a range of water depths, varying from 2 to 15 m, between the falling and rising stage, and depending on the gauge station. Estimates of sediment fluxes were calculated based on the relationship between the surface TSS and the mean concentration of the section, [TSS] (see Fig. 2). This relationship is not used for the JAT (Napo), PAS (Pastaza) and TOA (Esmeraldas) stations, where only a surface sample was taken due to high turbulence and the difficultly of sampling.

At the Esmeraldas station, measurements were made at different periods of the hydrological year, but it was difficult to take measurements at different depths and, with the turbulence, it can be dangerous. Solid load measurements did not reach the maximum values observed at the surface. The results from this station present the same behaviour as for the other basins (i.e. there is no vertical gradient for high and medium concentrations), which is why we prefer to use an interpolation curve for Esmeraldas based on the other stations. This is one of the reasons why measurements are taken every ten days.

The calculations of the discharge, solid and dissolved yields were performed using HYDRACCESS (http://www.orehybam.org/index.php/eng/Software/Hydraccess) software developed by P. Vauchel in 2005. For stable hydrological conditions, standard deviations of the concentrations are 15% and 36% of the mean value for samples taken at the surface and at <1 m from the bottom, respectively. To determine the sampling uncertainty in the section, repeated sampling was performed every week in low and high water conditions. The maximum standard deviation of the mean [TSS] is 20% at the gauging stations. The uncertainty of the suspended flux determinations was approx. ±25% (Vauchel 2009, Armijos *et al*. 2013).

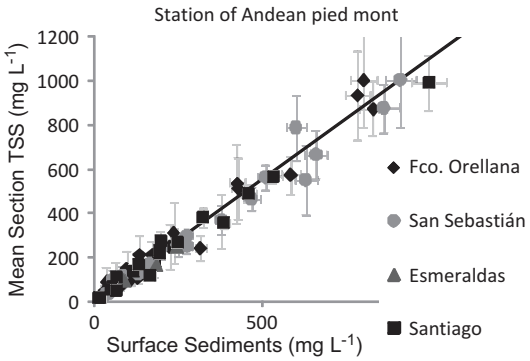

Fig. 2 Relationship between the surface TSS and mean TSS concentration for the gauge section, [TSS], in the Amazon basins of Ecuador (2001–2009); 72 samples.

RESULTS AND DISCUSSION

The results from the 9-year period can be used to supplement previous observations based on shorter periods (Armijos 2002, Cerón 2004, Laraque *et al*. 2004, 2009). We focused our analysis on two basins, Esmeraldas and Santiago, to determine the difference in behaviour between the Pacific and Amazonian basins. Figure 3 shows that the Esmeraldas basin is not completely Andean; for this reason, we calculated the dissolved and suspended sediment flux considering only the percentages of area meeting Andean criteria (i.e. altitude >500 m) to compare with that at Santiago. We chose Santiago because of its dynamic tectonic and seismic characteristics, and because very few suspended sediment studies have been performed in this region.

Hydrology

The Pacific and Amazon regions have high-frequency hydrological regimes associated with climate variability. However, in SAN (Amazon basin), there is a weak seasonal regime with strong peaks from May to July. The ESM station (Pacific region) presents a markedly seasonal hydrology with an extended flood season from February to May and a dry season from July to November (Fig. 4). This difference is due to the spatially homogenous rainfall distribution, rainfall amounts increasing with elevation (Buytaert *et al.* 2006, Galeas and Melo 2007, Rossel and Cadier 2009), whereas SAN has a spatially heterogeneous

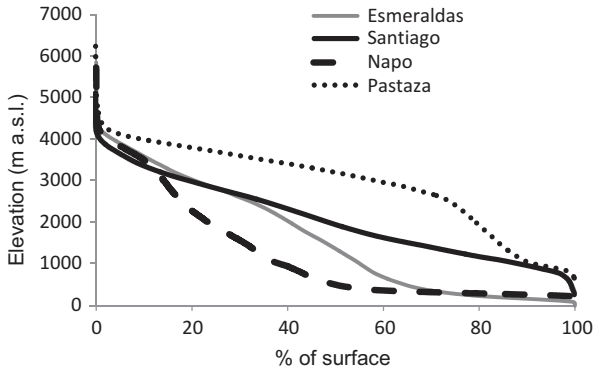

Fig. 3 Hipsometry curve from SRTM data (Source: Mialocq 2005). Percentage of area meeting Andean criteria (i.e. at elevation >500 m a.s.l.): Esmeraldas 58%, Santiago 98%, Napo 49%, and Pastaza 100%.

rainfall distribution that has no relationship with altitude (Laraque *et al*. 2007, Espinoza *et al*. 2009) (Fig. 1).

The coefficients of variation (CV) for discharge at ESM, JAT and SAN are large (0.7–0.8) relative to those for SEB, ORE and ROC (Table 3). The former basins experienced large events, such as in June 2004 when JAT recorded floods up to nine times higher than the daily average; ESM had a large discharge value in February, due to a low-intensity El Niño event (2004–2005, 2006–2007).

The mean annual discharge for 2001–2009 from the Amazon area of Ecuador was approx. 4590 $m^3\ s^{-1}$ (considering the three basins: Napo, Pastaza and Santiago ≅ 64 000 km^2). In Peru, the Borja gauging station on the Marañón River located in the Andean piedmont recorded a mean annual discharge of 4670 $m^3\ s^{-1}$ (Guyot *et al*. 2007), of which 35% corresponded to the Santiago River (SAN) discharge.

At the eastern station of La Union on the Pastaza River (PAS), the minimum flow rate recorded was 57 $m^3\ s^{-1}$ and the average flow rate was 752 $m^3\ s^{-1}$. It was difficult and dangerous to measure the discharge at this station because of the strong flash floods: e.g. a 9-m change in flood stage occurred in four hours (Laraque *et al.* 2004).

The specific discharge ranged from 42 to 97 L s^{-1} km^{-2}. The highest values were recorded in the

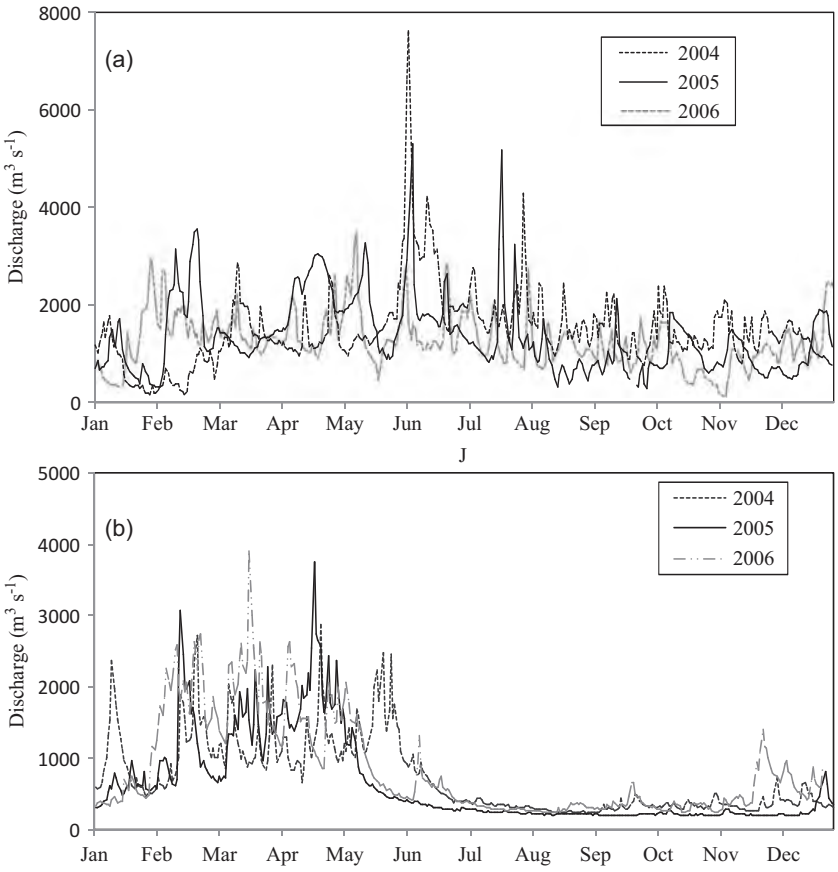

Fig. 4 Daily discharge (1 January 2004–31 December 2006) of (a) SAN (Amazon basin) and (b) ESM (Pacific basin).

Table 3 Daily discharge, monthly TDS (2001–2008), and 10-day estimates of TSS for 2001–2009 (No.: number of gauge readings; Samples: number of samples; CV: coefficient of variation; σ: standard deviation; x: average).

Code	Discharge					TDS					TSS				
	No.	Min. ($m^3\ s^{-1}$)	Mean ($m^3\ s^{-1}$)	Max. ($m^3\ s^{-1}$)	CV σ/x	Samples	Min. ($mg\ L^{-1}$)	Mean ($mg\ L^{-1}$)	Max. ($mg\ L^{-1}$)	CV σ/x	Samples	Min. ($mg\ L^{-1}$)	Mean ($mg\ L^{-1}$)	Max. ($mg\ L^{-1}$)	CV σ/x
JAT	144	63	260	2557	0.7	104	7	68	122	0.3	304	0.4	193	7338	3.0
SEB	27	163	484	1923	0.4	111	45	91	162	0.2	324	7	329	2961	1.5
ORE	43	351	1335	5036	0.5	86	38	57	117	0.2	337	3	192	3684	1.7
ROC	32	758	2313	6664	0.3	89	22	59	216	0.3	307	5	218	1481	0.9
PAS	17	–	–	–	–	67	41	89	160	0.3	125	1	316	1974	1.4
SAN	26	385	1311	12960	0.7	96	28	55	94	0.2	285	2	294	1977	1.2
TOA	29	33	103	412	0.6	69	46	122	196	0.3	132	0.3	128	1811	1.8
ESM	67	156	798	3360	0.8	81	19	103	200	0.4	313	2	162	2628	1.4
	385					679					2117				

Table 4 Annual rainfall (P), runoff (R), discharge, TDS (2001–2008) and TSS yields for 2001–2009 (Source of rainfall data: Perez 2000, Galeas and Melo 2007, Laraque *et al*. 2007).

Code	P ($mm\ year^{-1}$)	R ($mm\ year^{-1}$)	Discharge		TDS			TSS			TDS/ TSS+TDS (%)	TSS+TDS ($t\ km^{-2}\ year^{-1}$)
			($m^3\ s^{-1}$)	($L\ s^{-1}\ km^{-2}$)	($mg\ L^{-1}$)	($10^3\ t\ d^{-1}$)	($t\ km^{-2}\ year^{-1}$)	($mg\ L^{-1}$)	($10^3\ t\ d^{-1}$)	($t\ km^{-2}\ year^{-1}$)		
JAT	1961	2544	252	81	66	1	169	253	5	644	20	813
SEB	2691	2850	482	90	69	3	196	415	17	1183	14	1379
ORE	3209	3053	1200	97	52	5	158	216	22	659	19	817
ROC	3150	2538	2204	80	55	10	139	305	58	774	15	913
PAS	2207	1851	748	59	90	6	166	369	24	682	20	848
SAN	2305	2167	1641	69	56	7	110	335	47	725	13	836
TOA	1512	1324	98	42	111	0.9	147	170	1.4	221	39	368
ESM	2065	1313	818	42	88	6	115	214	15	281	33	342

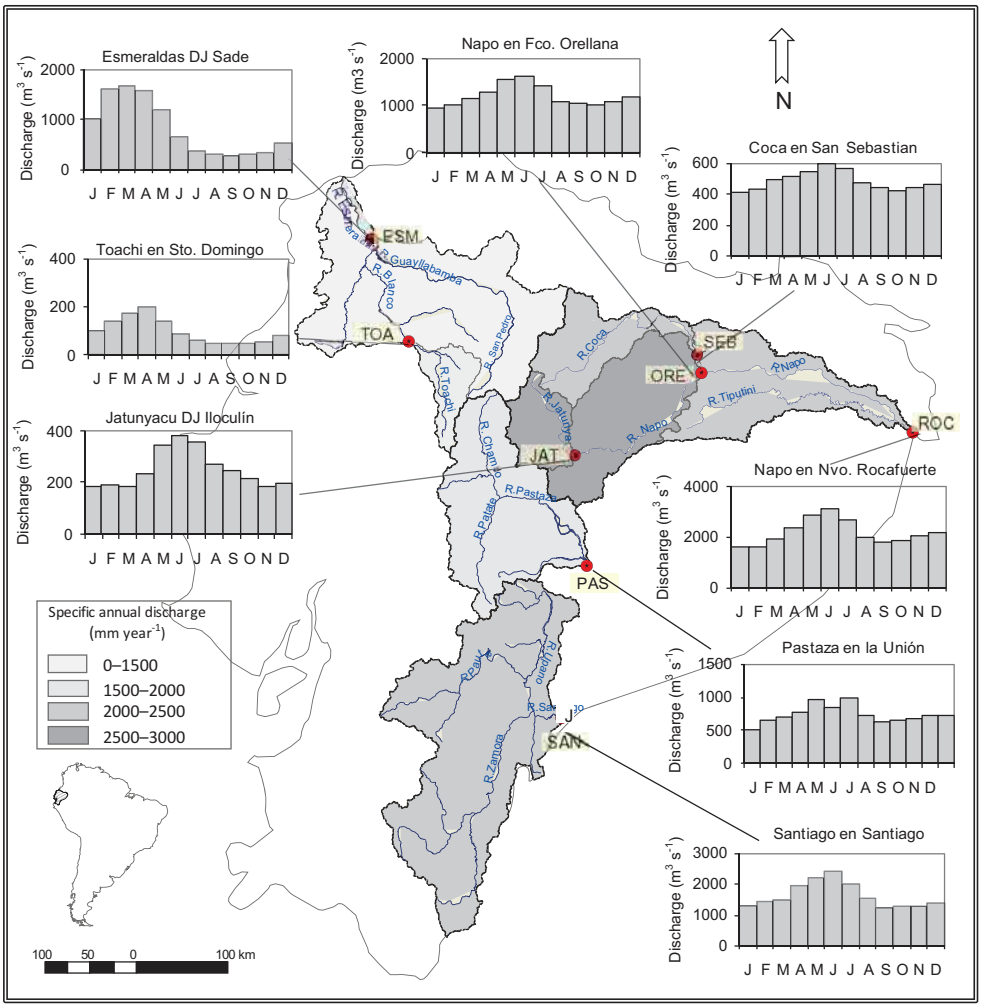

Fig. 5 Annual specific discharge (runoff) map and mean monthly discharge (January–December) for the Napo, Pastaza, Santiago and Esmeraldas rivers (2001–2009).

Amazon region, which may be due to the high specific humidity and convection in this region (Table 4, Fig. 5).

Total dissolved solids (TDS)

To better understand and visualize the dissolved solids, we considered only the period from 2002 to 2005 in Fig. 6; however, the data (tables) and the analysis concern the entire 8-year period. Figure 6(a) shows that at the Santiago River station (SAN), the variation of dissolved solids was almost constant in time (monthly sampling frequency). This behaviour is similar to that of other Ecuadorian Amazon gauging stations and can be linked to groundwater contributions to flow in the dry season. In the Pacific zone (Fig. 6(b)), the Esmeraldas River station (ESM) presented strong seasonality in TDS that is not linked to discharge but is a result of solute dilution during the flood season.

There was an inverse relationship between the TDS and the discharge at both the Pacific and Amazon stations (Fig. 7). However, at SAN the relationship was weak, with values of 50–110 mg L^{-1}, whereas for ESM, the inverse relationship was clear, with values ranging from 45 to 200 mg L^{-1} (Table 3). Guyot *et al.* (1996) observed the same behaviour in the Andean rivers of the Bolivian Amazon basin, where TDS concentrations range from 100 to 200 mg L^{-1}.

The primarily silico-clastic lithology of the sedimentary rocks of the Andean basins of Ecuador, as in Peru and Bolivia, influences their weathering (Stallard and Edmond 1983, Moquet *et al.* 2011). The

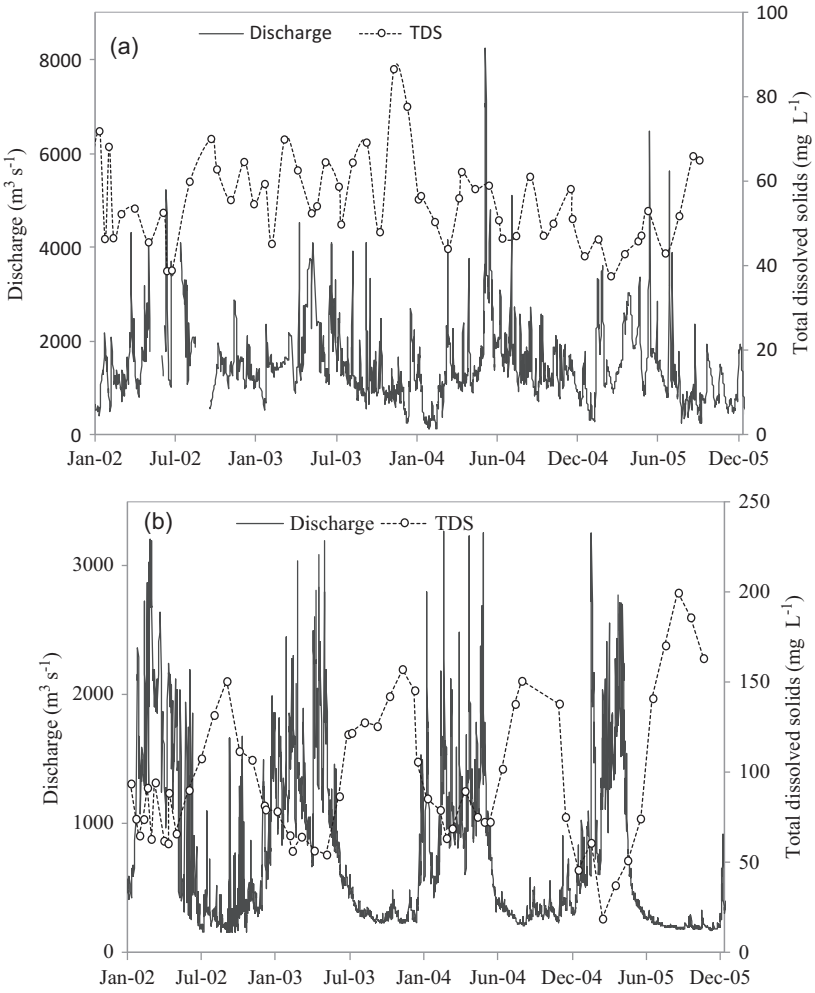

Fig. 6 Daily discharge and monthly TDS concentration (January 2002–December 2005) for (a) SAN and (b) ESM.

higher concentrations of dissolved materials at ESM and PAS are due to the presence of volcanic rocks (Table 2), which weather more rapidly (Goldsmith *et al*. 2008, Moquet *et al*. 2011). The higher concentrations of dissolved solids in the ROC and SAN basins are due to the presence of carbonates and evaporites.

Volcanic activity is also important. The maximum TDS concentrations in the Napo and Pastaza basins (Table 3) were observed in 2002 at SEB and ROC after the eruptions of Reventador. This volcano, a product of the subduction of the Nazca plate, is characterized by explosive eruptions of ash and lahars that contain SO_2 and HCl, which are readily dissolved in runoff (Gondran 2004, Hall *et al.* 2004, Bernal *et al*. 2007).

Within the study period (2001–2008), in 2005 and 2006, there was an approximately 50% increase in TDS concentrations in the Esmeraldas and Santiago basins. This increase may be related to the water discharge, being one of the lowest recorded in the dry season.

These results show that the rainfall, lithology and volcanism also influence the variability and distribution of the TDS concentrations.

The seasonal variability of TDS concentration is less than that of discharge, which implies that the hydrological variability controls the TDS flux during the annual cycle (Fig. 8). The Andean basins in the Pacific and Amazon regions generate the following amounts (10^6 t year^{-1}) annually: ESM, 2; ORE+SEB, 3; PAS, 2; and SAN, 3. The plains produce 0.38 $\times$ 10^6 t year^{-1} (40% from plains of the Esmeraldas basin) and 0.73 $\times$ 10^6 t year^{-1} (35% from plains of the Napo basin). These results indicate that approximately 80% of the TDS flux is produced by the Andean region of these basins (Table 4).

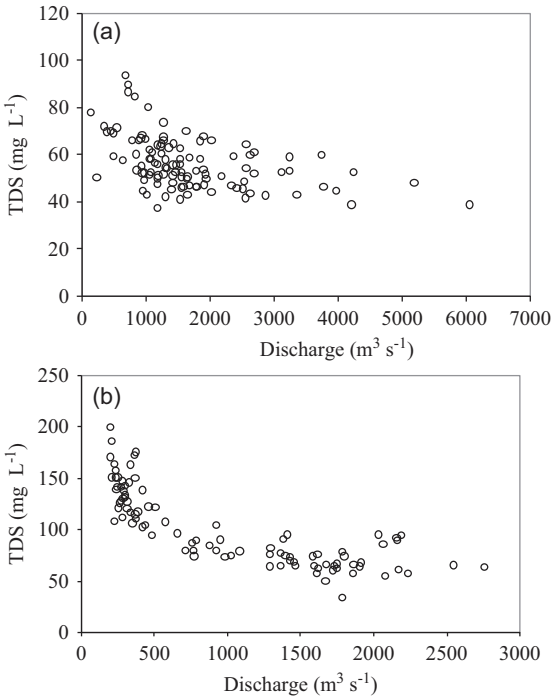

Fig. 7 Relationship between the monthly TDS concentration and discharge (2001–2008) for (a) SAN and (b) ESM.

In another region of the Andes, Guyot *et al.* (1996) showed that the dissolved sediment load from the Bolivian Andes (Beni and Grande rivers) was approx. 40 t km^{-2} year^{-1}. Restrepo *et al.* (2006) calculated that the weathering rate of the Magdalena River in Colombia was 120 t km^{-2} year^{-1}, resulting from both rock weathering (limestone) and anthropogenic effects (a well-known factor that affects all ecosystems in the Caribbean region).

In Peru, Moquet (2011) observed that the dissolved solid flux of the Upper Marañón River basin reached up to 23 $\times$ 10^6 t year^{-1}, of which the Andean contribution from the Santiago River sub-basin is 3 $\times$ 10^6 t year^{-1}, equivalent to 13%. Due to the great number of calcareous rock and salt rock outcrops in this part of the basin, the Peruvian Andes are the largest source of dissolved material in the Amazon basin (Gibbs 1972, Stallard and Edmond 1983).

Total suspended sediment (TSS)

In the Andean basins, the concentration of suspended material at the surface and the average concentration of the river section, [TSS], showed a relationship close to one (see Fig. 2), i.e. there was no concentration gradient. This behaviour was different from that generally observed in other Amazon rivers and the rest of the world. During high flow, the high-speed streamflow (>2 m s^{-1}) passing through shallow sections (max. depth 15 m) creates strong turbulence that maintains the homogeneous concentration of suspended sediments; hence, we perform an extrapolation to high flow. A vertical gradient was apparent during the dry season, but the concentrations were low; thus, this influence in the relationship is minimal. Regarding the three mountain rivers, Jatunyacu (JAT), Pastaza (PAS) and Toachi (TOA), which are very turbulent and where very high concentration peaks occur (e.g. maximum recorded 7000 mg L^{-1} on 10 May 2004 at JAT station), deep measurements are difficult and dangerous to perform. Hence, sampling was shallow, and the relationship described above should not be applied to these stations.

In the Amazon region, the concentrations of suspended sediment varied widely over time (even when only three samples per month were collected), but did not show clear seasonality (Fig. 9(a)), although higher peaks were observed from May to July, a similar pattern to that seen in the discharge. In contrast, there was pronounced seasonality in the Pacific region (Fig. 9(b)), with high suspended sediment concentrations during the flood season (February–May) and low concentrations during the dry season (July–November). The Esmeraldas transported 70% of its annual load in high-water periods. During intense rainfall events, we observed an increase in suspended sediment in the months of December to May. In 2008 it is evident that the El Niño event influenced 50% of suspended sediment concentrations.

In the Pacific basin, as in the Amazon basin, temporal fluctuations of the suspended sediment load were strong, with peaks of 6 and 14 times the mean, respectively. These fluctuations resulted in large coefficients of variation: the CV is greater in the upper basin and decreases in the plains (Table 2). The relationship between discharge and suspended sediments in both the Amazon and Pacific regions showed a positive slope and clockwise hysteresis, but this was more evident in the Esmeraldas River (Fig. 10(b)) than in the Santiago River (Fig. 10(a)) due to the difference in seasonality between the rivers.

The hypsometric curve (Fig. 3) indicates that the PAS and SAN are young basins and able to erode 100% of the Andean surface. The ESM and ROC are in a mature stage and, respectively, 40 and 35% of their basin area is represented by plains (slope

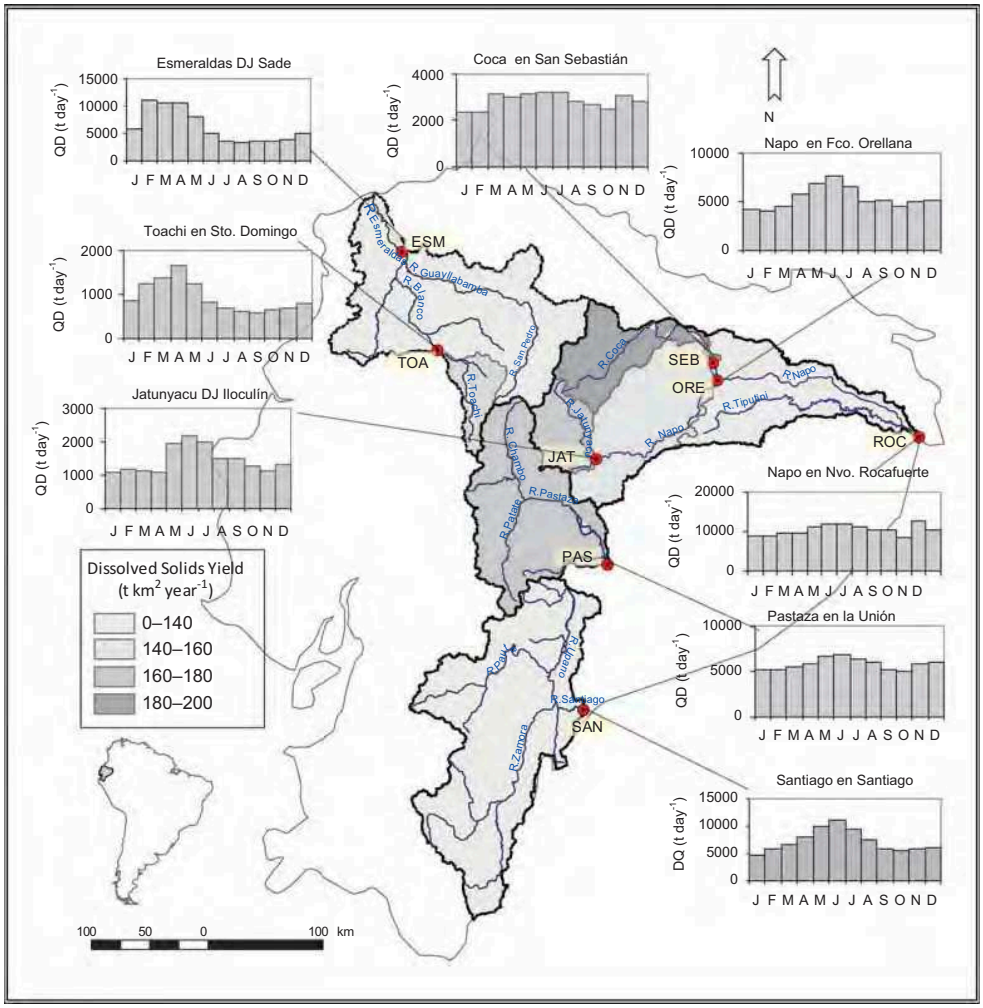

Fig. 8 Map of TDS specific production and monthly TDS flux (January–December) for the Napo, Pastaza, Santiago and Esmeraldas rivers (2001–2008).

<2%). Based on the percentage of the Andean surface, the sediment load (10^6 t year^{-1}) is as follows: Napo (SEB+ORE), 14; Pastaza, 8.8; Santiago, 17; and Esmeraldas, 3. The plains generate a sediment load representing 43% (ESM) and 32% (ROC) of the total load, which means that the plains produce sediment on both sides (Fig. 11). Noni and Trujillo (1989), Venacker *et al*. (2007) and Melo (2010), indicated that the zones susceptible to erosion are areas where agriculture is intensified and not areas with the greatest slope. However in the plain of the Napo basin, the cultivated area did not exceed 7%.

Dadson *et al*. (2004) observed in Taiwan that the presence of earthquakes greater than 5 Mw (moment magnitude scale) in this region caused high rates of erosion. This phenomenon disaggregates the sediments, facilitating their erosion by rainfall and runoff, and the effect is noticeable for five years after the earthquake occurrence.

In Ecuador, the highest rate of erosion is located in the Amazon region, which may be because the sub-Andean foothills have two large uplift zones separated by the depression of Pastaza (Bès de Berc *et al*. 2005): a relatively simple uplift is located to the north (Levantamiento Napo) and the complex structure of the Cutucú Cordillera is located to the south (Santiago). This complex structure results from the meeting of reverse faults, which penetrate into the Cutucú uplift (Legrand *et al.* 2005). Consequently, the Santiago basin has a higher probability of earthquakes occurring. In 1995, an earthquake with a magnitude of Mw = 7 was observed in the Santiago basin and several of Mw < 5.6 then occurred to 2000. In November 2007, another earthquake with a

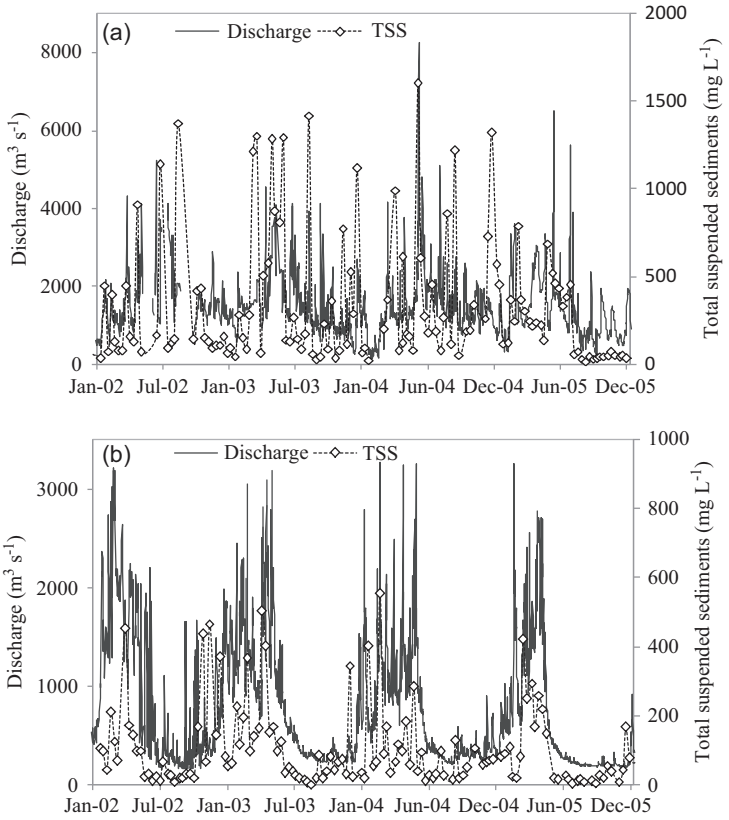

Fig. 9 Daily discharge and 10-day estimates of TSS concentration (January 2002–December 2005) for (a) SAN and (b) ESM.

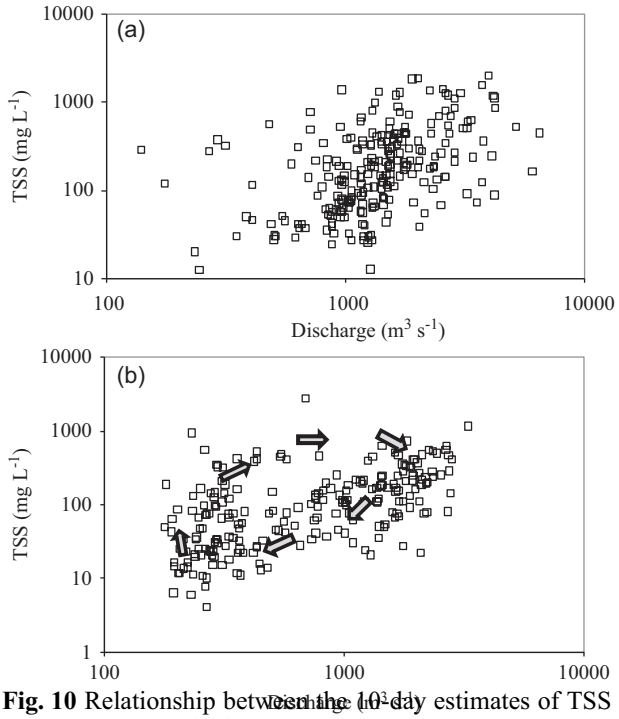

Fig. 10 Relationship between the 10-day estimates of TSS concentration and discharge (2001–2009) for (a) the Santiago River at Puerto Santiago and (b) the Esmeraldas River at DJ Sade.

magnitude of Mw = 5.8 occurred, and in May 2008, a third earthquake occurred with a magnitude of Mw = 5.9. These events coincide with the largest measured [TSS] as a result of sediment being washed out by rain. In the ORE-HYBAM data set, the 2005 earthquake (Mw = 5.3) coincided with the greatest [TSS] value (569 mg L^{-1}).

The SEB had the highest recorded [TSS] in 2003 (509 mg L^{-1}) due to the volcanic activity of Reventador in November 2002 (Laraque *et al*. 2004). In addition to the seismicity and volcanism, lithology plays an important role.

Guyot *et al*. (1996) estimated that the Bolivian Andean basin exported a total of 500–600 × 10^6 t $year^{-1}$ of suspended solids, which was controlled by relief (Aalto *et al*. 2006) and climate factors, primarily rainfall seasonality (Pepin *et al*. 2008).

In total, the Napo, Pastaza and Santiago rivers contributed 46 × 10^6 t $year^{-1}$ of suspended sediments, which corresponds to 8% of the total load of the Amazon River at the Óbidos station (the lowest station before the Atlantic Ocean).

In Ecuador, the comparison between the TDS and TSS fluxes showed that, in the Amazon basins, the TSS was approx. 80% of the total yield, whereas in the Pacific zone, the value was only 60% (Table 4).

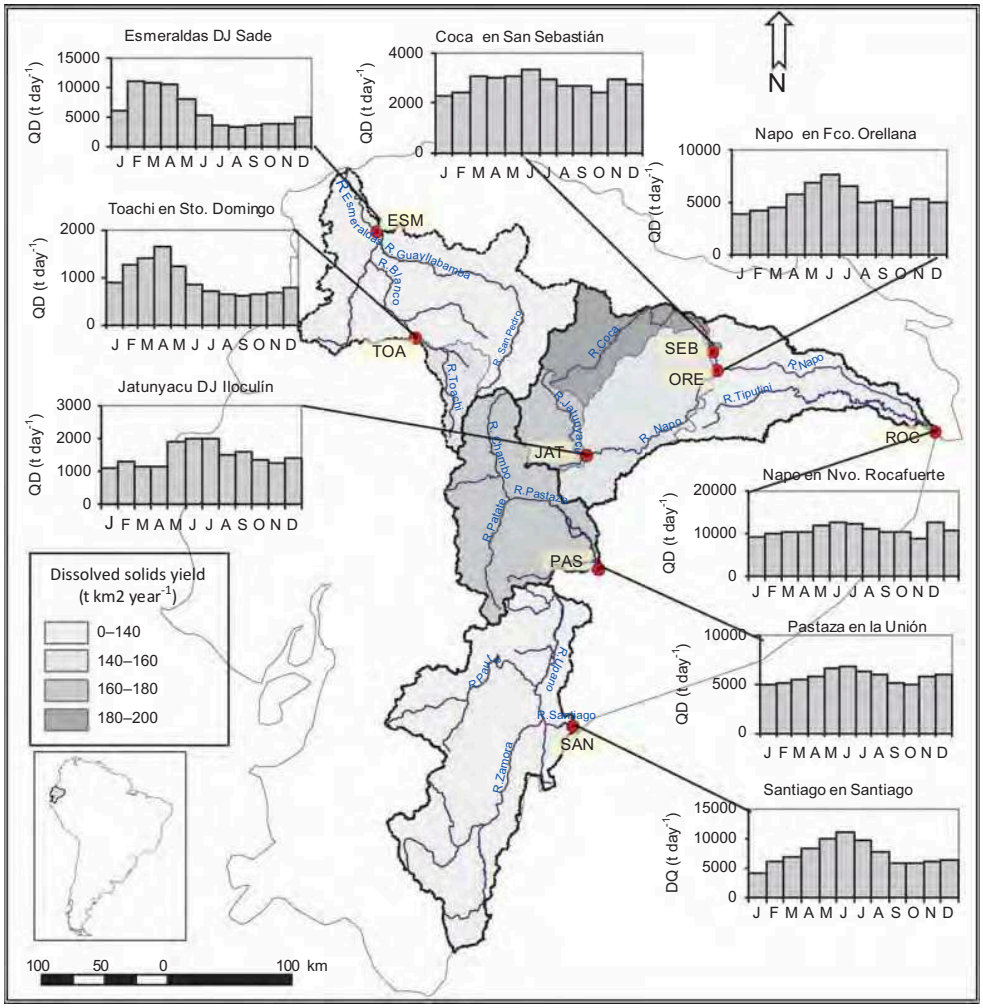

Fig. 11 Map of TSS specific production (erosion map) and monthly TSS flux (January–December) for the Napo, Pastaza, Santiago and Esmeraldas rivers (2001–2009).

CONCLUSIONS

This work provides the scientific community with a 9-year hydrological data set containing the dissolved solid and suspended sediment data from three major basins in the Amazon (ROC, PAS, SAN) and in the Pacific (ESM) regions of Ecuador.

The hydrology shows strong variability governed by the spatial heterogeneity of rainfall in both the Amazon and Pacific zones. However, in the Esmeraldas basin the hydrological regime is more defined, with intensification of precipitation when El Niño events occur.

The lithology and volcanic activity are driving factors that influence the high concentrations of dissolved sediments. However, anthropogenic activity may also be a factor that leads to higher concentrations of dissolved sediments in the Esmeraldas basin. It should be noted that in this basin there was a dilution of the concentration of dissolved sediments that was not measured and needed tracking in the piedmont basin.

Erosion is important in the Andean basins, but the plains are also a source of sediment in both regions. These results are linked to precipitation, lithology, volcanic activity, seismic activity and human activity factors, which act in different ways. In the Esmeraldas basin, heavy rainfall coincident with the El Niño phenomenon can be a trigger for erosion, especially in areas of pasture crops and arboriculture. However, in the Amazon basin, seismic activity is the trigger for the disaggregation of sediments and, together with volcanic activity and variable precipitation, cause higher concentrations of sediments in this region. In addition, the plain in the Napo basin showed the occurrence of erosion linked to tectonic activity. As there are no dissolved and suspended

sediment concentration measurements for the Andean Esmeraldas basin, we present a first estimate of the fluxes.

No sedimentation was observed along the river profile in the Bolivian, Peruvian or Brazilian Amazon basin. The lithology and volcanic activity are driving factors that influence the high concentrations of dissolved and suspended sediments. Seismic activity contributes to increases in the concentration of suspended sediments, particularly in the Santiago basin. The annual dissolved and sedimentary fluxes from the Ecuadorian Amazonian basin are 9 and 47 $\times$ 10^6 t year^{-1}, respectively (3 and 6% of the total Amazon yield), which corresponds to a yield of 131 and 736 t year^{-1} km^{-2}, respectively. In the Pacific region (Esmeraldas basin), the dissolved and sedimentary fluxes are 2 and 5 $\times$ 10^6 t year^{-1}, respectively, which are equivalent to 111 and 279 t year^{-1} km^{-2}.

Acknowledgements This study was performed with support from the *Instituto Nacional de Meteorología e Hidrología* of Ecuador (SENAMHI) and the Institut de recherche pour le développement (IRD), France. We would like to thank participants in the ORE-HYBAM Observatory from Ecuador, and the observers at the different gauging stations.

REFERENCES

Aalto, R., Dunne, T., and Guyot, J.L., 2006. Geomorphic controls on Andean denudation rates. *Journal of Geology*, 114 (1), 85–99.

Armijos, E., 2002. Estudio *hidrofísico de las cuencas de los ríos Napo, Pastaza y Santiago dentro del proyecto Hybam*. Thesis (Tesis de graduación), Universidad Central de Ecuador, Quito, Ecuador.

Armijos, E., 2010. *Cuantificación de flujos sedimentarios de las cuencas Amazónicas del Perú*. Thesis (Tesis para la obtención del título de Máster en Recursos Hidricos), Universidad Nacional Agraria La Molina, Lima, Perú.

Armijos, E., *et al*., 2013. Suspended sediment dynamic in the Amazon River of Peru. *Journal of South American Earth Sciences*, doi:10.1016/j.jsames.2012.09.002.

Aspiazu, P. and Luna, M., 1993. *Geografía e historia del Ecuador*. Madrid, Spain: Cultural.

Baldock, J.W., 1982. *Geología del Ecuador*. Quito, Ecuador: Dirección General de Geología y Minas.

Bernal, C., *et al*., 2007. Influence de l'activité volcanique dans la chimie du Rio Napo: affluent de l'Amazone venant des Andes équatoriennes. *Poster presented at*: Water quality and sediment behaviour of the future, July 2007. Perugia, Italy: IAHS.

Bès de Berc, S., *et al*., 2005. Geomorphic evidence of active deformation and uplift in a modern continental wedge-top–foredeep transition: example of the eastern Ecuadorian Andes. *Tectonophysics*, 399, 351–380, doi:10.1016/J.TECTO.2004.12.030.

Buytaert, W.. *et al*., 2006. Spatial and temporal rainfall variability in mountainous areas: a case study from the south Ecuadorian Andes. *Journal of Hydrology*, 329 (3–4), 413–421, doi:10.1016/j.jhydrol.2006.02.031.

Callède, J., *et al*., 2010. Les apports en eau de l'Amazone à l'Océan Atlantique. *Revue des Sciences de l'Eau*, 23 (3), 247–273.

Cerón, C., 2004. *Flux sédimentaires des basins amazoniens d'Equateur*. Mémoire de DEA, Université Paul Sabatier, Toulouse, France.

CLIRSEN (Centro de Levantamientos Integrados de Recursos Naturales por Sensores Remotos), 2003. Análisis de cobertura. Quito, Ecuador: Boscosa del Ecuador.

Dadson, S., *et al*., 2004. Earthquake-triggered increase in sediment delivery from an active mountain belt. *Geology*, 32, 733–736.

Degens, E.T., Kempe, S., and Richey, J.E., 1991. Summary: biogeochemistry of major world rivers. *In*: E.T. Degens, S. Kempe, and J.E. Richey, eds. *Biogeochemistry of major world rivers*. Chichester, UK: John Wiley & Sons Ltd., Scope 42, 323–347.

DINAGE (Dirección Nacional de Geologia), 1997. Primer catálogo de información técnica. Quito, Ecuador: Ministerio de Energía y Minas.

Dunne, T., *et al*., 1998. Exchanges of sediment between the flood plain and channel of the Amazon River in Brazil. *Geological Society of America Bulletin*, 110, 450–467.

ECORAE (Instituto para el Ecodesarrollo Regional Amazónico), 2002. *Zonificación Ecológica–Económica de la Amazonía Ecuatoriana*. Quito, Ecuador: ECORAE.

Espinoza, J.C., *et al*., 2009. Spatio-temporal rainfall variability in the Amazon Basin Countries (Brazil, Peru, Bolivia, Colombia and Ecuador). *International Journal of Climatology*, 29, 1574–1594.

Filizola, N. and Guyot, J.L., 2004. The use of Doppler technology for suspended sediment discharge determinations in the River Amazon. *Hydrological Sciences Journal*, 49 (1), 143–153.

Filizola, N. and Guyot, J.L., 2009. Suspended sediment yields in the Amazon basin: an assessment using the Brazilian national data set. *Hydrological Processes*, 23, 3207–3215, doi:10.1002.hyp.7394

Galeas, R. and Melo, P., 2007. *Estudio comparativo del comportamiento hidro-sedimentológico de las cuencas del río Napo (vertiente amazónica) y del río Esmeraldas (vertiente pacífica). Influencia de la morfometría y del fenómeno del Niño*. Thesis (Tesis de graduación), Pontificia Universidad Católica del Ecuador, Quito, Ecuador.

Gibbs, R.J., 1967. The Geochemistry of the Amazon River System. Part I. The factors that control the salinity and the composition and concentration of the suspended solids. *Geological Society of America Bulletin*, 78, 1203–1232.

Gibbs, R.J., 1972. Water chemistry of the Arnazon River. *Geochimica et Cosmochimica Acta*, 36, 1061–1066.

Goldsmith, S.T., *et al*., 2008. Geochemical fluxes and weathering on high standing islands: Taranaki and Manawatu-Wanganui Regions, New Zealand. *Geochimica et Cosmochimica Acta*, 72 (9), 2248–2267.

Gondran, R., 2004. *Impact de l'éruption du Reventador sur la chimie de la phase dissoute du Rio Coca*. Rapport de Stage, Université Paul Sabatier, Toulouse, France.

Goulding, M., Barthem, R., and Ferreira, E., 2003. *The Smithsonian Atlas of the Amazon*. Washington, DC: Smithsonian Institution Press.

Gutscher, M.A., *et al*., 1999. Tectonic segmentation of the North Andean margin: impact of the Carnegie Ridge collision. *Earth and Planetary Science Letters*, 168, 255–270.

Guyot, J.L., 1993. *Hydrogéochimie des fleuves de l'Amazonie bolivienne*. Thèse de doctorat, Université de Bordeux. Paris, France. ORSTOM.

Guyot, J.L., Bourges, J., and Cortez, J., 1994. Sediment transport in the Rio Grande, an Andean river of the Bolivian

Amazon drainage basin. *In*: L.J. Olive, R.J. Loughran, and J.A. Kesby, eds. *Variability in stream erosion and sediment transport*. Wallingford, UK: IAHS Press, IAHS Publ. 224, 223–231. Available from: http://iahs.info/redbooks/224.htm [Accessed 15 July 2013].

Guyot, J.L., Filizola, N., and Laraque, A., 2005. Régime et bilan du flux sédimentaire de l'Amazone à Óbidos (Pará, Brésil), de 1995 à 2003. *In*: D.E. Walling and A.J. Horowitz, eds. *Sediment budgets*. Wallingford, UK: IAHS Press, IAHS Publ. 291, 347–356. Available from: http://iahs.info/redbooks/291.htm [Accessed 15 July 2013].

Guyot, J.L., et al., 1996. Dissolved solids and suspended sediment yields in the Rio Madeira basin, from the Bolivian Andes to the Amazon. *In*: D.E. Walling and B.W. Webb, eds. *Erosion and sediment yield: Global and regional perspectives*. Wallingford, UK: IAHS Press, IAHS Publ. 236, 55–63. Available from: http://iahs.info/redbooks/236.htm [Accessed 15 July 2013].

Guyot, J.L., et al., 2007. Suspended sediment yields in the Amazon basin of Peru, a first estimation. *In*: B.W. Webb and D. De Boer, eds. *Water quality and sediment behaviour of the future: Predictions for the 21st century*. Wallingford, UK: IAHS Press, IAHS Publ. 314, 3–10. Available from: http://iahs.info/redbooks/314.htm [Accessed 15 July 2013].

Hall, M., *et al*., 2004. Volcanic eruptions with little warning: the case of Volcán Reventador's surprise November 3, 2002 eruption, Ecuador. *Revista Geologica de Chile*, 31 (2), 349–358.

Heredia, E. and Pombosa, R., 1999. Influencia del ENSO sobre los caudales mensuales de las grandes cuencas hidrográficas del Ecuador. *In*: *Hydrological and geochemical processes in large scale river basins*. Manaus, Brazil: HYBAM 11/1999.

La Condamine, C.M., 1751. Mesure des trois premiers degrés du méridien dans l'Hémisphère Austral. Paris: Académie Royale de Sciences.

Laraque, A., *et al*., 2004. Sediments yields and erosion rates in the Napo River Basin: an Ecuadorian Andean Amazon tributary. *In*: V. Golosov, V. Belyaev, and D.E. Walling, eds. *Sediment transfer through the fluvial system*. Wallingford, UK: IAHS Press, IAHS Publ. 288, 220–225.

Laraque, A., *et al*., 2007. Heterogeneous distribution of rainfall and discharge regimes in the Ecuadorian Amazon basin. *Journal of Hydrometeorology*, 8 (6), 1364–1381.

Laraque, A., *et al*., 2009. Sediment budget of the Napo River, Amazon basin, Ecuador and Peru. *Hydrological Processes*, 23 (25), 3509–3524.

Legrand, D., *et al*., 2005. The 1999–2000 seismic experiment of Macas swarm (Ecuador) in relation with rift inversion in Subandean foothills. *Tectonophysics*, 395, 67–80.

Martinez, J.M., *et al*., 2009. Increase in suspended sediment yield of the Amazon River assessed by monitoring network and satellite data. *CATENA*, 79, 257–264.

Meade, R.H., *et al*., 1979. Sediment loads in the Amazon River. *Nature*, 278, 161–163.

Meade, R.H., *et al*., 1985. Storage and remobilization of suspended sediment in the lower Amazon River of Brazil. *Science*, 228, 488–490.

Melo, P., 2010. *Estudio de los riesgos potenciales de erosión en dos cuencas de la vertiente pacifica ecuatoriana bajo la influencia del fenómeno ENSO. Los casos de la cuenca del Rio Guayas y Esmeraldas*. Thesis (Master 2 SGT), Prefalc. Ciencias y Gestión de la Tierra, Geologia, riesgos y gestión del territorio, Université Nice Sophia Antipolis, Nice, France.

Mialocq, L., 2005. *Délimitation des bassins versants à l'aide d'ArcGis8*. Lima, Peru: HYBAM.

Molina, A., *et al*., 2008. Environmental factors controlling spatial variation in sediment yield in central Andean mountain area. *Geomorphology*, 98, 178–186.

Monzier, M. and Robin, C., 1995. Volcans à risques du Vanuatu à l'Équateur. *ORSTOM Actualités*, 45, 13–20.

Moquet, J., *et al*., 2011. Chemical weathering and atmospheric/soil CO_2 uptake in the Andean and foreland amazon basins. *Chemical Geology*, 287, 1–26.

Moquet, J.S., 2011. *Caractérisation des flux hydrogéochimiques des bassins andins de l'Amazone*. Thèse de doctorat, Université Paul Sabatier, Toulouse, France.

Moreno, F. and Tapia, A., 2001. *Regionalización hidrometeorológica de las cuencas amazónicas*. Thesis (Tesis de graduación), Universidad Central de Ecuador, Quito, Ecuador.

Mortatti, J. and Probst, J.L., 2003. Silicate rock weathering and atmospheric/soil CO_2 uptake in the Amazon basin estimated from river water geochemistry: seasonal and spatial variations. *Chemical Geology*, 197, 177–196.

Narvaéz, P. and Vera, A., 2007. *Estudio comparativo del comportamiento geoquímico de las aguas superficiales de las cuencas del río Napo en el oriente y del río Esmeraldas en la costa ecuatoriana e identificación de factores naturales y antrópicos que determinan sus diferencias*. Thesis (Tesis de graduación), Universidad Central del Ecuador, Quito, Ecuador.

Noni, G. and Trujillo, G., 1986. *La Erosión en el Ecuador*. Quito, Ecuador: Centro Ecuatoriano de Investigación Geográfica.

Neil, D.A., 1997. *Ecuadorian Pacific coast mesic forest. In: A guide and strategy for their Conservation*. *The Americas*, Vol. 3. Cambridge, MA: UICN, 508–518.

Olivera, F., Dodson, B., and Bristow, E., 2002. *PrePro2002 User's Manual*. Houston: Texas University and Dodson Associates, Inc.

Pepin, E., *et al*., 2008. Tectonic or climate control on modern catchment-scale erosion rates. In: 4th Alexander von Humboldt International Conference – The Andes: *Challenge for Geosciences*. Santiago, Chili, 12/2008, EGU.

Pérez, V., 2000. *Balance hídrico superficial de la cuenca del Río Napo*. Thesis, Universidad Central del Ecuador, Quito, Ecuador.

Pombosa, R., INAMHI- ORE .2001–2010-Informes de campo. Available from: http://www.ore-hybam.org

Rabus, B., *et al*., 2003. The Shuttle Radar Topography Mission a new class of digital elevation models acquired by spaceborne radar. *Photogrammetry and Remote Sensing*, 57, 241–262.

RDI (RD Instruments), 1999. Acoustic Doppler Current Profilers – Principles of Operation: A Practical Primer. Second Edition for broadband ADCPs. San Diego, CA: RD Instruments.

Restrepo, J.D., *et al*., 2006. Fluvial fluxes into the Caribbean Sea and their impact on coastal ecosystems: The Magdalena River, Colombia. *Global and Planetary Change*, 50, 33–49.

Rivadeneira, M. and Baby, P., 1999. La Cuenca Oriente: Estilo tectónico, etapas de deformación y características geológicas de los principales campos de Petro-producción. Quito, Ecuador: IRD, Publ. Petroproducción.

Rossel, F. and Cadier, E., 2009. El Nino and prediction of anomalous monthly rainfalls in Ecuador. *Hydrological Processes*, 23 (22), 3253–3260.

Stallard, R.F. and Edmond, J.M., 1983. Geochemistry of the Amazon. The influence of geology and weathering environment on the dissolved load. *Journal of Geophysical Research*, 88, 9671–9688.

Vanacker, V., *et al*., 2007. Spatial variation of suspended sediments concentration in tropical Andean river system: The Paute River, southern Ecuador. *Geomrophology*, 87, 53–67.

Vauchel, P., 2005. Hydraccess : Logiciel de gestion et traitement de données hydro-météorologiques, version 2.1.4. Téléchargeable sur. Available from: http://www.orehybam.org.

Vauchel, P., 2009. Tratamiento de datos hidrológicos y de sedimentos con Hydromesad. Informe interno técnico, Observatório ORE-Hybam, Lima-Perú.

Winckell, A., 1997. Los paisajes naturales del Ecuador. Centro Ecuatoriano de Investigación Geográfica, IPGH-ORSTOM, Quito, Ecuador.

Apêndice D

Propiedades óticas das águas do rio e da várzeas na Bacia Amazônica: Implicações baseadas em medidas do satélite e medidas de partículas em suspensão

The optical properties of river and floodplain waters in the Amazon River Basin: Implications for satellite-based measurements of suspended particulate matter

AGU PUBLICATIONS

JGR

Journal of Geophysical Research: Earth Surface

RESEARCH ARTICLE
10.1002/2014JF003404

Key Points:
- Water optical properties and characteristics were assessed in the Amazon Basin
- CDOM absorption and SPM show reduced variability (size and type) at river surface
- AOPs show robust correlation with SPM at infrared for all rivers and tributaries

Supporting Information:
- Figures S1–S9

Correspondence to:
J.-M. Martinez,
jean-michel.martinez@ird.fr

Citation:
Martinez, J.-M., R. Espinoza-Villar, E. Armijos, and L. Silva Moreira (2015), The optical properties of river and floodplain waters in the Amazon River Basin: Implications for satellite-based measurements of suspended particulate matter, *J. Geophys. Res. Earth Surf.*, *120*, doi:10.1002/2014JF003404.

Received 5 DEC 2014
Accepted 16 JUN 2015
Accepted article online 18 JUN 2015

The optical properties of river and floodplain waters in the Amazon River Basin: Implications for satellite-based measurements of suspended particulate matter

Jean-Michel Martinez[1,2], Raul Espinoza-Villar[1,2], Elisa Armijos[3], and Luciane Silva Moreira[4]

[1]GET, UMR 5563, IRD/CNRS/Université Toulouse 3, Toulouse, France, [2]Instituto de Geociências, Universidade Nacional de Brasília, Campus Universitário Darcy Ribeiro, ICC Centro, Brasília, Brazil, [3]CLIAMB, Instituto Nacional de Pesquisas da Amazônia-Universidade Federal do Amazonas, Manaus, Brazil, [4]Departamento de Geoquímica, Universidade Federal Fluminense, Niterói, Brazil

Abstract Satellite images can now be used to assess river sediment discharge, and systematic studies over rivers and lakes are required to support such applications and document the variability of inland water optical properties at the watershed scale. The optical properties of the Amazon Basin waters were analyzed from in situ measurements of the remote sensing reflectance (R_{rs}) at 279 stations and downwelling diffuse attenuation coefficients (K_d) at 133 stations. Measurements of the apparent optical properties, suspended particulate matter (SPM) contents, and characteristics and colored dissolved organic matter (CDOM) absorption spectra were performed during 16 cruises along the main Amazonian Rivers draining the Andes and for some tributaries. Surface-suspended sediment granulometry and mineralogy showed a stable distribution at the catchment scale, even over large distances and between tributaries. The particle number-size distribution was best described using a segmented distribution with a slope of 2.2 for the fine range (1–15 μm), and the CDOM absorption coefficient at 440 nm varied from 1.8 to 7.9 m^{-1}. Overall, both R_{rs} and K_d were strongly correlated with SPM, although strong CDOM absorption limited the use of the blue spectrum. Reflectance saturation from blue to red was observed at approximately 100 g m^{-3}, whereas the near-infrared (NIR) wavelength enabled the monitoring of the full SPM range (5–620 g m^{-3}). In contrast, K_d showed no saturation for SPM from green to NIR, and a linear model was calculated. The use of the reflectance ratio was investigated and shown to improve the suspended sediment concentration retrieval performance.

1. Introduction

Monitoring of inland water quality using remote sensing data represents a major challenge for water-color research due to the complexity of their optical properties relative to oceanic and coastal waters (i.e., Case 1 and 2 waters). In inland waters, absorption and scattering by colored dissolved organic matter (CDOM) and mineral particles can mask the phytoplankton optical properties and show a very weak covariance, thereby invalidating most common retrieval models based on ocean color data that are used over marine water. The optical properties of mineral particles suspended in water depend on the material concentration, size distribution, and refraction index, which, in theory, could demonstrate a site- and/or time-dependent relationship between apparent optical properties (AOPs) and inherent optical properties (IOPs) with the inorganic particulate material.

Suspended sediment fluxes in rivers are the result of erosion, transport, and deposition processes that occur within catchments. The quantification of these fluxes is necessary to monitor and understand the impacts of human activities (e.g., land use and hydraulic infrastructure) and climate change (e.g., extreme events and changes in rainfall patterns) at the catchment scale. However, an accurate calculation of sediment budgets is often difficult due to the poor availability and reliability of sediment flux data in most developed and developing countries [*Walling and Fang*, 2003]. Water quality-monitoring networks are usually based on water sampling in different locations in a watershed (i.e., hydrological stations) to monitor the production, accumulation, and transfer of certain elements of interest within the river network. The efficiency of such monitoring is therefore a direct function of the number of sampling locations and sampling frequency. In this manner, the capacity of remote sensing imagery to frequently monitor different locations over a short

time span may be efficiently used to complete existing field hydrological station networks. Unfortunately, there is a lack of systematic measurements of the main AOPs in continental waters that may support the operational use of remote sensing imagery for water quality monitoring.

A large number of studies have been conducted to measure the relationship between AOPs, IOPs, and parameters of interest (often the pigment concentration), and various syntheses have been published for oceanic waters [*Bricaud et al.*, 1998; *Morel et al.*, 2007; *Stramski et al.*, 2001] and coastal regions [*Babin et al.*, 2003b; *Doxaran et al.*, 2009; *Neukermans et al.*, 2012; *Snyder et al.*, 2008]. These syntheses have paved the way for detailed optical modeling and robust remote sensing monitoring at both the regional and global scales. A significant number of studies have also been published on inland water optical properties [*Costa et al.*, 2013; *Giardino et al.*, 2007; *Gitelson et al.*, 2008; *Hoogenboom et al.*, 1998; *Kirk*, 1976; *Ma et al.*, 2006; *Whitlock et al.*, 1981]. However, unlike the progress that has been achieved for marine waters, there is a lack of systematic studies of rivers and lakes documenting the variability of the AOPs/IOPs in these areas to establish the foundation for the remote sensing-based operational monitoring of inland waters. In particular, it is necessary to consider the whole watershed, instead of a specific river/lake, and to determine the variation of AOPs/IOPs as a function of the hydrological cycle.

In recent years, several studies have shown that medium-resolution remote sensing imagery (few hundred meters per pixel) such as Moderate Resolution Imaging Spectroradiometer (MODIS) or Medium-Resolution Imaging Spectrometer (MERIS) may be efficiently used for the monitoring of the suspended sediment in large rivers [*Heege et al.*, 2014; *Martinez et al.*, 2009; *Park and Latrubesse*, 2014; *Wang and Lu*, 2010] and lakes [*Kaba et al.*, 2014; *Majozi et al.*, 2014; *Odermatt et al.*, 2010; *Wu et al.*, 2013]. *Martinez et al.* [2009] showed that robust empirical relationships between the suspended particulate matter (SPM) and surface reflectance using corresponding MODIS 250 m images and field samples collected over 7 years can be derived with significant accuracy (30%) and an absence of seasonal bias at an hydrological station along the Amazon River in Brazil. Using 10 years of MODIS data for the Amazon River in Peru, *Espinoza Villar et al.* [2012] compared upstream and downstream remote sensing-derived river sediment discharge estimates and demonstrated that satellite assessments are robust (root-mean-square error of 18%). *Mangiarotti et al.* [2013] analyzed methods of combining conventional network data and MODIS-derived SPM estimates to improve sediment budget assessments in the Amazonian Plain. However, all of these studies were based on empirical relationships between remote sensing reflectance (R_{rs}) and SPM, which may prevent a generalized use of reported remote sensing methods. In the context of a dramatic decrease of sediment monitoring stations across the world [*Covault et al.*, 2013], the use of remote sensing may be an efficient alternative to follow the fate of sediment discharge in river catchments. Therefore, it is necessary to investigate the robustness of the link between the optical properties of water and suspended sediment to ensure the robustness of the remote sensing-based retrieval.

The objective of this study is to understand how the optical properties of surface water vary across a large river basin and to determine the significance of this variability based on a large data set of water sampling and optical measurements. In particular, we assessed the variability of the remote sensing reflectance and of the vertical attenuation coefficient for different periods of the hydrological cycle, over floodplain lakes and river mainstreams as well as between different subcatchments, focusing on the mineral fraction of the SPM. This study also contributes to the field of bio-optic modeling by extensively documenting the optical properties of the world's largest watershed.

2. Materials and Methods

2.1. The Amazon Basin

The Amazon catchment covers 5.9×10^6 km^2 [*Callède et al.*, 2010] encompassing various soils and lithologies. The Amazon Basin is composed of three major morphostructural units: (i) the Brazilian and Guyana cratonic shields, (ii) the Andes and Subandean zones to the west, and (iii) the lowlands where the main rivers progressively join to form the Amazon River. The cratonic shields cover approximately 44% of the Amazonian Basin area and are composed of strongly weathered and metamorphosed igneous rocks. The Andes accounts for 11% of the Amazonian Basin area and consists of Paleozoic to Meso-Cenozoic metamorphic, igneous, and sedimentary rocks. The Amazonian lowlands cover approximately 45% of the Amazonian Basin and are composed of a very thick layer of Cenozoic sediments.

Interestingly, the first and most common classification used to describe the main Amazonian water types is based on their coarse optical properties, catalogued as white, clear, and black [*Sioli*, 1950]. White waters refer to waters loaded with sediment showing strong dissolved organic material, mainly originating from the Andes. Clear waters originate from the cratonic shields and show very low SPM loads but also low levels of organic matter. Black waters are of low biological productivity with near-zero SPM concentrations, have almost no nutrients, and are strongly acidic due to the organic material present in the colloidal fraction, which also gives them their dark color. The main black-water rivers drain the northern tributaries and cratonic shields, such as the Negro River and the Trombetas River, although black waters can also be found in a large number of smaller subcatchments in the Amazon lowlands that finally converge in the Amazon River main stem from the piedmont to the Atlantic Ocean. The white waters flow through the Madeira River and Solimões catchments that drain the southern Andes and the central and northern Andes, respectively. Herein, we mainly focus on these sediment-dominated waters along the Madeira River, the Solimões River, and the reach of the Amazon River that is formed by the Madeira, Solimões, and Negro Rivers.

The Amazon Basin crosses two hemispheres and experiences contrasting rainfall regimes. Consequently, the hydrological regime shows a distinct high-water period from March to April in the Madeira catchment in the south and from June to July in the Negro catchment in the north. The Amazon/Solimoes River shows an intermediate hydrological cycle as it receives waters from both the north and the south of the catchment [*Richey et al.*, 1989]. Overall, the hydrological regime becomes more consistent from upstream to downstream. From the Andes piedmont to the lowlands, the flood regime is monomodal with a steadily increasing water level during the rainy season. Consequently, during the majority of the hydrological cycle, the suspended sediment and geochemical characteristics of the surface water change slowly. The HYBAM network data (www.ore-hybam.org) allow for assessments of the suspended sediment cycle throughout the catchment. Variations in SPM concentration are correlated with the river discharge in the Andes [*Armijos et al.*, 2013], whereas the SPM becomes progressively disconnected with the river discharge through the confluence with other rivers draining the forested catchments that provide almost no SPM to the system [*Filizola and Guyot*, 2009]. Consequently, there is an overall decrease of the SPM concentration from upstream to downstream due to sedimentation and dilution processes [*Meade et al.*, 1979]. Several studies have noted that the dissolved organic carbon (DOC) concentrations show a low seasonal difference in the main stem of the river [*Ertel et al.*, 1986; *Hedges et al.*, 1986; *Moreira-Turcq et al.*, 2003] of between 3 and 5 g m^{-3}, whereas in black waters, the DOC concentrations are typically greater than 10 g m^{-3}. The proportion of humic acids versus fulvic acids, known to affect the extent of light absorption, has been shown to remain relatively constant seasonally, with a ratio of fulvic to humic acids in the Amazon River at Óbidos of 3.2 ± 0.3 [*Ertel et al.*, 1986]. The Amazon Basin is marked by a large floodplain that significantly contributes to the water fluxes and mass transfer. The open floodplain lakes are affected by different processes, such as the mixing of different water masses derived from the local catchments and the rivers, resuspension processes during the low-water period, and intense blooms of phytoplankton during the dry season. Such phytoplankton blooms extend over large areas during the period of decreasing water levels from July to September. The phytoplankton composition is dominated by Cyanophyceae with a significant proportion of Bacillariophyceae and Chlorophyceae [*Nogueira et al.*, 2010].

2.2. Calculation of Apparent Optical Properties: R_{rs} and K_d

Figure 1 shows the locations of the 42 stations where radiometric measurements were made from 2007 to 2011. Below- (133 measurements) and above-water (279 measurements) radiometric measurements were performed using TriOs RAMSES radiometers operating in the 350–900 nm spectral range. One radiometer was mounted with a cosine collector for irradiance measurements, and two other radiometers were equipped for radiance measurements with a field of view of 7° in air. All of the radiometers were synchronized to simultaneously measure the various optical properties.

For the majority of the locations, radiometric measurements were collected both from the boat deck to calculate the remote sensing reflectance R_{rs} (λ) and in the water to retrieve downward irradiance $E_d(z,\lambda)$ profiles. Above-water measurements of the upwelling radiance L_u (λ) were preferred to below-water measurements $L_w(\lambda)$ due to the strong light absorption in the blue and near-infrared (NIR)

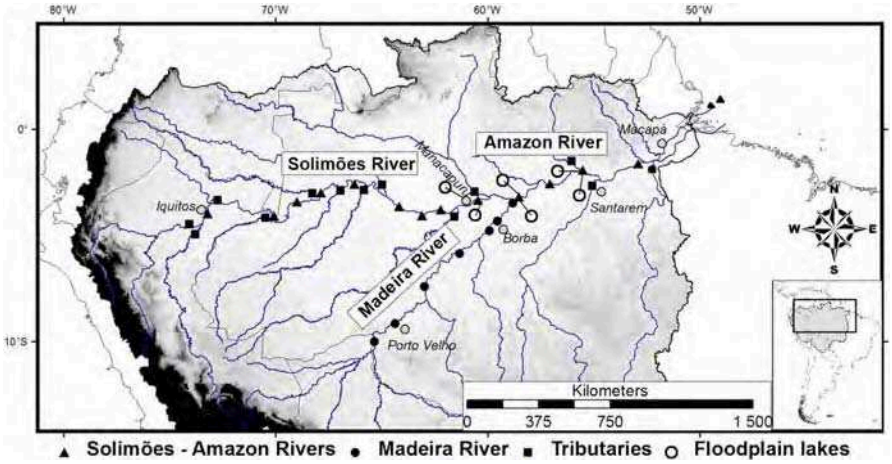

Figure 1. Location of the 42 stations for above-water (279 measurements) and below-water (133 measurements) sampling in the Amazon River Basin from 2007 to 2011 along the two main rivers draining the Andes: the Solimões and Madeira Rivers. Stations are partitioned into four subgroups: (1) the Amazon River and its main tributary, the Solimões River; (2) the Madeira River; (3) other tributaries; and (4) floodplain lakes.

domains by water, which may result in unreliable reflectance assessments at those wavelengths. The remote sensing reflectance was calculated as R_{rs} (λ):

$$R_{rs}(\lambda) = \frac{L_u(\lambda) - \rho.L_s(\lambda)}{E_d(\lambda)} \quad (1)$$

where $E_d(\lambda)$ is the downwelling irradiance above the water surface, $L_u(\lambda)$ is the upwelling radiance above the surface water, and $L_s(\lambda)$ is the sky radiance that is used to correct for the skylight reflection effect at the air-water interface. The above-water upwelling radiance L_u is the sum of the upwelling radiance $L_w(0^+)$ and the sky radiance directly reflected by the air-water interface L_r. Because only L_u is directly measureable, and $L_w(0^+)$ and L_r are not measured, L_r is assessed as $L_r = \rho.L_s$, where ρ is a proportionality factor. The factor ρ is not an inherent optical property of the surface and is dependent on the sky conditions, wind speed, solar zenith angle, and viewing geometry. *Mobley* [1999] used a radiative transfer code to estimate the variability of ρ as a function of the different forcing factors. These results showed that when L_u is acquired with a viewing direction of 40° from the nadir and 135° from the Sun, the variability of ρ is considerably reduced under clear-sky conditions, and a value of 0.028 is acceptable at wind speeds less than 5 m s^{-1}. Finally, $L_w(0^+)$ was assessed by the subtraction of L_u and $\rho.L_s$. To limit the effects of external factors, all radiometric measurements were acquired within the viewing geometry defined by Mobley and under low-wind conditions (0–4 m s^{-1}) and clear-sky conditions and for Sun zenith angle values ranging from 0 to 30°.

The in-water downward irradiance $E_d(z,\lambda)$ and upward radiance $L_u(z,\lambda)$ profiles were measured at discrete depths in rapid succession within the euphotic layer, which was usually less than 3 m in depth. The diffuse attenuation coefficients for downward irradiance $K_d(\lambda)$ were calculated by comparing the depth with the slope of the natural log plot for the downwelling irradiance. To retrieve robust estimates of K_d at each station, at least two vertical profiles were collected sequentially, and the more stable profile was selected.

2.3. Water Sampling

In situ water quality data were collected during 16 cruises along the main Amazonian Rivers in Peru and Brazil from 2007 to 2011 in different seasons (see Table 1). This sampling scheme made it possible to register the radiometric variability of the waters in the Amazonian catchment, the river main stems and floodplains and the estuary, representing locations separated by more than 3000 km. Although the sampling program was focused on the two rivers draining the Andes (Amazon and Madeira Rivers), samples were acquired from the tributaries and floodplain connected to these two streams to document the radiometric variability among the black and white waters. When possible, the above and in-water measurements were realized sequentially within approximately 15 min, with the surface water samples collected during each measurement for water quality assessments.

Table 1. Location and Dates of the 16 Sampling Campaigns Conducted for This Study

Campaign	Time Period		Water Stage	Sampling Location	Number of Stations Visited	
					Above Water	In Water
1	30/01/07	20/02/07	Rising	Santarem to Macapá	2	1
2	21/05/07	25/05/07	High	Manacapuru	19	0
3	10/11/07	15/11/07	Low/Rising	Manacapuru to Borba	34	2
4	15/03/08	20/03/08	Rising/High	Manacapuru to Borba	58	2
5	10/04/08	10/04/08	Rising	Amazon estuary	2	0
6	15/05/08	23/05/08	High	Manacapuru to Santarem	9	8
7	05/10/08	13/10/08	Low	Manacapuru to Santarem	14	5
8	20/06/09	06/07/09	High	Manacapuru to Santarem	18	13
9	19/11/09	28/11/09	Rising	Porto Velho to Manacapuru	7	11
10	26/03/10	30/04/10	High	Manacapuru to Porto Velho	5	7
11	08/06/10	02/07/10	Recession/High	Iquitos to Santarem	18	18
12	25/08/10	12/09/10	Recession	Manacapuru to Santarem	31	14
13	26/01/11	02/02/11	Rising	Manacapuru to Santarem	4	5
14	15/02/11	25/02/11	Rising	Manacapuru to Santarem	11	8
15	07/07/11	30/07/11	Recession	Porto Velho to Santarem	25	20
16	23/11/11	18/12/11	Low/Rising	Iquitos to Santarem	22	19
Total					279	133

At each of the visited stations, a single water sample used to determine SPM concentrations was collected at the surface from a small boat or research vessel during each R_{rs} and K_d measurement. It is important to note that for most of the locations, the water depth exceeded 20 m and reached up to 60 m at some stations. Water samples were processed on board the ship immediately after collection. When using small ships, water samples were stored in 2 L polyethylene containers and processed on land no later than 12 h after sampling. The samples were filtered using 0.45 μm cellulose acetate filters (Millipore) that were previously dried for 24 h at 60°C and weighted. After filtration, the filters were dried for 24 h at 60°C and weighed again to determine the concentration of suspended matter. Phytoplankton pigment concentrations were measured during 4 cruises by filtering 250 mL of water through GF/F filters, which were then frozen at −20°C on board the research vessel. At the laboratory, the pigments were extracted in acetone and analyzed for Chl *a* and phaeopigment concentrations using a calibrated fluorometer. Herein, Chl is defined as the sum of Chl *a* and phaeopigments.

Particle-size distribution analyses were performed on 39 5 L water samples collected during 6 cruises. Granulometric data were obtained using a laser grain-size measurement device (Mastersizer 2000 with a sample dispersion unit) at the Companhia de Pesquisa de Recursos Minerais (CPRM) Laboratory for Sediment and Water Quality. The results were modeled according to the classical Junge hyperbolic law to assess the variability of the slope coefficient and the range of sizes over which the fit could be performed.

Samples were collected during 3 cruises to assess the variability of the CDOM absorption coefficient for different types of waters and along an upstream to downstream profile of the Solimões and Amazon Rivers. Water was filtered under low vacuum on a 0.45 μm Millipore membrane using an all-glass filtering device. The filtered samples were stored and frozen in dark 10 cL bottles. At the Universidade Federal Fluminense (UFF) laboratory, a 5 cm quartz cuvette was used to measure the absorbance of the filtered water between 350 and 750 nm at 1 nm increments using a dual-beam spectrophotometer (Shimadzu UV/VIS UV-1800). Milli-Q water was used as a reference. After conversion to absorption coefficients, an exponential function was fitted between 350 and 500 nm by nonlinear regression to the data to assess the exponential slope S_{CDOM}. A baseline correction was not applied to obtain a null CDOM absorption at 685 nm as is usually performed for marine waters [*Babin et al.*, 2003b].

We analyzed 33 samples collected during 8 cruises to determine the temporal and spatial variations of the surface-suspended sediment mineral assemblage along the Madeira and Amazon Rivers. Samples were collected at the river surface in 25 L canisters and evaporated to a final volume of 500 mL. At the laboratory, water samples were prepared by evaporating the aqueous suspensions to dryness on a glass slide. The suspensions were prepared by the ultrasonic dispersion of 10 mg of sample in 2 mL of deionized water. The identification of minerals was based on their reactions to commonly used treatments: air drying, ethyl-glycol solvation, and heating to 550°C. Based on the glycolated sample diffractograms, semiquantitative estimates of the different clay minerals were performed manually by measuring the characteristic reflection areas.

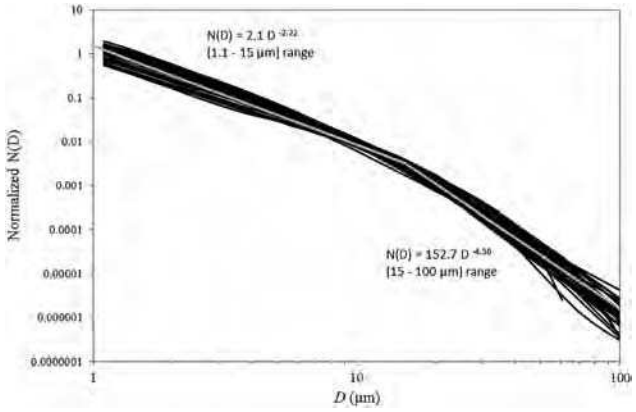

Figure 2. Particle-size distribution measurements for 39 surface water samples collected along the Madeira, Solimões, and Amazon Rivers. Segmented power law functions were fitted for the small (<15 µm) and large particle (>15 µm) ranges.

3. Results

3.1. Variability of the SPM Characteristics: Concentration, Granulometry, and Mineralogy

The SPM values of the water samples spanned more than 2 orders of magnitude (2–621.6 g m^{-3}), with a mean value of 140.8 g m^{-3}. There was a general decrease of the SPM from upstream to downstream areas along the rivers draining the Andes (the Maranon, Ucayali, Napo, Solimões, and Madeira Rivers). For each location, the highest SPM values were observed during the rising water period, and a decrease occurred during the remainder of the hydrological cycle. Black-water rivers showed very low SPM levels (i.e., <10 g m^{-3}), whereas in floodplains waters, SPM concentrations showed low to intermediate SPM values (0–76 g m^{-3}). Studies have reported that white-water rivers show low particulate organic carbon (POC) contents (1–4 wt % relative to the SPM concentration) [*Moreira-Turcq et al.*, 2003]. These relationships have been confirmed for a wide range of riverine environments throughout the world, demonstrating that the POC/SPM ratio decreases with increasing SPM, reaching approximately 1% for SPM levels of greater than 100 g m^{-3} [*Coynel et al.*, 2005; *Meybeck*, 1993]. In the Amazon River, it has been shown that the POC concentrations directly vary with the discharge volume, and higher concentrations occur during high-water periods (corresponding to low SPM concentrations). In black and floodplain waters, the POC concentrations are much higher, with weight percentages of up to 60%.

The nonalgal particle (NAP) scattering properties (i.e., the absolute values and spectral dependence) vary with the particle-size distribution and may influence the AOP/IOP relationship with the SPM [*Babin et al.*, 2003a]. Suspended sediment granulometry was obtained to assess the variability of the particle-size across the different white-water rivers, at different locations along the main stems and during different seasons. To characterize the particle-size distribution, hydrologists often use the *D*50 parameter, called the median grain size, which is the grain diameter at which half of the sample is smaller and half is larger. Studies of hydrologic optics use the number-size distribution $N(D)$, which represents the number of particles for a given size interval around the mean diameter D. It is often assumed that $N(D)$ follows the Junge distribution as a function of increasing particle size with

$$N(D) = K.D^{-j} \tag{2}$$

where K determines the scale and j is the slope of the distribution. Typical values of the factor "j" reported for marine waters (including organic and mineral fractions) vary between 2 and 5 [*Mobley and Mobley*, 1994]; although most studies assume a unique value for j of 4, experimental data are very limited. The value of this coefficient has been shown to be determinant because when $j < -4$, the relative contribution of the small particles to the total particle volume concentration decreases, and therefore, the contribution of small particles to the total light scattering decreases [*Babin et al.*, 2003a]. The composition of the Amazon white waters is, however, very different that than of the open ocean and coastal waters; thus, we tested the variability of the slope factor among the different rivers studied herein. *Mobley and Mobley* [1994] and *Morel and Ahn* [1991] suggest that the particle-size distribution in water is best described by a segmented distribution with a smaller value of j for smallest particles and a larger value of j for the largest particles. Our data demonstrate the same pattern with a slope of 2.22 ± 0.19 in the 1.1–15 µm range and 4.56 ± 0.61 at greater than 15 µm (see Figure 2). The limited variation in the size distribution for all of the studied samples is supported by the low *D*50 parameter variability of 12.0 ± 2.84 µm. Interestingly, no seasonal or spatial dependencies have been detected among the collected water samples.

We analyzed 33 samples collected during the field campaigns to determine the temporal and spatial variations of the surface-suspended sediment mineral assemblages. Our results confirmed those of previous reports [*Guyot et al.*, 2007] and showed a balanced composition of quartz (10–20%), kaolinite (20%), illite (20–40%), and smectite (20–40%). We detected a limited but significant increase in the smectite composition from low water to high water, which is consistent with a stronger contribution of lowland tributaries and floodplains to the main stemflow during the high flood phase [*Konhauser et al.*, 1994; *Moreira et al.*, 2013]. Comparisons between the Madeira and Solimoes systems showed higher smectite content in the Solimoes system and a higher illite content in the Madeira River, whereas the quartz and kaolinite remained stable. These observations highlight a limited but significant variability in the type of suspended sediment that may be related to the seasonal and/or spatial dependency of the reflectance over time.

3.2. Light Absorption by Dissolved Organic Matter

The water absorption is conventionally modeled as the sum of the absorption by pure water, SPM, phytoplankton, and CDOM. Unlike Case 1 and coastal waters, continental waters are marked by strong CDOM concentration originating from the degradation of terrestrial organic matter. Figure S1 in the supporting information shows the a_{CDOM} variation for 19 samples collected from black, clear, and white waters as well as floodplain lakes. The a_{CDOM} was higher in the black river waters ($a_{CDOM}(440) = 7.9\,m^{-1}$, $N = 1$) and floodplain lakes ($a_{CDOM}(440) = 4.8 \pm 0.8\,m^{-1}$, $N = 2$) and lower in white ($a_{CDOM}(440) = 3.3 \pm 1.0\,m^{-1}$, $N = 14$) and clear waters ($a_{CDOM}(440) = 1.8 \pm 0.8\,m^{-1}$, $N = 2$). Interestingly, at longer wavelengths, the CDOM absorption in white river waters remained significant (a_{CDOM} $(670) = 0.72 \pm 0.5\,m^{-1}$). The spectral slope S_{CDOM} showed small variations ($0.013\,nm^{-1} \pm 0.0016$) from one location to another. The CDOM absorption classes followed the usual water-type classification used to describe the main water types in the Amazon (clear/white/black), for which both DOC and POC have been shown to exhibit increasing carbon concentrations. The a_{CDOM} values reported here were much stronger than in any other measurements for the open ocean and can only be compared with coastal waters marked by large freshwater inputs from land. *Bowers et al.* [2000] monitored a CDOM absorption gradient from the Clyde Sea to an estuary and measured an a_{CDOM} value of 1.6 at zero salinity. The fact that S_{CDOM} does not show a strong variation is in accordance with other studies in which this parameter was assessed in other coastal waters. *Babin et al.* [2003b] reported a mean S_{CDOM} value of 0.018 ± 0.002 over 345 samples collected from six different coastal regions, and *Bowers et al.* [2000] reported a mean value of 0.018 ± 0.005 for 25 samples. In a previous work, Bricaud et al. [*Bricaud et al.*, 1981] found an S_{CDOM} value of 0.014 ± 0.003, and *Kirk* [1976], who studied lake waters, observed S_{CDOM} values between 0.013 and 0.016. In an analysis of CDOM in a tidal marsh area, *Tzortziou et al.* [2008] showed that S_{CDOM} was systematically lower at low tide (0.0149), as dissolved terrestrial material was drained out of the marshes, than during high tide ($S_{CDOM} = 0.0168$). Our study did not allow to document systematic variations of a_{CDOM} across the watershed, although our observations could be used to quantify the strong CDOM attenuation in the Amazonian waters and show the relative stability of those values for white-water rivers.

3.3. Classification of the R_{rs} Spectra

A cluster analysis was performed to classify the entire set of R_{rs} spectra into homogeneous groups. The objective of this classification was to highlight spatial or temporal dependencies in the remote sensing reflectance data set that may support the use of multiple retrieval algorithms for different rivers or a global retrieval algorithm. For this analysis, we used the *k*-means unsupervised classification technique, which categorizes the data set into classes based on the natural distribution of the data in multivariate space. In contrast to supervised classification techniques, this approach does not require predefined classes. To define the optimal number of classes, we used a hierarchical cluster method by applying Ward's algorithm to squared Euclidian distances between the spectra [*Lubac and Loisel*, 2007]. To enhance the spectral shape of the R_{rs} spectra in the classification, each R_{rs} spectrum was previously normalized by its integral calculated over the entire spectrum. The initial data set of 279 spectra was reduced to 171 spectra to avoid the overrepresentation of the Solimões River and Madeira River samples. The analysis of the hierarchical clustering showed that the partition into eight classes minimized the within-cluster variances. Figure S2 shows the mean spectrum of each class, and Figure S3 shows the mean and standard deviation for each class. Each group is described below.

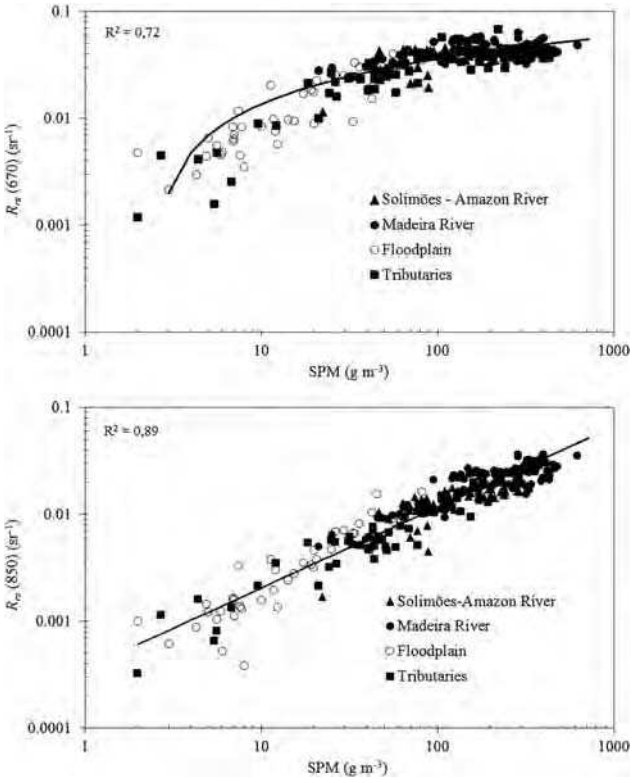

Figure 3. Variation of (top) $R_{rs}(670)$ and (bottom) $R_{rs}(850)$ as a function of the SPM concentration. The collected samples are identified based on their sampling location: the Solimões and Amazon Rivers (triangles), the Madeira River (black circles), the floodplain lakes (white circles), and all of the tributaries (squares).

Class 1 consisted of the Rio Negro black waters ($N = 3$). This class presented the lowest reflectance values of $<0.003\ sr^{-1}$ (nonnormalized reflectance values), with a slightly increasing reflectance from blue to red wavelengths. This pattern was directly related to the high CDOM concentrations associated with low Chl and SPM values. Class 2 included black- and clear-water stations primarily from the floodplain ($N = 4$). The class spectrum slowly increased from 400 to 570 nm and then declined gradually toward the higher wavelengths. Chl *a* absorption at approximately 665 nm was clearly apparent, although the other characteristic Chl *a* absorption peak at 440 nm was not detected. This class presented the lowest SPM loads and high Chl concentrations (mean = 34.4 mg m^{-3}). Class 3 mainly consisted of the productive floodplain waters ($N = 21$) and samples from river confluences. For this class, the reflectance increased sharply from 400 to 575 nm and presented a wide maximum up to 700 nm. The local minimum observed at approximately 675 nm most likely corresponded to the presence of Chl *a*. A second reflectance maximum was detected at 800 nm, and this class presented intermediate SPM values (mean = 21.9 g m^{-3}) and high Chl concentrations (mean = 21.5 mg m^{-3}). Class 4 was mostly composed of floodplain waters and river confluence stations ($N = 28$) and showed similar spectral patterns and reflectance values to those of Class 3, although the first reflectance maximum was shifted toward larger wavelengths at 585 nm, and the reflectance did not exhibit marked absorption troughs up to 700 nm. Class 4 was associated with intermediate SPM values (mean = 23.4 g m^{-3}) and lower Chl *a* concentrations (mean = 9.5 mg m^{-3}) compared with Class 3.

Class 5 consisted of floodplain waters ($N = 6$) and presented two distinct maxima of comparable amplitude: one near 550 nm and one near 705 nm. The first peak matched the Chl *a* absorption minimum in the green spectrum, whereas the second peak corresponded to the Chl *a* absorption minimum in the red spectrum. Two local minima detected at 625 and 675 nm corresponded to the absorption maxima of phaeopigments and chlorophyll *a* pigments, respectively. An absence of pigment-induced absorption patterns was observed in the blue part of the spectrum, which was likely because of the strong absorption by CDOM. Not surprisingly, Class 5 showed the highest Chl concentrations (66.9 mg m^{-3}) among all classes and an intermediate SPM value (mean = 39 g m^{-3}).

Classes 6–8 included river sediment-dominated waters with strong SPM concentrations. All of these classes showed similar spectral patterns, with sharply increasing R_{rs} values from 400 to 580 nm and a much less pronounced increase up to 700 nm. Class 6 ($N = 57$) presented intermediate SPM values (72 mg m^{-3}) and a low Chl value of 1.8 mg m^{-3}. Class 7 ($N = 33$) showed strong SPM values (187 mg m^{-3}), and Class 8 ($N = 19$) showed the highest SPM values (368 mg m^{-3}), which was associated with low Chl *a* concentrations (<1 mg m^{-3}). It is important to note that Classes 7 and 8 can only be discriminated based on the shapes of their NIR spectra, although they showed different SPM values. Interestingly, although the spectra were

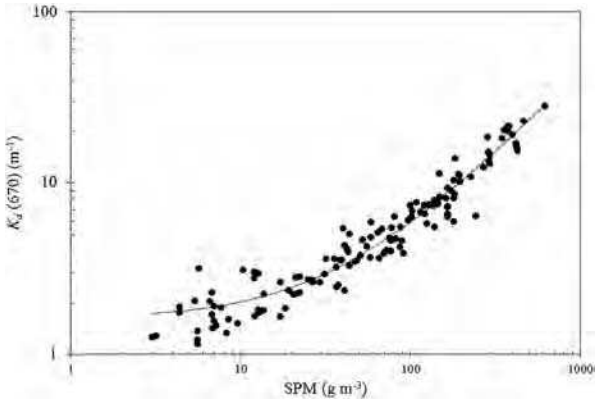

Figure 4. Variation of $K_d(670)$ as a function of the SPM concentration.

normalized to enhance the spectral shape in the classification, the R_{rs} classes represented homogeneous classes as a function of SPM or Chl, and spatial or temporal dependencies were not detected. These conclusions support the use of a global SPM retrieval algorithm for the entire catchment, which we will be detailed in the next two sections.

3.4. The Relationship of R_{rs} and K_d to SPM: Average Relationship

Figure 3 shows the variation of the remote sensing reflectance at 670 nm and 850 nm as a function of the SPM for 279 samples collected during the 16 cruises in of all the studied rivers and floodplain lakes. Although the reflectance in the red and NIR channels showed a clear increasing trend as a function of the SPM, we noted a strong difference between the channels. Although the red channel showed saturation at approximately 100 g m^{-3}, we could not identify a saturation point for the NIR channel up to 600 g m^{-3}, demonstrating a remarkable sensitivity to the SPM concentration over 2 orders of magnitude. The dispersion around the main trend appeared to be stronger for lower SPM values, specifically for the floodplain stations. Linear regressions between the natural logarithm of the wavelength and of R_{rs} for the Madeira River and Solimões River showed similar intercepts ($P = 0.763$) and slopes ($P = 0.461$). In contrast, the slopes and intercepts for Madeira River and Solimões River were different when compared with the tributary and floodplain samples ($P < 0.001$). However, the lower SPM range for the floodplains (mean SPM = 22.9 g m^{-3}) compared with that for the Madeira (mean SPM = 239.3 g m^{-3}) and Solimões (mean SPM = 128.9 g m^{-3}) Rivers limits the relevance of this statistical result. The clear correlation between SPM and reflectance for all of the water types and seasons demonstrated that SPM is clearly driving the water optical properties in the majority of the waters of the Amazon Basin. However, whereas the SPM was mainly composed of mineral particles at high concentrations and along the white-water rivers, the composition of the suspended matter may be much more diverse at low SPM values with a much larger organic fraction (living and nonliving), in particular in black river and floodplain waters. Relative importance and variability of the organic fraction relative to the inorganic fraction clearly affected the reflectance level at low SPM concentrations (i.e., <20 g m^{-3}).

Figure 4 shows the variation of $K_d(650)$ as a function of the SPM for 133 samples collected during the 16 cruises in all of the studied rivers and floodplain lakes. Unlike the R_{rs} at the red wavelength, saturation was not observed up to 620 g m^{-3}. The dispersion was relatively constant across the entire SPM range, and a simple linear function could be fit to model the K_d-SPM relationship. At low SPM levels, $K_d(650)$ appeared to be greater than 1, which is indicative of residual CDOM absorption at those wavelengths (see section 3.2). This result showed that K_d is a good predictor of SPM for all types of waters in the Amazon Basin.

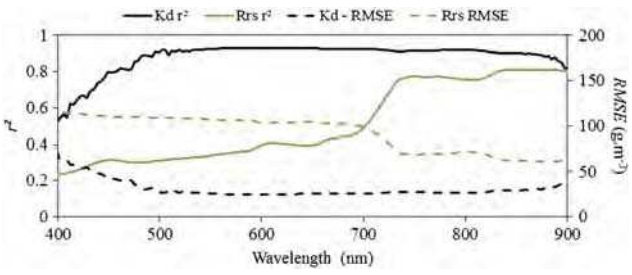

Figure 5. Variation of the square of the Pearson correlation coefficient (left axis) and the RMSE of the SPM concentration (right axis) as a function of the wavelength for K_d and R_{rs}.

We also investigated the spectral dependence of the relationship of R_{rs} and K_d with SPM, excluding all floodplain and nonwhite waters. The revised data set represented 229 stations for R_{rs} and 109 stations for K_d. To assess the accuracy of the AOPs in predicting SPM concentrations, two subsets were formed for each AOP. For R_{rs}, the calibration data set included 115 samples (mean SPM = 168.2 g m^{-3}) and the validation data set included 114 samples (mean SPM = 166.2 g m^{-3}).

For K_d, the calibration data set included 56 samples (mean SPM = 128.1 g m^{-3}) and the validation data set included 53 samples (mean SPM = 138.9 g m^{-3}).

Figure 5 presents the model-fitting and SPM retrieval performances for R_{rs} and K_d as a function of the wavelength. For R_{rs}, there was a clear increasing relationship with SPM from the blue to NIR wavelengths, with a square Pearson correlation factor of greater than 0.75 beyond 730 nm and an optimal range of 840–900 nm (r^2 of approximately 0.81). A lower correlation in the visible spectrum (400 to 700 nm) was induced by the rapid saturation of the R_{rs} as a function of the SPM at low concentrations. The least squares regression showed that a power law model $a.R_{rs}(\lambda)^b$ provides the best fit values. The model factors and performance were calculated based on the linear regression between the natural logarithm of the wavelength and of R_{rs}. The root-mean-square error (RMSE) of the retrieval model decreased as a function of increasing wavelength starting at 114.1 g m^{-3} (400 nm) down to 61 g m^{-3} (820–900 nm). The optimal wavelength occurred at 860 nm, and the corresponding model is as follows:

$$\mathrm{SPM} = 20.41[R_{rs}(860)]^{1.173} \tag{3}$$

Figure S4 shows the model performance over the validation data set. For K_d, there was a strong and robust correlation with SPM (see Figure 5) over a wide range of wavelengths in both the visible and NIR spectra from 495 to 860 nm ($r^2 > 0.90$). The lower Pearson correlation at short wavelengths and beyond 890 nm may have been induced by the strong absorption of light that makes it difficult to accurately assess the downwelling irradiance distant from the water surface. Accordingly, a linear best fit model between SPM and K_d performed better than for R_{rs} with an RMSE of better than 30 g m^{-3} from 500 to 870 nm.

$$\mathrm{SPM} = 20.5\,.K_d(650) - 22.94 \tag{4}$$

Figure S5 shows the model performance for the validation data set. These observations may be related to the link between the AOPs and IOPs (the absorption and scattering coefficients); i.e., whereas R_{rs} is related to the absorption to scattering ratio, K_d is assumed to vary as the sum of absorption and scattering. With increasing SPM, coefficients a and b will increase, meaning that K_d will increase indefinitely as a function of the suspended sediment concentration, whereas R_{rs} may reach a saturation point. Not surprisingly, K_d and R_{rs} were well correlated at 730 nm up to 900 nm ($r^2 > 0.80$). At 850 nm, we observed the following relationship ($r^2 > 0.85$):

$$K_d(850) = 559.17R_{rs}(850) + 3.98 \tag{5}$$

3.5. Improvement of SPM Retrieval Using the R_{rs} Ratio at Two Wavelengths

It has been shown that the ratio between R_{rs} at two wavelengths may lessen the dependence on the SPM type and thus is more robustly linked to the SPM concentration [*Doxaran et al.*, 2002; *Moore et al.*, 1999]. Irradiance reflectance is generally modeled as $R = f \cdot b_b/(a + b_b)$, where b_b is the backscattering coefficient and f is a factor determined by the incident light field and often assumed to be invariant as a function of the wavelength. *Doxaran et al.* [2002] analyzed the variation of the $b_b/(a + b_b)$ ratio for highly turbid waters in the Gironde estuary. These authors showed that when the contributions of pure water, algal pigments, and CDOM to light absorption can be neglected, the $b_b/(a + b_b)$ ratio becomes independent of the SPM concentrations, leading to the saturation phenomenon observed for R_{rs}. The total absorption by pure water is high at NIR, and thus, this simple model predicts that saturation will occur for higher SPM concentrations at infrared relatively to visible wavelengths. Interestingly, the same authors reported that the $b_b/(a + b_b)$ ratio at two wavelengths will be less sensitive to the refraction index and grain-size variation than to the SPM concentration at high SPM loads. Indeed, by assuming that the spectral variations of b_b are weak [*Moore et al.*, 1999; *Whitlock et al.*, 1981], it can be shown that the ratio is much more dependent on the absorption than on the backscattering, which, in turn, may limit the influence of the refraction indices and granulometry. This simple ratio model will perform better using wavelengths at which SPM absorption shows a strong variation and, together with the pure water absorption, dominates the total absorption. It can be deduced from our previous observations that the R_{rs} ratio should make use of the red and NIR wavelengths.

We investigated whether the use of the reflectance ratio $R_{rs}(\lambda_1)/R_{rs}(\lambda_2)$ improved the SPM-R_{rs} relationship in the river sediment-dominated waters. To determine the optimal position of λ_1, we selected an initial value of $\lambda_2 = 670$ nm within the range of the minimum total absorption in the red spectrum. We performed a

regression of the model [$R_{rs}(\lambda_1)/R_{rs}(670)$] versus SPM for the range of 730 to 900 nm; the RMSE of the SPM estimation showed minimal values over a wide range of λ_1 between 760 and 820 nm (see Figure S6a). In the second iteration, we determined λ_2 after fixing λ_1 at 805 nm and regressing the model [$R_{rs}(805)/R_{rs}(\lambda_2)$] versus SPM. Again, the RMSE was minimal over a wide range of λ_2 between 650 and 700 nm, with the best result obtained at $\lambda_2 = 680$ (see Figure S6b). Interestingly, the ratio model performed significantly better than with the use of a unique wavelength with an RMSE of approximately 38 g m^{-3} (Figures S7 and S8). In addition, the spectral bands showing a minimal RMSE at both the red and NIR regions of the spectrum included the spectral bands of commonly used water-color sensors, such as MERIS and MODIS, and future platforms, such as Sentinel-3, NPP/VIIRS, and JPSS.

We further investigated whether the efficiency of the R_{rs} ratio was global or varied from one river to another. For the Solimões River, the use of the ratio compared with that of a single-wavelength model at NIR increased slightly the model accuracy ($r^2 = 0.83$ versus 0.73, $N = 76$). For the Madeira River, the use of the ratio showed a strong improvement of the retrieval accuracy ($r^2 = 0.93$ versus 0.62, $N = 102$) (see Figure S9). However, when the regression lines assessed for both rivers were compared, the data supported the hypothesis that the slope ($P = 0.108$) and intercept ($P = 0.225$) are equal. From our data set, we concluded that the use of the R_{rs} ratio may not show an increased SPM retrieval efficiency globally, although it may be used as a general tool to homogenize a data set across a watershed.

4. Discusion and Conclusions

The Amazon Basin presents Case 2 waters with an absorption budget dominated by CDOM and SPM in rivers but with a significant contribution from Chl *a* in floodplains. A simple unsupervised classification of R_{rs} spectra made it possible to discriminate several classes: (1) one class presenting very low R_{rs} values corresponding to the so-called black waters with strong CDOM absorption and very low SPM concentrations; (2) four groups of floodplain lakes and river confluences, where a reduced water velocity allows the development of phytoplankton at high concentrations; and (3) three classes of sediment-dominated waters with relatively high SPM concentrations. R_{rs} shows saturation, with SPM at approximately 100 g m^{-3} in the green and red spectra. However, the use of R_{rs} in the infrared spectrum makes it possible to monitor the SPM range without saturation. Interestingly, the three main Amazonian Rivers having sediment-dominated water (the Madeira, Solimões, and Amazon Rivers) showed a similar behavior as a function of SPM, even though the samples were collected at stations that in some cases were separated by more than 3000 km. K_d proved to be a very robust predictor ($r^2 > 0.9$) of SPM through a simple linear relationship for a very wide range of SPM values (up to 622 g m^{-3}) and wavelengths.

The use of reflectance ratios has been previously presented as a means to reduce the sensitivity of R_{rs} to the sediment type or size distribution in sediment-dominated waters [*Doxaran et al.*, 2002; *Moore et al.*, 1999]. In our data set, we observed that the use of a ratio model does not improve the results uniformly for all of the studied water bodies. For example, although the retrieval model accuracy was slightly improved for the Solimões River when using a reflectance ratio instead of one wavelength, for the Madeira River, the improvement is much stronger. In an analysis of 11 years of MODIS red and infrared surface reflectance data and of SPM data acquired at two hydrological stations along the Madeira River in Brazil, *Espinoza Villar et al.* [2013] showed that the NIR reflectance does not exhibit a simple relationship with SPM. The authors detected a hysteresis effect in which for the same SPM concentration, the reflectance during rising water is higher than at the flood peak. It is important to note that using the same method, *Espinoza Villar et al.* [2012] did not detect such a seasonal variation for the Solimões River or its main tributaries (Marañon and Ucayali) in Peru.

For such sediment-dominated waters, it is expected that the AOP/IOP variations may be strongly impacted by spatial and seasonal changes in sediment type and particle-size distribution. However, our results showed that at the Amazon catchment scale, R_{rs} exhibits a relationship with SPM that is sufficiently robust to be used for the accurate monitoring of surface-suspended sediment discharge in the largest river of the world. Regarding the particle-size distribution, our granulometric results showed a relatively consistent grain-size distribution among different rivers and hydrological periods. The segmented grain-size distribution showed a more even distribution (slope 2.22) for the 1 to 15 μm diameter range than is usually predicted in optical modeling (approximately 4), which implies that the contribution of very fine particles

(<1 μm) to NAP scattering is limited. These observations agree with the classical results of sediment transport dynamics in a turbulent flow system that predict a relatively constant distribution of the fine-grained size fraction in the water column in which the coarse-grained size fraction increases from the surface to the river bottom [*Rouse*, 1938], resulting in an almost pure fine sediment composition at the river surface. Furthermore, most large rivers, such as the main rivers of the Amazon Basin, have been shown to display reduced grain-size range in the bed load and suspended sediment mainly because they flow across vast plains for a major part of their course with very low topographic gradient causing strong sedimentation in the foothills and floodplains [*Latrubesse*, 2008].

Our study did not allow for a detailed assessment of the variability of the mineral particle types, but it did confirm the results of previous studies in the Amazonian Plain showing a relatively consistent pattern of mineral compositions. *Guyot et al.* [2007] analyzed 229 sediment samples from throughout the entire Amazon Basin to document the spatial variability of the mineral assemblages. These authors reported that the sediment clay phase from the rivers draining the Andes contains a dominant illite + chlorite assemblage that is enriched in smectite during transport through the lowlands. The main minerals found in the SPM showed a limited refraction index range relative to water of 1.16–1.18. Furthermore, previous modeling studies [*Babin et al.*, 2003a; *Doxaran et al.*, 2009; *Wozniak and Stramski*, 2004] showed that even grain-size distribution (i.e., slope below 4) limited the impact of the variability of the refraction index. Our results demonstrated that the sediment-size distribution and mineralogy may present limited variations at the scale of a large river basin, thus supporting the development of robust SPM retrieval methods from main AOPs.

Although the R_{rs} seasonal variation as a function of SPM for the Madeira River case can be efficiently corrected using a simple reflectance ratio model, the cause of the R_{rs} variability remains unclear because the deviation may originate from variations of the physical properties of the inorganic SPM or variation in the organic fraction. *Viers et al.* [2008] analyzed the variations in the geochemical and physical properties of SPM from the Solimões River and Madeira River during one hydrological cycle. These authors showed that both rivers exhibit distinct suspended sediment chemical compositions but that these characteristics do not vary significantly over time except for in the Madeira River, where the strontium (Sr) isotopic composition showed clear variations between the high-water period and the remainder of the year. *Santos et al.* [2014] published a more exhaustive monitoring of the dissolved Sr isotopes for the main Amazonian Rivers based on the HYBAM water database. These authors confirm that only the Madeira River catchment waters exhibited a seasonal dependence in the dissolved strontium isotopic composition that can be tracked from the Andean piedmont downstream to the Amazon River confluence. This seasonal variability is attributed to increasing rates of erosion of Precambrian rocks during the rainy season in the upstream catchments (Beni River). This seasonal control of the Sr isotopic composition highlights the limited but significant variability in suspended sediment types in the Madeira River. This variability may be used to explain the seasonal dependency of the reflectance in this subcatchment and the lower R_{rs} values observed during high-water periods in particular.

This work is one of the first studies to assess the variation of the AOP of river waters across a large river basin and for all hydrological periods. The SPM retrieval performance assessed based on the AOPs varied from 37% (R_{rs} at a single wavelength in the NIR) to 23% (R_{rs} ratio at two wavelengths) to 18% (K_d in the visible spectrum) relative RMSE. These performances are consistent with the operational monitoring of suspended sediment in rivers. Uncertainties regarding both the sampling and calculation methods are known to affect the accuracy of in situ SPM concentration assessments in rivers by approximately 10 to 20% [*Cheviron et al.*, 2011; *Horowitz*, 2003]. In recent years, we have published several studies that used MODIS satellite imagery to retrieve surface SPM values for the Amazon Basin using correlations between R_{rs} and SPM data obtained from field samples. *Martinez et al.* [2009] found a 36% relative difference when comparing 7 years of MODIS-derived surface SPM estimates and 10 day surface field samples acquired at one station in Brazil. At two stations in Peru (Solimões and Marañon Rivers), *Espinoza Villar et al.* [2012] reported a 27% and 45% relative RMSE when comparing 4 years of MODIS-derived surface SPM estimates and 10 day surface field samples. The retrieval accuracy assessed based on the satellite data is consistent with the R_{rs}-based model performance we analyzed and demonstrates that significant improvement may be achieved using an appropriate reflectance model. The optical properties presented in this study cannot be extrapolated for global use over all the continental waters. However, considering the size of the catchment, our results support the notion that remote sensing monitoring may be used efficiently for sediment discharge monitoring in large river basins.

Acknowledgments
This work has been supported by the Brazilian Water Agency (ANA), CNPq, Ministry of Science and Technologies, and Program for Graduate Students-Agreement (PEC-PG) program in Brazil; IRD, Joint International Laboratory "Environmental Changes Observatory in Amazon Region," INSU "Reliefs," INSU "Syster," ANR "CARBAMA," and CNES/TOSCA programs in France. Our thanks also go to all the HYBAM program partners in Brazil and Peru: the University of Brasilia, the Amazonas State Federal University (UFAM), the Fluminense State University (UFF), the Brazilian Mineral Resources Research Company (CPRM), and the Peruvian Hydrologic and Meteorology Service (SENAMHI). The authors are grateful to the ship crews who accompanied them during the surveys. The data for this paper are available by contacting the corresponding author.

References

Armijos, E., A. Crave, P. Vauchel, P. Fraizy, W. Santini, J.-S. Moquet, N. Arevalo, J. Carranza, and J.-L. Guyot (2013), Suspended sediment dynamics in the Amazon River of Peru, *J. South Am. Earth Sci.*, *44*, 75–84.

Babin, M., A. Morel, V. Fournier-Sicre, F. Fell, and D. Stramski (2003a), Light scattering properties of marine particles in coastal and open ocean waters as related to the particle mass concentration, *Limnol. Oceanogr.*, *48*(2), 843–859.

Babin, M., D. Stramski, G. M. Ferrari, H. Claustre, A. Bricaud, G. Obolensky, and N. Hoepffner (2003b), Variations in the light absorption coefficients of phytoplankton, nonalgal particles, and dissolved organic matter in coastal waters around Europe, *J. Geophys. Res.*, *108*(C7), 3211, doi:10.1029/2001JC000882.

Bowers, D. G., G. E. L. Harker, P. S. D. Smith, and P. Tett (2000), Optical properties of a region of freshwater influence (the Clyde Sea), *Estuarine Coastal Shelf Sci.*, *50*(5), 717–726.

Bricaud, A., A. Morel, and L. Prieur (1981), Absorption by dissolved organic matter of the sea (yellow substance) in the UV and visible domains, *Limnol. Oceanogr.*, *26*(1), 43–53.

Bricaud, A., A. Morel, M. Babin, K. Allali, and H. Claustre (1998), Variations of light absorption by suspended particles with chlorophyll *a* concentration in oceanic (case 1) waters: Analysis and implications for bio-optical models, *J. Geophys. Res.*, *103*(C13), 31,033–31,044, doi:10.1029/98JC02712.

Callède, J., G. Cochonneau, F. V. Alves, J.-L. Guyot, V. S. Guimaraes, and E. De Oliveira (2010), Les apports en eau de l'Amazone à l'Océan Atlantique, *Rev. Sci. Eau*, *23*(3), 247–273.

Cheviron, B., M. Delmas, O. Cerdan, and J. M. Mouchel (2011), Parameter uncertainty and sensitivity analysis in sediment flux calculation, *Hydrol. Earth Syst. Sci. Discuss.*, *8*(1), 1469–1506.

Costa, M. P. F., E. Novo, and K. H. Telmer (2013), Spatial and temporal variability of light attenuation in large rivers of the Amazon, *Hydrobiologia*, *702*(1), 171–190.

Covault, J. A., W. H. Craddock, B. W. Romans, A. Fildani, and M. Gosai (2013), Spatial and temporal variations in landscape evolution: Historic and longer-term sediment flux through global catchments, *J. Geol.*, *121*(1), 35–56.

Coynel, A., P. Seyler, H. Etcheber, M. Meybeck, and D. Orange (2005), Spatial and seasonal dynamics of total suspended sediment and organic carbon species in the Congo River, *Global Biogeochem. Cycles*, *19*, GB4019, doi:10.1029/2004GB002335.

Doxaran, D., J. M. Froidefond, S. Lavender, and P. Castaing (2002), Spectral signature of highly turbid waters. Application with SPOT data to quantify suspended particulate matter concentrations, *Remote Sens. Environ.*, *81*, 149–161.

Doxaran, D., K. Ruddick, D. McKee, B. Gentili, D. Tailliez, M. Chami, and M. Babin (2009), Spectral variations of light scattering by marine particles in coastal waters, from visible to near infrared, *Limnol. Oceanogr.*, *54*(4), 1257.

Ertel, J. R., J. I. Hedges, A. H. Devol, J. E. Richey, and M. N. G. Ribeiro (1986), Dissolved humic substances of the Amazon River system, *Limnol. Oceanogr.*, *31*(4), 739–754.

Espinoza Villar, R., J.-M. Martinez, J.-L. Guyot, P. Fraizy, E. Armijos, A. Crave, H. Bazan, P. Vauchel, and W. Lavado (2012), The integration of field measurements and satellite observations to determine river solid loads in poorly monitored basins, *J. Hydrol.*, *444*, 221–228.

Espinoza Villar, R., J.-M. Martinez, M. Le Texier, J.-L. Guyot, P. Fraizy, P. R. Meneses, and E. d. Oliveira (2013), A study of sediment transport in the Madeira River, Brazil, using MODIS remote-sensing images, *J. South Am. Earth Sci.*, *44*, 45–54.

Filizola, N., and J. L. Guyot (2009), Suspended sediment yields in the Amazon basin: An assessment using the Brazilian national data set, *Hydrol. Processes*, *23*(22), 3207–3215.

Giardino, C., V. E. Brando, A. G. Dekker, N. Strambeck, and G. Candiani (2007), Assessment of water quality in Lake Garda (Italy) using Hyperion, *Remote Sens. Environ.*, *109*(2), 183–195.

Gitelson, A. A., G. Dall'Olmo, W. Moses, D. C. Rundquist, T. Barrow, T. R. Fisher, D. Gurlin, and J. Holz (2008), A simple semi-analytical model for remote estimation of chlorophyll-*a* in turbid waters: Validation, *Remote Sens. Environ.*, *112*(9), 3582–3593.

Guyot, J. L., J. M. Jouanneau, L. Soares, G. R. Boaventura, N. Maillet, and C. Lagane (2007), Clay mineral composition of river sediments in the Amazon Basin, *Catena*, *71*, 340–356.

Hedges, J. I., J. R. Ertel, P. D. Quay, P. M. Grootes, J. E. Richey, A. H. Devol, G. W. Farwell, F. W. Schmidt, and E. Salati (1986), Organic carbon-14 in the Amazon River system, *Science*, *231*, 1129–1131.

Heege, T., V. Kiselev, M. Wettle, and N. N. Hung (2014), Operational multi-sensor monitoring of turbidity for the entire Mekong Delta, *Int. J. Remote Sens.*, *35*(8), 2910–2926.

Hoogenboom, H. J., A. G. Dekker, and I. A. Althuis (1998), Simulation of AVIRIS sensitivity for detecting chlorophyll over coastal and inland waters, *Remote Sens. Environ.*, *65*(3), 333–340.

Horowitz, A. J. (2003), An evaluation of sediment rating curves for estimating suspended sediment concentrations for subsequent flux calculations, *Hydrol. Processes*, *17*(17), 3387–3409.

Kaba, E., W. Philpot, and T. Steenhuis (2014), Evaluating suitability of MODIS-Terra images for reproducing historic sediment concentrations in water bodies: Lake Tana, Ethiopia, *Int. J. Appl. Earth Observ. Geoinform.*, *26*, 286–297.

Kirk, J. T. O. (1976), Yellow substance (gelbstoff) and its contribution to the attenuation of photosynthetically active radiation in some inland and coastal south-eastern Australian waters, *Mar. Freshwater Res.*, *27*(1), 61–71.

Konhauser, K. O., W. S. Fyfe, and B. I. Kronberg (1994), Multi-element chemistry of some Amazonian waters and soils, *Chem. Geol.*, *111*, 155–175.

Latrubesse, E. M. (2008), Patterns of anabranching channels: The ultimate end-member adjustment of mega rivers, *Geomorphology*, *101*(1), 130–145.

Lubac, B., and H. Loisel (2007), Variability and classification of remote sensing reflectance spectra in the eastern English Channel and southern North Sea, *Remote Sens. Environ.*, *110*(1), 45–58.

Ma, R.-H., J.-W. Tang, and J.-F. Dai (2006), Bio-optical model with optimal parameter suitable for Taihu Lake in water colour remote sensing, *Int. J. Remote Sens.*, *27*(19), 4305–4328.

Majozi, N. P., M. S. Salama, S. Bernard, D. M. Harper, and M. G. Habte (2014), Remote sensing of euphotic depth in shallow tropical inland waters of Lake Naivasha using MERIS data, *Remote Sens. Environ.*, *148*, 178–189.

Mangiarotti, S., J. M. Martinez, M. P. Bonnet, D. C. Buarque, N. Filizola, and P. Mazzega (2013), Discharge and suspended sediment flux estimated along the mainstream of the Amazon and the Madeira Rivers (from in situ and MODIS satellite data), *Int. J. Appl. Earth Observ. Geoinform.*, *21*, 341–355.

Martinez, J. M., J. L. Guyot, N. Filizola, and F. Sondag (2009), Increase in suspended sediment discharge of the Amazon River assessed by monitoring network and satellite data, *Catena*, *79*, 257–264.

Meade, R. H., C. F. Nordin, W. F. Curtis, F. M. Costa Rodrigues, C. M. Do Vale, and J. M. Edmond (1979), Sediment loads in the Amazon River, *Nature*, *278*, 161–163.

Meybeck, M. (1993), Riverine transport of atmospheric carbon: Sources, global typology and budget, *Water Air Soil Pollut.*, *70*, 443–463.
Mobley, C. D. (1999), Estimation of the remote-sensing reflectance from above-surface measurements, *Appl. Opt.*, *38*(36), 7442–7455.
Mobley, C. D., and C. D. Mobley (1994), *Light and Water: Radiative Transfer in Natural Waters*, Academic Press, San Diego, Calif.
Moore, G. F., J. Aiken, and S. J. Lavender (1999), The atmospheric correction of water colour and the quantitative retrieval of suspended particulate matter in Case II waters: Application to MERIS, *Int. J. Remote Sens.*, *20*(9), 1713–1733.
Moreira, L. S., P. Moreira-Turcq, R. C. Cordeiro, B. Turcq, S. Caquineau, J. C. C. Viana, and N. Brandini (2013), Holocene paleoenvironmental reconstruction in the eastern Amazonian Basin: Comprido Lake, *J. South Am. Earth Sci.*, *44*, 55–62.
Moreira-Turcq, P., P. Seyler, J. L. Guyot, and H. Etcheber (2003), Exportation of organic carbon from the Amazon River and its main tributaries, *Hydrol. Processes*, *17*(7), 1329–1344.
Morel, A., and Y.-H. Ahn (1991), Optics of heterotrophic nanoflagellates and ciliates: A tentative assessment of their scattering role in oceanic waters compared to those of bacterial and algal cells, *J. Mar. Res.*, *49*(1), 177–202.
Morel, A., B. Gentili, H. Claustre, M. Babin, A. Bricaud, J. P. Ras, and F. Tieche (2007), Optical properties of the "clearest" natural waters, *Limnol. Oceanogr.*, *52*(1), 217–229.
Neukermans, G., H. Loisel, X. Mériaux, R. Astoreca, and D. McKee (2012), In situ variability of mass-specific beam attenuation and backscattering of marine particles with respect to particle size, density, and composition, *Limnol. Oceanogr.*, *57*(1), 124.
Nogueira, I. D. S., J. C. Nabout, M. D. S. R. Ibanez, and L. M. Bourgoin (2010), Determinants of beta diversity: The relative importance of environmental and spatial processes in structuring phytoplankton communities in an Amazonian floodplain, *Acta Limnol. Bras.*, *22*(3), 247–256.
Odermatt, D., C. Giardino, and T. Heege (2010), Chlorophyll retrieval with MERIS Case-2-regional in perialpine lakes, *Remote Sens. Environ.*, *114*(3), 607–617.
Park, E., and E. M. Latrubesse (2014), Modeling suspended sediment distribution patterns of the Amazon River using MODIS data, *Remote Sens. Environ.*, *147*, 232–242.
Richey, J. E., L. A. K. Mertes, T. Dunne, R. Victoria, B. R. Forsberg, A. C. F. N. S. Tancredi, and E. Oliveira (1989), Source and routing of the Amazon River flood wave, *Global Biogeochem. Cycles*, *3*(3), 191–204, doi:10.1029/GB003i003p00191.
Rouse, H. (1938), Experiments on the Mechanics of Sediment Suspension, paper presented at Fifth International Congress for Applied Mechanics, Wiley, Cambridge.
Santos, R. V., F. Sondag, G. Cochonneau, C. Lagane, P. Brunet, K. Hattingh, and J. G. S. Chaves (2014), Source area and seasonal $^{87}Sr/^{86}Sr$ variations in rivers of the Amazon Basin, *Hydrol. Processes*, *29*, 187–197, doi:10.1002/hyp.10131.
Sioli, H. (1950), Das Wasser im Amazonasgebiet, *Forsch. Fortschr.*, *26*(21/22), 274–279.
Snyder, W. A., R. A. Arnone, C. O. Davis, W. Goode, R. W. Gould, S. Ladner, G. Lamela, W. J. Rhea, R. Stavn, and M. Sydor (2008), Optical scattering and backscattering by organic and inorganic particulates in U.S. coastal waters, *Appl. Opt.*, *47*(5), 666–677.
Stramski, D., A. Bricaud, and A. Morel (2001), Modeling the inherent optical properties of the ocean based on the detailed composition of the planktonic community, *Appl. Opt.*, *40*(18), 2929–2945.
Tzortziou, M., P. J. Neale, C. L. Osburn, J. P. Megonigal, N. Maie, and R. Jaffe (2008), Tidal marshes as a source of optically and chemically distinctive colored dissolved organic matter in the Chesapeake Bay, *Limnol. Oceanogr.*, *53*(1), 148.
Viers, J., M. Roddaz, N. Filizola, J.-L. Guyot, F. Sondag, P. Brunet, C. Zouiten, C. Boucayrand, F. Martin, and G. R. Boaventura (2008), Seasonal and provenance controls on Nd/Sr isotopic compositions of Amazon Rivers suspended sediments and implications for Nd and Sr fluxes exported to the Atlantic Ocean, *Earth Planet. Sci. Lett.*, *274*(3), 511–523.
Walling, D. E., and D. Fang (2003), Recent trends in the suspended sediment loads of the world's rivers, *Global Planet. Change*, *39*(1), 111–126.
Wang, J. J., and X. X. Lu (2010), Estimation of suspended sediment concentrations using Terra MODIS: An example from the Lower Yangtze River, China, *Sci. Total Environ.*, *408*(5), 1131–1138.
Whitlock, C. H., L. R. Poole, J. W. Usry, W. M. Houghton, W. G. Witte, W. D. Morris, and E. A. Gurganus (1981), Comparison of reflectance with backscatter and absorption parameters for turbid waters, *Appl. Opt.*, *20*(3), 517–522.
Wozniak, S. B., and D. Stramski (2004), Modeling the optical properties of mineral particles suspended in seawater and their influence on ocean reflectance and chlorophyll estimation from remote sensing algorithms, *Appl. Opt.*, *43*(17), 3489–3503.
Wu, G., L. Cui, J. He, H. Duan, T. Fei, and Y. Liu (2013), Comparison of MODIS-based models for retrieving suspended particulate matter concentrations in Poyang Lake, China, *Int. J. Appl. Earth Observ. Geoinform.*, *24*, 63–72.